STAB

J A H R E S B E R I C H T

2016

zum

20. DGLR-Fach-Symposium der STAB

8. - 9. November 2016

Braunschweig

„Deutsche Strömungsmechanische Arbeitsgemeinschaft, STAB“

INHALT

Mitteilungen der Geschäftsstelle

Früher erschienen die STAB-Jahresberichte im Frühjahr des Folgejahres. Hiervon wird seit 2011 abgewichen. Die Berichte werden bei den alternierenden Veranstaltungen Symposium und Workshop als Sammlung der Kurzfassungen der Vorträge an die Teilnehmer verteilt. Somit erscheint dieser STAB-Jahresbericht 2016 zum 20. DGLR-Fach-Symposium der STAB, das am 8. und 9. November 2016 in Braunschweig stattfindet.

Der Bericht enthält 82 „Mitteilungen" über Arbeiten aus den Projektgruppen und Fachkreisen, über die beim Symposium vorgetragen wird. Den „Mitteilungen" vorangestellt ist ein Inhaltsverzeichnis (Seite 16 bis 21), das nach Projektgruppen/Fachkreisen gegliedert ist. Innerhalb der Rubriken ist alphabetisch nach Verfassern sortiert. Die Beiträge verteilen sich (bezogen auf den Erstautor) zu 5 % auf die Industrie, 45 % auf die Hochschulen, 50 % auf Forschungseinrichtungen (DLR, DNW, ISL). Auf Seite 186 sind die Autoren und Koautoren dieses Berichtes aufgelistet.

Die Jahresberichte werden nur an den tatsächlich daran interessierten Personenkreis verteilt. Alle Teilnehmer des diesjährigen STAB-Symposiums erhalten zur Veranstaltung ein Exemplar. Weiterhin wird der Jahresbericht an die Mitglieder der STAB-Gremien und weitere Interessierte versandt.

Falls Sie ein Exemplar des nächsten Jahresberichts, in diesem Fall 2017, wünschen, schicken Sie bitte den unten beigefügten Abschnitt zurück. Der Bezug muss jährlich neu angefordert werden.

Dieser Jahresbericht erscheint in einer Auflage von 200 Exemplaren. Einige Rest-Exemplare sind erfahrungsgemäß bis zum Ende des jeweiligen Jahres verfügbar.

Aktualisierte Informationen über STAB finden Sie auch unter: *www.dlr.de/agstab*

Göttingen, im Oktober 2016

Auch über e-mail: stab@dlr.de	O Ich bitte um Zusendung des STAB-Jahresberichts 2017
	Name:
Geschäftsstelle der STAB	Organisation:
c/o DLR	Anschrift:
Prof. Dr. C. Wagner	Telefon:
Bunsenstraße 10 37073 Göttingen	E-mail:

Zielsetzungen, chronologische Entwicklung und Organisation

Die Arbeitsgemeinschaft „Strömungen mit Ablösung“ (STAB) wurde auf Initiative der Deutschen Gesellschaft für Luft- und Raumfahrt (DGLR) - Lilienthal-Oberth, e.V. - 1979 von Strömungsforschern, Aerodynamikern und Luftfahrtingenieuren aus DLR, Hochschule und Industrie ins Leben gerufen.

Sie entstand aus „dem gemeinschaftlichen Bestreben, die Strömungsforschung in Deutschland generell zu fördern und durch Konzentration auf ein wirtschaftlich und forschungspolitisch zukunftsträchtiges Teilgebiet zu vertiefen“ (Auszug aus der Präambel der Verfahrensordnung der STAB).

In Zeiten knapper werdender Kassen bei gleichzeitig massiv erhöhtem Wettbewerbsdruck sind diese Ansätze notwendiger denn je. Die öffentlichen Finanziers setzen diese Kooperationsbereitschaft inzwischen aber auch voraus. Da dieser Leitgedanke der STAB dadurch inzwischen anderweitig verfolgt wird, konzentriert sie sich mehr auf fachliche Veranstaltungen.

STAB ist als ‚Kompetenznetzwerk’ der DGLR angegliedert. Auf der DGLR-Webseite findet man STAB unter: *http://www.dglr.de/index.php?id=2428*

In der STAB sind alle wichtigen Gebiete der Strömungsmechanik - insbesondere die der Luft- und Raumfahrt - aus Grundlagenforschung, Großforschung und Industrie in Deutschland zusammengeschlossen. Bei der Gründung Ende der 70er Jahre stand die Idee dahinter, über ein hochaktuelles fachliches Thema - identifiziert wurde seinerzeit „Strömungen mit Ablösung“ - Forschungsverbünde aus der Industrie, den Hochschulen und der Großforschung zu organisieren. In den folgenden Jahren sind auch andere strömungsmechanische Fragestellungen aufgegriffen worden, womit die STAB sich in der Fachwelt einen wohlbekannten Namen erworben hat. Es sind aber nicht nur diejenigen angesprochen, die sich mit den traditionellen Themen der Strömungsmechanik beschäftigen, sondern es können auch Probleme aus dem Automobilbau, der Gebäudeaerodynamik, der Verfahrenstechnik, dem Motorenbau, usw. diskutiert werden.

Die Programmleitung hat im November 2000 entschieden, zukünftig das „AG“ im Namen wegzulassen.

Die öffentlichkeitsrelevanten wissenschaftlichen Aktivitäten spiegeln sich in der nachfolgenden chronologischen Entwicklung wider:

DGLR-Symposium „Forschung und Entwicklung auf dem Gebiet der Strömungsmechanik und Aerodynamik in der Bundesrepublik Deutschland“	Bonn, 29.11.-01.12.1978
„Gespräch über Strömungsforschung in Deutschland“	Ottobrunn, 30.01.1979
„Memorandum über zukünftige nationale Zusammenarbeit in der Strömungsforschung, insbesondere der Aerodynamik auf dem Gebiet der Strömungen mit Ablösung“	Oktober 1979
Programmpräsentation anlässlich der BDLI-Jahrestagung	Bonn, 01.07.1980

Programm der Arbeitsgemeinschaft „Strömungen mit Ablösung“	September 1980
Programmpräsentation im Bundesministerium für Forschung und Technologie	Bonn, 19.03.1981
Konstituierung des Kuratoriums und Neuorganisation der Arbeitsgemeinschaft „Strömungen mit Ablösung" (AG STAB)	Köln-Porz, 23.02.1982
Konstituierung von Programmleitung/Programmausschuss	Göttingen, 24.03.1982
Erfassung STAB-relevanter Aktivitäten in der Bundesrepublik Deutschland (Stand Mitte 1981)	April 1982
Fachtagung anlässlich der ILA '82 „Strömungen mit Ablösung“	Hannover, 19.05.1982
Neue Impulse für die Strömungsforschung- und Aerodynamik; Vortrag von H.-G. Knoche, DGLR-Jahrestagung	Hamburg, 01.-03.10.1984
DGLR Workshop „2D-Messtechnik“	Markdorf, 18.-19.10.1988

Symposium

1. DGLR-Fach-Symposium	München, 19.-20.09.1979
2. DGLR-Fach-Symposium	Bonn, 30.06.-01.07.1980
3. DGLR-Fach-Symposium	Stuttgart, 23.-25.11.1981
4. DGLR-Fach-Symposium	Göttingen, 10.-12.10.1983
5. DGLR-Fach-Symposium	München, 09.-10.10.1986
6. DGLR-Fach-Symposium	Braunschweig,08.-10.11.1988
7. DGLR-Fach-Symposium	Aachen, 07.-09.11.1990
8. DGLR-Fach-Symposium	Köln-Porz, 10.-12.11.1992
9. DGLR-Fach-Symposium	Erlangen, 04.-07.10.1994
10. DGLR-Fach-Symposium	Braunschweig,11.-13.11.1996
11. DGLR-Fach-Symposium	Berlin, 10.-12.11.1998
12. DGLR-Fach-Symposium	Stuttgart, 15.-17.11.2000
13. DGLR-Fach-Symposium	München, 13.-15.11.2002
14. DGLR-Fach-Symposium	Bremen, 16.-18.11.2004
15. DGLR-Fach-Symposium	Darmstadt, 29.11.-01.12.2006
16. DGLR-Fach-Symposium	Aachen, 03.-04.11.2008
17. DGLR-Fach-Symposium	Berlin, 09.-10.11.2010

18. DGLR-Fach-Symposium	Stuttgart, 06.-07.11.2012
19. DGLR-Fach-Symposium	München, 04.-05.11.2014
20. DGLR-Fach-Symposium	Braunschweig,08.-09.11.2016

Workshop

1. STAB-Workshop	Göttingen, 07.-08.03.1983
2. STAB-Workshop	Köln-Porz, 18.-20.09.1984
3. STAB-Workshop	Göttingen, 10.-11.11.1987
4. STAB-Workshop	Göttingen, 08.-10.11.1989
5. STAB-Workshop	Göttingen, 13.-15.11.1991
6. STAB-Workshop	Göttingen, 10.-12.11.1993
7. STAB-Workshop	Göttingen, 14.-16.11.1995
8. STAB-Workshop	Göttingen, 11.-13.11.1997
9. STAB-Workshop	Göttingen, 09.-11.11.1999
10. STAB-Workshop	Göttingen, 14.-16.11.2001
11. STAB-Workshop	Göttingen, 04.-06.11.2003
12. STAB-Workshop	Göttingen, 08.-09.11.2005
13. STAB-Workshop	Göttingen, 14.-15.11.2007
14. STAB-Workshop	Göttingen, 11.-12.11.2009
15. STAB-Workshop	Göttingen, 09.-10.11.2011
16. STAB-Workshop	Göttingen, 12.-13.11.2013
17. STAB-Workshop	Göttingen, 10.-11.11.2015

Kurs über „Application of Particle Image Velocimetry, PIV“:
findet seit 1993 regelmäßig im DLR-Göttingen statt,
letztmalig am 14.-18.03.2016

Die STAB-Symposiums-Tagungsbände durchlaufen einen Begutachtungsprozess. Die Bände der letzten zehn Jahre finden Sie hier aufgelistet.

- Notes on Numerical Fluid Mechanics, Vol. 60; Ed.: H. Körner, R. Hilbig; Vieweg, Braunschweig/Wiesbaden, 1997
- Notes on Numerical Fluid Mechanics, Vol. 72; Ed.: W. Nitsche, H.-J. Heinemann, R. Hilbig; Vieweg, Braunschweig/Wiesbaden, 1999
- Notes on Numerical Fluid Mechanics, Vol. 77; Ed.: S. Wagner, U. Rist, H.-J. Heinemann, R. Hilbig; Springer, Berlin Heidelberg New York, 2002

- Notes on Numerical Fluid Mechanics and Multidisciplinary Design, Vol. 87; Ed.: Chr. Breitsamter, B. Laschka, H.-J. Heinemann, R. Hilbig; Springer, Berlin Heidelberg New York, 2004
- Notes on Numerical Fluid Mechanics and Multidisciplinary Design, Vol. 92; Ed.: H. J. Rath, C. Holze, H.-J. Heinemann, R. Henke, H. Hönlinger; Springer, Berlin Heidelberg New York, 2006
- Notes on Numerical Fluid Mechanics and Multidisciplinary Design, Vol. 96; Ed.: C. Tropea, S. Jakirlic, H.-J. Heinemann, R. Henke, H. Hönlinger; Springer-Verlag Berlin Heidelberg, 2007
- Notes on Numerical Fluid Mechanics and Multidisciplinary Design, Vol. 112; Eds.: A. Dillmann, G. Heller, M. Klaas, H.-P. Kreplin, W. Nitsche, W. Schröder; Springer-Verlag Berlin Heidelberg, 2010
- Notes on Numerical Fluid Mechanics and Multidisciplinary Design, Vol. 121; Eds.: A. Dillmann, G. Heller, H.-P. Kreplin, W. Nitsche, I. Peltzer; Springer-Verlag Berlin Heidelberg, 2013
- Notes on Numerical Fluid Mechanics and Multidisciplinary Design, Vol. 124; Eds.: A. Dillmann, G. Heller, E. Krämer, H.-P. Kreplin, W. Nitsche, U. Rist; Springer-Verlag Berlin Heidelberg, 2014
- Notes on Numerical Fluid Mechanics and Multidisciplinary Design, Vol. 132; Eds.: A. Dillmann, G. Heller, E. Krämer, C. Wagner, C. Breitsamter; Springer-Verlag Berlin Heidelberg, 2016

<u>Vorschau:</u>

18. STAB-Workshop	Göttingen, November 2017 (aktuelle Informationen dazu werden regelmäßig auf die STAB-Website gestellt)
26. Kurs „PIV“	Göttingen, 20.-24. März 2017

Programmleitung

Dipl.-Ing. R. Behr roland.behr@astrium.eads.net	(Astrium-Space, München) Tel.: 089 / 607-251719
Prof. Dr. C. Breitsamter christian.breitsamter@aer.mw.tum.de	(Technische Universität München) Tel.: 089 / 289-16137
Prof. Dr. A. Dillmann (Sprecher) andreas.dillmann@dlr.de	(DLR, Göttingen) Tel.: 0551 / 709-2177
Prof. Dr. G. Eitelberg dnw@nlr.nl	(DNW, Emmeloord) Tel.: 0031 527 / 248521
Prof. Dr. J. Fröhlich jochen.froehlich@tu-dresden.de	(TU Dresden) Tel.: 0351 / 463 37607
Dr. R. Höld roland.hoeld@mbda-systems.de	(LFK Schrobenhausen) Tel.: 08252 / 99 8845
Dr. G. Heller (Sprecher) gerd.heller@airbus.com	(Airbus, Bremen) Tel.: 0421 / 538-2649
Prof. Dr. E. Krämer (Sprecher) kraemer@iag.uni-stuttgart.de	(Universität Stuttgart) Tel.: 0711 / 685-63401
P. Nöding peter.noeding@astrium.eads.net	(EADS Astrium GmbH, Bremen) Tel.: 0421 / 539-4752
Dipl.-Ing. T. Pinar thilo.pinar@cassidian.com	(EADS Cassidian, Manching) Tel.: 08459 / 81-7 92 50
Prof. Dr. R. Radespiel r.radespiel@tu-braunschweig.de	(Technische Universität Braunschweig) Tel.: 0531 / 391-94250
Prof. Dr. C.-C. Rossow (DLR, Braunschweig)	(DLR, Braunschweig) Tel.: 0531 / 295-2400
Prof. Dr. U. Rist rist@iag.uni-stuttgart.de	(Universität Stuttgart) Tel.: 0711 / 685-63432
Dipl.-Ing. D. Schimke dieter.schimke@eurocopter.com	(Eurocopter Deutschland, München) Tel.: 089 / 6000-6566
Prof. Dr. W. Schröder office@aia.rwth-aachen.de	(RWTH, Aachen) Tel.: 0241 / 80 95410
Prof. Dr. L. Tichy lorenz.tichy@dlr.de	(DLR, Göttingen) Tel.: 0551 / 709-2341

Projektgruppen	**Sprecher:**
Transportflugzeuge einschl. Triebwerksintegration	Dr. A. Seitz (DLR, Braunschweig) Tel.: 0531 / 295-2888 E-mail: arne.seitz@dlr.de
Multidisziplinäre Optimierung und Neue Konfigurationen	Dr. M. Hepperle (DLR, Braunschweig) Tel.: 0531 / 295-3337 E-mail: martin.hepperle@dlr.de und Dipl.-Ing. D. Reckzeh (Airbus, Bremen) Tel.: 0421 / 538-2136 E-mail: daniel.reckzeh@airbus.com
Turbulenzforschung/-modellierung	Prof. Dr. W. Schröder (RWTH, Aachen) Tel.: 0241 / 80 95410 E-mail: office@aia.rwth-aachen.de und Prof. Dr. N. Adams (Technische Universität München) Tel.: 089 / 289-16120 E-mail: Nikolaus.Adams@tum.de
Hyperschallaerothermodynamik	Dr. T. Eggers (DLR, Braunschweig) Tel.: 0531 / 295-2436 E-mail: Thino.Eggers@dlr.de
Flow Control, Transition und Laminarhaltung	Dr. G. Schrauf (Airbus Deutschland, Bremen) Tel.: 0421 / 538-3232 E-mail: geza.schrauf@airbus.com
Hochagile Konfigurationen	Dr. R. Höld (LFK-Lenkflugkörpersysteme GmbH, Schrobenhausen) Tel.: 08252 / 99 8845 E-mail: roland.hoeld@mbda-systems.de
Drehflügleraerodynamik	Dr. K. Richter (DLR, Göttingen) Tel.: 0551 / 709-2631 E-mail: kai.richter@dlr.de
Technische Strömungen	Prof. Dr. C. Wagner (DLR, Göttingen) Tel.: 0551 / 709-2261 E-mail: claus.wagner@dlr.de

Fachkreise:

siehe hierzu die

‚Querschnittsthemen (Q)' der DGLR unter www.dglr.de:

Aeroelastik und Strukturdynamik Q 1.2	Dipl.-Ing. J. Schweiger (EADS, Deutschland) Tel.: 08459 / 8178847 E-mail: johannes.schweiger@cassidian.com
Fluid- und Thermodynamik Q 2	Dr. B. Eisfeld(DLR, Braunschweig) Tel.: 0531 / 295-3305 E-mail: Bernhard.Eisfeld@dlr.de
Numerische Aerodynamik Q 2.1	Prof. Dr. N. Kroll (DLR, Braunschweig) Tel.: 0531 / 295-2440 E-mail: norbert.kroll@dlr.de
Experimentelle Aerodynamik Q 2.2	Dr. C. Breitsamter (Technische Universität München) Tel.: 089 / 289-16137 E-mail: christian.breitsamter@aer.mw.tum.de
Strömungsakustik / Fluglärm Q 2.3	Prof. Dr. J. Delfs (DLR, Braunschweig) Tel.: 0531 / 295-2170 E-mail: jan.delfs@dlr.de
Versuchsanlagen Q 2.4	Prof. Dr. G. Eitelberg (DNW, Emmeloord) Tel.: 0031 527 / 248521 E-mail: dnw@nlr.nl
Wissenschaftlicher Koordinator	Prof. Dr. Claus Wagner (DLR Göttingen) Tel. 0551 / 709-2261 E-mail: claus.wagner@dlr.de

Stand: Oktober 2016

Verfassen von „Mitteilungen“:

Auf der Sitzung der Programmleitung von STAB am 09.11.2010 in Berlin wurde der Beschluss gefasst, den Jahresbericht in der bisherigen Form abzuschaffen. Stattdessen sollen die Anmeldungen zum STAB-Symposium bzw. STAB-Workshop zusammengefasst werden und bei der jeweiligen Veranstaltung als Bericht/Proceedings an die Teilnehmer verteilt werden. Diese zum Ende des laufenden Jahres erscheinende Broschüre ersetzt somit den bisher im ersten Quartal des Folgejahres erstellten Jahresbericht.

Die bisherige recht starre Vorgabe für die Form der Mitteilungen wird ersetzt durch eine zweiseitige Kurzfassung des Beitrags, bei der nur der Kopf vorgegeben ist mit:

Mitteilung

Projektgruppe / Fachkreis:

Thema / Titel des Beitrags

Autor(en)
Institution
Adresse
E-mail

Bitte halten Sie sich bei der Anmeldung zur STAB-Veranstaltung unbedingt an die vorgegebenen zwei Seiten pro „Mitteilung“.
Tragen Sie bitte keine Seitenzahlen ein.
Der Druck erfolgt weiterhin ausschließlich in schwarz/weiß.

Für Rückfragen steht Ihnen die Geschäftsstelle gerne zur Verfügung:

Tel.: 0551 / 709 - 2261
Fax: 0551 / 709 - 2241
E-mail: stab@dlr.de

Mit freundlichen Grüßen
Ihre Projektgruppenleiter / Ihre Fachkreisleiter / Ihre Geschäftsstelle

The **CEAS Aeronautical Journal** and the **CEAS Space Journal** were created under the umbrella of CEAS to provide an appropriate platform for excellent scientific publications submitted by scientists and engineers. The German Aerospace Center (DLR) and the European Space Agency (ESA) support the Journals.

CEAS Aeronautical Journal

An Official Journal of the Council of European Aerospace Societies
ISSN: 1869-5582 (print version)
Journal no. 13272
Springer Wien
http://www.springer.com/13272

Editor-in-Chief: Rolf Henke, DLR, Cologne
Managing Editors: Cornelia Hillenherms, DLR, Cologne

The CEAS Aeronautical Journal is devoted to publishing new developments and results in all areas of aeronautics-related science and technology. Also of interest are (invited) in-depth reviews of the status of development in specific areas of relevance to aeronautics and descriptions of the potential way forward. The topics of the journal are aeroacoustics, aeroelasticity, air transport system, air traffic management, flight mechanics, flight physics and aerodynamics, propulsion, structures and materials. Reports on new developments in design and manufacturing of aircraft, rotorcraft, missiles and unmanned aerial vehicles are also welcome .

The journal publishes peer-reviewed original articles, (invited) reviews and short communications.

CEAS Space Journal

An Official Journal of the Council of European Aerospace Societies
ISSN: 1868-2502 (print version), 1868-2510 (electronic version) Journal no. 12567
Springer Wien
http://www.springer.com/12567

Editor-in-Chief: Constantinos Stavrinidis (London, Imperial College)
Managing Editor: Wilhelm Kordulla, Torben Henriksen (ESA)

The CEAS Space journal is devoted to publish new developments and results in all areas of space-related science and technology, including important spin-off capabilities and applications as well as ground-based support systems and manufacturing advancements. Of interest are also (invited) in-depth reviews of the status of development in specific areas of relevance to space, and descriptions of the potential way forward. Typical disciplines of interest include mission design and space systems, aerothermodynamics, environmental control and life support systems, guidance, navigation and control, mechanisms, propulsion, power, robotics, structures, testing and thermal issues.

The journal publishes peer-reviewed original articles, (invited) reviews and short communication

1. Projektgruppe „Transportflugzeuge einschl. Triebwerksintegration“

2. Projektgruppe „Turbulenzforschung/-modellierung“

3. Projektgruppe „Hyperschallaerodynamik“

4. Projektgruppe „Flow Control, Transition und Laminarhaltung“

5. Projektgruppe „Hochagile Konfigurationen“

6. Projektgruppe „Drehflügleraerodynamik“

7. Fachkreis „Aeroelastik und Strukturdynamik“

8. Fachkreis „Numerische Aerodynamik“

9. Fachkreis „Experimentelle Aerodynamik“

10. Fachkreis „Strömungsakustik / Fluglärm"

11. Themenkreis „Fahrzeugaerodynamik”

12. Themenkreis „Windenergie”

13. Themenkreis „Biofluidmechanik”

Mitteilung

Projektgruppe / Fachkreis: Transportflugzeuge, Flow Control

Numerical Investigation of Slot and Configuration Impact on the Efficiency of Tangential Blowing at a Vertical Tailplane with Infinite Span

Anna Gebhardt, Jochen Kirz
Deutsches Zentrum für Luft- und Raumfahrt e. V. (DLR),
Institut für Aerodynamik und Strömungstechnik,
Lilienthalplatz 7, 38108 Braunschweig
anna.kroehnert@dlr.de, jochen.kirz@dlr.de

Introduction

The vertical tailplane (VTP) of a transport aircraft is needed for stability and control of the aircraft about the yaw axis. One case determining the size of the VTP is the failure of the critical engine. In the one-engine inoperative (OEI) condition, the resulting asymmetric thrust condition creates a moment around the yaw axis. This must be counteracted by the VTP. Here take-off is a critical flight segment where relatively low flight speed and high thrust requirements coincide to necessitate large aerodynamic forces to be generated by the VTP. On the other hand, in cruise flight at high aircraft velocity, the VTP is larger than necessary to satisfy cruise stability requirements for modern transport aircraft with electronic flight control systems. It follows that the VTP size is determined by a rarely occurring failure case. In this critical OEI case the rudder is highly deflected to achieve maximum side force but this also leads to partial separation on the rudder. If the size of the VTP could be reduced by applying some means to increase the side force, drag and weight could be lowered which in turn would lead to a reduction in fuel burn. One possibility is the use of active flow control (AFC). With this the side force coefficient produced by the VTP can be increased without increasing its size by delaying flow separation to higher sideslip and/or rudder deflection angles.

Previous Work

Sensitivities of different active flow control parameters were investigated in a previous study using a 2D VTP airfoil [1]. The results showed that the flow on the rudder can, with sufficiently high blowing velocity and mass flow rate, remain attached on the rudder also at high deflection angles. This was accompanied by an increase of the lift coefficient of the airfoil. Also unsteady blowing using a pulsing jet has been investigated for this 2D geometry [2]. As intended and also known from other studies the mass flow rate for the actuation could be reduced for a similar increase in the lift coefficient.
Tangential blowing has already been investigated experimentally and numerically in several studies, e.g. [3], but mainly for the use on wings. Due to the small aspect ratio and the large sweep angle of the VTP the results obtained for the wing might not be directly transferable. Currently research is done at NASA and Boeing with a VTP geometry using an experimental approach. However, no study was found in which the underlying mechanism driving the variable efficacy of different slot configurations along the VTP span was investigated.

Aim of this Study

In the frame of the current study the numerical investigation to increase the side force coefficient by tangential blowing is extended to 3D. This allows examining effects in span wise direction. Here the width of discrete slots and the size of the gap between them

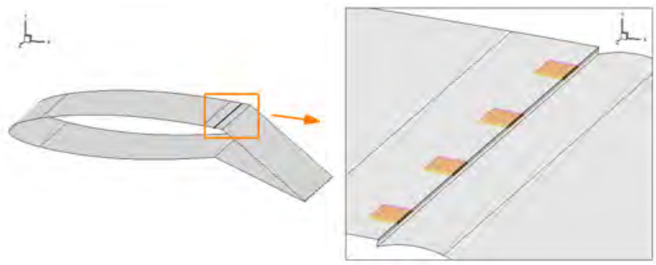
Fig. 1: Geometry with detail view of four slots (orange)

are varied. An example of one resulting geometry is shown in Fig. 1. In addition, the blowing velocity is varied.
In this study, starting from a continuous jet, the slot area is reduced in span wise direction. Keeping the blowing velocity constant, this can again lead to a reduction of required mass flow rate to achieve the same increase in side force on the VTP compared to a configuration with a continuous slot.
Since a whole 3D VTP would mean a large mesh resulting in excessive calculation time, a 2.5D geometry is used. It has an infinite span and a constant chord length but incorporates the sweep angle of the VTP. In addition to a variation of the slots the leading edge sweep angle is also altered since it is expected to have an impact on the lift increase at a constant momentum coefficient as well as the curvature of the rudder shoulder just behind the blowing slots.

Results

Without blowing the deflected rudder is separated. Using tangential blowing with a sufficiently high mass flow rate leads to an attached flow on the rudder. This in turn leads to an increase of the side force coefficient up to 60% for a discrete slot configuration at a comparatively low momentum coefficient C_μ=0.5%. For the continuous slot a C_μ=1% was needed to achieve the same side force coefficient. This large difference makes it obvious that when moving from a continuous slot to discrete slots additional and beneficial effects occur in the flow field over the rudder. This improvement is due to a vortex pair which develops for each discrete jet as show in Fig. 2. It is not present for the continuous slot. The effect of the vortex system will be analyzed.
Changing the slot spacing alters the impact on the side force. For example a too dense spacing reduces the possible side force coefficient since the vortex system on the rudder cannot fully develop. Due to the underlying vortex development mechanism discussed by the authors, the leading edge sweep angle should also influence the generation of the vortex system.
This is the case as shown in Fig. 3. For three different sweep angles the side force coefficient C_Y is shown for three different jet blowing velocities. It can be seen that the side force coefficient increases with increasing blowing velocity. However, with a reduction of the leading edge sweep angle also the gain in C_Y decreases. In addition, a change of the curvature of the rudder shoulder is analyzed which also has an impact on the generated side force.

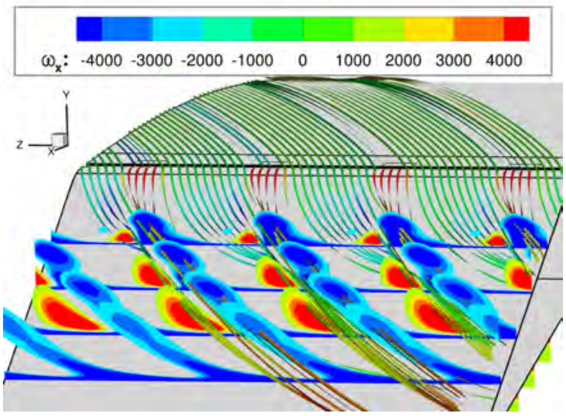

Fig. 2: Rear view onto the rudder: field stream traces and vortices generated by several discrete slots

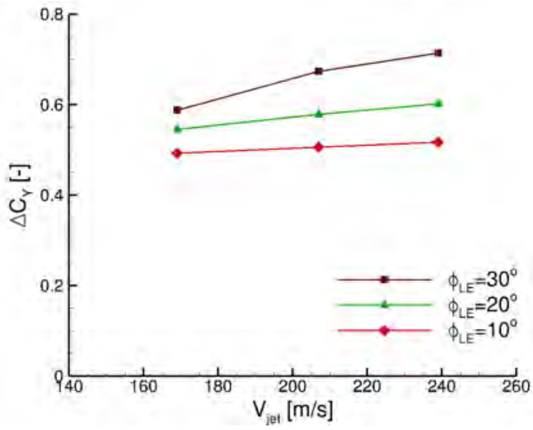

Fig. 3: Change of side force for a variation of the leading edge sweep angle for three different velocities

References

[1] Kröhnert, A., "Numerical Investigation of Tangential Blowing at the Rudder of a Vertical Tailplane Airfoil", AIAA Paper 2014-2143, 2014
[2] Kröhnert, A., "Numerical Investigation of Unsteady Tangential Blowing at the Rudder of a Vertical Tailplane Airfoil", Proceedings STAB Symposium 2014, München, 2014
[3] Pfingsten, K.-C., "Experimentelle und numerische Untersuchung eines spaltlosen Hochauftriebssystems mit Zirkulationskontrolle", Campus Forschungsflughafen FB 2011-04, 2011

Mitteilung

Projektgruppe / Fachkreis: SFB880

Aerodynamic Assessment of Embedded Over-the-Wing Engine Installations on a STOL Commercial Aircraft Concept

Heykena, Constance*; Ronzheimer, Arno†; Friedrichs, Jens*
*Institut für Flugantriebe und Strömungsmaschinen, Hermann-Blenk-Str. 37, 38108 Braunschweig, c.heykena@ifas.tu-bs.de; j.friedrichs@ifas.tu-bs.de
† DLR, Deutsches Zentrum für Luft- und Raumfahrt
Institut of Aerodynamics and Flow Technology, Department of Transport Aircrafts
Lilienthalplatz 7, 38108, Braunschweig

The numerical study presented here deals with the integration of an Over-Wing-Nacelle (OWN) to a Wing-Body aircraft configuration at high flight velocities. Nacelles installed over the wing offer a great variety of benefits like noise reduction during take-off and landing, landing gear length and weight reduction as well as short take-off and landing potential. Moreover, this configuration can also accommodate nacelles for efficient jet engines with increasing bypass ratios (BPR). These benefits used to be more than offset by a poor aerodynamic leading to a unfavorable higher overall airframe drag.

Recent studies have shown, however, that OWN installations can also improve aerodynamic performance. By positioning the nacelle at the wing trailing edge the inlet slows down the flow approaching the nacelle. As a result the wing shock strength can be reduced. This leads to a better overall aircraft performance at high cruise velocities. To connect a nacelle to the airframe pylons are commonly used, not only for conventional under wing configurations but also for OWN configurations. Within the presented study a more integrative approach was chosen. The purpose of the presented study is to analyze the aerodynamic performance of an OWN, which is embedded into the wing, and to evaluate the influence of the placement of the nacelle.

The aircraft investigated in this study is sized for short distance missions with 100 passangers, 45t max. payload and a cruise speed at Ma = 0.78. It is a low wing configuration powered by two ultra-high bypass ratio (UHBR) geared turbofan engines with a bypass ratio of 18 and max. thrust of 100kN at take-off to ensure short take-off and landing attributes of the aircraft. The corresponding generic UHBR-nacelle was designed to fit the geometric requirements derived from the propulsion system's thermodynamic cycle, which is dimensioned to meet the thrust requirements of the aircraft. The DLR-FNG airfoil profile is used for shaping the wing geometry. Figure 1 below shows the half model of the aircraft in the clean configuration without nacelle on the left side, which serves as a reference for the performance evaluation of the configuration. The right hand side of Figure 1 is to illustrate the postion of the OWN at the trailing edge of the wing.

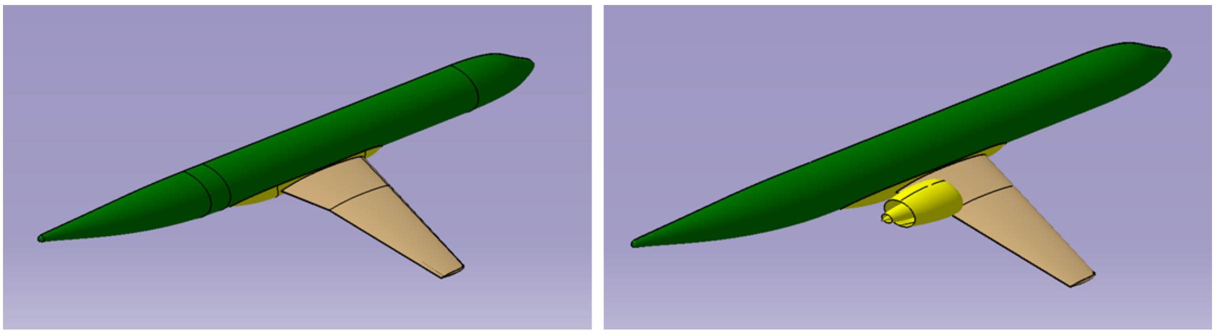

Figure 1: Clean configuration (left) and position of OWN (right)

The generation of the surface model of the wing/body/nacelle configuration was done using CATIA V. A suitable parameterization for the junction of the wing and nacelle was to be implemented to establish a easy to vary surface model for the following placement study of the embedded OWN. For the grid generation the commercial grid generator CENTAUR from CentaurSoft was chosen. Previous studies have shown that the hybrid grid setup can easily be transferred to modified configurations while achieving the same level of mesh quality for all investigated positions of the OWN. For the steady 3D RANS simulations the DLR TAU-Code was used which is an established tool for this kind of aerodynamic problems.

In the numerical study a half model of the aircraft with UHBR nacelle installed at the wing trailing edge is examined. From an aerodynamic point of view it is expected on one hand that the nacelle influences the wing shock by weakening the shock strength due to the deceleration of the flow in front of the nacelle. On the other hand it is assumed that the inlet length to fan diameter ratio of the UHBR-nacelle can be significantly reduced because of the influence of the wing flow field. This leads to a decline in wetted area which has a positive impact on the drag of the configuration. To decrease the wetted area of the configuration further the nacelle is also embedded into wing, which is supposed to lead to a better performance in terms of thrust to drag of the investigated configuration.

For the described configuration a fundamental engine placement study will be conducted to asses aerodynamic characteristics of an embedded OWN installation at cruise conditions. Several positions will be investigated while keeping the spanwise position of the OWN constant. Figure 2 shows the schematic wing/nacelle reference position at the spanwise position of the wing. During the sensitivity study the OWN will be varied in x-direction from 0.9 to 1.4 while the z position will be shifted from 0.9 to 1.2. Thus, a representative parameter space for an embedded OWN will be covered to gain an understanding on the impact of the engine placement for such a configuration.

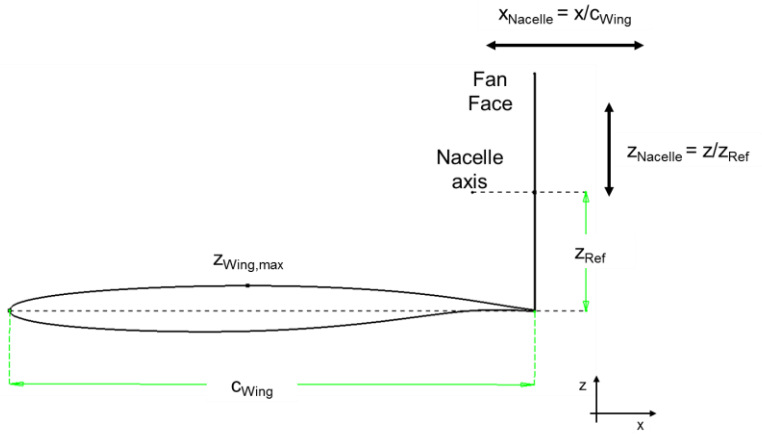

Figure 2: Reference position of the Nacelle in relation to the wing

The project lies within the framework of the Collaborative Research Center (Sonderforschungsbereich) SFB880. As an alternative to the embbeded OWN installation a pylon-mounted OWN configuration for the same baseline aircraft and engine will be analyzed by DLR, Institut of Aerodynamics and Flow Technology, Department of Transport Aircrafts.

Mitteilung

Projektgruppe / Fachkreis: Triebwerksintegration

Steady and Unsteady CFD Simulation of a Bent Intake Geometry

Thomas Kächele[1], Tim Schneider[2], and Reinhard Niehuis[1]
1. Universität der Bundeswehr München, Werner-Heisenberg-Weg 39,
85577 Neubiberg, thomas.kaechele@unibw.de
2. MTU Aero Engines AG, Dachauer Str. 665, 80995 München

Modern aircraft concepts often feature complex engine intake configurations. Whereas the reduction of aircraft drag through boundary layer ingestion motivates the development of such civil configurations, a low observability by means of hiding the highly reflective fan plane of the jet engine lies in the focus of military applications. These unconventional geometries provoke a disturbed flow regime towards the compression system of the jet engine leading to performance deficits and a reduced stability margin. The generated flow distortion within the aerodynamic interface plane (AIP) between intake and engine is both dependent on the duct geometry as well as the upstream influence of the distorted compressor. To improve the knowledge about this interaction and to validate different simulation approaches, a highly bent intake geometry (cf. Figure 1) was developed for an experimental investigation within the engine test facility of the Institute of Jet Propulsion at the University of the German Federal Armed Forces in Munich [1] in cooperation with MTU Aero Engines AG. This paper presents results of steady and unsteady RANS computations of the inner aerodynamics of this intake geometry obtained with the flow solver TRACE.

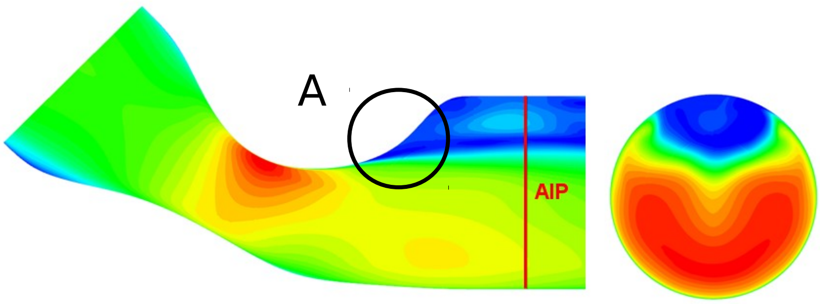

Figure 1: Flow regime inside duct (l.) and AIP total pressure distortion (r.)

As this solver is developed and optimized for turbomachinery applications, no best practice for s-duct simulations was available. Hence, results of an experimental NASA-test campaign of a single s-bent duct [2] were used for the calibration of the numerical setup. The flow field of this duct is characterized by a high subsonic Mach number and a large flow separation due to an increase of cross-sectional area and wall curvature – the same flow features, which are present within the bent intake geometry. In this context, sensitivity studies included mesh density, wall treatment, turbulence modeling, and a variation of the inflow conditions. The accuracy of the obtained simulation results with the final setup were comparable or even superior to those of other RANS-solvers also deploying two-equation eddy viscosity turbulence models. Additionally, a strong influence of the inflow turbulent length scale on the wall pressure distribution was observed, while a high mesh resolution did not lead to an increased accuracy.

The setup showing best predictive capabilities was then applied on the bent intake geometry where steady RANS-simulations were carried out with undisturbed inflow conditions as well as flow conditions as they are expected to occur during the experiment within the engine test facility. Again, mesh density had a minor impact on the duct flow, while a strong dependence on the inflow conditions illustrates the importance of a precise acquisition of the experimental inflow conditions for successful post-test calculations. In both cases, convergence problems and asymmetric flow solutions occurred for some numerical setups which had produced valid results for the NASA case. This suggested an unsteady flow regime within this more aggressive duct geometry. URANS computations were thus carried out.

Again, no experience for duct simulations was available. Thus, a broad range of numerical settings was investigated. In addition, a time-step study as well as a variation of the extent of computational domain was necessary. Results include global performance and distortion parameters as well as unsteady probe data and an analysis of the dominant frequencies such as shown in Figure 2.

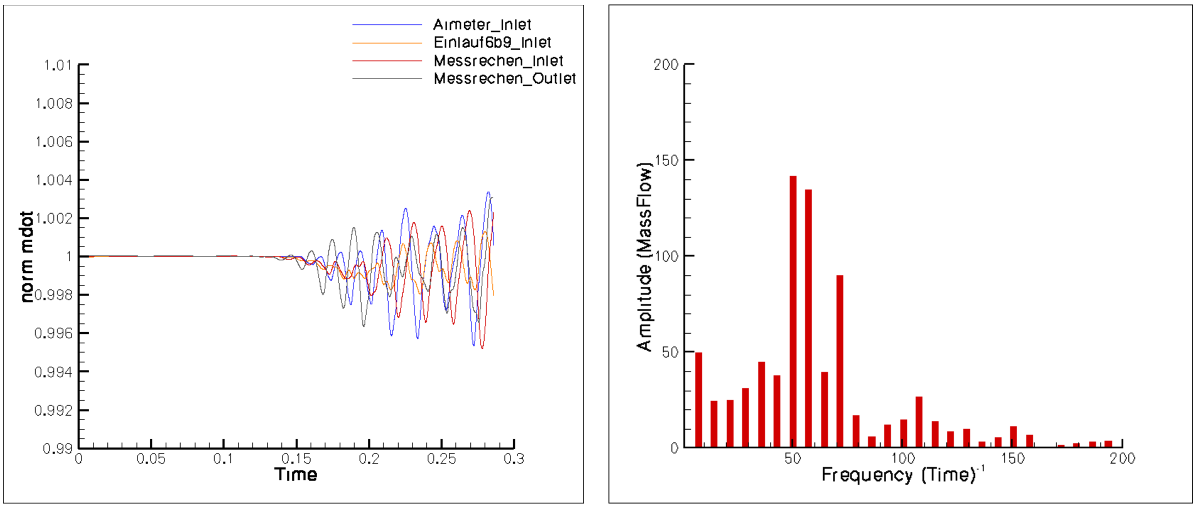

Figure 2: Unsteady mass flow fluctuations (l.) and the frequency spectrum of the signal (r.)

The unsteady character of the large flow separation close to the location of the smallest cross-section (denoted as "A" in Figure 1) dominates the mass flow and total pressure ratio fluctuations of the duct geometry. While the separation location remains almost unchanged, the AIP flow conditions, especially flow angles and local total pressure, exhibit a strong unsteady behavior due to the oscillation of the separation wake. The resulting frequencies are independent on a broad time step range but are sensitive to turbulence modelling and wall treatment.

As a conclusion, an uncertainty range for the numerical simulation results of the bent intake geometry can be estimated. This information is important for two reasons: First for an assessment of the expected loads during the experiment defining the strength of the duct structure as well as support structures, second, for the prediction of the produced flow distortion towards the jet engine to enable a save operation during the experiment.

References:

[1] Rademakers, R.P.M., Kächele T., and Niehuis, R., "Integration of a Highly Bent Engine Inlet in an Engine Test Facility", Proceedings of ISROMAC Symposium of Rotating Machinery, Honolulu, USA, ISAROMAC2016-112, 2016

[2] Wellborn, S.R. and Okiishi, T.H., "A Study of the Compressible Flow through a Diffusing S-Duct," NASA Technical Memorandum 106411, 1993

Mitteilung

Triebwerksintegration / Numerische Aerodynamik:

Numerical and Experimental Investigation of a Helicopter Engine Side Intake

Dipl.- Ing. Florian Knoth*, Prof. Dr. C. Breitsamter*

*Chair of Aerodynamics and Fluid Mechanics, TU München
Boltzmannstr. 15, 85748 Garching bei München
Tel.: +49 89 289 16439, Fax: +49 89 289 16139,
e-mail: florian.knoth@aer.mw.tum.de

Summary:

Engine installation plays an important role to guarantee fuel-efficient engine operation and decrease emissions. For this purpose, in the sub-project Green RotorCraft 2 within the Clean Sky JTI (Joint Technology Initiative) an aerodynamic optimization of novel engine air intakes was conducted at the example of a light twin-engine helicopter. As a part of GRC 2 in the ATHENAI project (Aerodynamic Testing of Helicopter Novel Air Intakes) wind tunnel (W/T) tests have been performed on a full-scale model of a helicopter fuselage section at the Institute of Aerodynamics and Fluid Mechanics of the Technische Universität München (TUM-AER), Fig.1.

In order to evaluate the aerodynamic performance of three engine side intake variants, the flow field characteristics in the AIP (Aerodynamic Interface Plane: directly upstream of the compressor inlet) are determined using a circumferentially adjustable 5-hole pressure probing system. For the evaluation a pressure drop coefficient, swirl angle and distortion parameter are investigated, Ref.[1]. A reduction of total pressure losses in the inflow region results in a raised thermal efficiency. Decreased swirl and total pressure distortion further improve the engine efficiency which leads to reduced fuel consumption and emissions. The total pressure distortion level and distribution in the AIP gives information about the change of the surge margin due to the intake flow [2].

For the wind tunnel model design several aspects have been taken into account. In order to fulfil local Mach and Reynolds numbers simultaneously, the wind tunnel model is designed in full scale. The fuselage is truncated to achieve a blockage of 7-8%. To ensure a flow field upstream of the intake comparable to in-flight conditions parts of the fuselage section are incorporated. Components with little influence on the intake flow field in level flight are not accounted for in the model. For the reproduction of engine mass flow rates suitable to in-flight operation, a system including a fan and a venturi meter are connected to the W/T model as depicted in Fig.1. Three baseline intake variants were tested in the first wind tunnel campaign of the project, Ref.[1]. The Baseline variant 1 (BSL 1), which is investigated further as part of this research, is developed as a static side intake configuration.

In addition to the experimental investigations, CFD simulations of the helicopter fuselage section including the ATHENAI BSL 1 intake with the use of ANSYS CFX have been carried out taking into account the complete inner structure of the engine air intake. The W/T nozzle, collector and test section geometry are modelled to reproduce the flow field around the fuselage section and intake parts in accordance with the experiments, Fig. 1. For the complete domain a structured meshing approach has been chosen using ICEM CFD. A high resolution discretization scheme in space and an implicit second order backward Euler scheme in time have been applied. The use of the k-ω SST turbulence model with a boundary layer resolution ($y+ < 1$) led to a good accordance of the measured AIP velocity distributions with the CFD results, see Fig. 3, Ref [3].

Further, numerical investigations are performed for the entire helicopter fuselage geometry including the side intake to assess the influence of a truncated fuselage section, i.e. the wind tunnel configuration, with respect to the entire fuselage geometry. As basis for this assessment the flow field on the truncated fuselage section is analyzed for the cases with and without wind tunnel test section geometry.

As reference data the experimental results of the first ATHENAI wind tunnel campaign are considered.

Acknowledgment:
The research leading to the experimental results have received funding from the European Commission's Framework Program 7 for the Clean Sky Joint Technology Initiative under grant agreement number 619819. The authors would like to thank the project partner Airbus Helicopters Deutschland GmbH for the support and the successful cooperation. Further thanks is given to ANSYS Inc. for providing the simulation software CFX / Fluent as well as to the Leibniz Rechenzentrum (LRZ) for computing time on SuperMUC.

Literature:

[1] Knoth, F. and Breitsamter, C., *Aerodynamic Analysis of Helicopter Side Intake Variants by Full Scale Wind Tunnel Measurements* in 41st European Rotorcraft Forum, Munich, 2015.

[2] AGARD, Working Group 13, *Air Intakes for High Speed Vehicles*, AR-270, 1991, pp. 8-10

[3] Knoth, F., Stuhlpfarrer, M. and Breitsamter, C, *Numerical and Experimental Investigation of Helicopter Engine Air Intakes*, in 64. Deutscher Luft- und Raumfahrtkongress 2015, Rostock, 2015.

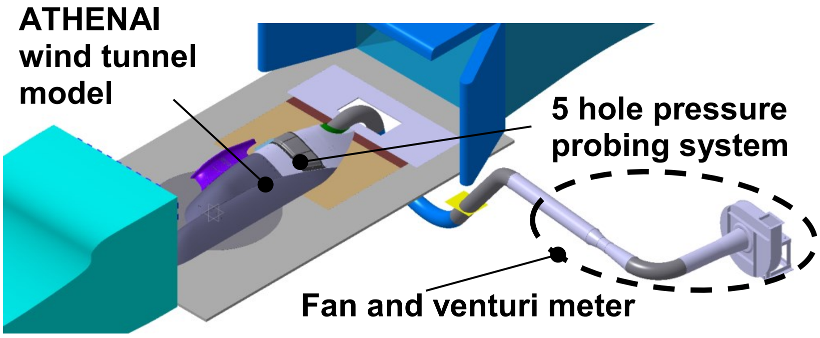

Fig. 1 Setup of the truncated ATHENAI W/T model [1].

Fig. 2 Baseline 1 intake geometry [1].

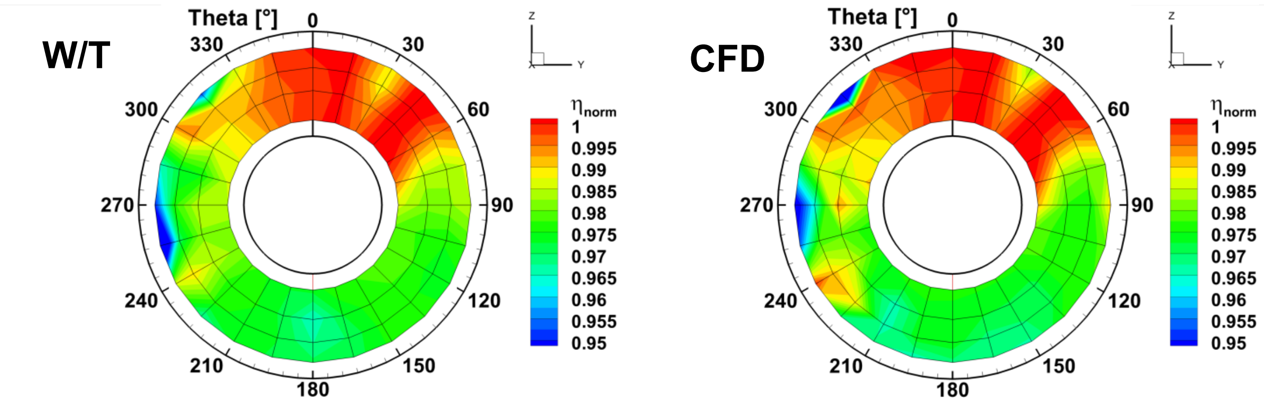

Fig. 3 Distribution of normalized total pressure ratio in the AIP for the truncated ATHENAI fuselage section wind tunnel experiment and CFD simulation [3].

Mitteilung

Projektgruppe / Fachkreis: Transportflugzeuge einschl. Triebwerksintegration

Simulations of Streamwise Vortices on a High-Lift Wing with UHBR-Engine

Tim Landa(1), Rolf Radespiel(1) and Sebastian Ritter(2)

(1) Institute of Fluid Mechanics, Technische Universität Braunschweig,
Hermann-Blenk-Str.37, 38108 Braunschweig, Germany, t.landa@web.de
(2) Institute of Aerodynamics and Flow Technology, DLR Braunschweig,
Lilienthalplatz 7, 38108 Braunschweig, Germany

Abstract

In the flow field around modern aircraft in high-lift configuration, streamwise vortices occur at various positions on the wing. One of these positions is the region downstream of an engine, which is integrated under the wing. The pylon of the engine is in a geometric conflict with the slat. To avoid this conflict, for realistic aircraft the slat is intercepted in spanwise direction. At this slat cut-out different vortices arise. In addition, another vortex develops at the nacelle, and this is advected downstream over the suction side of the wing. The resulting system of streamwise vortices strongly influences the flow in this region, which in general leads to a loss of maximum lift. One possibility to reduce these losses is to create a particular vortex by a nacelle strake that in turn positively influences the flowfield [1, 2].

Against this background, numerical simulations have been performed to study the prediction of streamwise vortix effects on high-lift. The simulations have been performed with the DLR TAU-Code with two turbulence models of different type. As an eddy-viscosity model, the Menter-SST turbulence model has been applied. This model is numerically rather robust and thus, it has been used to create a fundamental understanding of the flow around this geometry. Nevertheless, the ability of this model to accurately simulate vortices is limited. To obtain improved predictions of the behavior of the vortex system, the JHh-v2 turbulence model has been applied, which belongs to the class of Reynolds-Stress models [3].

Recently, the authors presented results of simulations on a simplified high-lift configuration without engine [4, 5]. This configuration has a slat outboard, which is cut off instead of an intercepted slat along the whole span. At this configuration, a vortex system with reduced complexity occurs. Thus, a deeper insight into the flow physics and knowledge about the numerical settings and the influence of the computational grid on the prediction of the vortices was achieved.

Within the present contribution, a more complex configuration with an intercepted slat and an UHBR-engine is investigated based on the findings obtained from the simplified configuration. With both turbulence models simulations at different angles of attack have been performed to characterize the dependency of the vortex behavior on the incidence. In particular the effect on stall behavior of the high-lift wing is of great interest.

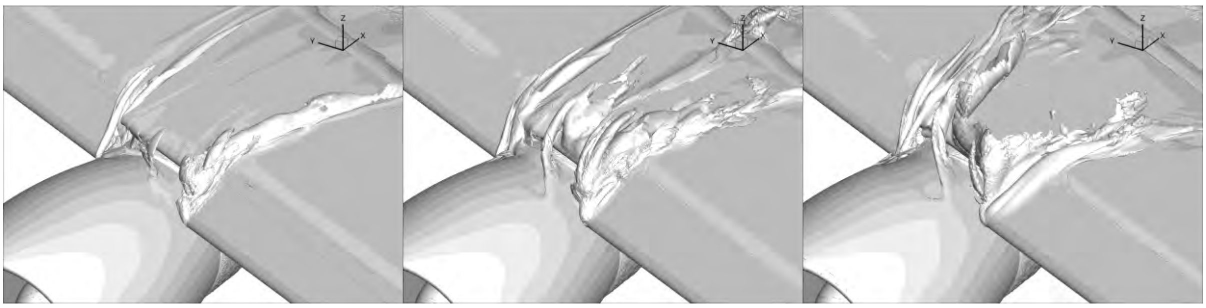

Figure 1: Visualization of the vortex system (Iso-Surfaces of vorticity) at α=6° (left), α=10° (middle) and α=14° (right), Menter-SST turbulence model, Re=15.687×10^6

Exemplarily, figure 1 shows the visualization of the vortex system at the position of the integrated UHBR-engine, as simulated with the Menter-SST turbulence model. It appears, that different vortex systems occur. Two vortices arise at the outboard edge of the slat and at the corresponding step of the clean nose. Another vortex develops on the upper side of the engine from the flow around the nacelle, proceeding on the suction side of the wing. Furthermore, a system of vortices comes from the inboard interception of the slat. The strength, the appearance and the behavior strongly depend on the incidence, which will be discussed in detail in the final paper.

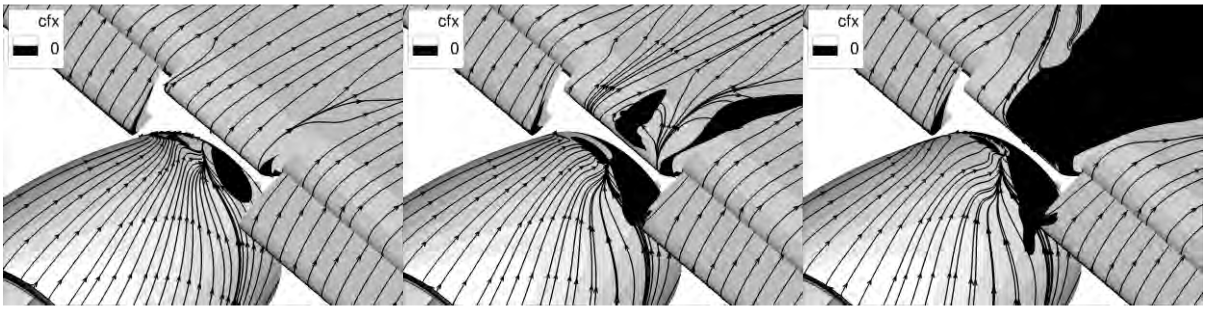

Figure 2: Streamtraces and regions of separated flow close to the UHBR-engine simulated with the Menter-SST turbulence model at α=6° (left), α=10° (middle) and α=14° (right), Re=15.687×10^6

Figure 2 exhibits streamtraces and regions of separated flow close to the UHBR engine. At low angles of attack (α=6°), the flow on the wing is completely attached. At moderate incidences (α=10°), local regions of separated flow occur downstream of the engine and at the inboard slat interception. With increasing incidence, these regions of separated flow grow. At an angle of attack of α=14°, both regions have growninto a large, single flow separation. As a result, the flow on the wing downstream of the engine is detached.
The final paper will also display and analyze simulations with the JHh-v2 Reynolds-Stress model. Differences regarding the prediction of the vortices and the mechanism of stall will be discussed and evaluated. Of particular interest will be signs of vortex burst and resulting unsteadyness of flow fields.

References

[1] Frhr. v. Geyr, H., Schade, N., v. d. Burg, J. W., Eliasson, P. and Esquieu, S., CFD Prediction of Maximum Lift Effects on Realistic High-Lift-Commercial Aircraft-Configurations within the European project EUROLIFT II, AIAA 2007-4299, Miami, 2007.

[2] Bier, N., Rohlmann, D. and Rudnik, R., Numerical Maximum Lift Prediction of a Realistic Commercial Aircraft in Landing Configuration, AIAA 2012-0279, Nashville, 2012.

[3] Cécora, R.-D., Radespiel, R., Eisfeld, B. and Probst, A., Differential Reynolds-Stress Modeling for Aeronautics, Journal of Aircraft, Vol. 53, No. 3, pp. 739-755, 2015.

[4] Landa, T., Wild, J. and Radespiel, R., Numerical Simulations of Streamwise Vortices on a High-Lift Wing, Deutscher Luft- und Raumfahrtkongress, 22.-24. September 2015, Rostock, 2015.

[5] Landa, T., Radespiel, R. and Wild, J., Numerical Simulations of Streamwise Vortices on a Generic High-Lift Configuration, AIAA 2016-0304, AIAA SciTech 2016, 04.-08. January 2016, San Diego, 2016.

Mitteilung

Projektgruppe / Fachkreis: SFB880

Aerodynamic Assessment of Pylon-Mounted Over-the-Wing Engine Installations on a STOL Commercial Aircraft Concept

Luciana Savoni, Ralf Rudnik
DLR, Deutsches Zentrum für Luft- und Raumfahrt
Institut of Aerodynamics and Flow Technology, Department of Transport Aircrafts
Lilienthalplatz 7, 38108, Braunschweig
luciana.savoni@dlr.de, ralf.rudnik@dlr.de

Introduction

Low noise emissions, low fuel consumption and subsequently low pollution are some of the most compelling requirements of an aviation technology which is striving to become every day more "environmental friendly". These requirements can, however, be in net contrast with the growing need of increasing the number of passengers and flights. As shown in [1], the worldwide passenger traffic, measured in Revenue Passenger Kilometers (RPK), is expected to double in the next fifteen years and it will grow by 145% to 15.2 trillion RPKs by 2034. In this scenario, it is quite appealing to make operational those airports which are at present not accessible due to their limited size or because of their proximity to residential areas. The Collaborative Research Center (Sonderforschungsbereich) SFB880 aims to address this need with short take-off and landing (STOL) vehicles with a capacity of 100 passengers that feature low noise emission characteristics. As determined in [2], the capability of taking-off and landing on 800 m runway would double the possible point-to-point connections with respect to the current situation. Figure 1 depicts one of two reference configurations of the SFB880 [3]. The so-called REF3 configuration is characterized by a low wing allowing the installation of a UHBR turbofan over the wing aft of the trailing edge. This design has proven to offer a potential for an efficient aerodynamic engine installation, a significant noise reduction potential and a decrease of FOD risk during ground operations [4]. Neverthless, the engine installation presents many challenges, especially to manage the interference drag at transonic conditions. Combining this with STOL capabilities has not yet been attempted.

Figure 1: REF3 configuration for SFB880 with Over the Wing Mounted Engines

The present study aims to provide results of a first investigation of the effects of the installation of an UHBR turbofan engine over the wing, in terms of wing and nacelle interference drag in the transonic regime and lift drop. The engine will firstly be considered in the reference position and subsequently a variation of the vertical position of the engine will be analysed.

Description of the geometry and of the numerical approach

To the aim of evaluating the aerodynamic performance of an OWM engine aircraft, the REF3 wing/body/engine (WBE) configuration has been studied and compared to the wing/body (WB) configuration. To be able to separate aerodynamic installation effects, the pylon is omitted in this phase of the studies and it will be considered later. The engine is mounted aft of the wing trailing edge, since this proved to be beneficial for drag reduction in previous studies [4]. The reference position used for the preliminary analysis is the one prescribed in [3].

The CFD simulations have been carried out with the DLR TAU-Code using a 3D RANS approach, with a *Central* main discretization scheme using the 80% of matrix dissipation and Backward-Euler time integration scheme. The turbulence model is Spalart-Allmaras in the so-called negative formulation.
The computational grid has been generated with the CENTAUR grid generation package. 9,000,000 grid points are used for the WB configuration and around 14,000,000 nodes for the WBE. The study is carried out for cruise conditions corresponding to M=0.78, CL=0.46 and an altitude of 11277 m.

Preliminary results

The analyzed test case corresponds to start of cruise, with both engines operative and a Mach number equal to 0.78. Furthermore, off-design conditions with Mach numbers between 0.70 and 0.82 will be computed to examine in detail transonic flow phenomena and the interaction of the engine with the upper wing shock as this represents the key for a potential aerodynamically superior engine integration compared to conventional configurations [4]. Figure 3 depicts the surface grid of the configuration with engine. Figure 4 shows isobars on the upper surface of the WB configuration indicating the extent of the supersonic areas and the shock location.

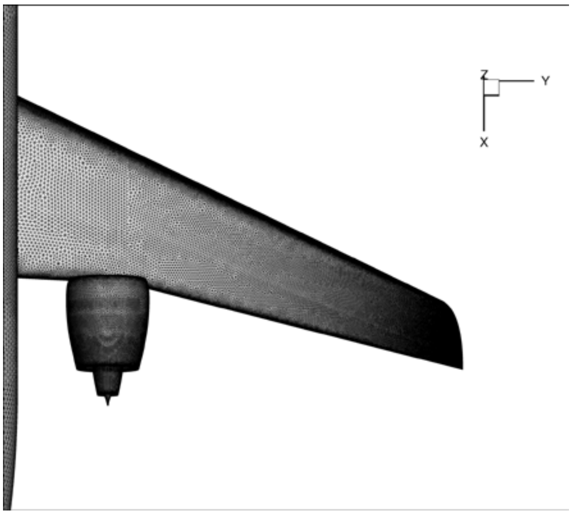

Figure 3 Detail of WBE grid

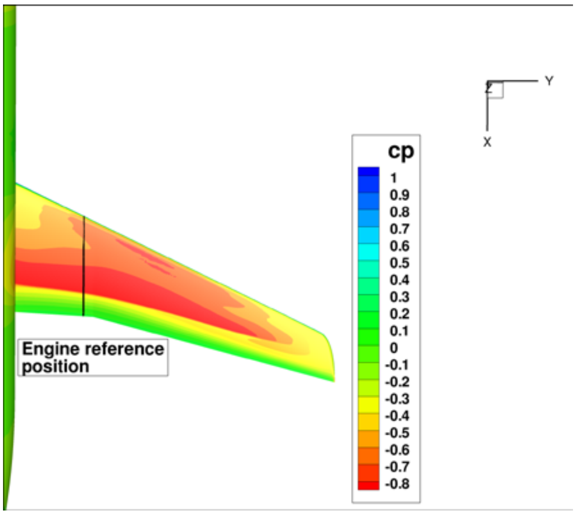

Figure 4 WB surface isobars

Outlook

The final paper will provide a study of aerodynamic interference effects of over-the-wing-mounted engine aircraft concepts for different engine position and thrust settings. The wing/body configuration will serve as a reference. Special attention will be devoted to the mutual interference of the engine inlet streamtube and the supersonic flowfield of the wing. A complementary study, dealing with the same baseline configuration and an embedded turbofan engine, will be proposed by the Institute of Jet Propulsion and Turbomachinery (IFAS) of the Technical University of Braunschweig.

Bibliography

[1] "Flying by numbers", Global Market Forecast 2015-2034, Airbus S.A.S., Blagnac, France, 2015, p. 9.
[2] "Aerodynamic Installation Effects of an Over-the-wing Propeller on a High-Lift Configuration", L. Müller, W. Heinze, D. Kozulovic, M. Hepperle, R. Radespiel, Journal of Aircraft, Vol. 51, No. 1, January-February 2014, p. 249.
[3] "Main Data Sheet. A/C Type: SFB880 Reference Aircraft REF3-2015", June 2015, W. Heinze, T. Weiss.
[4] "Over Wing Nacelle Installations for Improved Energy Efficiency", J.R. Hooker, A. Wick, C. Zeune, A. Agelastos, 31st AIAA Applied Aerodynamics Conference, June 24-27 2013, San Diego, CA.

Mitteilung

Projektgruppe / Fachkreis: Transportflugzeuge einschl. Triebwerksintegration

Instationäre Simulation des abgelösten Nachlaufs eines Verkehrsflugzeuges mittels Detached Eddy Simulation

A. Waldmann, T. Lutz, E. Krämer
Institut für Aerodynamik und Gasdynamik, Universität Stuttgart
Pfaffenwaldring 21, 70569 Stuttgart
waldmann@iag.uni-stuttgart.de

Einführung

Im Rahmen von in den vergangenen Jahren innerhalb der Arbeitsgruppe Luftfahrzeugaerodynamik des IAG durchgeführten Arbeiten [1,2,3] wurden Möglichkeiten erarbeitet, mittels hochaufgelöster instationärer Simulationen das Verständnis für massiv abgelöste Nachlaufströmungen an Verkehrsflugzeugen zu stärken. Dabei wurden sowohl instationäre RANS-Verfahren als auch hybride RANS/LES-Ansätze verfolgt, die jeweils im Rahmen ihrer Anwendbarkeit zu zuverlässigen Ergebnissen führten. Die Erkenntnisse dieser Vorarbeiten sollen durch Variation der räumlichen und zeitlichen Auflösung der numerischen Simulationen vertieft werden.

Vorgehen

Das NASA Common Research Model (CRM) [4] ist eine Verkehrsflugzeugkonfiguration, die speziell zum Zwecke der Validierung von CFD-Daten entworfen und publiziert wurde. Dabei ist das CRM eine generische Repräsentation eines modernen für transsonische Machzahlen konzipierten Großraumflugzeuges. Die Verfügbarkeit der Geometrie und die weitreichende Verwendung des CRM haben zu einer großen Anzahl von Veröffentlichungen geführt, die sich mit verschiedensten Aspekten der Luftfahrzeugforschung beschäftigen.

In [1] und [2] wurden mit dem Strömungslöser TAU durchgeführte instationäre Simulationen des CRM bei hohen Anstellwinkeln sowie hohen Reynoldszahlen im subsonischen Bereich beschrieben. In diesem Rahmen wurde auch eine teilweise Vailidierung dieser Rechnungen durchgeführt, wobei eine gute Übereinstimmung mit den im Windkanal ETW ermittelten Daten festgestellt wurde. Gleichzeitig wurde aufgezeigt, in welchen Bereichen noch Unzulänglichkeiten existieren. So gibt es Verbesserungsbedarf in Bezug auf Wiedergabe der Nachlaufdelle im zeitlichen Mittel sowie des Oberflächendruckes. Mittels einer Variation von numerischen Parametern wie der zeitlichen und räumlichen Auflösung soll in der vorliegenden Arbeit erörtert werden, inwiefern diese Einstellungen die Simulationsergebnisse beeinflussen. Dabei werden wiederum die in [1] beschrieben experimentellen Datensätze zum Vergleich herangezogen.

Neben der Validierung mittels Messdaten wird der Einfluss der Auflösung auf die Strömungsphänomene in der Flügel- und Nachlaufströmung untersucht. Ein Beispiel hierfür ist die Ablösung, die beim betrachteten Anstellwinkel unmittelbar hinter der Flügelvorderkante stattfindet. So konnte beispielsweise beobachtet werden, dass das Verhalten der Strömung in diesem Bereich von der zeitlichen Auflösung abhängt, s. Abb. 1.

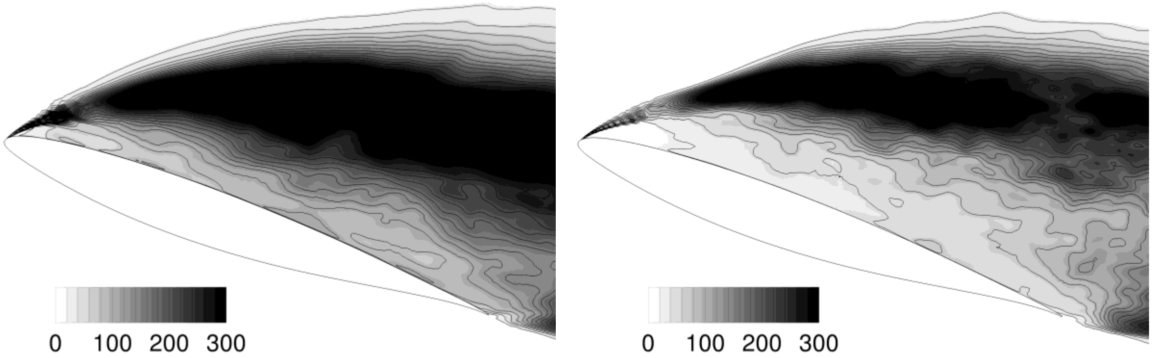

Abbildung 1: Aufgelöste Reynoldsspannungskomponente uu in Anströmrichtung am Flügel des CRM. Physikalischer Zeitschritt entsprechend $0.01t_{conv}$ (links) und $0.005\ t_{conv}$ (rechts).

Da davon ausgegangen werden kann, dass die Ablösung und darauf folgende Ausbildung der turbulenten Strukturen eine wichtige Rolle für das Verhalten des Nachlaufes spielen, werden diese Zusammenhänge detailliert beleuchtet. Die Auswirkungen der räumlichen und zeitlichen Auflösung werden anhand der Druckfluktuationen an den Flügeloberflächen sowie anhand der Entwicklung der turbulenten Fluktuationen im Nachlauf verglichen. Neben der Betrachtung der Statistiken wie beispielsweise der in Abb. 1 gezeigen Reynoldsspannungen liefern spektrale Analysen weitere Informationen über die turbulenten Fluktuationen. Die so durchgeführten Vergleiche sollen Aussagen über Auflösungsanforderungen ermöglichen und so Anhaltspunkte für zukünftige Studien dieser Art liefern.

Referenzen :

[1] Lutz, T.; Gansel, P. P.; Waldmann, A.; Zimmermann, D.-M.; Schulte am Hülse, S A.: “Prediction and Measurement of the Common Research Model Wake at Stall Conditions”, AIAA Journal of Aircraft, Vol. 53, No. 2, DOI 10.2514/1.C033351, 2016.

[2] Waldmann, A., Gansel, P.P., Lutz, T., Krämer, E.: “Unsteady Wake of the NASA Common Research Model in Low-Speed Stall”, accepted for publication in AIAA Journal of Aircraft, DOI 10.2514/1.C033413, 2015.

[3] Zimmermann, D.-M., Waldmann, A., Lutz, T., Krämer, E.: Development of Flow Structures in the Near-Field Wake Region of the Common Research Model. 5^{th} CEAS Air & Space Conference, Delft, Netherlands (2015).

[4] Vassberg, J.C., DeHaan, M.A., Rivers, S.M.B., Wahls, R.A.: “Development of a Common Re-search Model for Applied CFD Validation Studies,” AIAA 2008-6919, 2008.

Mitteilung

Projektgruppe/Fachkreis: Turbulenz

Revisiting the Higher-order Statistical Moments in Turbulent Pipe Flow using Direct Numerical Simulations

Christian Bauer, Daniel Feldmann & Claus Wagner
Institut für Aerodynamik und Strömungstechnik, DLR, Bunsenstr. 10, 37073 Göttingen
christian.bauer@dlr.de

Outline: Statistical moments of fully developed turbulent pipe flows have been investigated by means of direct numerical simulations (DNS), such as Wagner et al. (2001). While the latter study was restricted to pipe lengths of $L = 5D$, experimental investigations revealed the need for larger domains in order to capture so-called very large-scale motions (VLSM), which are known to appear in wall-bounded turbulence (Kim and Adrian, 1999). According to Monty et al. (2009) and others, VLSM contribute to Reynolds stresses but their influence on even higher statistical moments, such as skewness and kurtosis has not been rigorously studied yet. Furthermore, the origin of high kurtosis levels of wall-normal velocity fluctuations in the very vicinity of the wall was found to be caused by very strong events (velocity spikes) that are rare both in time and in space (Xu et al., 1996). Due to their large normal velocities they are difficult to observe within experiments, which is, according to the author of the latter study, the reason why such high kurtosis levels have not been measured in experiments yet. In order to resolve both high gradients near the wall and VLSM, a DNS requires a fine near-wall grid resolution as well as a large flow domain. Besides the computational requirements the convergence of higher statistical moments is yet to be studied, since they correspond to rare events, as stated above. The aim of the current study is to revise statistical moments in turbulent pipe flows, such as turbulent intensities, skewness and flatness factors in large domains with high near-wall grid resolutions. The influence of outer flow motions, which penetrate into the buffer layer on turbulent statistics shall be revealed and scaling laws for higher statistical moments are to be found.

Numerical Methodology: In order to elucidate the effect of VLSM on higher statistical moments a DNS based on the incompressible Navier-Stokes equation is carried out within a domain of $L = 21D$, where D is the pipe diameter. The governing equations

$$\frac{\partial \boldsymbol{u}}{\partial t} + \boldsymbol{u} \cdot \nabla \boldsymbol{u} + \nabla p = \frac{1}{Re_\tau} \nabla^2 \boldsymbol{u} \tag{1}$$

$$\nabla \cdot \boldsymbol{u} = 0, \tag{2}$$

where $Re_\tau = u_\tau D/\nu$ is the friction Reynolds number, based on friction velocity, pipe diameter and kinematic viscosity, are integrated in time using a Leapfrog-Euler scheme, after being discretized by means of a fourth-order finite volume method (Shishkina and Wagner, 2007). The scheme is based on the projection method of Chorin (1968) and consists of three basic steps. First, an auxiliary velocity field is computed from the momentum equation (2) neglecting the pressure term. Then a Poisson equation is solved in order to fulfil the divergence free condition, before the actual velocity and pressure fields are updated from the auxiliary field and the solution of the Poisson equation. Due to the flow geometry, an explicit time integration scheme would require very small time steps (Δt) in the vicinity of the cylindrical axis in order to fulfil stability conditions. To overcome this problem, a semi-implicit scheme, as proposed by Kim and Moin (1985), is applied in the region of interest, where flow variables are treated implicitly with respect to the azimuthal direction. Furthermore, a second semi-implicit region will be introduced in the vicinity of the pipe wall with respect to the radial direction, to make small grid resolutions affordable. Based on a coarse grid simulation a convergence criteria for higher statistical moments will be stated and a finer grid simulation will be integrated in time until turbulent statistics reach a fully converged state. Table 1 shows the current simulation setups used within this study, which are settled in the low Reynolds number regime. The grid resolution in wall units satisfies commonly accepted values of $\Delta z^+ < 5$, $R^+\Delta\varphi < 5$ and $\Delta r^+_{max} < 5$. The wall-normal grid spacing at the wall was chosen to be somewhat smaller than comparable studies ($\Delta r^+_{min} = 0.11$). Besides the mentioned ones, higher Reynolds number cases will be set up to determine scaling laws of higher statistical moments.

case	Re_τ	L	$N_z \times N_\varphi \times Nr$	Δz^+	$R^+\Delta\varphi$	Δr^+_{min}	Δr^+_{max}
PIPE360CO	360	$21D$	$1536 \times 256 \times 84$	4.9	4.4	0.31	4.4
PIPE360FI	360	$21D$	$1536 \times 256 \times 104$	4.9	4.4	0.11	4.4

Table 1: Turbulent pipe flow simulation cases

Results and Outlook: Figure 1 shows isocontours of wall-normal velocity fluctuations within an instantaneous flow field realization from turbulent pipe flow DNS. A highly energetic velocity spike can be found in the vicinity of the wall near the dashed line. Such motions contribute to the high wall-normal kurtosis level as shown in figure 2 (b). Cases involving finer grid resolutions and higher Reynolds numbers will be carried out until the symposium, which gives us the possibility to perform convergence studies and investigate the impact of outer flow motions on the higher-order statistics.

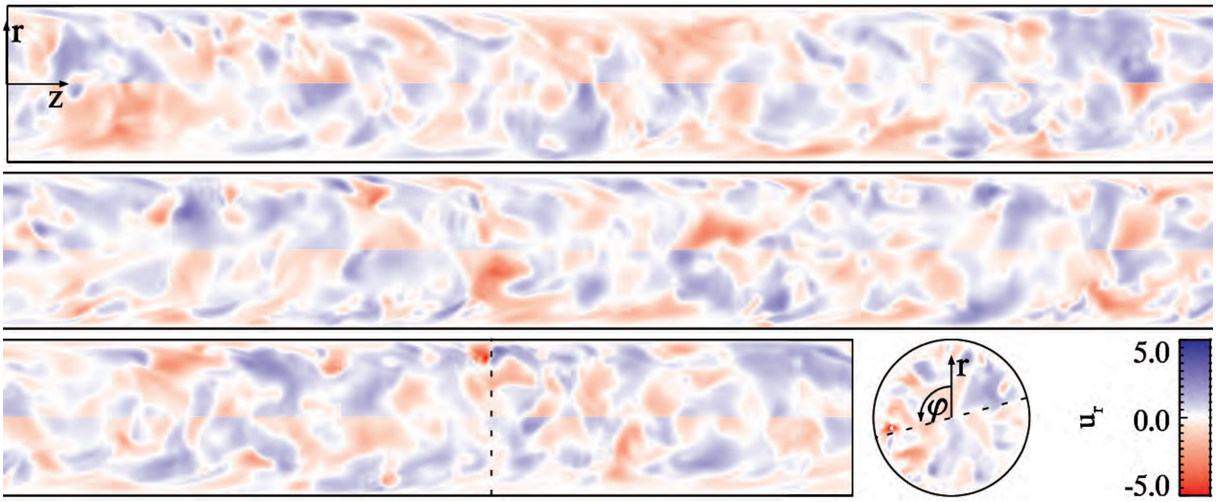

Figure 1: Isocontours of instantaneous wall normal velocity fluctuations u_r' in the rz-plane in fully developed turbulent pipe flow *PIPE*360*CO*, Re_τ = 360.

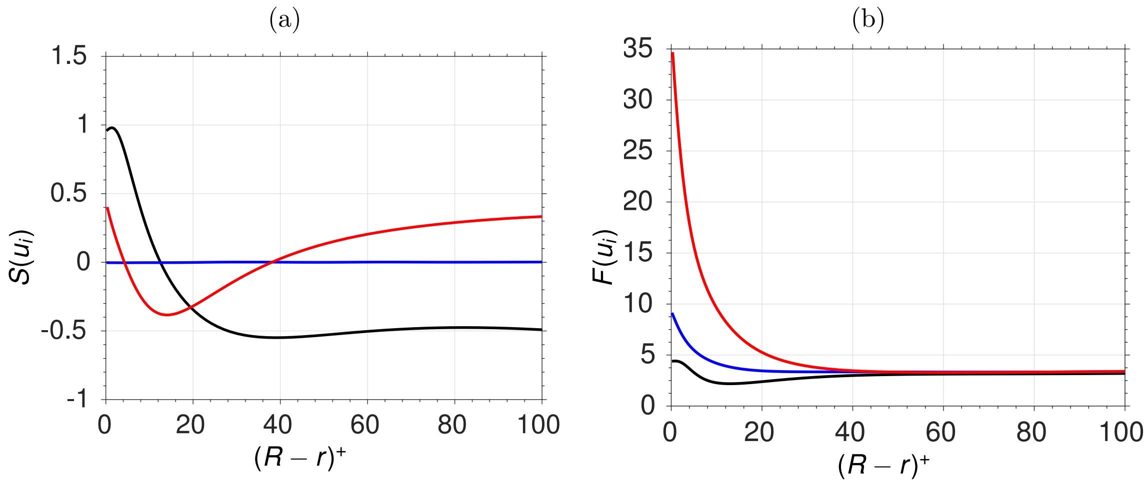

Figure 2: Skewness (a) and flatness (b) profiles from turbulent pipe DNS *PIPE*360*CO* in wall units with focus on the near-wall region and R the pipe radius. (a): —, $S(u_z)$; —, $S(u_r)$; —, $S(u_\varphi)$. (b): —, $F(u_z)$; —, $F(u_r)$; —, $F(u_\varphi)$.

References:

Chorin, A. J. (1968). Numerical solution of the Navier-Stokes equations. *Mathematics of Computation*, 22:745–762.

Kim, J. and Moin, P. (1985). Application of a fractional-step method to incompressible Navier-Stokes equations. *Journal of Computational Physics*, 59(2):308–323.

Kim, K. C. and Adrian, R. J. (1999). Very large-scale motion in the outer layer. *Physics of Fluids*, 11(2):417.

Monty, J. P., Hutchins, N., Ng, H. C. H., Marusic, I., and Chong, M. S. (2009). A comparison of turbulent pipe, channel and boundary layer flows. *Journal of Fluid Mechanics*, 632:431–442.

Shishkina, O. and Wagner, C. (2007). A fourth order finite volume scheme for turbulent flow simulations in cylindrical domains. *Computers & Fluids*, 36(2):484–497.

Wagner, C., Hüttl, T. J., and Friedrich, R. (2001). Low-Reynolds-number effects derived from direct numerical simulations of turbulent pipe flow. *Computers & Fluids*, 30:581–590.

Xu, C., Zhang, Z., den Toonder, J. M. J., and Nieuwstadt, F. T. M. (1996). Origin of high kurtosis levels in the viscous sublayer. Direct numerical simulation and experiment. *Physics of Fluids*, 8(May 2015):1938.

Mitteilung

Projektgruppe/Fachkreis: Numerische Simulation

Ansprechpartner: Tobias Knopp

Institution: DLR – Institute of Aerodynamics and Flow Technology (AS)
C²A²S²E Center for Computer Applications in AeroSpace Science and Engineering (CAS)

Adresse: Bunsenstr. 10
37073 Göttingen
Telefon: 0551 7092451
E-Mail: Tobias.Knopp@dlr.de

Weitere Partner: Daniel Schanz, Matteo Novara, Andreas Schröder, DLR-AS EXV, Bunsenstr. 10, 37073 Göttingen
Erich Schülein, DLR-AS HGK, Bunsenstr. 10, 37073 Göttingen
Nico Reuther, Christian Kähler, Institute for Fluid Mechanics and Aerodynamics, Universität der Bundeswehr (UniBw) München, 85577 Neubiberg

Thema: A new experiment of a turbulent boundary layer flow at adverse pressure gradient for validation and improvement of RANS turbulence models

The prediction of pressure induced separation of a turbulent boundary layer (TBL) in the low-speed regime using RANS-based CFD is still associated with significant uncertainties. Well-defined and documented validation test cases at an adverse pressure gradient (APG) and at Reynolds numbers relevant for aircraft flows are rare in the literature. Therefore, a new boundary layer experiment was designed. The design includes the lessons learned from a previous experiment which was performed within the DLR internal project RETTINA, see [2]. The aim is to ensure well-defined flow conditions and to reach higher values of the Reynolds number by increasing the flow velocity up to 36m/s, yielding Re_θ=64000 in the APG region. The measurements were performed in the Atmospheric Windtunnel (AWM) at the UniBw in München. The work was funded by DFG. Highly resolved data for the Reynolds stresses were obtained using the 3D PTV STB approach. The wall shear stress was determined directly using oil film interferometry and from the mean velocity profiles in the viscous sublayer obtained using the 2D μPTV technique.

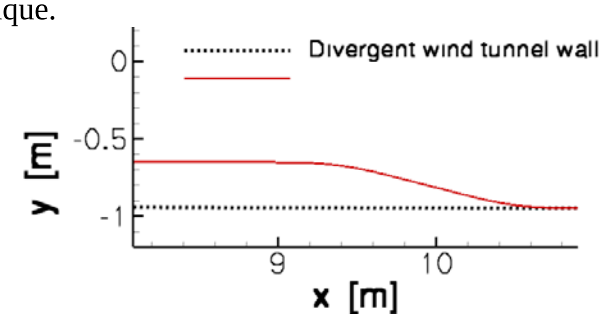

Fig. 1 – Left: Geometry of the experiment mounted to the wind tunnel wall in the AWM.

The first step for RANS modelling at APG is to derive a new wall-law for the mean velocity in the inner 15% of the boundary layer. This wall-law is based on a log-law formulation in the inner part and a square-root-law (sqrt-law) formulation in the outer part [1]. We present an empirical blending correlation based on the pressure gradient parameter in inner scaling Δp_x^+. For $\Delta p_x^+ \rightarrow 0$, the log-law is recovered for the entire inner layer. The value of the slope parameter (κ in the log-law at zero pressure gradient) is a function of Δp_x^+ and is decreasing with increasing values of Δp_x^+. Then we derive a composite formula for the turbulent viscosity ν_t. From the profiles for the mean velocity and for ν_t in the log-law region and in the square-root-law region at APG, we derive the solutions for the turbulence quantities k and ω in both regions.

In the second step, we study the boundary-layer equations for k and ω in the log-law region and in the sqrt-law region at APG. The ω-equation is consistent with the derived solution at APG in the log-layer, but needs to be modified in the sqrt-law region.

In the third step we consider state-of-the-art eddy-viscosity based models (SA, k-ω SST) and differential Reynolds stress models (DRSM), i.e., the SSG/LRR-ω model and different versions of the JHh-model. In the sqrt-law region, the mean velocity profiles predicted by the SST model and the SSG/LLR-ω model show a different behaviour than the JH-type models. This can be explained by the inexact transformation of the ε-equation to the ω-equation used in the SST model and in the SSGLRR-ω model. We use the exact ω-equation given in [4]. Then we modifiy the SSG/LRR-ω model by combining the exact ω-equation with the sensitivity terms at APG developed for the SST model in [1]. The resulting model gives good agreement for the mean velocity profiles with the experimental data, see. Fig. 2, both in dimensional units and in viscous units.

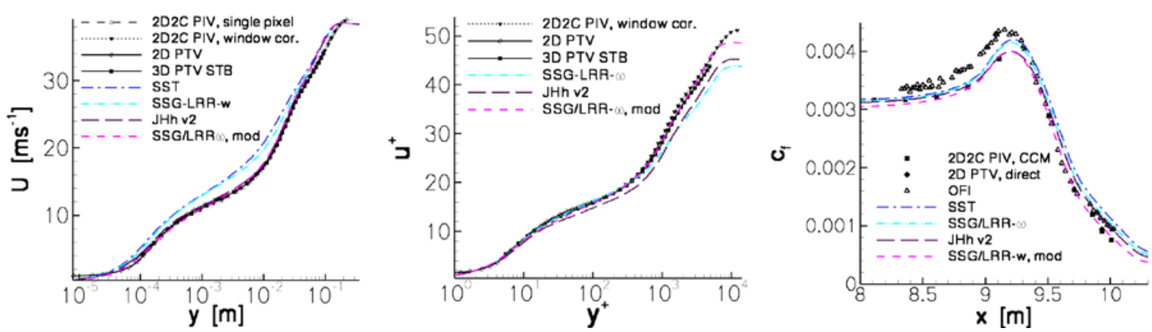

Fig. 2 – Mean velocity in the APG region at U_∞=36m/s in dimensional units (left), in inner viscous units (center) and surface distribution for the skin-friction c_f including the OFI data (right).

Literatur:

[1] Knopp, T.: „A new wall-law for adverse pressure gradient flows and modification of k-ω type turbulence models". AIAA 2016-0588.

[2] Knopp, T. et al.: „Investigation of scaling laws in a turbulent boundary layer flow with adverse pressure gradient using PIV". J. Turbulence, 16:250-272, 2015.

[3] Reuther et al.: „Experimental investigation of adverse pressure gradient boundary layers by means of large-scale PIV". Proc. PIV15, Santa Barbara, USA, 2015.

[4] Wilcox, D.C.: „Turbulence Modeling for CFD". DCW Industries, 2nd ed., 1998.

Datum: 10.06.2016 **STAB**

Mitteilung

Fachkreis: Turbulenzforschung

Der turbulente Weg zum Gleichgewicht

Ulrich Nehring*, Keith Weinman, Anthony Gardner. DLR-Göttingen,
Institut fürAerodynamik u. Strömungstechnik (*ehemals, email: unehring@t-online.de)

Ausgangspunkte

In dem STAB-Workshop 2015 wurde das anliegende Gleichungssystem vorgeschlagen, das auf der Grundlage elementarer Erhaltungssätze Welle- und Teilcheneigenschaften von Fluidelementen korreliert. Als raum-zeit-abhängige Variable kommen dabei, wie in der molekularen Theorie, die vektoriellen Größen Translation $\vec{\boldsymbol{v}}$,Vibration $\vec{\boldsymbol{e}}$ und Rotation $\widehat{\boldsymbol{b}}$ in Betracht, sowie die skalare Gesamtenergie $\boldsymbol{\phi}$ eines Systems. Die Skaleninvarianz dieses Ansatzes bedeutet dass die irreversible Entwicklung eines Strömungsfeldes von Mittelwerten, also makroskopisch, bestimmt wird. Empirisch begründete statistische Annahmen werden zunächst nicht benutzt. Das ist möglich, weil sich im Gleichgewicht (stabil oder instabil) unterschwellige positive und negative Vibrationen und Rotationen zu null kompensieren, sodass in geschlossenem Raum allein die energetische Anfangsverteilung maßgeblich ist. Das umgebende Feld beeinflusst so das Fluidelement, das seinerseits dank der Integralsätze von Gauß und Stokes auf die Umgebungrückwirkt. Die Welleneigenschaft dieses Modells folgt aus einer Analogie zu den Maxwell-Gleichungen für elektrische und magnetische Felder.

$$\frac{D\vec{v}}{Dt} + grad\phi = \frac{1}{Re_v}\Delta\vec{v} + \vec{e}$$

$$\frac{D\phi}{Dt} + \phi div\vec{v} = \frac{1}{Re_\phi}\Delta\phi$$

$$\frac{\partial\vec{e}}{\partial t} - rot\hat{b} = \frac{1}{Re_e}\Delta\vec{v}$$

$$\frac{\partial\hat{b}}{\partial t} + rot\vec{e} = 0$$

Ein Welle-Teilchen-Dualismus

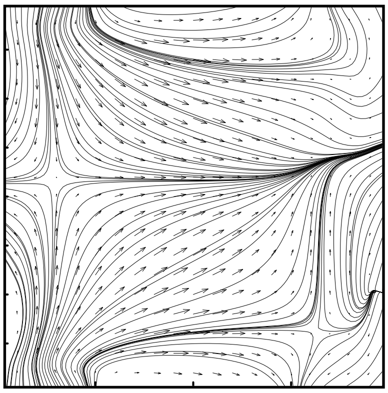

Abb.1 $\vec{v}$-Feld

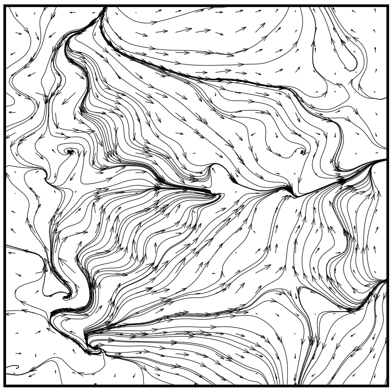

Abb.2 $\vec{v}$-Feld + $\vec{e}$, $\hat{b}$

Ausgehend von einer anisotropen energetischen Anfangsstörung entwickelt sich das Strömungsfeld in einer Simulation (Kubus) unterschiedlich, je nachdem ob Mittelwerte (verborgener) unterschwelliger $\vec{e}$ und $\hat{b}$ Fluktuationen berücksichtigt werden oder nicht. ***Abb.1*** zeigt Geschwindigkeitenohne „unelastische“ Reibungsarbeit, während andernfalls Wellen und Verwirbelungen auftreten (***Abb.2***). Ein derartiger Prozess verläuft irreversibel und führt schließlich zu einem chaotischen Gleichgewicht.

Abb.3/4zeigenden Verfall anfänglicher Information - Vibrationen und Rotationen betreffend. Die Vektoren bilden die jeweiligen lokalen Größen ab, zusammengefasst als Linien zur besseren Anschauung.

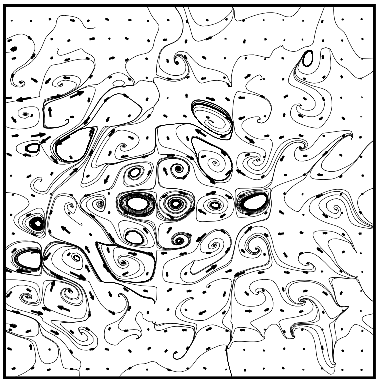

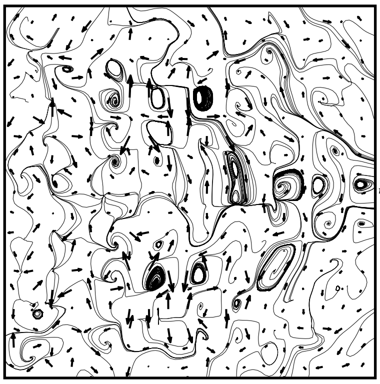

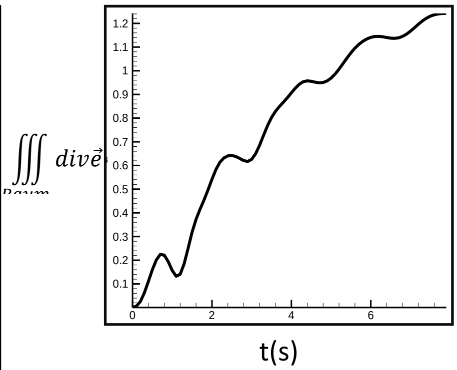

Abb.3Vibrationen$\overrightarrow{e}$, t> t_0 Abb.4 Rotationen$\hat{b}$, t> t_0Abb.5Fluktuationen (t)

Auf dem Weg zum Gleichgewicht ist die zeitliche Entwicklung der Divergenz der Vibrationen $\vec{e}$ pro Raumgebiet (Abb.5) maßgeblich. Verglichen mit logarithmischen Kurven einer Entropiezunahme zeigen sich allerdings Stufen einer negativen Entwicklung, die fern vom Gleichgewicht stärker sind als in Gleichgewichtsnähe. Dies könnte als Austauschzwischen äußerer und innerer Entropieproduktion interpretiert werden, konkret als Wechselwirkung zwischen Vibration und Rotationbzw.als Energieübertragung auf Wirbel,formal ähnlich den Stufen im Franck-Hertz-Versuch, die auch auf unelastische Stöße (mit Gasatomen) zurückzuführen sind.

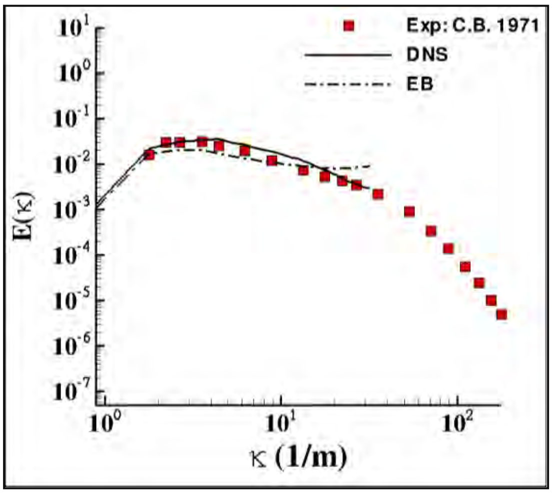

Abb. 6 3D Energiespektrum gegen Wellenzahl

Die vorliegenden Gleichungen (EB-Modell) wurden in Open FOAM implementiert und für reibungsfreie Flüsse mittels eines hybriden aufwind/zentralen Verfahren für die reibungsfreie Flüsse gelöst. Für abnehmende isotrope Turbulenz wurde dieses Modell mit der DNS-Simulation eines Experiments von Comte-Bellot at al [1] verglichen. Das Rechengebiet bestand aus einem Kubus mit 64 Elementen in jede Richtung, und eine Kantenlänge von 2π. Zur Anpassung an ein gemessenes Energiespektrum [2] wurde anfangs ein Divergenz-freies Geschwindigkeitsfeld vorgegeben, angepasst an die gemessenen Energiespektren für Re=1000. Außerdem war eine zusätzliche Initialisierung erforderlich: eine normal verteilte ϕVariable, iterativ gelöst bei eingefrorenem Geschwindigkeitsfeld - bis ϕ bei abklingenden Geschwindigkeitsfeld konvergierte. Anliegend zeigt Abb. 6 einen Vergleich experimenteller Ergebnisse mit DNS- und EB Modellrechnungen. Das neue Modell gibt die k=2 Steigung bei kleine Wellenzahlen korrekt wieder. Die Energieverteilung über die mittleren Wellenzahlen weicht leicht von den DNS Ergebnissen ab-es wird nochversucht, den Ursprung dieser Differenzen zu klären. Das numerische Schema ist zwischen DNS und das EB Modell identisch.

[1] H.G. Weller, G. Tabor, H.Jasak, C.Fureby: Atensorial approach to computational continuum mechanics using object-oriented techniques, Computers in Physics, Vol.12, No 6, Nov/Dec 1998

[2] G.Comte-Bellot, S.Corrsin: Simple Eulerian time correlation of full- and narrow-bandvelocity signals in grid-generated, 'isotropic' turbulence, J. Fluid Mech Vol 48, pp. 273-337, 1971

Mitteilung

Projektgruppe / Fachkreis: Turbulenzforschung

Optische Messung der Wandschubspannung in turbulenten Grenzschichten mit Druckgradient

Erich Schülein[1], Nico Reuther[2], Tobias Knopp[1]
[1]DLR, Institut für Aerodynamik und Strömungstechnik (AS),
Bunsenstr.10, 37073 Göttingen, erich.schuelein@dlr.de
[2]Institut für Strömungsmechanik und Aerodynamik, Universität der Bundeswehr (UniBw) München, 85577 Neubiberg

Im Rahmen des Projekts RETTINA wurde ein Windkanalexperiment zur Untersuchung von turbulenten Grenzschichten unter Einfluss von positiven Druckgradienten bei hohen Reynoldszahlen konzipiert [1]. Das großskalige Windkanalmodell besteht aus zwei S-förmigen Umlenkflächen, die durch eine 4 m lange ebene Platte getrennt sind. Diese ebene Platte dient als Beruhigungsbereich für die turbulente Grenzschicht, die stromab einem vordefinierten Druckgradienten ausgesetzt ist. Um eine möglichst dicke natürliche Grenzschicht in diesem Bereich zu etablieren, wurde das Modell bündig in der Wand des Atmosphärischen Windkanals München (AWM) der Universität der Bundeswehr (UniBw) in München eingebaut, der nominell über eine 22 m lange Messstrecke mit einem Querschnitt von 2.0 × 1.8 m² verfügt.
Die Wandschubspannung gehört bekanntlich zu den wichtigsten Oberflächengrößen in der Strömungsmechanik. Die Ölfilminterferometrie (OFI) ist seit Jahren bekannt als zuverlässige berührungslose Messtechnik zur Erfassung von Wandschubspannungen [2, 3]. Beim parallelen Wandstromlinienverlauf in 2-D Strömungen reicht die Kenntnis über die zeitliche Änderung der Ölschichtdicke auf der Testoberfläche um die Schubspannung auszurechnen. Die Ölschichtdicke wird dabei nach dem Prinzip eines Fizeau-Interferometers erfasst (Bild 1).
Die aktuelle Arbeit beschreibt die Ergebnisse einer OFI-Messkampagne am AWM, die Juli 2015 durchgeführt wurde. Die eigentliche Herausforderung dabei war der ausgedehnte Messbereich von ca. 1.7 m Länge. Um eine ausreichende Auflösung der Interferenzbilder zu erhalten wurde diese Strecke in mehrere Abschnitte aufgeteilt. Fünf handelsübliche hochauflösende Digitalkameras NIKON D7100 wurden parallel eingesetzt um die gesamte Messzeit möglichst kurz zu halten. Die Oberfläche des Modells ist für die Messungen mit einer schwarzen reflektierenden PVC-Folie (0.1 mm dick) beklebt worden. Als Lichtquellen kamen Natriumdampf-Niederdrucklampen SOX-E 18W zum Einsatz, die jeweils mit weißen diffusen

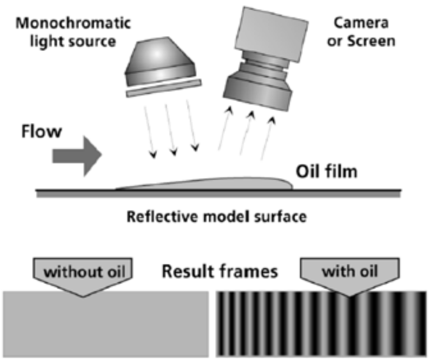

Bild 1: Prinzip der Ölfilminterferometrie nach [3]

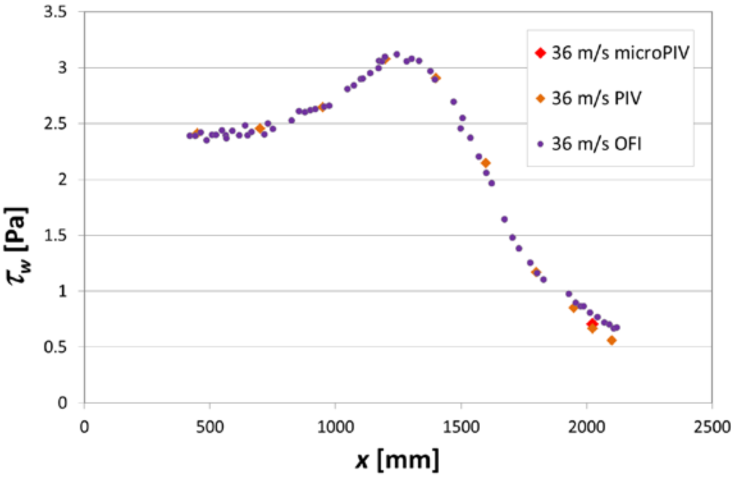

Bild 2: Vergleich der Wandschubspannungsverteilungen im Längsschnitt z = -10mm bei 36 m/s (gemessen mittels OFI, PIV und µPIV).

Reflektoren (0.6 × 0.6 m²) ausgestattet waren und somit als ausreichend große Flächenleuchten dienten. Die einzelnen Leuchtfelder waren von außen an den vorhandenen Fenstern des Windkanals angebracht. Aufgrund der gewählten örtlichen Auflösung konnte von jeder Kamera ein Feld von ca. maximal 0.18 × 0.25 m² beobachtet werden. Zum Einsatz kamen ELBESIL-Silikonöle verschiedener kinematischer Viskosität zwischen 5 und 50 mm²/s, die abhängig vom Einsatzbereich und Testbedingungen verwendet wurden. Die Messungen sind gleichzeitig an mehreren Stellen entlang des Testbereichs durchgeführt worden, wobei der Ölfilm vor dem Versuch in dünnen Streifen senkrecht zur Strömungsrichtung aufgetragen wurde. In mehreren kurzen hintereinander folgenden Versuchen konnte somit die gesamte Wandschubspannungsverteilung in einem Streifen von ca. 1.70 × 0.16 m² erfasst werden.
Drei verschiedene Strömungsgeschwindigkeiten von 10, 23 und 36 m/s wurden untersucht. Ein Beispielergebnis der Wandschubspannungsmessung für 36 m/s in einem Längsschnitt bei z = -10mm (parallel zur Mittelachse des Modells) ist in Bild 2 dargestellt. Der gewählte Schnitt entspricht der Lage der früheren PIV- und µPIV-Messungen [4], die unabhängig am gleichen Modell durchgeführt wurden. Ein direkter Vergleich der Daten demonstriert eine verlässliche Verteilung der Wandschubspannung entlang der Längskoordinate. Der Grund für eine leichte Abweichung in der Tendenz im letzten Abschnitt (x > 1950mm) konnte bislang nicht geklärt werden.
Im Bild 3 ist eine interpolierte flächige Darstellung der gleichen OFI-Ergebnisse im gesamten Messbereich präsentiert, die eine leichte Dreidimensionalität der Grundströmung am Testmodell aufweist. Bei geringeren Strömungsgeschwindigkeiten (nicht gezeigt) ist dieser Effekt noch weniger ausgeprägt.
Weitere Ergebnisse zum Effekt der Anströmgeschwindigkeit (Reynoldszahl) sowie des dimensionslosen Druckgradientenparameters (nach Clauser) auf die Wandschubspannung werden im endgültigen Artikel präsentiert und analysiert.

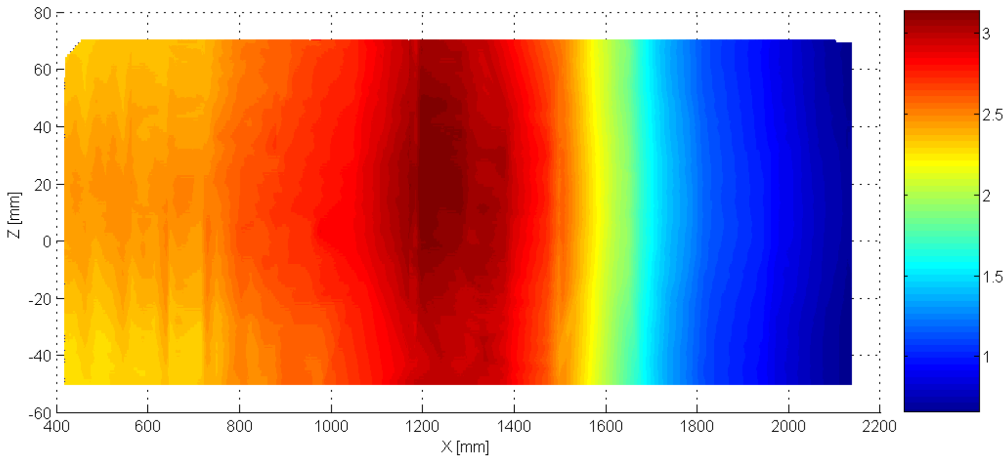

Bild 3: 2D-Wandschubspannungsverteilung aus OFI-Messung bei 36 m/s

Literatur :

[1] Knopp T. et al. (2011) Experimental investigation of a turbulent boundary layer flow at high Reynolds number without and with separation using PIV, *CFD and Experiment – Integration of Simulation Workshop*, 05. - 06. April 2011, Göttingen, Germany

[2] Naughton J., Sheplak M. (2002) Modern developments in shear-stress measurement, *Progress in Aerospace Science*, 2002

[3] Schülein E. (2006) Skin friction and heat flux measurements in shock/boundary layer interaction flows, *AIAA Journal*, 44(8), 2006

[4] Reuther N., Scharnowski S., Hain R., Schanz D., Schröder A., Kähler C.J. (2015) Experimental investigation of adverse pressure gradient turbulent boundary layers by means of large-scale PIV, 11th International Symposium on Particle Image Velocimetry – PIV15, Santa Barbara, California, Sep. 14-16, 2015.

Mitteilung

Projektgruppe / Fachkreis: Turbulenzforschung / -modellierung

Characterization of Turbulence Generated by an Active Grid
with Individually Controllable Paddles

T. Skeledzic, H. Lienhart, Ö. Ertunc, J. Jovanovic, J. Krauss, A. Delgado
Lehrstuhl für Strömungsmechanik, Friedrich-Alexander-Universität Erlangen-Nürnberg, Cauerstraße 4, 91058 Erlangen
tanja.skeledzic@fau.de

When it comes to studying turbulence in basic research well-defined and repeatable means to generate turbulence are needed. Typically static grids are used for this purpose but the possible variety of mesh size and blockage of the grid is very much restricted as long as homogenous turbulence is under consideration. Makita (1991) proposed a so called active grid to generate turbulence of large integral scale, high turbulence intensity and high turbulence Reynolds number. Exactly with the same aims an active grid was designed and built at Lehrstuhl für Strömungsmechanik (LSTM) at Friedrich-Alexander-Universität Erlangen-Nürnberg.

The active grid finally shall be installed in the Refractive Index Matched Tunnel (RIMT) at LSTM which uses a cosmetic white oil as the test fluid. Therefore, the size and the construction of the active grid is adapted to its final use. It spans a cross section of 600 x 450 mm^2 and its components are made from stainless steel. The cross section is covered by 24 paddles arranged in 6 columns and 4 rows, the axis of rotation of each paddle is under 45° in an alternating orientation. In contrary to Makitas approach we decided to go for individually driven paddles, this means each paddle is activated by its own servo motor, which gives additional degrees of freedom in the possible patterns of paddle movement. The 24 independent actuators can give a rotation of maximum 90° each. In other words it can fully open and fully close the cross section. However, the geometry of the paddles is designed in such a way that at the fully closed state, the tunnel is not blocked completely due to the circular openings and spacing between the paddles. These openings also initiate smaller scales of turbulent fluctuations and in this way promote the generation of an equilibrium spectrum of scales in the turbulence cascade. A photograph of the active grid is shown in Figure 1, left.

Control of 24 servo motors is made by a real time FPGA (Field Programmable Gate Array) system installed inside of the tunnel. Motion parameters (driving protocols) are delivered to the FPGA by WLAN so that only power cables have to pass into the tunnel which minimizes leakage problems. A sketch of the control electronics can be found in Figure 1, right.

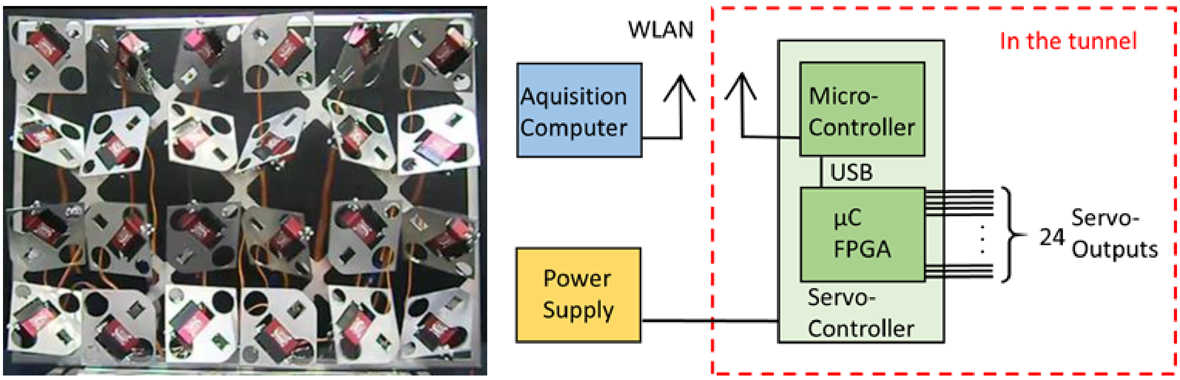

Figure 1: Active grid on left side, control electronics on right hand side

Due to the very time-consuming and costly operation of the Refractive Index Matched Tunnel, a first set of characterization tests were conducted in the wind tunnel of LSTM. As the kinematic viscosity of air and the white oil used in RIMT are approximately the same, the achievable turbulence Reynolds number Re_λ is very much the same. Because the cross section of the test section of the wind tunnel is much larger than the cross sectional area of the active grid, the active grid is mounted inside a specific closed test section insert which is positioned in the open test section of the wind tunnel. The measurements were performed using a DANTEC StreamLine constant temperature hot-wire system, the probe was mounted on the computer controlled wind tunnel traversing unit which had access to the test section insert through a slot in the top lid. A sketch of the set-up is shown in Figure 2.

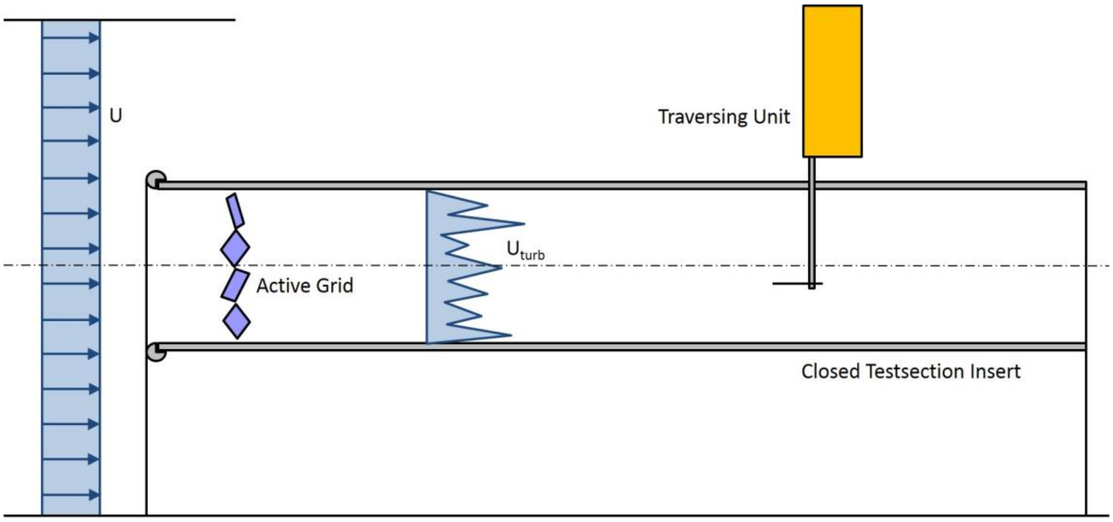

Figure 2: Test set-up with test section insert in LSTM wind tunnel

The results of the measurements presented were acquired along the vertical symmetry plane in the wake of the active grid. Statistical quantities of the fluctuating velocity such as mean and rms values, correlation functions and spectra will be shown to characterize the turbulence generated depending on the motion scheme of the paddles. In order to find appropriate motion schemes to generate high turbulence Reynolds numbers and large scale homogeneous turbulent flows different driving protocols of the servo motors were tested. As large scales in turbulence means high correlation, an increase in correlation of the motion scheme of neighbouring paddles shall result in an increase of the integral length scale. Results and limitations of this approach will be presented.

References:

H. Makita: Realization of a large-scale turbulence field in a small wind tunnel. Fluid Dynamics Research 8 (1991) 53-64

Mitteilung

Projektgruppe / Fachkreis: **Hyperschallaerothermodynamik**

Thema:

Freistrommessungen mit Stausonden im Hyperschall

Autor(en) : Syed Raza Christopher Ali, Rolf Radespiel
Institution : Institut für Strömungsmechanik,
Technische Universität Braunschweig
Adresse : Hermann-Blenk-Strasse 37, 38108 Braunschweig
e-mail : s.ali@tu-bs.de

Ausgangssituation : Experimentelle Untersuchungen von Transitionsvorgängen in Hyperschall-Grenzschichten von stumpfen oder schlanken Körpern können bei großen Reynoldszahlen nur in sogenannten konventionellen Hochgeschwindigkeitskanälen durchgeführt werden, die kanaltypische Störpegel der Strömung in der Messstrecke haben. Dieser Störpegel beeinflusst die Transition laminar-turbulent, so dass in vielen Fällen ein anderer physikalischer Ablauf des Transitionsvorgangs und eine geringere laminare Lauflänge der Grenzschichten am Modell im Vergleich zum Freiflug erwartet werden muss. Daher ist die Kenntnis über die Art und die räumliche Verteilung der Störung der Zuströmung im Windkanal bedeutsam. Störspektren setzen sich aus 3 unterschiedlichen Grundstörmoden zusammen und hierbei dominieren die akustischen Störungen für Hochgeschwindigkeitsanlagen [1]. Diese Störungen werden vom Strömungslärm der turbulenten Grenzschicht der Kanaldüse verursacht.
In einer Kooperation der TU Braunschweig mit der RWTH Aachen wurde bereits der Versuch unternommen, aus den Messdaten einer Kegelsonde und mit Hilfe von zugehörigen DNS-Simulationen der Wechselwirkungen von generischen Störmoden mit der Sonde die tatsächlichen Pegel der ungestörten Zuströmgrößen im hypersonischen Windkanal HLB der TU Braunschweig zu bestimmen. Das gelang nur mit Einschränkungen aufgrund der Ähnlichkeit der Übertragungsprozesse, die initiale Entropiemoden und akustische Moden bis zum Erreichen der Sensorposition erfahren [1].
Ziel und Ergebnisse: In der Fortführung dieses Vorhabens haben erste Berechnungen gezeigt, dass Staupunktssonden ein signifikant besseres Antwortverhalten (response coefficient) von Schwankungen der Zuströmung zu Schwankungen der beobachteten Größe an der Sensorposition besitzen und somit eine eindeutige Zerlegung der Fluktuaktionsgrößen ermöglichen sollten.

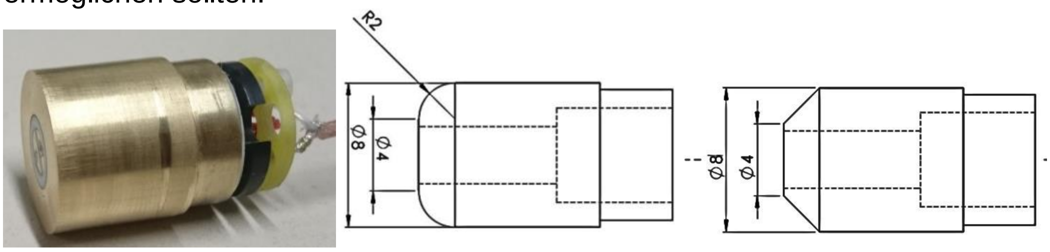

Bild1 : von links nach rechts : zyindrisch, runde und abgeschrägte Frontkontur der Stausonde

Im nächsten Schritt wird die geometrische Form (s. Bild 1) des Sondenkopfes, in der die Sensorik oberflächenbündig sitzt, bewertet. Hierfür werden zunächst numerische Simulationen der laminaren Strömung um den Sondenkopf herangezogen, die z.B. Ablösungen und die Gleichförmigkeit des Drucks und des Wärmeübergangs im Bereich des Sensors anzeigen. Für die Bewertung sind auch die kürzlich veröffentlichten Arbeiten um Chaudhry et al [2] sehr hilfreich, die anhand von mehreren untersuchten Stausondengeometrien zeigen, dass die Antwort von Staupunktssonden auf akustische Wellen einen welligen Verlauf im Spektrum aufweist und dass die lokalen Maxima des Druckspektrums an der Sensorposition durch Wechselwirkungen der akustischen Wellen mit der Kopfwelle des Sonde hevorgerufen werden.

Mit neuen Messungen der Fluktuationen für Druck und Wärmestromdichte mit 3 verschiedenen Sondenköpfen für variierende Einheits-Reynoldszahlen wird nun der Störpegel von akustischen Wellen und Entropiewellen genauer als zuvor bestimmt. Hierzu kommen dynamisch hochauflösende Wärmestrom- und Drucksensoren (ALTP und PCB) zum Einsatz, s. Bild 2. Zusätzlich werden mit einer Referenzsonde als Nachbau einer Stausonde des amerkanischen Hyperschallkanals AEDC T9 vergleichbare Staumessungen durchgeführt. In der weiteren Auswertung werden diese Daten für schmale Frequenzbänder gefiltert und mit den Ergebnissen der DNS, den response coefficients, ausgewertet um daraus die Störmoden der Anströmung zu bestimmen. Weiterhin sind in den nächsten Monaten noch Hitzdrahtmessungen geplant, um die ggf. vorhandenen Vorticitystörungen in der Messstrecke des Windkanals HLB zu detektieren.

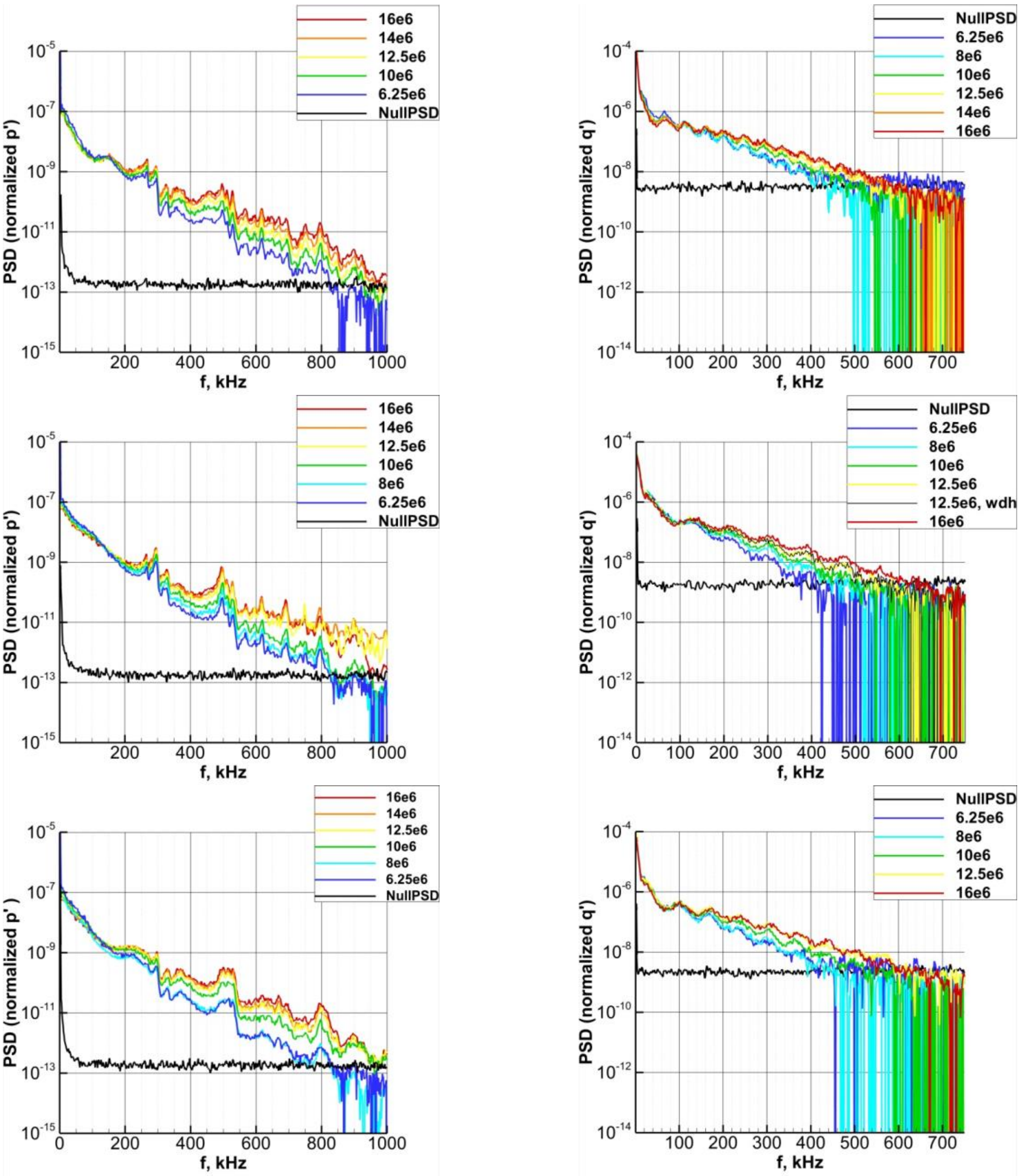

Bild 2 : Linke Spalte : dynamisches Verhalten der normierten Druckschwankungen (oben nach unten : zylindrisch, konisch, rund). Rechte Spalte : Dynamisches Verhalten der normierten Wärmestromdichteschwankungen

Literatur:

[1] Schilden et al “Analysis of acoustic and entropy disturbances in a hypersonic wind-tunnel”, Phys. Fluids 28(5), 2016

[2] Chaudhry et al “Recovery of Freestream Disturbance Spectrum from Stagnation Pressure Spectrum for Hypersonic Pitot Probes ”, AIAA 2016-2059

Mitteilung

Projektgruppe / Fachkreis: Aerodynamik und Aeroakustik

PIV measurements of shock/cooling-film interaction at varying shock impingement position

Pascal Marquardt[1], Michael Klaas[1], Wolfgang Schröder[1]
[1]Institute of Aerodynamics, RWTH Aachen University, 52062 Aachen, Germany
corresponding author p.marquardt@aia.rwth-aachen.de

1. Introduction

In supersonic applications with high thermal loads, e. g., scramjet combustors, supersonic film cooling through two-dimensional slots is a promising cooling concept for surface temperature reduction [1, 2, 3]. In those combustors, shocks occur that interfere with the cooling film, which leads to a locally reduced cooling effectiveness.
The scope of this study is to analyze the effect of the impingement position of an oblique shock impinging upon a supersonic cooling film flow by means of high-speed particle-image velocimetry (PIV). The cooling film is injected tangentially to the main flow with an injection Mach number of $Ma_i = 1.8$ through a two-dimensional slot nozzle into a supersonic turbulent boundary layer at a freestream Mach number of $Ma_\infty = 2.45$. An oblique shock generated by a 5° flow deflection impinges upon the cooling film. In this study, the flow field is analyed in detail for two impingement positions, namely 15 nozzle heights and 37 nozzle heights downstream of the injection point using high-speed 2C/2D PIV measurements. The comparative analysis comprises the mean flow fields as well as turbulence statistics.

2. Experimental setup

The experiments have been conducted in the trisonic wind tunnel of RWTH Aachen University. This wind tunnel is an intermittent working vacuum storage tunnel that is able to provide flows at Mach numbers reaching from 0.3 to 4.0 which are stable up to 3 seconds. The unit Reynolds number varies between $6 \cdot 10^6$ and $16 \cdot 10^6\ m^{-1}$ depending on the Mach number and the ambient conditions.

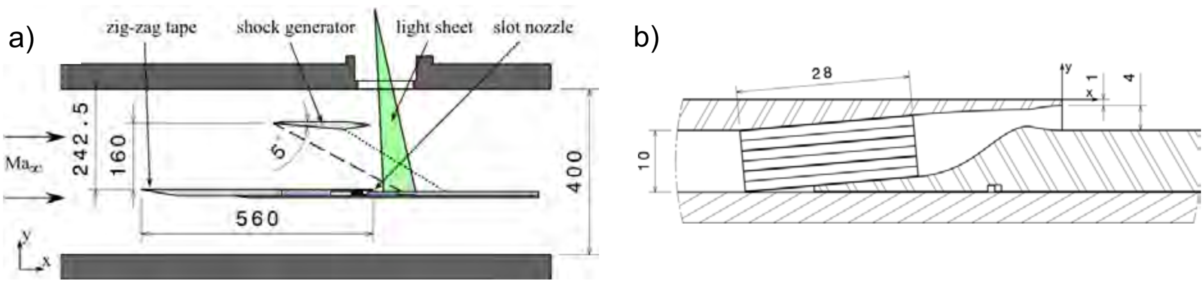

Fig. 1. Dimensions of the wind tunnel model and its location in the test section (a) and cross section of the slot nozzle (b)

The model, mainly made of aluminum, spans across the entire 400 mm x 400 mm test section of the wind tunnel, has an overall length of 960 mm, and possesses a thickness of 20 mm. The dimensions of the model and its position in the test section are sketched in figure 1a. The incoming flow is tripped by a 0.2 mm thick zigzag tape 10 mm downstream of the wedge-shaped leading edge to ensure a uniform turbulent boundary layer at the position of injection. The cooling flow is injected 560 mm downstream of the leading edge through a 200 mm wide, centered slot nozzle and develops on a 400 mm long flat plate. The nozzle is designed as a symmetric, bell-shaped nozzle with an exit height of *S* = 4 mm and a lip thickness of 1 mm (Fig. 1b). The oblique shock is generated by a 5° wedge spanning the entire test section. The expansion fan emanating from the shock generator reaches the model 120 mm downstream of the shock impingement location.

The PIV setup consists of a Quantronix Darwin Duo laser (527-40-M) and a Photron Fastcam SA5 which are synchronized by an ILA synchronizer. In the current setup, the PIV system records 1000 samples per second with a resolution of 1024 x 1024 px². The light sheet enters the test section through a window in the ceiling of the test section and is oriented vertical and parallel to the flow on the centerline of the model, as sketched in figure 1a. The camera is equipped with a 180 mm Tamron tele macro lens to realize a field of view of 20 mm x 20 mm in the measurement plane. The main flow as well as the cooling flow are seeded with DEHS particles. The effective mean diameter of the particles is $d_p = 1.2\ \mu m$ and the corresponding relaxation time is $\tau_p = 7.1\ \mu s$.
Each measurement consists of 1000 snapshots recorded over 1 s. After subtraction of a background image, the particle images are preprocessed using a non-linear Gaussian blur working in the logarithmic scale to reduce camera noise. The image evaluation uses an iterative correlation scheme with subpixel-accurate image deformation. The window size used for PIV evaluation is 48 x 48 px² with 75% overlap. Outliers in the vector field are determined using a normalized median test.

3. Results

The freestream Mach number is $Ma_\infty = 2.45$, with air being injected at an injection Mach number of $Ma_i = 1.8$. The total temperature of both the freestream and the cooling flow varies between 290 K and 295 K and depends on the ambient conditions. The unit Reynolds number is $10 \cdot 10^6\ m^{-1}$ leading to a thickness of the boundary layer developing on the model of $\delta_{99} = 8\ \mathrm{mm}$ at the point of injection.

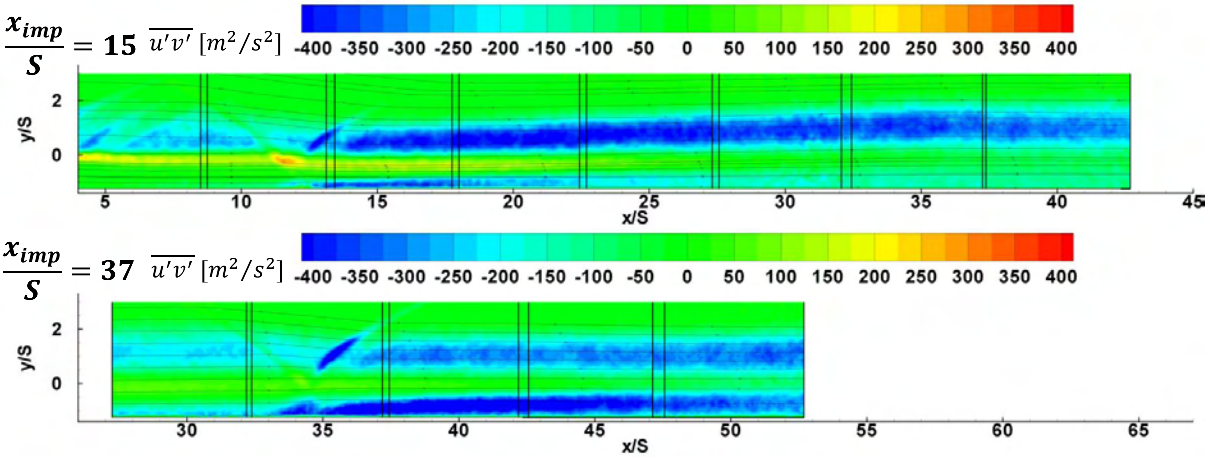

Fig. 2. Contours of the Reynols stress $\overline{u'v'}$ in the model centerplane. Results of several test runs with different streamwise measurement position. Shock impingement at $x/S = 15$ (top); shock impingement at $x/S = 37$ (bottom).

The distributions of the Reynolds stress $\overline{u'v'}$ for the cases with shock impingement at $x/S = 15$ (top) and $x/S = 37$ (bottom) are presented in figure 2. In both cases, the Reynolds stress is greatly increased by the shock interaction. In the case with the shock interaction closer to the nozzle, the increase in $\overline{u'v'}$ is more pronounced in the shear layer, whereas in the case with the shock impingement further downstream, the turbulent mixing is more intense in the boundary layer on the bottom wall. In the final paper, the shock/cooling-film interaction will be discussed in detail. The analysis will comprise the mean velocity distributions as well as turbulence statistics at various positions downstream of the cooling film injection.

4. References

[1] Juhany, K., Hunt, M., (1994) Flowfield Measurements in Supersonic Film Cooling Including the Effect of Shock-Wave Interaction, AIAA Journal, Vol. 32, No. 3, pp 578–585 (1994).
[2] Konopka, M., Meinke, M. & Schröder, W., (2012) Large-eddy simulation of shock-cooling-film interaction, AIAA Journal Vol. 50, No. 10, pp 2102-2114
[3] Konopka, M., Meinke, M. & Schröder, W., (2013) Large-eddy simulation of shock-cooling-film interaction at helium and hydrogen injection, Phys. Fluids, 25(10), 106101

Mitteilung

Projektgruppe / Fachkreis: Hyperschall

Development of Ultra-fast Temperature Sensitive Paints for Hypersonic High Speed Flows

Jan Martinez Schramm
Jan.Martinez@dlr.de

Frank Edzards
Frank.Edzards@dlr.de

DLR Göttingen
Bunsenstrasse 10
37073 Göttingen

The precise experimental determination of the heat loads acting on vehicles traveling at hypersonic speeds is crucial for the design of the vehicle's thermal protection system (Bertin and Cummings, 2006). Computational fluid dynamics methods provide increasingly powerful possibilities for the simulation of such hypersonic configurations. Nevertheless, the difficulties in the accurate modeling of high-temperature effects in chemically reacting flows, boundary-layer transition and shock-wave/boundary-layer interactions, mean that ground-based testing will remain an important tool for evaluating the heating levels encountered by high-speed vehicles for the foreseeable future. Conventional heat-flux sensors, such as thin-film gauges and thermocouples, have been employed successfully in hypersonic wind tunnels in general and also in the High Enthalpy Shock Tunnel Göttingen (HEG) for a few decades (Schultz and Jones (1973)). Such gauges are limited in terms of the spatial resolution they provide and occasionally geometrical constraints may prevent the installation in complex model geometries. An attractive nonintrusive alternative, providing global heat-transfer measurements at potentially much lower costs and efforts, is the use of temperature sensitive paints, TSP.

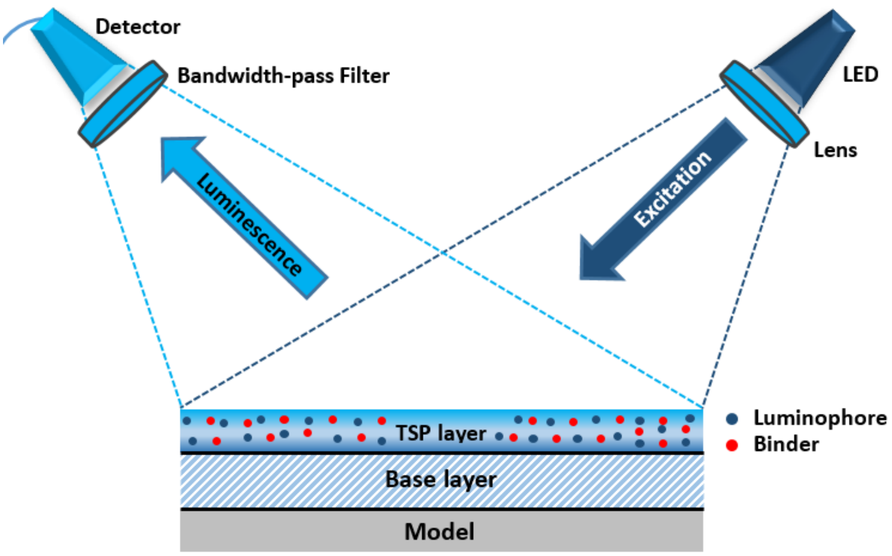

Figure: Schematics of the TSP measurement technique.

A TSP consists of a luminescent molecule, the luminophore, dissolved in a suitable binder and applied to the surface of the body to be inspected. When illuminated with light at appropriate wavelengths, the intensity of the emitted light of the color is reciprocal dependent on the mean temperature of the luminophores in the TSP layer. Thus, the emission intensity recorded by an imaging device can be related to the temperature at any visualized location on the surface during an experiment in HEG. The heat transfer rate can subsequently be determined from the time evolution of the temperatures on the surface.

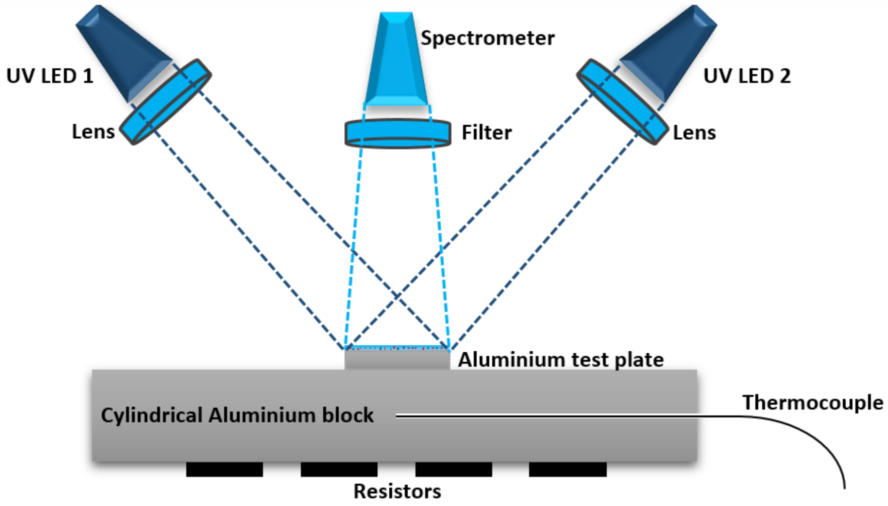

Figure: Schematics of the TSP calibration appartus.

The paper will describe the development and deployment process of TSP in HEG. Special care has been taken to bring the technique up to recording frequencies to the ranges needed to derive time resolved heat fluxes within a few milliseconds of test time in HEG. Among a lot of matters considerd, e.g. linearity, repeatability, accuracy, the degradation of the TSP layers with time has been measured and quantified. The paper will demonstrate the feasibility of usage of this measurement technique by discussing various applications in HEG.

References

Bertin J, Cummings R (2006) : Critical hypersonic aerothermodynamic phenomena. Annu Rev Fluid Mech 38:129–157.

Schultz DL, Jones TV (1973) : Heat transfer measurements in short-duration hypersonic facilities. AGARD-AG-165.

Liu T, Campbell BT, Sullivan JP (1995) : Accuracy of Temperature-Sensitive Fluorescent Paint for Heat Transfer Measurements. AIAA Paper 95-2042.

Hubner JP, Carroll BF, Schanze KS, Ji HF, Holden MS (1999) : Temperature- and Pressure-Sensitive Paint Measurements in Short-Duration Hypersonic Flow. AIAA Paper 99-0388.

Hubner JP, Carroll BF, Schanze KS (2002) : Heat Transfer Measurements in Hypersonic Flow Using Luminescent Coating Techniques. AIAA paper 2002-0741.

Nagai H, Ohmi S, Asai K (2008) : Effect of Temperature-Sensitive-Paint Thickness on Global Heat Transfer Measure-ment in Hypersonic Flow. J Thermophysics and Heat transfer 22(3):373-381.

Nakakita K, Osafune T, Asai K (2003) Global Heat Transfer Measurement in a Hypersonic Shock Tunnel Using Tempera-ture-Sensitive Paint. AIAA Paper 2003-0743

Mitteilung

Projektgruppe/Fachkreis: Laminarhaltung und Transition

Redesigned swept flat-plate experiment for crossflow-induced transition studies

Hans Peter Barth, Stefan Hein, Henning Rosemann
DLR, Institute of Aerodynamics and Flow Technology, Department of High Speed Configurations, Bunsenstr. 10, 37073 Göttingen
peter.barth@dlr.de, stefan.hein@dlr.de, henning.rosemann@dlr.de

1 Introduction

In the 80s and 90s, Bippes et al. performed comprehensive experiments on crossflow-induced laminar-turbulent transition mostly using an experimental setup consisting of a swept flat plate with a displacement body arranged above [1]. The displacement body imposed a pressure gradient on the plate surface with a constant acceleration along most of the chord length. Saric et al. showed that artificial excitation of a stationary crossflow instability with a wavelength smaller than the naturally most amplified can delay transition [3]. This transition control strategy has been comprehensively studied using Direct Numerical Simulation at the University of Stuttgart where it has been named "upstream flow deformation" (UFD) [4]. In order to reestablish a setup suitable for detailed studies on crossflow-dominated transition and its control, a new swept flat-plate experiment has been designed, constructed and tested at DLR Göttingen.

2 Goals and Design

The original design of Bippes et al. offered some key advantages over comparable experiments. The choice of a flat surface over a curved wing greatly facilitates boundary layer measurements while surface curvature effects could be neglected in numerical treatment. The experiment also offered a good approximation of infinite swept-wing conditions. However, for the study of the UFD method, a new pressure distribution with varying degrees of acceleration over the length of the plate chord was needed. A strong acceleration in the first 20% and a weaker acceleration further downstream cause stationary crossflow instabilities with a wavelength smaller than the integrally most amplified instability mode to be amplified stronger initially than the latter. This means that even for weak actuation, instabilities at these smaller wavelengths reach locally higher amplitudes compared to the integrally most amplified ones. This enables the nonlinear effects of UFD and ultimately the desired transition delay. In order to design a displacement body which imposes a suitable pressure distribution on the plate surface, an inverse design method was used. The resulting pressure distribution is shown in comparison to the original Bippes et al. experiment in Fig. 1(b) and the resulting shape can be seen in a cross-section of the new setup in Fig. 1(a). This design process was accompanied by local stability (LST) analyses in order to ensure the desired instability conditions. At u_∞ = 30m/s, Ma = 0.087, Re $= 1.54 \cdot 10^6$ (based on the plate chord length in the direction of the oncoming freestream) the most amplified stationary crossflow instabilities have a wavelength of λ = 9mm, and laminar-turbulent transition is expected on the upper side of the plate.

3 Results

The experimentally determined pressure distribution is in good agreement with the numerical design and can be seen in Fig. 1(b). Using a smoke generator, the flow around the setup was visualized and it was verified that no unexpected flow separation occurs. Using hot-wire anemometry the infinite swept wing conditions were verified and the flow field in the plate's

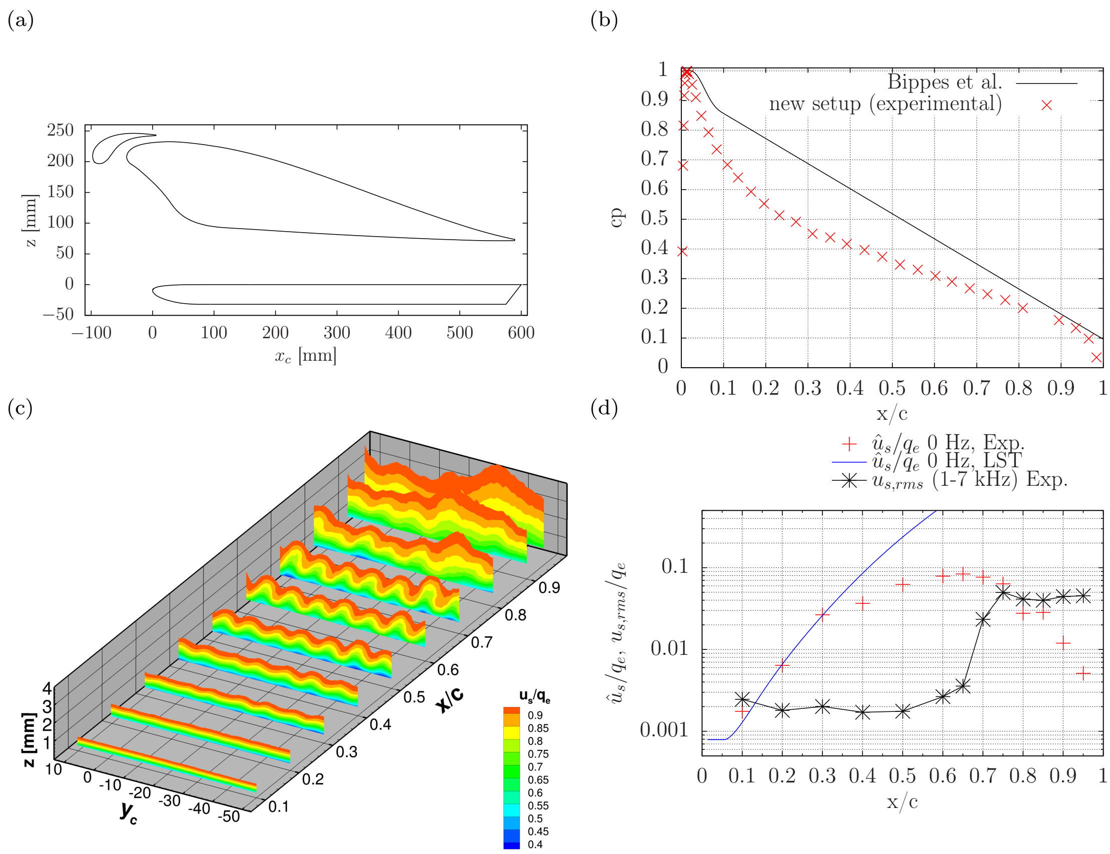

Figure 1: (a): Cross-section of the new experimental setup, (b): pressure distribution compared to the idealized pressure distribution in experiments of Bippes et al., (c): 3D boundary-layer visualization of the mean streamwise velocity component with visible deformation by stationary crossflow vortices, (d): Development of the integrally most amplified stationary crossflow instability amplitudes and onset of transition as sudden rise in high-frequency disturbance amplitudes

upper surface boundary layer was investigated comprehensively. Especially the development of stationary and travelling crossflow instabilities, as well as the appearance of high-frequency secondary instabilities have been investigated in detail for the new setup, see Fig. 1(c) and Fig. 1(d). The newly designed swept flat-plate experiment offers a platform for pursuing new research ideas in crossflow-induced laminar-turbulent transition. First experiments on transition delay using active flow control methods with pneumatic actuation and plasma actuators were conducted within the LuFo IV-4 project AKSA in cooperation with TU Berlin and TU Darmstadt, the results of which will be presented separately (see e.g. [2]).

4 Bibliography

[1] H. Bippes. Basic experiments on transition in three-dimensional boundary layers dominated by crossflow instability. *Progress in Aerospace Sciences*, 35(4):363 – 412, 1999.

[2] J. Lohse, H. P. Barth, and W. Nitsche. Active control of crossflow-induced transition by means of in-line pneumatic actuator orifices. *Experiments in Fluids*, 57(8):1–10, 2016.

[3] W. Saric, R. Carrillo, and M. Reibert. Leading-edge roughness as a transition control mechanism. *AIAA 98-0781*, 1998.

[4] P. Wassermann and M. Kloker. Mechanisms and passive control of crossflow-vortex-induced transition in a three-dimensional boundary layer. *Journal of Fluid Mechanics*, 456:49–84, 2002.

Mitteilung

Projektgruppe / Fachkreis: Flow Control

Experimental and Numerical Investigation on Delta-Wing Post-Stall Flow Control

Andrei Buzica, Christian Breitsamter
Chair of Aerodynamics and Fluid Mechanics, Technical University of Munich,
Boltzmannstraße 15, 85748 Garching b. München, andrei.buzica@aer.mw.tum.de

Large vortex flow structures are typical for high maneuverable aircraft configurations with high sweep angle and low aspect ratio (e. g. delta wings). Starting from the leading edge the flow around this type of wing separates even at moderate incidence angles resulting in a free shear layer which rolls up into a large scale vortex. This flow structure produces high suction peaks over the wing, responsible for a nonlinear increase in lift compared to attached flow. Therefore wings with leading-edge vortices generally achieve higher maximal angles of attack. Due to the unsteady nature of these vortical structures, instabilities with non-linear interaction occur over a broad frequency spectrum. Vortex breakdown is a phenomenon of great importance. It causes undesired effects such as structural excitation and loss of flight stability thus limiting the flight envelope. In the post-stall flight regime the flow completely detaches from the suction side and generates a sudden lift drop. The active manipulation of the separating shear layer at the leading edge is of great interest in increasing the aerodynamic performance of delta wing configurations and extending the flight envelope. This study focuses on the vortex flow control through pulsed blowing and oscillating miniature flaps along the sharp leading edge of a slender, 65° swept generic half wing model. Wind tunnel investigations as well as time accurate CFD simulations demonstrate the receptivity of vortex breakdown and shear layer roll-up to actuation at moderate to high angles of attack.
The above mentioned investigations comprise experiments with two half wing models in a low speed wind tunnel. The models represent the geometry of the Vortex Flow Experiment 2 configuration (VFE-2). The wing measures a chord root of c_r = 0.977 m, a half span of s = 0.456 m and a thickness of δ = 0.033 m, resulting in an aspect ratio of Λ = 1.867. Two actuation systems are integrated in each leading edge. Both wind tunnel models generate at the formation of the shear layer unsteady flow disturbances in a mechanical and pneumatic manner: by flap excitation from two segments and by dynamic blowing through three segments with evenly arranged air slots respectively (see Figure 1). The measurement techniques consist of force balance measurements, hot wire anemometry, surface pressure monitoring and stereo particle image velocimetry. Figure 2 compares the measured lift and rolling moment coefficients of both configurations with the best typical actuation frequency. For the configuration with the blowing slots a dimensionless frequency of F^+ = 1.0 was selected, whereas the flaps oscillate at F^+ = 2.7. The first mechanism injects additional momentum into the outer flow, thus achieving greater lift increase in the post-stall flight regime. Greater rolling moments are also resulting, which is important for flight control and stability at this extreme flight conditions. By exciting the shear layer through the miniature flaps the typical post-stall lift drop between 42° and 43° is shifted by $\Delta\alpha \approx 1°$ towards higher angles. In the rolling-moment coefficient plot no significant change is depicted.
The PIV measurements show good agreement with the aerodynamic loads. The three dimensional averaged velocity field around the wing is reconstructed in Figure 3 and compared to selected URANS-SAS results for an angle of attack of α = 45°. The unsteady blowing reattaches the separated flow as suggested by the spiraling of the streamlines and reduces the backflow region. Thus a vortex-like structure producing additional suction on the upper side is generated. CFD simulations on the same configuration with and without pulsed blowing shows good agreement with the experiments.

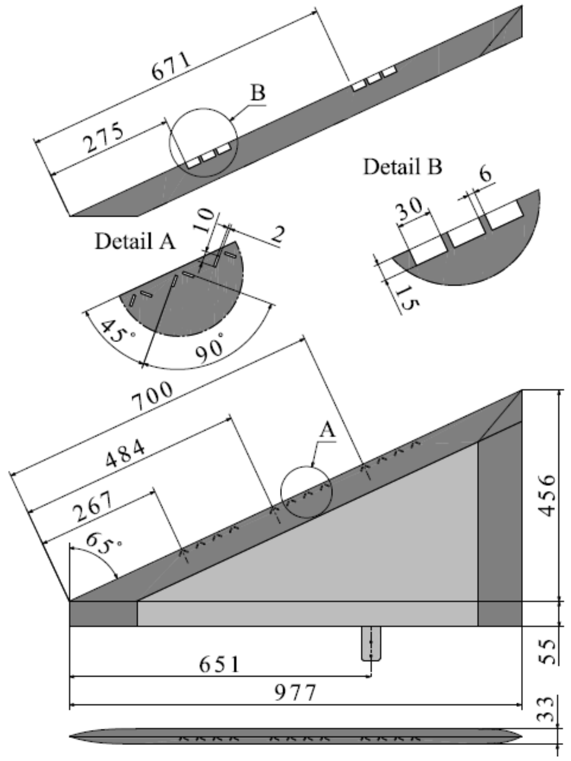

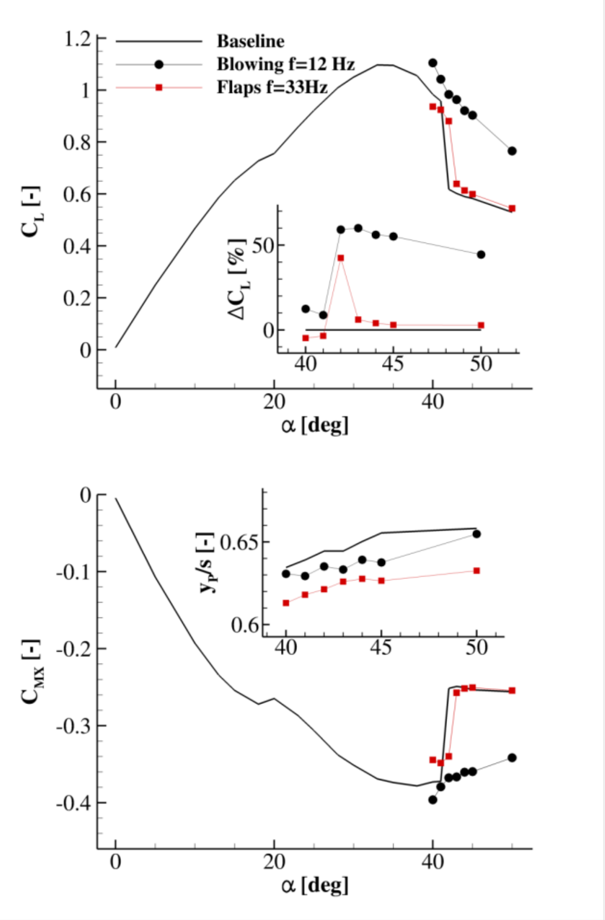

Figure 1: Sketch of the VFE-2 half-wing model: Leading edge with integrated oscillating flaps (above) and blowing sections (beneath).

Figure 2: Lift (above) and rolling moment coefficient (beneath) versus the angle of attack for the baseline compared to both flow control mechanisms.

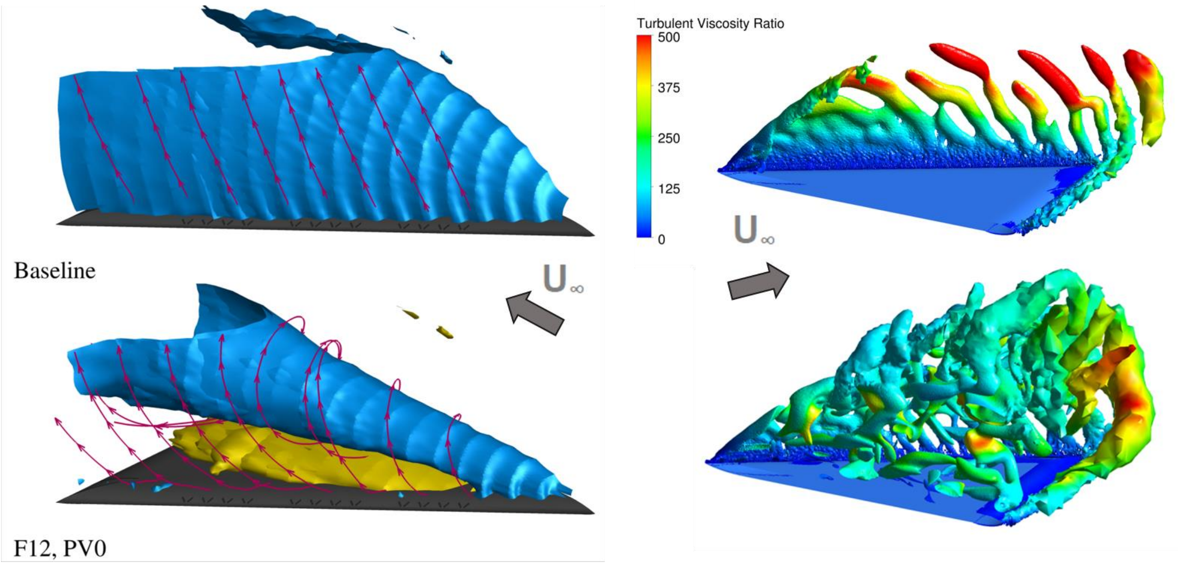

Figure 3 : Isosurface of the zero axial velocity and streamlines obtained from multiple averaged PIV cross-flow planes (left) and Q-criterion coloured by the turbulent viscosity ratio from URANS-SAS simulations (right) at α = 45° and U_∞ = 12 m/s.

Mitteilung

Projektgruppe / Fachkreis: Laminarhaltung und Transition

Extension of the PSE code NOLOT for transition analysis in rotating reference frames

Xavier Dechamps, Stefan Hein
DLR, Institut für Aerodynamik und Strömungstechnik, Abteilung Hochgeschwindigkeitskonfigurationen
Bunsenstraße 10, 37073 Göttingen
xavier.dechamps@dlr.de, stefan.hein@dlr.de

Introduction

Flows subject to rotating geometries are encountered in a great number of aeronautical applications (e.g. propellers, rotors, wind turbines, helicopter blades, etc.). However the effects of rotation on the stability of boundary layers are still only partially understood. It is well-known that the laminar-turbulent transition is postponed for propellers and wind turbines in comparison with a non-rotating configuration [1,2]. A physical interpretation is that the radial velocity component generated through the centrifugal force leads to an azimuthal Coriolis force, which acts as a negative pressure gradient and thus stabilizes the boundary layer. The main consequence is a delayed separation on the suction side.

The present work aims at contributing to a better understanding of the effect of rotation on the stability properties of boundary layers. For this purpose, the *Parabolized-Stability-Equations* based NOLOT code [3] was extended to rotating reference frames through the inclusion of the centrifugal and Coriolis forces. Stability analyses of two flow configurations were then considered for verification: the rotating Blasius profile and the Görtler instability. A third flow configuration, which is currently studied, is the three-dimensional flow due to a rotating disk. This last configuration is intrinsically more similar to a rotating propeller and is more challenging than the two other test cases.

Test cases

The first considered flow configuration is the standard Blasius profile for boundary layers on which a rotation is applied along the spanwise direction (see Fig. 1). The dimensionless inviscid instability criterion of the rotating shear flow is $Ro\ \partial u/\partial x_3>1$ where $Ro=u_\infty/2\Omega\delta$ is the Rossby number. This means that a negative rotation vector tends to destabilize the flow and inversely for a positive rotation number. This artificial flow configuration was thoroughly studied by Yecko and Rossy [4]. Local parallel stability computations are performed in this case.

The second flow configuration is the Görtler instability subject to spanwise rotation. The basic flow is identical to the previous case except that streamwise curvature is now included. The most unstable mode appears as steady longitudinally elongated vortices. Rotation in the same direction as the flow stabilizes the flow and inversely for a rotation opposed to the flow. Local parallel and non-parallel stability computations are performed in this case.

Results

Figure 1 shows the neutral curves for the rotating Blasius profile for different values of the Rossby number. A perfect matching is observed with the numerical results of [4]. One sees that rotation affects only marginally the modified Tollmien-Schlichting (TS) instability. A more pronounced effect is observed at high spanwise wavenumbers with the appearance of a new kind of instability at low streamwise wavenumbers. This new instability is characterized by much higher growth rates than the TS instability.

Figure 2 shows the neutral curves for the Görtler instability for different values of the rotation number $N=\Omega R/ u_\infty$. At high spanwise wavenumbers, a perfect matching is observed with the local non-parallel results of Zebib et al. [5] (with rotation) and Floryan et al. [6] (without rotation). As expected, a stabilization is observed when the rotation is in the same direction as the flow and inversely for a rotation opposed to the flow.

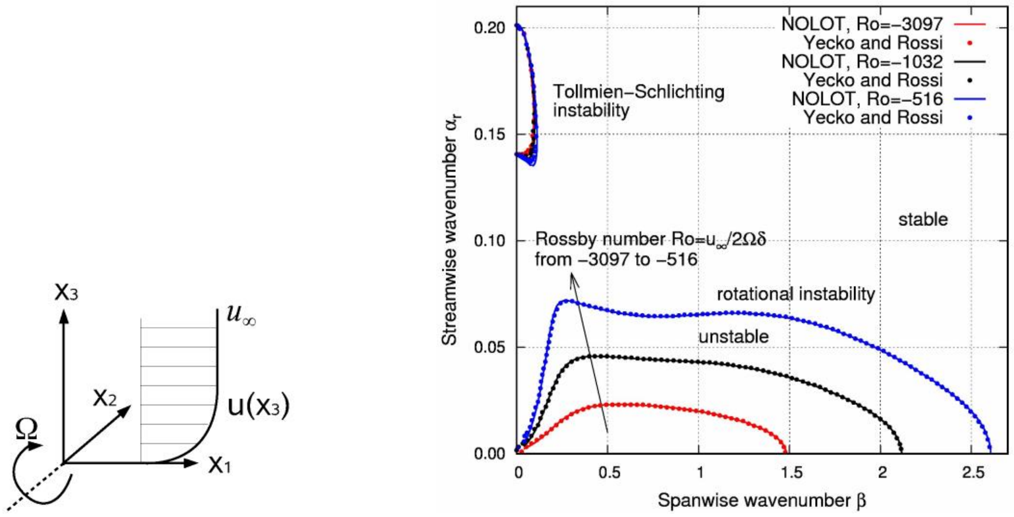

Fig. 1: Geometry (left) and neutral curves (right) for the rotating Blasius profile. Because of the use of different reference length, the Rossby number Ro had to be adjusted in order to match the numerical results of Yecko and Rossy [4] (dots).

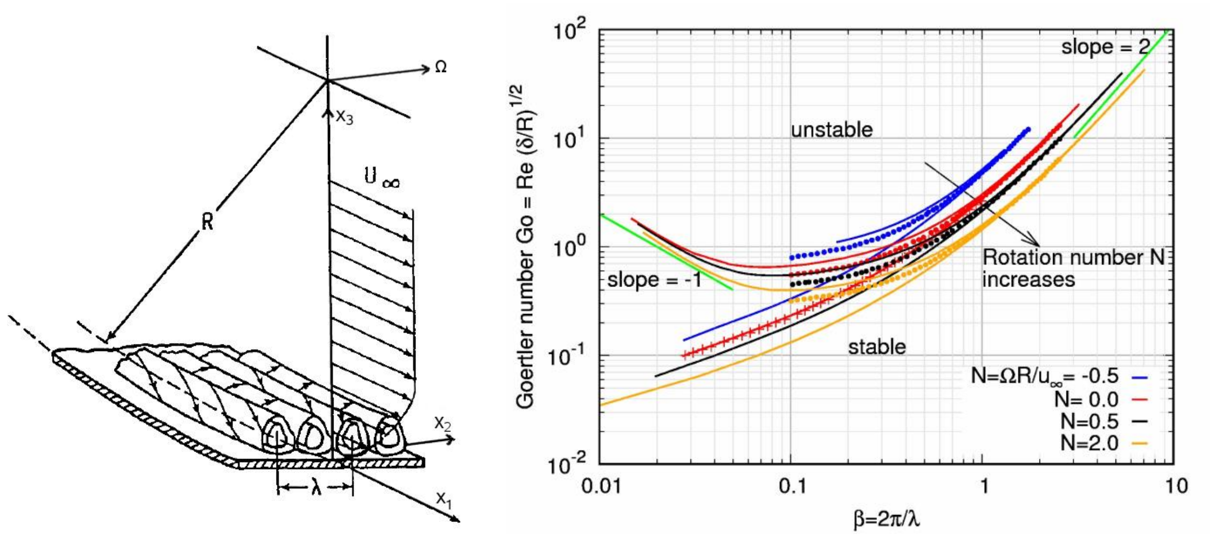

Fig. 2: Geometry (left) and neutral curves (right) for the Görtler instability. Present computations based on local parallel theory (lines), local non-parallel theory (dashed lines), local non-parallel results of Zebib [5] (dots) and Floryan [6] (crosses).

References

[1] Du Z. and Selig M.S., The effect of rotation on the boundary layer of a wind turbine blade, Renewable Energy 20, pp, 167-181, 2000

[2] Dumitrescu H. and Cardos V., Rotational effects on the boundary-layer flow in wind turbines, AIAA Journal 42(2), pp. 408-411, 2004

[3] Hein S., Bertolotti F.P., Simen M., Hanifi A. and Henningson D., Linear nonlocal instability analysis - The linear NOLOT code, DLR-IB 223-94 A56, 1995

[4] Yecko P. and Rossy M., Transient growth and instability in rotating boundary layers, Physics of Fluids 16(7), pp. 2322-2335, 2004

[5] Zebib A. and Bottaro A., Goertler vortices with system rotation: linear theory, Physics of Fluids A 5(5), pp. 1206-1210, 1993

[6] Floryan J.M. and Saric W.S., Stability of Görtler vortices in boundary layers, AIAA Journal 20(3), pp. 316-324, 1982

Mitteilung

Projektgruppe / Fachkreis: Laminarhaltung und Transition

Numerical Simulations of the High-Enthalpy Boundary Layer on a Generic Capsule Geometry with Roughness

Antonio Di Giovanni, Christian Stemmer

Lehrstuhl für Aerodynamik und Strömungsmechanik,
Technische Universität München,
Boltzmannstr. 15, 85748 Garching b. München.
Email : antonio.digiovanni@aer.mw.tum.de

Reentry capsules are equipped with ablative Thermal Protection Systems (TPS) to protect and insulate the vehicle. Since turbulent heat-transfer rates at the wall can be much higher than laminar ones, the prediction of the laminar-turbulent transition of the boundary layer on the capsule surface is a crucial issue in the realisation of the TPS. Although the flow on the wind-ward side of the capsule is laminar in the first phase of typical return paths, with transition moving from back to front with decreasing altitude, uncertainties on predicting hypersonic transition and the lack of transition criteria have so far constrained the design of the TPS to be based on a fully turbulent flow.

Transition on a reentry capsule with laminar ablated TPS is largely affected by the surface roughness, as classical, linear instabilities are absent for the strongly accelerated boundary layer. Even though extensive experimental investigations have been conducted on capsule models with distributed roughness, further numerical investigations based on new computational methods are still needed [1]. Direct Numerical Simulations (DNS) represent a valuable investigation tool as wind-tunnel experiments at reentry conditions matching all relevant dimensionless parameters including the Damköhler number are extremely difficult.

The presented work is part of a joint effort to investigate laminar-turbulent transition on a generic Apollo capsule geometry and focuses on the influence of the high-temperature effects, such as molecular dissociation and thermal non-equilibrium, on the high-enthalpy boundary layer of the capsule under reentry conditions. By means of the finite-volume code NSMB, DNS are performed for a three-dimensional geometry (capsule at 24° angle of attack) for both the smooth and the rough wall geometry. The gradual inclusion of chemical reactions and non-equilibrium will show the influence of the gas modelling on the stability of linear perturbations in the case of smooth geometry as well as on the steady disturbances developing in the presence of roughnesses.

Parallel DNS are performed on a grid including the shock ahead of the capsule (Fig. 1a). Results from these simulations are used to generate inflow profiles for a more refined, restricted domain for the boundary-layer flow on the wind-ward side of the capsule. On the restricted domain, a 4th-order central discretisation scheme is used on a grid consisting of more than 50 millions points. With regard to reentry missions, a realistic scenario at Ma = 20 at an altitude of H = 57.7 km has been chosen. The roughness patch is modelled modulating the capsule wall with a superposition of sinusoidal functions with different wavelengths and quasi-random phase and amplitude.

To validate the method used to generate the base flows, a comparison between experimental data and numerical results at wind-tunnel conditions are presented for both cold and high-temperature flows.

In the case of a smooth wall, flow profiles under reentry conditions have been analysed by means of Linear Stability Analysis. As a consequence of the strong acceleration of the boundary layer, the base flow was found to be stable with regard to linear perturbations. However, the analysis revealed that the incorporation of dissociation as well as of chemical non-equilibrium significantly reduces the damping rate of the stable modes.

In the case of a rough wall, a simulation database of boundary-layer flows has been generated, including various roughness parameter (e.g. roughness average, roughness-based Reynolds number) and different gas models (ideal gas, chemical/ thermal equilibrium as well as non-equilibrium). The development of the steady disturbance downstream of the roughness patch (Fig. 1b), which is a starting point for stability investigations, is analysed and compared.

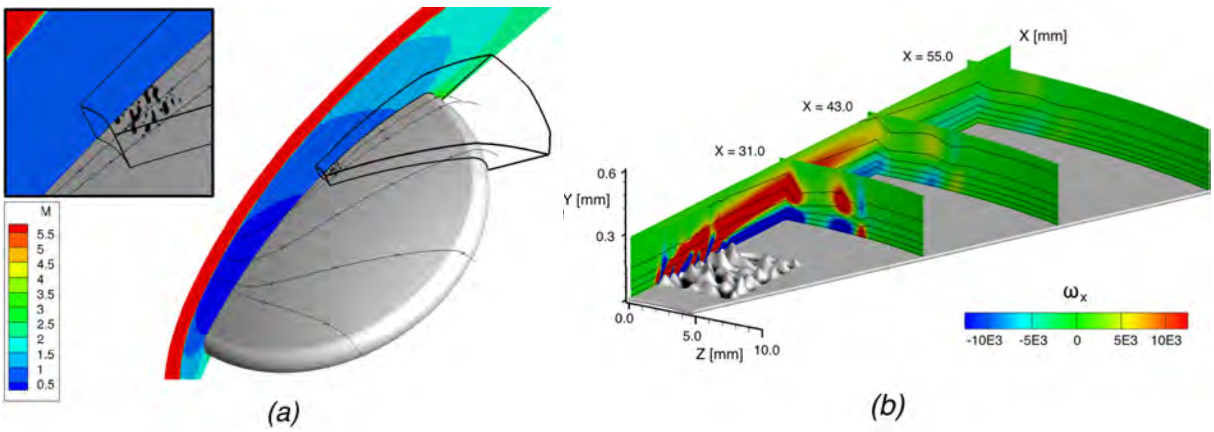

Figure 1: (a) Capsule with roughness patch and schematic representation of the restricted computational domain; symmetry plane coloured by the value of the Mach number (wind-tunnel conditions); (b) vorticity disturbance downstream of the roughness patch.

References

[1] Schneider, S. P., "Hypersonic boundary-layer transition on blunt bodies with roughness", AIAA Paper 2008-501, January 2008.

[2] Stemmer C., Adams N.A., Hein S., Schröder W., Meinke M., Olivier H., Radespiel R., Heitmann D.: Experimental and numerical investigation of hypersonic instabilities in a boundary layer on a capsule with and without high-temperature gas effects. RTO-AVT 200 Specialists Meeting on "Hypersonic Laminar-Turbulent Transition", 32.1-32.26, April 16-19, 2012, San Diego, USA.

[3] Stemmer C., Fehn J.: High-temperature gas effects at a capsule under re-entry and wind-tunnel conditions, AIAA-Paper 2014-2645.

Mitteilung

Projektgruppe / Fachkreis: Laminarhaltung und Transition

Ein-Gleichungs-Transitionsmodell für Profil- und Tragflügelaerodynamik

Michael Fehrs
Institut für Aeroelastik, DLR, Bunsenstraße 10, 37073 Göttingen,
michael.fehrs@dlr.de

Hintergrund

Aeroelastische Probleme beinhalten in der Regel ein Zusammenspiel aus Trägheits-, aerodynamischen und elastischen Kräften. Für die Behandlung aeroelastischer Fragestellungen ist daher eine Modellierung eben dieser Kräfte notwendig, um auftretende Effekte hinreichend genau abzubilden. Die vorliegende Mitteilung behandelt den Effekt der Grenzschichttransition auf die aerodynamischen Kräfte im Rahmen der numerischen Strömungsberechnung mittels Reynolds-gemittelten Navier-Stokes-Gleichungen. Laminare Grenzschichtströmungen haben einen erheblichen Einfluss auf die aerodynamischen Kräfte, das Ablöseverhalten der Grenzschicht und Stoßsysteme, die an Profilen und Tragflügeln auftreten. Aus diesem Grund werden valide und robuste Modelle zur Transitionsbestimmung im Bereich der Aeroelastik benötigt.

Zielsetzung

In Bereich hoher Reynolds- und Machzahlen und niedrigen Turbulenzgraden liefern bisherige Korrelationsmodelle unbefriedigende Ergebnisse. Ziel der Arbeit ist eine valide Transitionsbestimmung für die genannten Randbedingungen zu ermöglichen. Hierbei soll das Modell mit modernen CFD-Codes kompatibel sein und nur geringe Vorgaben von Nutzerseite benötigen.

Lösungsansatz

Ein Transitionsmodell wird vorgeschlagen, das auf dem existierenden γ-Re_θ Transitionsmodell [1] aufbaut, dieses vereinfacht und speziell für externe Aerodynamikanwendungen erweitert. Das γ-Re_θ Transitionsmodell wird auf die Transportgleichung für die Intermittenz-Variable γ reduziert:

$$\frac{\partial \rho\gamma}{\partial t} + \frac{\partial \rho U_j \gamma}{\partial x_j} = P_\gamma - E_\gamma + \frac{\partial}{\partial x_j}\left[(\mu + \mu_t)\frac{\partial \gamma}{\partial x_j}\right] \qquad (1)$$

Der Produktionsterm P_γ und der Destruktionsterm E_γ sind gegenüber dem γ-Re_θ Transitionsmodell modifiziert und das Transitionskriterium wird neu bestimmt. Dieses hängt vom Turbulenzgrad τ der freien Strömung und dem Beschleunigungsparameter K ab:

$$Re_{\theta t} = \frac{\rho U \theta_t}{\mu} = f(\tau,\, K)\,. \qquad (2)$$

Hierbei wird der Turbulenzgrad vom Anwender vorgegeben und K direkt in der Grenzschicht berechnet. Das Transitionskriterium genügt daher einer algebraischen Gleichung und die $\widetilde{Re}_{\theta t}$ Transportgleichung entfällt. Das neue Modell wird in Anlehnung an das γ-Re_θ Transitionsmodell als γ Transitionsmodell bezeichnet.

Ergebnisse

Es werden mit dem kalibrierten Modell berechnete Profilumströmungen bis zu Reynoldszahlen $Re = 50{,}0 \cdot 10^6$ und Machzahlen $Ma = 0{,}825$ präsentiert. Dabei zeigt sich, dass befriedigende Ergebnisse im Hinblick auf Reynoldszahl-Effekte erzielt werden. Im Fall von transsonischen Strömungen wird das Ergebnis der Transitionsbestimmung durch die Eigenschaften des zugrundeliegenden Turbulenzmodells im Bezug auf Ablösungen und Stoßlagen beeinflusst.
Abbildung 1 zeigt die Auftriebs- und Widerstandspolare eines modifizierten NLF(2)-0415–Profils bei $Re = 15{,}0 \cdot 10^6$ und $Ma = 0{,}38$. Die e^N-Methode und das γ Transitionsmodell sagen eine Laminardelle voraus, die vom γ-Re_θ Transitionsmodell nicht berechnet wird. Die Bestimmung der Laminardelle und die Änderung der aerodynamischen Beiwerte beim Übergang aus oder in die Laminardelle ist für aeroelastische Fragestellungen von großer Bedeutung, da die Luftkraftderivative Eingangsgrößen für Flatterberechnungen sind.

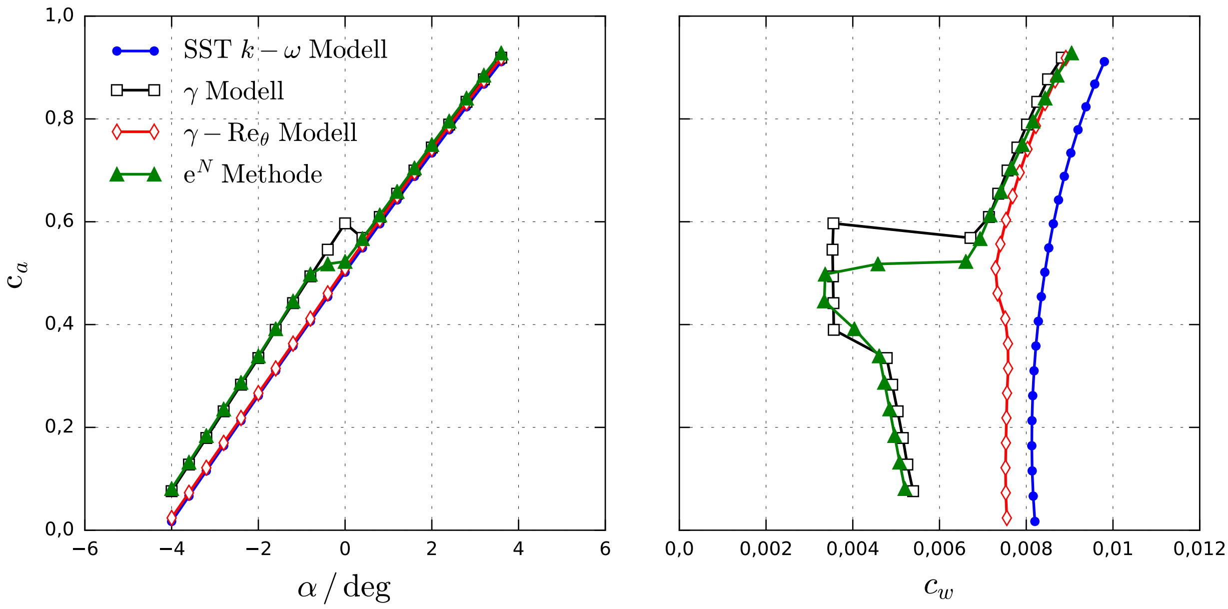

Abbildung 1: NLF(2)-0415M: Auftriebs- und Widerstandspolare.

Literatur

[1] Langtry, R. B. and Menter, F. R., "Correlation-Based Transition Modeling for Unstructured Parallelized Computational Fluid Dynamics Codes," *AIAA Journal*, Vol. 47, No. 12, 2009, pp. 2894–2906.

Mitteilung

Projektgruppe / Fachkreis: Flow Control, Turbomachine, Internal Cooling

Titel: Experimental Investigation of Dynamically Forced Impingement Jet Arrays

Dr.-Ing. Frank Haucke
Technische Universität Berlin, Fakultät V – Verkehrs- und Maschinensysteme,
Institut für Luft- und Raumfahrt, FG Aerodynamik, Sekr. F2
Marchstraße 12-14, 10587 Berlin,Germany,
Frank.Haucke@ilr.tu-berlin.de

Within the framework of the German Collaborative Research Centre "SFB 1029", dynamically forced impingement cooling is investigated experimentally. This will provide a contribution to compensate the critical effects of a turbine inlet temperature increase induced by innovative combustion concepts. The present study describes experimental investigations regarding dynamically forced heat transfer between a flat surface and an array of up to 7 by 7 circular impingement jets. Fast switching solenoid valves are used to periodically pulse each cooling jet separately by changing frequency, duty cycle and phasing. Depending on the excitation parameters, strong ring vortices can be generated around each single jet. Thereby, the maximum velocity within the core zone of each single jet can be extremely increased. Simultaneously, the vorticity is increased, which induces higher local and temporal wall shear stress after impinging on the wall and thus enhanced convective heat transfer as well. Considering a multi nozzle arrangement, the vortex structures of each impingement jet will interfere with the adjacent ones, which strongly influences convective heat transfer.

Liquid crystal thermography (LCT) is employed to determine the distribution of the Nusselt number in the impingement area under steady state and dynamically forced flow conditions. The LCT foil is of type Hallcrest "TKTLCR25C5WM" and has an adhesive backing, which is used to attach it to a thin steel foil. The unaffected side of the steel foil is directed to the impingement jets. The visible side of the LCT foil is placed on a transparent, even glass plate, which is used as an impingement plate. In order to fix the LCT assembly on the glass plate, the edges are sealed and the trapped air is sucked out by a vacuum pump, thus creating a vacuum and pressing the laminate together. The steel foil is connected to a power source and can be heated by controlling the electrical current. Simultaneously, each impinging jet is cooling the steel foil, which affects a wall heat flux. Depending on the resulting local wall temperatures, the liquid crystals reflect specific wave lengths originating from a light source through the glass plate back to a color camera. These wave lengths are read out from the camera sensor as RGB values. In a post process, these RGB values will be converted in values of Hue, saturation and intensity. In order to complete this temperature measurement technique, both a geometrical and a color calibration are necessary for dewarping and allocating the real quasi wall temperatures.

In order to achieve a better physical insight, a time resolved PIV measurement system is used to achieve the two-dimensional velocity flow field. DEHS-droplets, each with a diameter of about $1\mu m$, are used as tracer particles and are produced by a seeding generator, which is integrated in the compressed air supply of the corresponding impingement jets. Two pulses of high energy laser light with a wavelength of $527nm$ are used in order to visualize the DEHS-tracer particles. Therefore, a ND:YLF double pulse laser *Quantronix Darwin-Duo-PIV-80* is employed, which allows a maximum repetition rate of the laser pulses of 10kHz. The pulse energy depends on the repetition rate and varies between $15mJ$ and $30mJ$. Two high speed cameras of the type *Photron APX RS* are arranged stereoscopically to capture the laser light scattered by the DEHS-droplets. In this case, the determination of all three velocity components in the analyzed two dimensional layer is possible. The cameras are equipped with a CMOS-sensor, which allows a maximum frame rate of 3 kHz at full resolution of 1024px by 1024px. Thereby 2048 single images can be buffered on the internal memory. Based on these specifications, 1024 double images at a frame rate of 1.5 kHz can be captured. Case by case, the spatial resolution is reduced to 640px by 480px in order to achieve a higher frame rate of 8 kHz and thus a higher temporal resolution.

In the present experimental study, detailed heat transfer investigations have been performed at a Reynolds number of Re_D = 8000. Thereby, the effect of impingement distance and pulse frequency on the local heat transfer is analyzed in more detail. The results show a significant potential in heat transfer enhancements due to the dynamic forcing. Using the most effective pulse parameter, the percentage rise of the local Nusselt number is up to 50%, compared to corresponding steady state blowing case. Generally, the convective heat transfer rises with decreasing impingement distances.

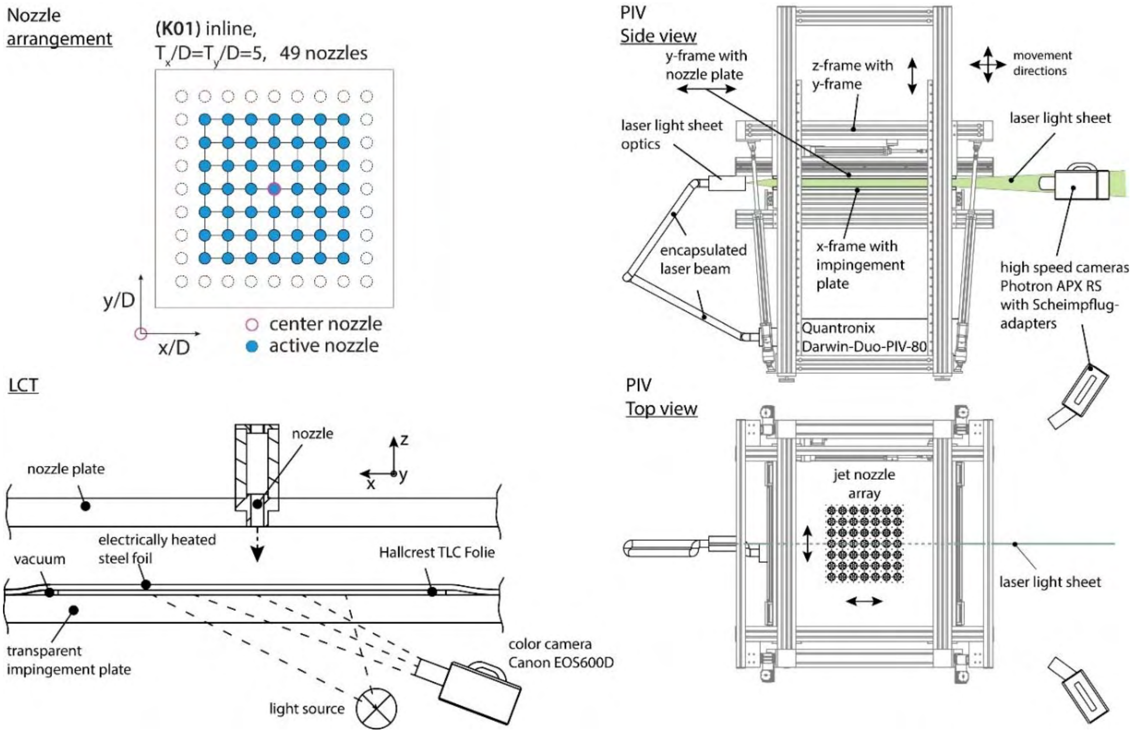

Fig. 1: Experimental Setup.

Furthermore, the results show that pulsed blowing at an impingement distance of *z/D* = 5 is capable to outperform the Nusselt number profile for *z/D*=1 determined under steady state blowing conditions. The most efficient combination of pulse parameters is found at a Strouhal number of Sr_D = 0.12, which corresponds to a pulse frequency of f=100Hz, and an amplitude of *AMP* = 0.8. These values are valid for the employed actuator system. Accompanying PIV measurements clarify the impact of dynamic forcing on the local flow field. Per pulse cycle a sequence of several toroidal vortices can be generated that are capable to reach and to interact directly with the impingement plate. Thereby, on time average the level of velocity and vorticity close to the wall is increased compared to the steady blowing case, which is the main reason for the increase in time averaged Nusselt numbers.

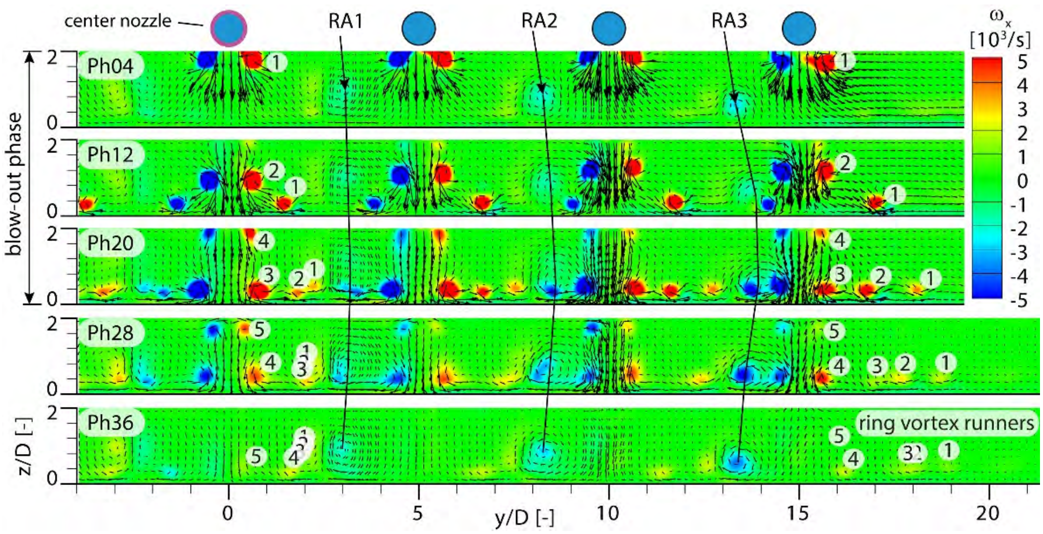

Fig. 2: Vorticity distribution of interacting impingement jets.

ACKNOWLEDGMENT

The authors gratefully acknowledge support by the Deutsche Forschungsgesellschaft (DFG) as part of the Collaborative Research Centre SFB 1029 “Substantial efficiency increase in gas turbines through direct use of coupled unsteady combustion and flow dynamics”.

Mitteilung

Projektgruppe/Fachkreis: Flow Control, Transition und Laminarhaltung

Linear and nonlinear growth of secondary instabilities of stationary crossflow vortices studied by PSE

S. Hein
DLR – Institut für Aerodynamik und Strömungstechnik
Abteilung Hochgeschwindigkeitskonfigurationen
Bunsenstr.10, 37073 Göttingen, stefan.hein@dlr.de

Introduction

Laminar–turbulent transition in three-dimensional boundary layers is often caused by stationary or travelling crossflow instabilities. At low turbulence levels, as in free flight, stationary crossflow vortices usually dominate in amplitude because they are promoted by surface roughness. Further downstream those stationary crossflow vortices reach rather high amplitudes and thus tend to saturate in amplitude. High–frequency secondary instability modes that finally trigger laminar–turbulent breakdown probably are introduced directly into the disturbed boundary layer by environmental disturbances via a yet unknown receptivity mechanism in this case. In some previous work this transition scenario was therefore studied by successive application of two different numerical methods. In a first step the nonlinear development of the stationary crossflow vortices and their subsequent saturation in amplitude was either simulated by PSE (e.g. in [1],[2]) or the saturation stage was directly modelled by nonlinear equilibrium solutions [3]. The resulting steady flow was then used as input for a subsequent linear secondary instability analysis based on Floquet theory or a more general 2D eigenvalue problem formulation.

Numerical approach

In contrast to previous literature the numerical approach used here makes use of a bi–directional coupling of a nonlinear PSE code (the DLR/FOI NOLOT code) with a secondary instability analysis code based on Floquet theory (see [3] for details about the latter code). The NOLOT/PSE code provides the primarily disturbed mean flow needed as input for a secondary instability analysis as described above. However, selected secondary eigenmodes computed with the secondary instability analysis code then are imported back into the nonlinear PSE computations and used there as initial conditions for subsequent studies on linear and nonlinear development of the secondary instability modes further downstream. Thereby, both the effects of flow non–parallelism on the secondary instability growth and the nonlinear stages of secondary instability development are covered. Hence, the feedback of the finite-amplitude secondary instability modes on the stationary crossflow vortices during the later stages of crossflow-dominated laminar-turbulent transition is also modelled by the present approach, i.e. stages where the usual classification into primary and secondary disturbances is no longer justified.

Results

The new approach has been tested for the setup of the DLR swept–flat plate experiment. Stationary crossflow vortices of fundamental spanwise wavelength were initialized at a chord position $x_c/c \approx 0.04$, represented by Fourier mode (0,1) in the nonlinear PSE computations. Slightly further downstream the stationary crossflow vortex mode starts to be amplified and

a) b)

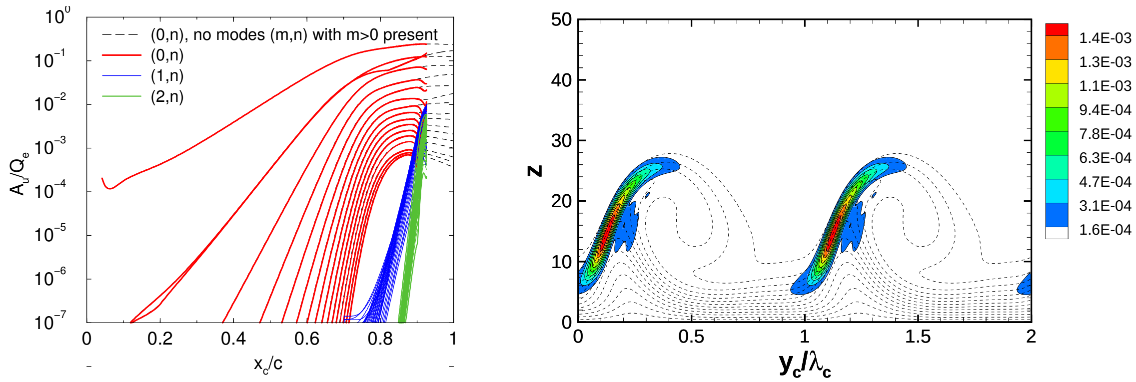

Figure 1: a) PSE results showing the nonlinear development of stationary crossflow vortices represented by modes (0,n), the linear and nonlinear growth of a high-frequency secondary instability (modes (1,n)) and its first higher harmonic (modes (2,n)). b) RMS isocontours of the u_v-velocity component of the high-frequency secondary instability in a wall-normal plane at chord position $x_c/c = 0.85$ plotted on top of the isolines (dashed) of the time–averaged velocity component in x_v-direction. The x_v-direction is locally aligned with the direction of the primary stationary crossflow vortex axis.

as its amplitude increases successively higher harmonics (0,n) are generated nonlinearly (Fig. 1a). Due to these modes, regions of high shear develop in the mean flow which support the growth of high–frequency secondary instabilities. A low-amplitude high–frequency secondary instability was added to the PSE computation at $x_c/c \approx 0.70$ (Fig. 1a). This secondary mode develops into the structure shown in Fig. 1b and nonlinearly generates higher harmonics. The subsequent nonlinear disturbance development could be studied up to the stages where the feedback of the finite–amplitude secondary instability modes on the stationary crossflow vortices is no longer negligible (Fig. 1a). At those stages of laminar-turbulent transition the skin-friction coefficient starts to deviate from that due to the mean flow distortion caused by the stationary crossflow modes alone. This could be used as a criterion for imminent laminar–turbulent transition within the saturation region of the stationary crossflow modes, which was lacking in any nonlinear PSE analysis of crossflow–dominated transition until now.

Literature

[1] Janke E., Balakumar P.: On the secondary instability of three–dimensional boundary layers. *Theoret. Comput. Fluid Dynamics* **14**:167-194, 2000.

[2] Li F., Choudhari M.M.: Spatially developing secondary instabilities in compressible swept airfoil boundary layers. *Theoret. Comput. Fluid Dynamics* **25**:65-84, 2011.

[3] Koch W., Bertolotti F.P., Stolte A., Hein S.: Nonlinear equilibrium solutions in a three–dimensional boundary layer and their secondary instability. *J Fluid Mech.* **406**:131-174, 2000.

Mitteilung

Projektgruppe / Fachkreis: Flow Control

Flow manipulation by standing acoustic waves and visualization with background oriented schlieren (BOS)

Christian Kiefer*, Dara Feili and Helmut Seidel
Saarland University – Chair of Micromechanics,Microfluidics/Microactuators
Uni Campus, Gebäude A5.1, 66123 Saarbrücken, Germany
c.kiefer@lmm.uni-saarland.de

A novel approach for flow manipulation to reduce the frictional losses of turbulent flow zones is presented: flow manipulation by focused acoustic waves. Focused acoustic waves are well known and can be used to levitate small objects. This effect is called acoustic levitation and was first described in 1933 [1]. It can also be used as a trap for cold gases, revealing visual patterns in the shape of a fir tree. This was shown by R. Tuckermann and S. Bauerecker at a frequency of 40 kHz [2]. Acoustic levitation is possible when a standing wave with very high sound pressure (>120 dB) is generated by a setup of a transducer and a reflector in a distance of $n \cdot \lambda/2$. Alternatively, one or more arrays of acoustic transducers can be used, focusing in one point to highly increase the sound pressure (shown by Y. Ochiai *et al*. [3]). With this method it is even possible to create three-dimensional standing waves.

This principle can also be used for flow manipulation. The underlying idea is that the standing waves are like ”virtual riblets”, which can lead to a reduction of turbulent friction analogous to a shark skin. Figure 1 shows the influence of a standing wave on a hot convective current generated by a halogen bulb with 50 W. This effect is visualized by the background-oriented schlieren method (BOS) [4]. In direct comparison it can be seen that by the influence of the standing wave the hot gas is streaming in expanded and lamellar form. For additional visualization, levitating polystyrene balls were placed in the acoustic nodes (black points).

Our intention is to use this approach for drag reduction on airplanes. For this purpose a planar actuator incorporating an array of ultrasound transducers is required that can be fully integrated into the surface of an airfoil. Figure 2 shows a schematic diagram of the planned actuator with an array of 5x5 single transducers operating at a frequency of 40 kHz. Driving the transducers in a phase shifted mode generates a focus zone in the center which alternates into the plus and minus sound pressure like an antinode. By building a cluster of several arrays and driving the actuators pair wise with a phase-shift of 180° generates a ”virtual standing wave” with only planar actuators.

The sound patterns can be adjusted continuously by adapting the phase and the frequency of the individual transducers, which can be implemented in a closed loop control system, including appropriate sensors. This opens up the future prospect to control and reduce the turbulent drag significantly.

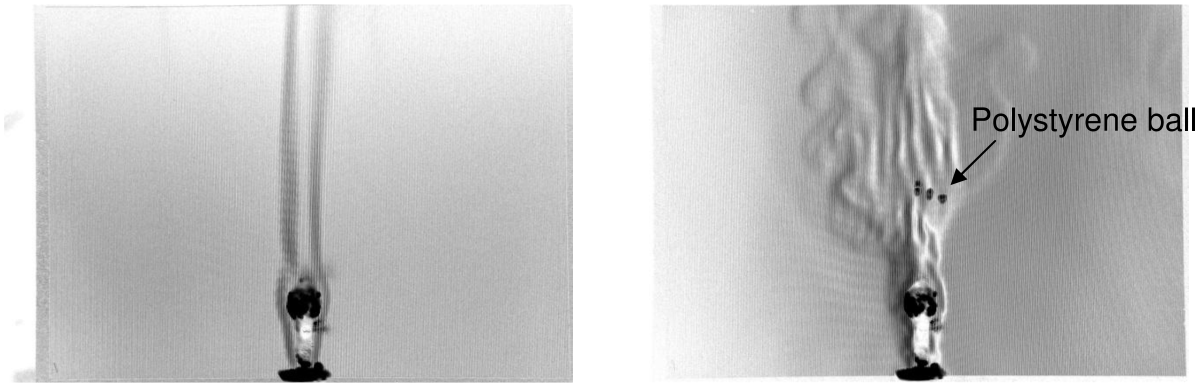

Figure 1: BOS visualization of hot streaming generated by a halogen bulb. Left: uninfluenced, right: influenced by a standing wave.

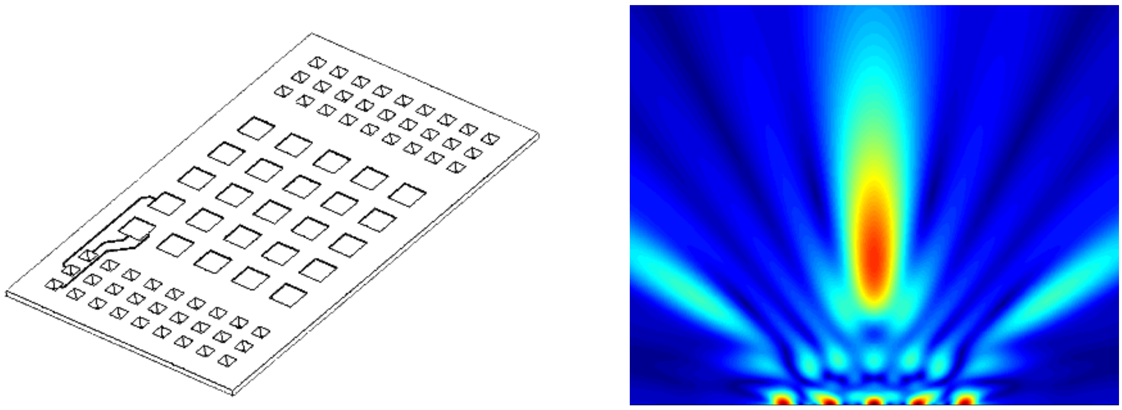

Figure 2: Left: Drawing of the planned planar transducer with 5x5 single ultrasonic transducer. Right: Simulated sound field (pressure distribution) of an array (5x5) of planar transducers operating at 40 kHz. A phased array operation generates a focus in the center.

[1] K. Bücks, H. Müller: Über einige Beobachtungen an schwingenden Piezoquarzen und ihrem Schallfeld, Zeitschrift für Physik Volume 84, Issue 1-2 , pp 75-86, January 1933
[2] R. Tuckermann and S. Bauerecker: Wie akustische Kaltgasfallen wirken. ”Tannenbäume” im stehenden Ultraschallfeld, Chemie in unserer Zeit, Volume 42, Issue 6, pages 402-407, December 2008
[3] Y. Ochiai, T. Hoshi, and J. Rekimoto: Pixie Dust: Graphics Generated by Levitated and Animated Objects in Computational Acoustic-Potential Field, ACM Transactions on Graphics, vol. 33, article no. 85, 2014
[4] H. Richard and M. Raffel: Principle and applications of the background oriented schlieren (BOS) method, Measurement Science and Technology, Volume 12, Number 9, August 2001

Mitteilung

Projektgruppe / Fachkreis: Flow Control

AIR OUTLET DESIGN FOR A PASSIVELY DRIVEN HYBRID LAMINAR FLOW CONTROL SYSTEM

Udo Krause, Peter Kreuzer, Hubert Stuke

Airbus Operations GmbH, Component Aerodynamics Bremen
Airbus Allee 1, 28199 Bremen

e-mail: udo.krause@airbus.com, peter.kreuzer@airbus.com, hubert.stuke@airbus.com

Abstract:
Hybrid Laminar Flow Control (HLFC) is one of various promising future aircraft applications intended to reduce drag and hence also fuel consumption. Airbus investigated laminar flow control technology in previous decades with active suction at the leading edge of the vertical tail plane (VTP). These previous investigations lead to several flight test campaigns. The most important projects were ELFIN, ELFIN II, A320 HLF fin ([1] and [2]), HYLTEC and ALTTA [3], where the focus was mainly on suction of the wing or VTP leading edge region to keep the flow laminar.

Recent HLFC approaches concern not only laminar flow control but also system details such as internal compartment shape and air outlet design. One possible technical solution involves passively driving the system through suction at an air outlet. The current CFD investigation is intended to aid the definition of a robust system solution that will be implemented on a flight test aircraft in upcoming years. Here, HLFC will be applied at a specified VTP section.

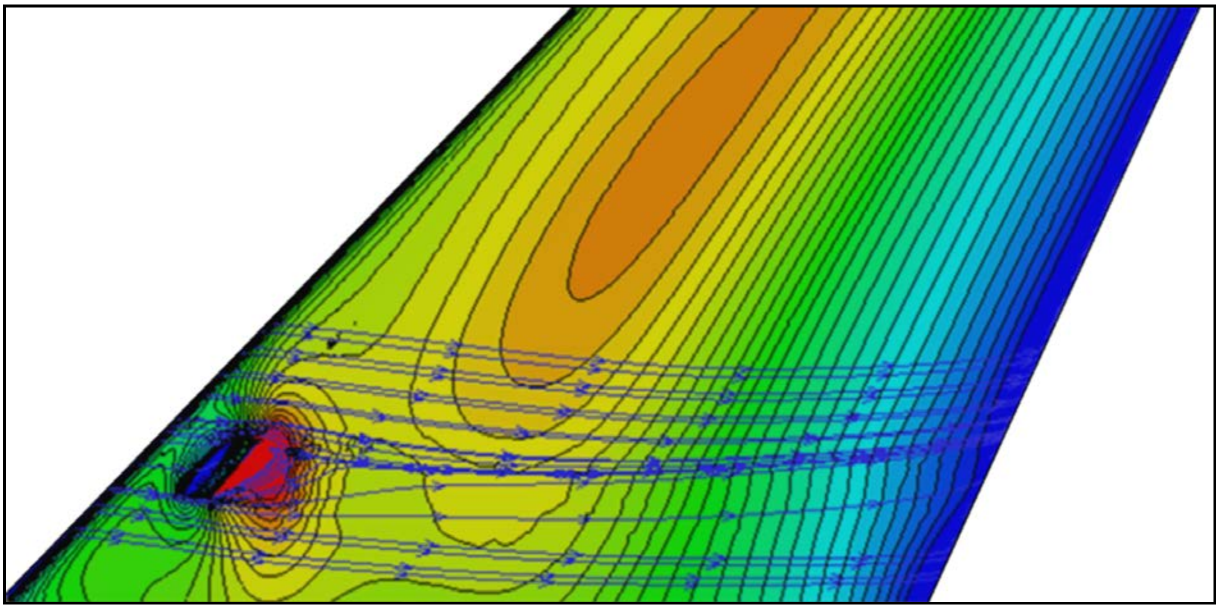

Figure 1: Vertical Tail Plane with lower air outlet location to passively drive HLFC

This CFD investigation was carried out on a typical passenger aircraft. Variations of outlet size, shape, opening angle and location were investigated. A detailed analysis

of typical cruise flight conditions, i.e. variations of Mach number, flight level, AoA and sideslip angle, was performed.
The focus of this investigation is the aerodynamic performance of the outlet; laminar flow control is not included in the CFD simulations.

The DLR-TAU RANS solver was used for this investigation. A sensitivity study was first performed with application of different turbulence models. Finally the Menter-SST (Shear Stress Transport) turbulence model was chosen for all subsequent computations. This two-equation eddy-viscosity turbulence model is very robust and gives reasonable physical outcomes. Additionally this turbulence model is also commonly used and has been validated for other air intake and air outlet applications.

The main results of the investigation were the achieved suction pressures and hence the mass flows driven through the system. There were large differences in system efficiency depending upon the outlet location and shape. A system mass flow requirement in order to apply HLFC at a specified VTP section was fulfilled by all three investigated air outlet locations: at the VTP tip, at a middle location and at a close-to-root location. However, the aerodynamic performance of these air outlets was very different. The locations at the VTP tip and mid-VTP required large outlet areas and / or large flap opening angles. This generated high aerodynamic drag. The lower VTP location was found to be the most promising compromise with respect to the achieved suction pressures and associated aerodynamic drag.

References

[1] R. Henke, “A320 HLF FIN Flight Tests Completed”. *Air&Space Europe* Vol. 1 No 2, 78-79, 1999.

[2] G. Schrauf, “Evaluation of the A320 Hybrid Laminar Fin Experiment”. ECCOMAS 2000, Barcelona, Spain, September 11-14, 2000.

[3] G. Schrauf, H. von Geyer, “Simplified Hybrid Laminar Flow Control for Transport Aircraft”. ECCOMAS 2012, Vienne, Austria, September 10-14, 2012.

[4] H. Hansen, „Laminar Flow Technology – The Airbus View”. ICAS 2010, Nice, France, September 19-24, 2010.

Mitteilung

Projektgruppe / Fachkreis: Laminarhaltung und Transition

Bestimmung des kritischen N-Faktors für Querströmungsinstabilität für den Niedergeschwindigkeits-Windkanal Braunschweig (DNW-NWB)

Martin Kruse[1], Albert Küpper[2], Rouven Petzold[3], Federico Munoz[4]
[1]DLR, Lilienthalplatz 7, 38106 Braunschweig, martin.kruse@dlr.de
[2]DNW-NWB, Lilienthalplatz 7, 38106 Braunschweig, albert.kuepper@dnw.aero
[3]Volkswagen AG, Brieffach 1737, 38436 Wolfsburg, rouven.petzold@volkswagen.de
[4]Institut für Strömungsmechanik, TU-Braunschweig, Hermann-Blenk-Straße 37, 38108 Braunschweig, f.munoz@tu-braunschweig.de

Zusammenfassung

Nach dem Umbau des DNW-NWB zum turbulenzarmen Akustikkanal bietet sich dieser Windkanal für experimentelle Untersuchungen mit freier Transition im Niedergeschwindigkeitsbereich besonders an. Durch die Verbesserung der Strömungsqualität sind jedoch ältere Angaben zu kritischen *N*-Faktoren für den NWB überholt und bedürfen der neuerlichen Bestimmung anhand von Validierungsexperimenten. Küpper & Rohhardt [1] zeigten bereits an einem 2D-Profil, das im NWB für Tollmien-Schlichting Instabilität kritische Werte von N_{TScrit} = 11.8 erzielt werden können. Mit Hilfe eines weiteren Transitionsexperiments soll nun der kritische *N*-Faktor für Querströmungsinstabilität N_{CFcrit} bestimmt werden.
Als geeignetes und verfügbares Modell für Experimente mit Transition durch Querströmungsinstabilität wurde das Sichelflügelmodell der TU-Braunschweig ausgewählt [2]. Das Modell ist durch seine, in drei Segmenten spannweitig veränderliche Pfeilung charakterisiert. Abhängig vom Anstellwinkel, der Reynoldszahl und der Flügelseite, können verschiedenste Umschlagszenarien in den einzelnen Flügelsektionen erzielt werden. Eine im Modell integrierte Heizung sowie der Aufbau der Oberfläche ermöglichen hohen Kontrast für Transitionslagenbestimmung mittels Infrarotthermographie. Weiterhin ist der Flügel mit insgesamt 108 Druckmessbohrungen in drei Schnitten ausgerüstet. Abbildung 1 zeigt das in die geschlossene Messstrecke des NWB eingerüstete Windkanalmodell.
Im Rahmen der Messkampagne wurden zahlreiche Anstellwinkelreihen bei Reynoldszahlen zwischen $2{,}7 \cdot 10^6$ – $4{,}5 \cdot 10^6$ gefahren. Das Transitionsverhalten wurde dabei anhand der Wärmeabstrahlung des beheizten Modells gemessen. Pro Seite des Flügels stand hierzu jeweils eine IR-Kamera mit Weitwinkeloptik (f=12mm) zur Verfügung. Eine dritte IR-Kamera wurde für Detailaufnahmen eingesetzt. In Folge schräger Betrachtungswinkel der Hauptkameras sowie der Linsenaberration der Weitwinkelobjektive entsteht eine Bildverzeichnung, die durch einen entsprechenden Entzerralgorithmus korrigiert wird. Der entwickelte Entzerralgorithmus nutzt vorab erstellte Kalibrieraufnahmen des installierten Flügels, so dass während der Transitionsmessungen keine Störung der Grenzschicht durch Positionsmarkierun-

Abbildung 1: Sichelflügel im DNW-NWB

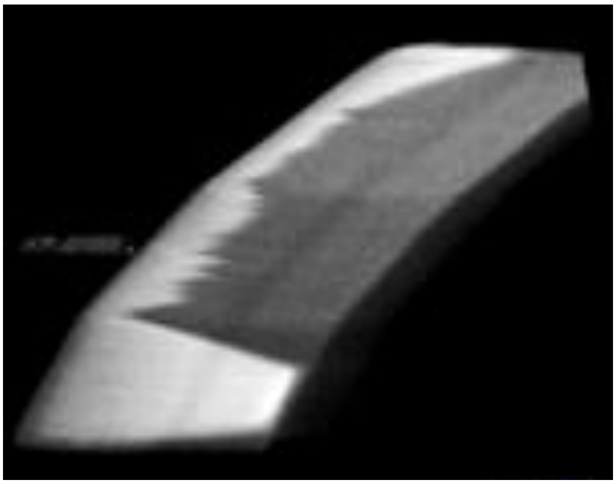

Abbildung 2: entzerrte IR-Aufnahme

gen auftritt. Abbildung 2 zeigt eine derart bearbeitete IR-Aufnahme.
Für die Auswertung der spannweitigen Transitionslinie wurde ein automatisiertes Bildverarbeitungsverfahren entwickelt. Dieses detektiert den Ort des Grenzschichtumschlags anhand eines Temperaturgradientenkriteriums. Um Fehler durch Bildrauschen zu vermeiden, wird ein eigenschaftserhaltenes Filterungsverfahren eingesetzt. Alle Arbeitsschritte der Transitionslagenbestimmung einschließend, ergibt sich für die Standartabweichung der Ortsauflösung ein Wert 3,25mm, entsprechend 0,41% der Flügeltiefe.
Zur Berechnung der 3-D Grenzschichtdaten werden hochaufgelöste numerische Simulationen unter Vorgabe der experimentell bestimmten Transitionslage mit dem RANS Strömungslöser *TAU* durchgeführt. Um eine möglichst exakte Nachrechnung der im Experiment vorliegenden Bedingungen zu erreichen, wird die Messstrecke des Windkanals sowie die Düse für die Berechnung mit modelliert. Es zeigt sich, dass hierdurch eine sehr gute Übereinstimmung zwischen experimenteller und numerisch gewonnener Druckverteilung erzielt wird.
Für die Stabilitätsanalyse der Grenzschicht wird das lokale, lineare Stabilitätsanalyseverfahren *lilo* eingesetzt. Die Integration der lokalen Anfachungsraten erfolgt entlang von Grenzschichtrandstromlinien, welche als Approximation der Gruppengeschwindigkeitstrajektorie herangezogen werden [3]. Für eine nahezu flächenhafte Abtastung werden pro Seite des Flügels 108 Stromlinien ausgewertet. Für jede der Stromlinien wird am Ort der vorgegebenen Transitionslinie das Wertepaar N_{TScrit} und N_{CFcrit} ermittelt. Durch Selektion von genügend Testfällen mit querströmungsdominiertem Umschlagverhalten ($e^{N_{CF}} >> e^{N_{TS}}$) lässt sich ein Unsicherheits-gewichtetes, arithmetisches Mittel für den gesuchten Wert N_{CFcrit} bilden. Von der Auswertung ausgenommen werden Bereiche stark veränderlicher Querströmung (siehe Schraffur Abb. 4, Pfeilungsübergänge, Flügelspitze), da hier Grundannahmen der lokalen linearen Stabilitätstheorie verletzt werden. Auf Grundlage der bisher ausgewerteten Fälle ergibt sich für den NWB ein kritischer *N*-Faktor für Querströmungsinstabilität von $\overline{N_{CFcrit}} = 8{,}4 \pm 0{,}8$.
Eine auffällige Abhängigkeit der ermittelten kritischen N_{CF}-Faktoren von der Flügelseite ist Gegenstand aktueller Arbeiten, in denen der Einfluss von Krümmungs- und nichtlokalen Effekten sowie der Einfluss der Oberflächenrauhigkeit untersucht wird.

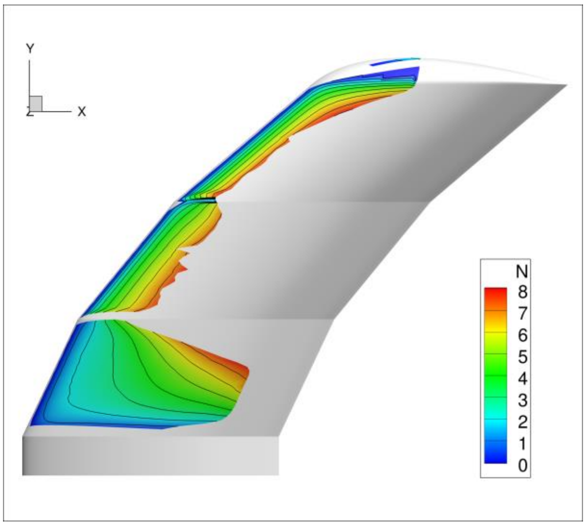

Abbildung 3: Konturdarstellung N_{CF}

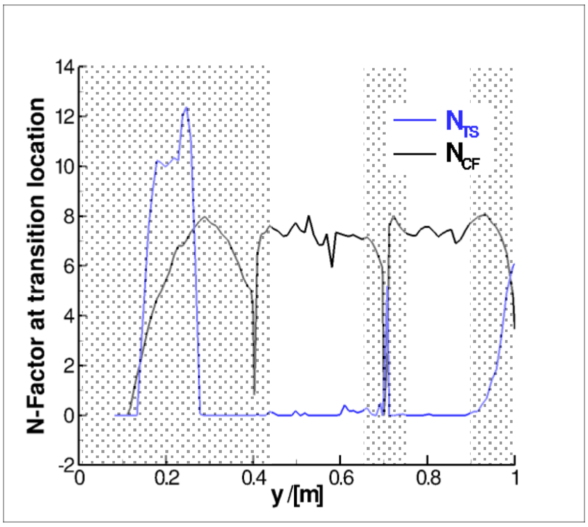

Abbildung 4: Spannweitige N_{TS} & N_{CF} Verteilung

1] Rohardt, C.-H., Küpper, A. : *Determination of the NTS-factor for the DNW-NWB.* 19. DGLR-Fach-Symposium der STAB, 4.-5. November 2014, München.
[2] Petzold, R. : Einfluss stark veränderlicher Querströmung auf den laminar turbulenten Grenzschichtumschlag, NFL-Forschungsbericht 2014-10, Dissertation TU-Braunschweig, ISBN 9783844032505, 2014.
[3] Krimmelbein, N., Radespiel, R.: Transition prediction for three-dimensional flows using parallel computation. Comp. Fluids, 2008. doi:10.1016/j.compfluid.2008.01.004

Die gezeigten Arbeiten wurden im Rahmen einer Beauftragung des DLR durch den DNW-Research-Fond durchgeführt.

Mitteilung

Projektgruppe / Fachkreis: Laminarhaltung und Transition

Experimental studies on the receptivity of stationary crossflow modes to pneumatic actuation

J. Lohse, A. Berthold and W. Nitsche
TU Berlin, Institut für Luft- und Raumfahrt, Marchstraße 12, 10587 Berlin
jakob.lohse@ilr.tu-berlin.de

The transition process induced by stationary crossflow vortices has been extensively studied in the last 30 years experimentally, theoretically and by means of DNS. Saric et al. (1998) successfully employed a passive control mechanism where the crossflow disturbance is forced with a spanwise row of distributed roughness elements (DRE), Wassermann & Kloker (2002) proposes nearly the same concept, named Upstream Flow Deformation (UFD). Both introduced a system of narrower spaced longitudinal crossflow vortices into the three-dimensional boundary layer in order to weaken the growth of the naturally most amplified crossflow mode. Thus, the onset of high frequency secondary instability and the following laminar-turbulent transition is shifted farther downstream. Using this control strategy in combination with a pneumatic actuator, experiments have been performed in the redesigned Bippes experiment at the DLR Göttingen. It was shown that both methods, steady blowing as well as steady suction are suitable for transition control. Although blowing enables a significant shift of the transition position in chordwise direction, it is limited by bypass transition at the actuator position while this was not an issue in the suction case (Lohse et al. (2016)).
In the present work we experimentally continue this control strategy and investigate the possibility of a pneumatic actuator system for generating high-amplitude artificial crossflow vortices with a selected wavelength without bypass transition. All experiments were conducted in a closed-loop wind tunnel at TU Berlin. The test section used for the measurements in the three-dimensional boundary layer is depicted in figure 1. A displacement body imposes a negative and thus favorable pressure gradient on a swept flat plate. In conjunction with the geometric sweep angle of 45°, crossflow instabiliti es are amplified while Tollmien-Schlichting waves are suppressed. Curved end plates minimize spanwise gradients in the flow field and the Reynolds number based on the chord length C was Re_C=960000.

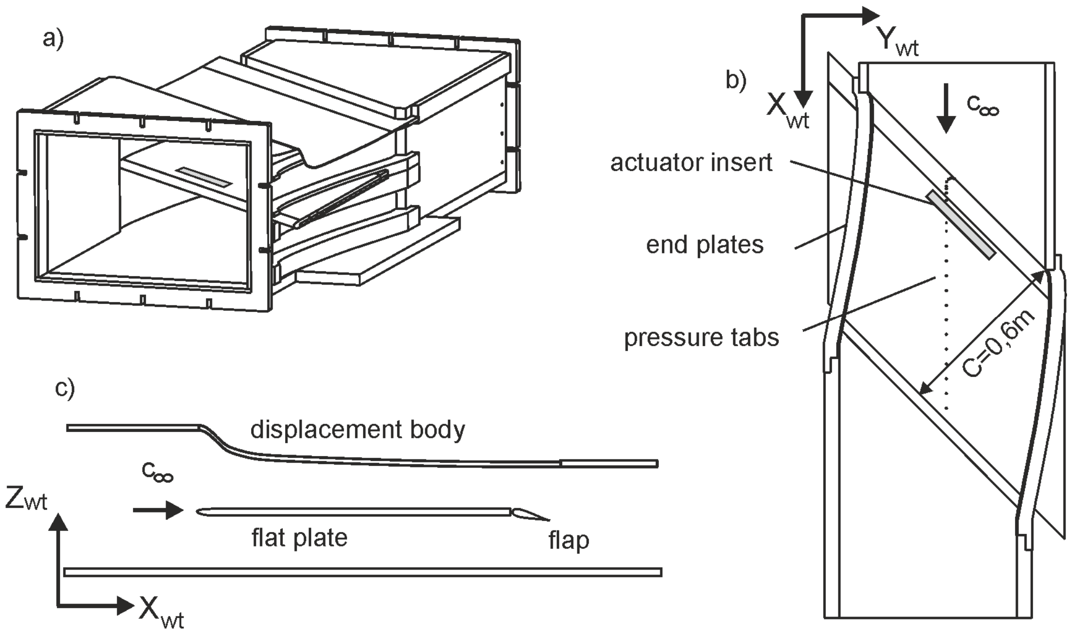

Fig. 1: Experimental setup: a) isometric view b) top view and c) section along the axis of the wind tunnel X_{wt}

The actuator insert enables steady blowing or suction through spanwise-periodic orifices at X/C=0.1. After identifying the base flow properties experimentally with subsequent Linear Stability Analysis, the influence of different actuator parameters were investigated. Therefore the size, the shape and the angle of the actuator orifices was varied. The spanwise distance was kept constant at λ=8mm which is equal to the naturally most amplified crossflow mode. In consequence, the present work rather addresses the receptivity of stationary crossflow modes to different pneumatic actuation parameters than the transition control.

The flow field was investigated using a miniature three-hole pressure-probe mounted on a three-axis traverse indicating the two velocity components parallel to the flat plate. Figure 2 shows the streamwise velocity contours at different chordwise positions for the baseflow and the case with steady blowing through drilled holes with a diameter of 0.3mm. In the baseflow case, stationary crossflow instabilities can be observed in the rear part of the flat plate. Their weak amplification is caused by the interaction of travelling and stationary crossflow waves due to the turbulence level of the wind tunnel. By switching on steady blowing through the actuator holes, the amplitude of the stationary crossflow vortices has increased and the spanwise distribution of the vortices is more homogenous.

The pneumatic concept allows to control the amplitude of the introduced stationary crossflow mode over a wide range by varying the applied momentum coefficient c_μ, which is calculated as a ratio between the introduced momentum by the actuator and the momentum of the boundary layer at the actuator position.

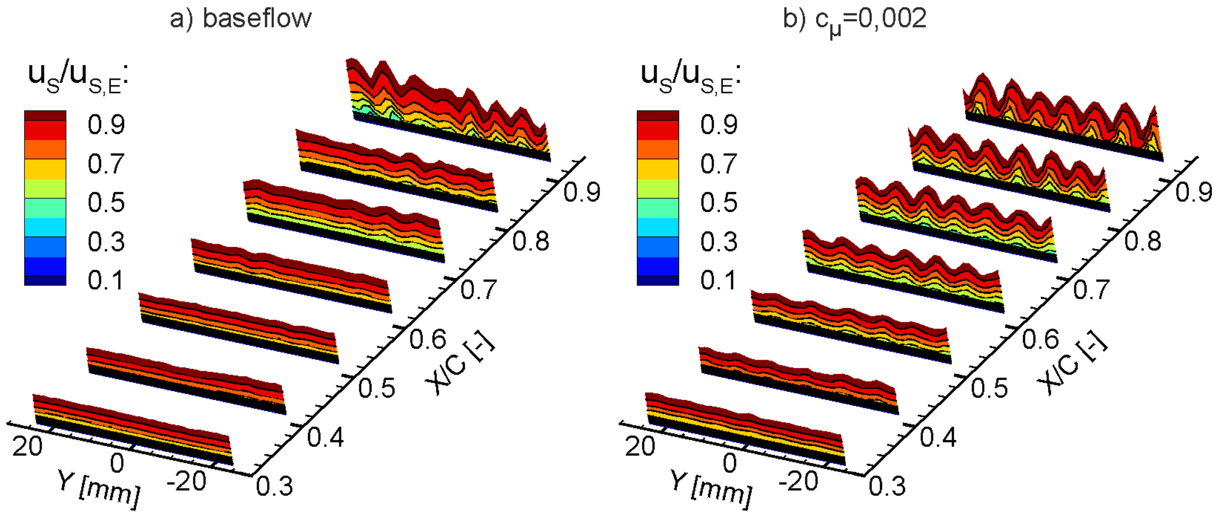

Fig. 2: Streamwise velocity contours: a) baseflow and b) steady blowing through drilled holes with c_μ=0.002

References

Saric, W.S., Carrillo Jr., R.B. and Reibert, M.S. 1998 Leading-edge roughness as a transi tion control mechanism. AIAA Paper 98-0781, 1-13.

Wassermann, P. & Kloker, M. 2002 Mechanisms and passive control of crossflow-vortex-induced transition in a three-dimensional boundary layer. J. Fluid Mech. 456, 49–84.

Lohse, J., Barth, H.P. and Nitsche, W. 2016 Active control of crossflow-induced transition by means of in-line pneumatic actuator orifices. (Accepted for publication in Experiments in Fluids)

Mitteilung

Projektgruppe / Fachkreis: Laminarhaltung und Transition

Direkte numerische Simulation von TS-Wellen hinter der generischen Stufe eines Laminarprofils für Windkanaluntersuchungen

Heinrich Lüdeke
DLR, Lilienthalplatz 7, Heinrich.Luedeke@dlr.de

Kai Backhaus
TU Braunschweig, Hermann-Blenk-Str. 37, Backhaus.Kai@gmail.com

Für die Vorhersage des laminar-turbulenten Überganges an einem umströmten Körper existiert für ebene Fälle mit dem linearen Ansatz der e^N-Methode eine angepasste Theorie, die auch praxisnah einsetzbar ist. Für komplexere Szenarien, wie gescherte oder abgelöste Grenzschichten, Stufen, Wellen oder auch Anlegelinientransition sind fundierte Theorien teilweise erheblich aufwändiger und müssen umfangreich validiert werden. Mit Hilfe der direkten numerischen Simulation (DNS) können einerseits wichtige Validierungsfälle für verbesserte Theorien gestellt werden, vgl. *Kloker (1993)*, andererseits ist für einzelne komplexe Problemstellungen die DNS auch direkt zur Vorhersage des Transitionvorgangs nutzbar.

Direkte Simulationen der Anfachungs-Vorgänge von Tollmien Schlichting (TS) Wellen erlauben die Validierung von Vorentwurfsverfahren auch für Geometrien mit Oberflächenstörungen wie vor- oder rückspringenden Stufen (siehe auch *Lüdeke (2010)*). Ziel der vorliegenden Arbeit ist die direkte numerische Simulation und Untersuchung von lokalen Instabilitäten einer Stufenströmung an einem Laminarprofil. Als Referenz dient das im Rahmen des „ProWinGS"-Projektes im NWB untersuchte Laminarprofil mit einstellbarer Stufe. Für die experimentellen Untersuchungen wurde ein Windkanalmodell ausgelegt, dessen Druckverteilung im Mittelschnitt einem generischen Laminarprofil für eine Transportflugzeugkonfiguration entspricht. Da es sich bei den betrachteten TS-Wellen um zweidimensionale Störungen einer Grenzschicht ohne Querströmkomponente handelt, genügt eine zweidimensionale Simulation der Strömung.

Um hierzu effiziente Einstellungen für die verwendete Numerik zu finden, wurden in früheren Studien durch *Backhaus (2014)* verschiedene DNS-Auswertungen mit Ergebnissen der linearen Stabilitätstheorie erfolgreich verglichen. Zur hochgenauen Lösung der Navier-Stokes-Gleichungen steht mit dem DLR FLOWER-Code ein strukturiertes Finte-Differenzen-Verfahren 4. Ordnung zur Verfügung.

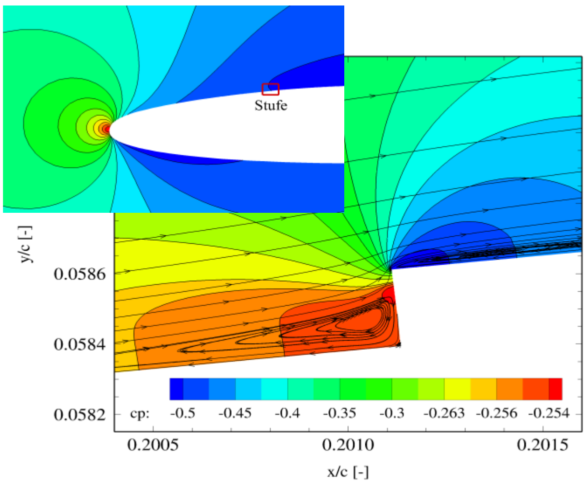

Abb. 1: Strömung über Stufe mit Ablösung, Stufenposition: 20%

Die Rechnungen werden unter Verwendung der Profil-Geometrie und der vollständig vernetzten Stufe durchgeführt. Die Extraktion des kritischen Bereichs vor und hinter der Stufe und eine Netzverfeinerung zur Auflösung der TS-Wellen erlaubt die effiziente zeitgenaue Simulation der Instabilitäten in dieser Region. Für die extrahierte Grenzschicht werden am Einströmrand zeitgenau Störungen vorgegeben, die in Frequenz und wandnormalem Amplitudenverlauf den erwarteten TS-Wellen entsprechen. Aus den Anfachungsraten der TS-Wellen hinter der Stufe lassen sich Rückschlüsse auf die Position des laminar-turbulenten Übergangs ziehen.

Abbildung 1 zeigt die Grundströmung an der Stufe bei 20% Profiltiefe. Als Stufenhöhe wurde der Nominalwert von 0.6 mm, bezogen auf eine Profiltiefe von 2.75 m gewählt, der auch im NWB intensiv vermessen wurde und somit Vergleiche mit der experimentellen Auswertung erlaubt.

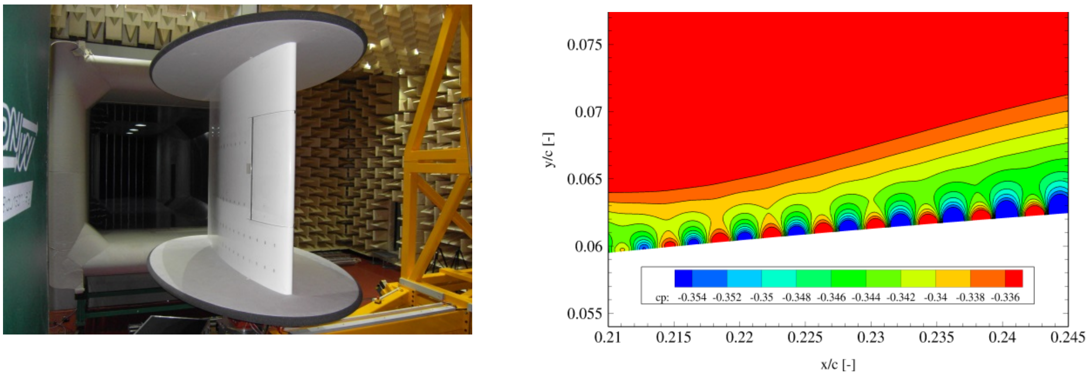

Abb. 2 : Windkanalmodell im DNW-NWB und TS-Wellen Verlauf stromab der Stufe

In Abbildung 2 ist links der Aufbau im Windkanal gezeigt, der mittlere Nasenbereich des Laminarprofils ist mit einem verstellbaren Einsatz versehen, der die Betrachtung unterschiedlicher vor- oder rückspringende Stufen erlaubt und seitlich durch Grenzschichtzäune zur Verbesserung der Grenzschichtqualität erweitert wurde.

Lokale DNS auf unterschiedlich feinen Rechennetzen wurde bei mehreren Strouhalzahlen und Störamplituden über mehrere Millionen Iterationen durchgeführt. Exemplarisch zeigt Abbildung 2 rechts die Ausbildung der TS-Wellen als räumlich angefachte Druckstörung mit einem ausgeprägten Verlauf Stromab der Stufe.

Die in dieser Arbeit vorgenommenen Simulationen liefern die Grundlage für weitere lokale DNS zur Untersuchung von Stufeneinflüssen auf die Stabilität der Grenzschicht. Die verwendete Prozesskette, von der Ermittlung des Strömungsfeldes bis hin zur lokalen DNS mit Implementierung einer Störung, konnte erfolgreich nachvollzogen werden und erlaubt Vergleiche mit den gezeigten Windkanalversuchen.

Die Anwendbarkeit von DNS Ergebnissen zur Validierung von LST-Vorhersageverfahren an Oberflächenstörungen bestätigt sich somit durch die gezeigte Studie erneut.

Kloker, M. (1993) *Direkte numerische Simulation des laminar-turbulenten Strömungsumschlages in einer stark verzögerten Grenzschicht*, Dissertation, Fakultät Verfahrenstechnik der Universität Stuttgart, Institut für Aerodynamik und Gasdynamik

Lüdeke, H., Wartemann, V., Seitz, A. (2010) *Direct Numerical Simulation of Tollmien Schlichting Waves to Support Linear Stability Analysis*, In: Notes on Numerical Fluid Mechanics and Multidisciplinary Design, New Results in Numerical and Experimental Fluid Mechanics VIII, Vol. 121. Springer Verlag, Seiten 227-234.

Backhaus K. (2014) Direkte numerische Simulation der Anfachungsraten von Tollmien-Schlichting-Wellen. Bachelorarbeit Nr. 628 an der TU-Braunschweig.

Mitteilung

Projektgruppe / Fachkreis: Laminarhaltung und Transition

Reattaching Flow Behind a Square Bar Investigated with Temperature-Sensitive Paint

J. Ost*, E. Mäteling§, C. Klein*, D. Puckert°, U. Rist°
*Deutsches Zentrum für Luft- und Raumfahrt e.V. (DLR),
Bunsenstraße 10, D-37073 Göttingen, Germany, jonathan.ost@dlr.de
§ Institut für Luft- und Raumfahrtsystheme, RWTH Aachen
Wuellnerstraße 7, D-52062 Aachen, Germany
°Institut für Aerodynamik und Gas Dynamik, Universität Stuttgart
Pfaffenwaldring 21, D-70569 Stuttgart, Germany

Introduction

Reattaching flow is of major concern for airfoils with steps and separation bubbles. In combination with heat flux a separated flow with reattachment on a surface is significant for the design of heat exchangers. Also for future application of laminar wings this combination is relevant for non-adiabatic wall conditions, e.g. in cases of warmed fuel [8] or batteries providing momentarily great amounts of power.

The flow phenomena of backward facing steps are extensively studied, i.e. the reattachment length of the flow with respect to the step Reynolds number [2] and the coherent structures in the reattached flow [3]. These experiments were mostly conducted in ducts of small aspect ratio and rather large expansion ratios. For square bars, primarily the excrescence's influence on laminar to turbulent transition is investigated [11] or tests were performed in turbulent flow [7]. The combination of excrescences and heat flux is investigated mainly for heat exchanger configurations [1].

Temperature-Sensitive Paint (TSP) is used to visualize flow phenomena which cause a variation in surface temperature or heat transfer coefficient, respectively, e.g. laminar to turbulent transition, vortex footprints, and laminar separation bubbles [10]. The TSP application in water [5], [6] is especially favorable due to the low flow speed and the resulting low propagation speed of flow structures. A systematic study of the wall bound flow phenomena caused by a square bar in a Blasius flow is performed with the TSP method. The Reynolds number Re_{kk} based on the bar height k and the velocity at the upper edge of the bar u_k spans $127 \leq Re_{kk} \leq 1898$.

Experimental Setup

The experiments were conducted in the IAGs Laminarwasserkanal, which is a laminar water tunnel with the test section being an open channel flow [9]. The facility has a turbulence level of 0.02 % (0.1-10 Hz) and velocities up to 0.2 m/s are possible. For the experiment a thin TSP element was manufactured, which is placed on top of the already installed flat plate. This element consists of a substrate made of glass fiber reinforced plastics, an embedded layer of carbon fiber reinforced plastic to electrically heat the model [10] and the TSP coating. The entire TSP element measures 1.07 m in length, 1 m in width and 0.85 mm in thickness. Only the mid third of the model can be heated, the area coated with TSP is 0.25 m wide and symmetric to the model center. The heating is split into two parts, which causes the dark area about 14 square bar heights downstream of the bar, see Figure 1. Due to the high flow quality it was possible to acquire the TSP images through the free water surface. The 2D flow is disturbed by a rectangular bar (height to width ratio of 0.5) with sharp edges, which is placed at x_k = 0.9 m downstream of the leading edge directly on top of the TSP coating.

Result

During the test conditions of laminar, transitional and turbulent reattachment ($127 \leq Re_{kk} \leq 1898$) have been investigated. An example for transitional reattachment ($Re_{kk} = 732$) is given in Figure 1. The flow separation upstream of the square bar is clearly distinguishable because of the low heat flux in the vicinity of flow separation. This leads to the bright line about one bar height in front of the square bar. The flow structures downstream of the excrescence are less distinct. The first part, which is mainly a region of low heat flux, also exhibits streaks of increased heat flux roughly aligned with the main flow direction. These structures end about six bar heights downstream. Between the square bar and the beginning of the first impinging structures, which is roughly 17 square bar heights downstream of the obstacle, the temperature gradually decreases in downstream direction. These structures are characterized by the tips of vortex-like structures that are aligned with the flow. These have a spacing of about 30 mm (indicated by white lines in Figure 1), which is in accordance with Beaudoin et al. [3]. The maximum heat transfer is located approximately at $(x - x_k) / k \approx 22$ and is just preceding the reattachment location [4]. The reattached region has a good heat transfer and is therefore well cooled. The location shift of flow reattachment and the variation of the impinging flow structures to characterize the flow will be shown in the final paper. Furthermore, the influence of the temperature difference between model surface and fluid, which is required for the TSP method, will be addressed, especially for low Re_{kk} at low flow speed.

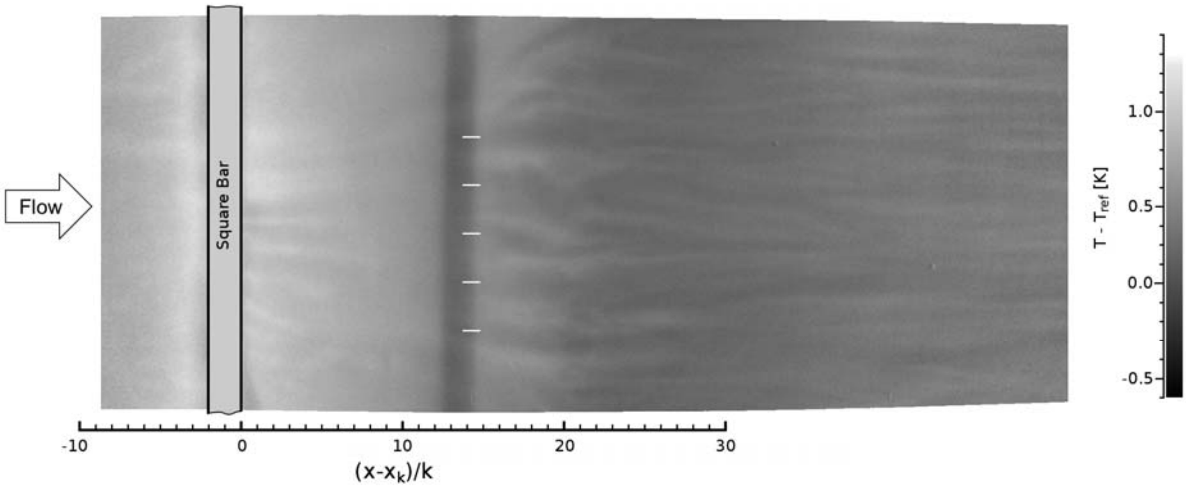

Figure 1: Visualization of the flow over a square bar at $Re_{kk} = 732$. Bright regions correspond to low heat transfer and are therefore warmer than dark regions.

[1] Abu-Mulaweh H.I.: *A review of research on laminar mixed convection flow over backward- and forward-facings steps*, Int. Journal of Thermal Sciences, vol. 42, 2003, pp. 897-909

[2] Armaly B.F., Durst F., Pereira J.C., Schönung B.: *Experimental and theoretical investigation of backward-facing step flow*, J. Fluid Mech., vol. 127, 1983, pp. 473-496

[3] Beaudoin J.-F., Cadot O., Aider J.-L., Wesfreid J.E.: *Three-dimensional stationary flow over a backward-facing step*, European Journal of Mechanics B/Fluids, vol. 23, 2004, pp. 147-155

[4] El-Mehlawy F., Mankbadi R.: *Transient Heat Transfer in Backward Facing Step Flows*, AIAA 90-0554, 1990

[5] Fey U., Klein C., Möller T.J., Pöttner J., Radespiel R., Ondrus V. Beifuß U.: *Investigation of circular cylinder flow in water using Temperature-Sensitive Paint*, New Results in Numerical and Experimental Fluid Mechanics VIII: Contributions to the 17th STAB/DGLR Symposium Berlin, Germany 2010, 2013

[6] Miozzi M., Capone A., Di Felice F., Klein C., Liu T.: *Skin friction fields from TSP surface patterns on an underwater cylinder in crossflow*, 18th Lisbon 2016 Symp. Laser tech. fluid mech., 2016

[7] Moss W.D., Baker S.: *Re-Circulating Flows Associated with Two-Dimensional Steps*, Aeronautical Quarterly, vol. 31, 1980, pp. 151-172

[8] Stock H.W.: *Wind tunnel-flight correlation for laminar wings in adiabatic heating flow conditions*, Aerospace Science and Technology, vol. 6, 2002, pp. 245-257

[9] Strunz M., Ein Laminarwasserkanal zur Untersuchung von Stabilitätsproblemen in der Strömungsgrenzschicht, PhD thesis, University Stuttgart, 1987

[10] Tropea C., Yarin A.L., Foss J.F. (eds.): Chap. 7.4 Transition-Detection by Temperature-Sensitive Paint, Springer Handbook of Experimental Fluid Mechanics, Springer-Verlag, Berlin Heidelberg, 2007

[11] Wang Y.: *Instability and Transition of Boundary Layer Flows Disturbed by Steps and Bumps*, PhD thesis, 2004

Mitteilung

Projektgruppe / Fachkreis: Laminarhaltung und Transition

Transition downstream of cylindrical roughness elements on a flat plate boundary layer

Dominik Puckert, Ulrich Rist
Institut für Aerodynamik und Gasdynamik, Universität Stuttgart
Pfaffenwaldring 21, 70569 Stuttgart
puckert@iag.uni-stuttgart.de

The need for drag-reduction of aircraft increases continuously and a deeper understanding of the laminar-turbulent transition of boundary layers is essential for future designs. In this context, roughness elements in laminar boundary layers have been found to either promote or delay transition, depending on the parameters [1, 3]. A recently published, three-dimensional analysis using linear stability theory (LST) predicts the instability of 'global' modes in the wake of a roughness without parallel-flow assumption [2]. This numerical tool is promising for future stability predictions, but is yet lacking a comparison to a physical experiment. This article provides hot-film measurements to verify theoretical predictions of the critical roughness height, disturbance frequencies and symmetry of the eigenfunctions found by the global LST.

The Laminarwasserkanal (LaWaKa, laminar water channel) is a unique facility with low turbulence intensity that allows experiments with greater time and lenght scales than most wind tunnels in this field of research. A hot-film probe has been traversed in a plane downstream of the roughness element with height k at X / k = 20 to measure the time-averaged mean flow and rms disturbances (Figure 1). The time-averaged flow reveals a central low-speed streak, surrounded by a pair of symmetrical high-speed and low-speed streaks. A high disturbance level, indicated by grey-scale contours, is located on top of the central low-speed streak and at locations of high spanwise velocity gradients. As predicted theoretically [2], spanwise shear of an streamwise elongated region nurtures disturbances in the wake of the roughness. The central peak of disturbances is the result of shear in vertical direction, which can develop into hairpin vortices when the Reynolds number is high enough.

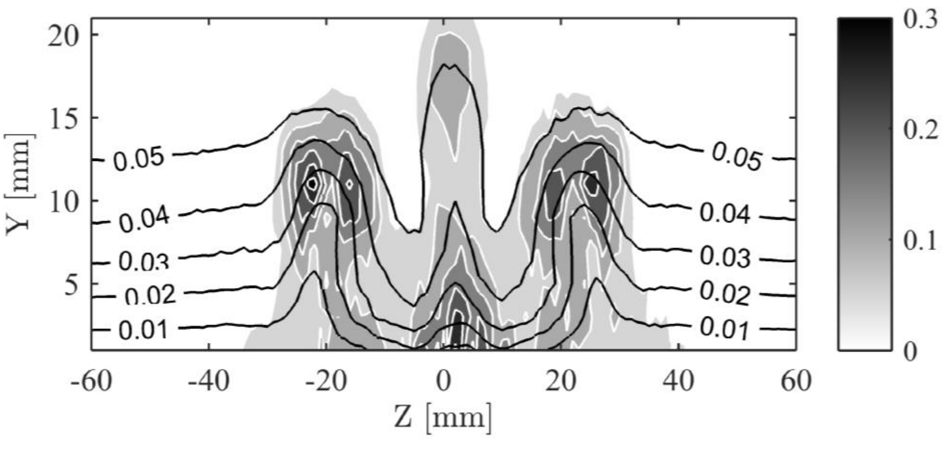

Figure 1 : Streaky baseflow downstream of a roughness element. Time-averaged, mean flow (solid black lines) and rms-disturbances (contours).

The hot-film probe has then been traversed in downstream direction to measure the disturbance growth. The time-signal shows strong initial, transient growth of a dominant frequency (Figure 2) at X = 8, followed by a decay to a rather chaotic signal. A Fourier transform of the signal shows a clear energy-density peak at a frequency of 0.75 Hz, which is in good agreement with the frequency of the most unstable mode of the global LST [2]. Rms and skewness of the signal are analyzed in streamwise direction to find the transition region for different Reynolds numbers Re_k based on the roughness height. An increase of rms can be seen when Re_k reaches 574 in this set-up (Figure 3), which is also in good agreement with the critical Reynolds number predicted by the global LST. Further, a rms peak occurs upstream of the turbulent region in the case with Re_k = 574 at X / k = 10, which results from self-induced vorticity in the wake of the roughness. This experiment has been repeated for different positions in the boundary layer. Interestingly, there are cases where the rms functions show an initial peak, but then settle down to a level of laminar flow. In these cases, the vorticity is not self-sustaining and viscosity has a damping effect on the disturbances.

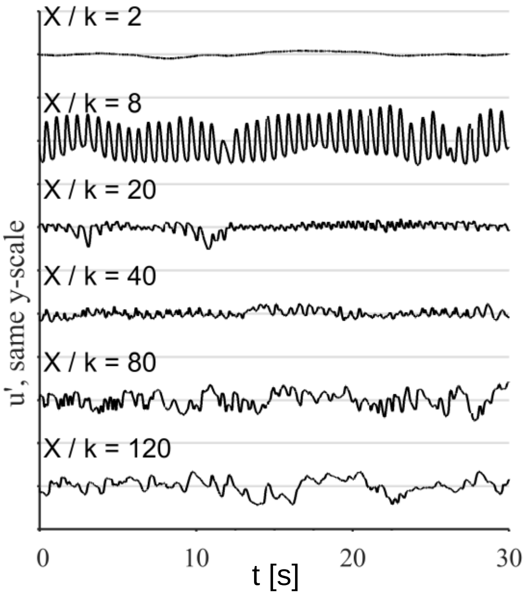

Figure 2: Hot-film signals of u' at downstream positions for Re_k = 574

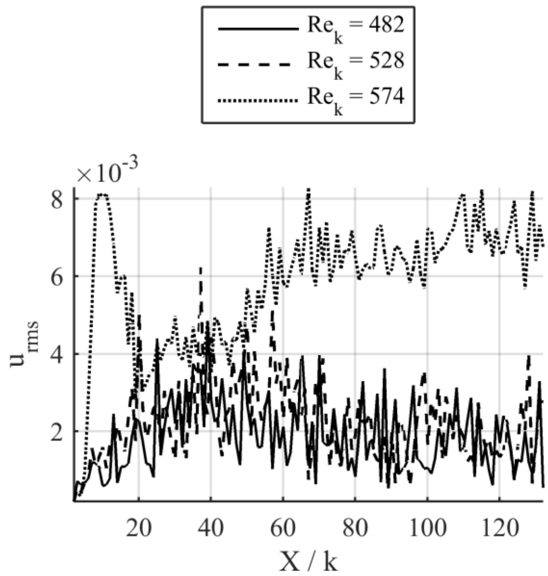

Figure 3: Downstream development of rms fluctuation for different Re_k-numbers

References :

[1] Y. Shin, U. Rist und E. Krämer, „Stability of the laminar boundary-layer flow behind a roughness element,“ *Experiments in Fluids,* 2015.

[2] J.-C. Loiseau, J.-C. Robinet, S. Cherubini und E. Leriche, „Investigation of the roughness-induced transition: global stability analyses and direct numerical simulations,“ *Journal of Fluid Mechanics,* pp. 175- 211, 12 2014.

[3] J. H. M. Fransson und L. Brandt, „Experimental study of the stabilization of Tollmien–Schlichting waves,“ *Physics of Fluids,* 2005.

Mitteilung

Projektgruppe / Fachkreis: Laminarhaltung und Transition

Experimental investigation of Mach number and pressure gradient effects on two-dimensional laminar-turbulent boundary layer transition

S. Risius, M. Costantini, S. Hein, C. Klein
Deutsches Zentrum für Luft- und Raumfahrt e.V. (DLR),
Bunsenstraße 10, D-37073 Göttingen, Germany, steffen.risius@dlr.de

Introduction

Drag reduction by means of natural laminar flow technology is a promising way to reduce wall shear stress, which can significantly reduce fuel consumption of commercial aircraft [1]. Tollmien-Schlichting (T-S) waves are the dominating mechanism to trigger 'natural' transition in low free-stream disturbance environments for boundary layers developing on smooth two-dimensional surfaces. At these conditions the linear stability theory [2], in particular the e^N method, predicts a stabilizing effect of compressibility on boundary layer transition [3]. However, there is only limited experimental verification of this effect for Mach numbers up to highly subsonic conditions. In this work we show a systematic experimental investigation of pressure gradients ($dc_p/dx = -1.2$ to 0.25 1/m), Mach numbers ($M = 0.35$ to 0.77) and chord Reynolds numbers ($Re_c = 3.5*10^6$ to $16.0*10^6$, with $c = 0.2$ m).

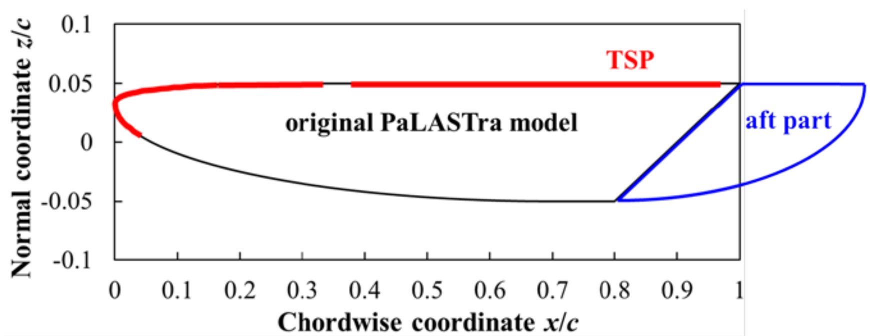

Figure 1: Side view (cross section) of the *PaLASTra* model with an additional aft part at the trailing edge and temperature-sensitive paint (TSP) on top.

Experimental setup

The experiments were performed in the low-turbulence ($Tu_{\rho u} \sim 0.06$ %) Cryogenic Ludwieg-Tube Göttingen (DNW-KRG) [4, 5], with a two-dimensional wind tunnel model that is based on the *PaLASTra* model [6, 7]. In order to reduce the size of the separation region at the rear edge of the original *PaLASTra* model an additional aft part was added to the model (fig. 1). The surface pressure distribution was measured using pressure taps, while the temperature distribution and transition location was detected by means of temperature-sensitive paint (TSP) on the upper side only [8]. A systematic variation of the pressure gradient was possible by adjusting the angle-of-attack between -3.5 and 0 degrees. Boundary layer computations were performed using the boundary layer solver *COCO* [9], which was modified in order to incorporate not only the measured surface pressure but also surface temperature distributions as inputs. These computations were used in order to determine displacement (δ_1) and momentum thickness (δ_2), as well as the shape factor $H_{12} = \delta_1/\delta_2$, which was used to characterize the boundary layer velocity profile. Amplification rates of T-S waves for the computed boundary layer were determined by means of *LILO* [10]. The results of the stability computations were then correlated with the measured transition location to assess the critical N-factors.

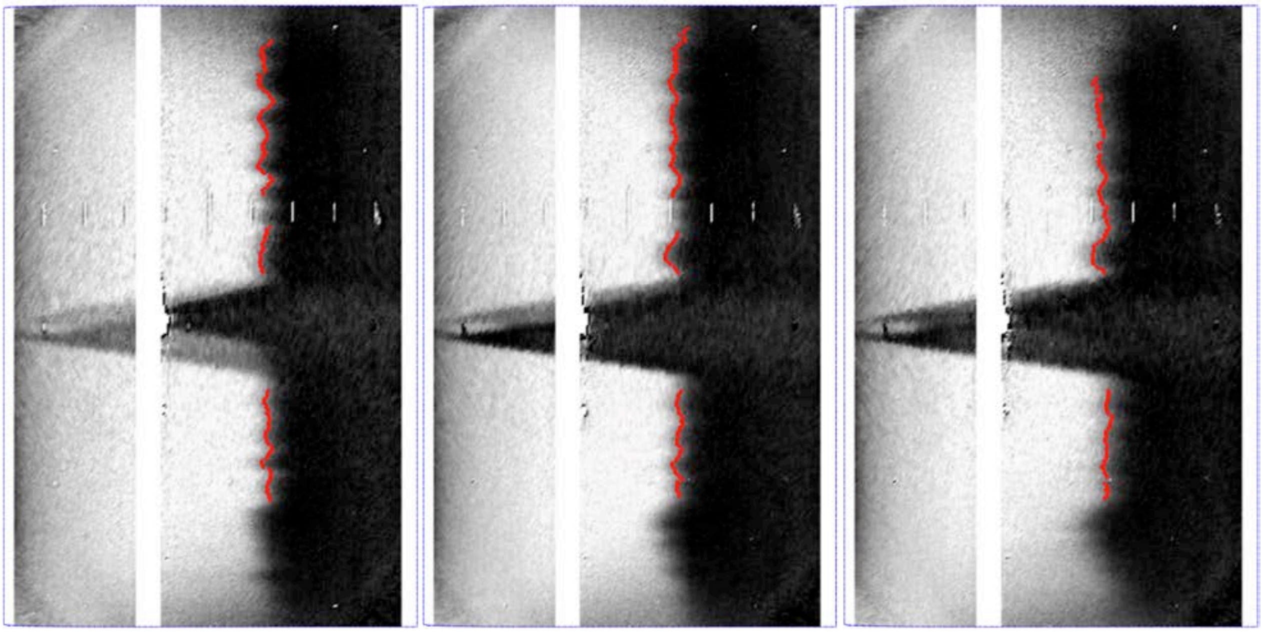

Figure 2: TSP results, which indicate laminar (white) and turbulent regions (black) and detected transition locations (red line). The flow is from left to right and pressure taps cause two turbulent wedges in the middle of the model. An uncoated region at x/c = 35 +/- 2 % has been masked with a white strip. Measurements at three different Mach numbers 0.35, 0.65 and 0.77 (from left to right) are shown. The acceleration of the flow increases from left to right due to more favorable pressure gradients with dc_p/dx = -0.10 1/m, -0.30 1/m and -0.52 1/m respectively. The corresponding average transition locations are at x_{tr}/c = 63.5 %, 61.3 % and 62.7 %.

Results and conclusions

Figure 2 shows TSP images that were taken at three different Mach numbers (0.35, 0.65 and 0.77) at the same chord Reynolds number $Re_c = 6*10^6$ (with c = 0.2 m). It can be seen that the average transition location remains at approximately 62.5 +/- 1.2 %. The corresponding transition Reynolds number is $Re_{tr} = x_{tr}*U_\infty/v_\infty = 3.75 +/- 0.05*10^6$, which is within the measurement uncertainty. Thus, the transition Reynolds number remains essentially unchanged although Mach number and flow acceleration increase. These results appear to stand in contrast with the stabilizing effect of compressibility and pressure gradient as predicted by linear stability theory [3]. However, due to the operation principle of DNW-KRG also wall temperature effects and the free-stream disturbance environment (which are both Mach number dependent) have to be taken into account in order to conduct a comprehensive assessment of Mach number effects on transition Reynolds numbers. These influences will be discussed in the final version of the paper.

References

[1] Schrauf, G. Status and Perspectives of Laminar Flow, *The Aeronautical Journal*, Vol. 109, No. 1102, 2005, pp. 639-644.

[2] Schlichting, H., and Gersten, K., Boundary-Layer Theory, 8th ed., Springer-Verlag, Berlin/Heidelberg, 2000, Chap. 15.

[3] Arnal, D., and Vermeersch, O. Compressibility effects on laminar-turbulent boundary layer transition. *Int. J. Engineering Systems Modelling and Simulation*, Vol. 3, Nos. 1/2, 2011, pp. 26-35.

[4] Rosemann H. The Cryogenic Ludwieg-Tube Tunnel at Göttingen. AGARD-R-812, Cologne, Germany, 1996, pp. 8-1 to 8-13.

[5] Koch S. Zeitliche und räumliche Turbulenzentwicklung in einem Rohrwindkanal und deren Einfluss auf die Transition an Profilmodellen. DLR-FB-04-19, 2004.

[6] Costantini, M., Risius, S., Klein, C. Effect of Forward-Facing Steps on Boundary Layer Transition at a Subsonic Mach Number. *New Results in Numerical and Experimental Fluid Mechanics X,* edited by Dillmann, A., Heller, G., Krämer, E., Wagner, C., and Breitsamter, C., Vol. 132, Notes on Numerical Fluid Mechanics and Multidisciplinary Design (NNFM), Springer–Verlag, Berlin/Heidelberg, 2016, pp. 203-213.

[7] Costantini, M., Risius, S., Klein, C. Experimental Investigation of the Effect of Forward-facing Steps on Boundary Layer Transition. *IUTAM_ABCM Symposium on Laminar Turbulent Transition, Procedia IUTAM*, edited by Medeiros, M. A. F., and Meneghini, J. R., Vol. 14, 2015, pp. 152-162.

[8] Liu T, Sullivan J. P. Pressure and Temperature Sensitive Paint. Springer-Verlag, Berlin/Heidelberg, 2005.

[9] Schrauf, G. COCO – A Program to Compute Velocity and Temperature Profiles for Local and Nonlocal Stability Analysis of Compressible, Conical Boundary Layers with Suction. *ZARM Technik Report*, 1998.

[10] Schrauf, G. LILO 2.1 – Users Guide and Tutorial. *GSSC Technical Report 6*, 2006.

Mitteilung

Projektgruppe / Fachkreis: Flow Control, Transition, Wirbelgenerator

Grenzschichtbeeinflussung mittels definierter Oberflächenstrukturierung am Beispiel des rotierenden Zylinders

Thomas Schomberg
Student der Universität Kassel, Institut für Mechanik
Thomas.Schomberg@Student.Uni-Kassel.de

Markus Rütten
DLR, Institut für Aerodynamik und Strömungsmechanik,
Abteilung Hochgeschwindigkeitskonfigurationen,
Bunsenstr.10, 37073 Göttingen
Markus.Ruetten@dlr.de

Einleitung:

In der technischen Umwelt kommt es häufig zur ungewollten Grenzschichtablösung an gekrümmten Oberflächen. Zur Verzögerung der Grenzschichtablösung werden u.a. erfolgreich Wirbelgeneratoren eingesetzt, da diese der Grenzschicht kinetische Energie zuführen. In dieser Arbeit wird die radiale Umströmung eines rotierenden Zylinders analysiert, da auch hier eine Grenzschichtablösung auftreten kann. Zusätzlich erzeugt der rotierende Zylinder eine Magnus-Kraft, welche beispielsweise für zukünftige Schiffsantriebe genutzt werden kann. So zeigte bereits das Enercon E-Ship-1 im Jahr 2011 das Potential sogenannter Flettner-Rotoren im Bereich der Schifffahrt [1]. Zur Grenzschichtbeeinflussung wird in dieser Arbeit eine definierte Oberflächenstrukturierung, ähnlich eines Golfballs, gewählt. Achenbach [2] konnte einen Unterschied zwischen einer Golfballstruktur (sogenannter Dimples) und rauen Oberflächen auf die Umströmung einer Kugel zeigen (vgl. Abb 1). Der Effekt scheint über eine reine Transitionsverlagerung hinaus zu gehen. In den Arbeiten von Kovalenko et al. [3] und Vincent et al. [4] werden Strömungsformen innerhalb einzelner Dimples auf einer ebenen Platte analysiert. Es können dabei definierte Wirbelstrukturen gezeigt werden. Das Ziel dieser Arbeit ist es, Strömungsformen innerhalb von Dimples auf einem rotierenden Zylinder zu analysieren und deren Einfluss auf die Zylinderumströmung zu bewerten.

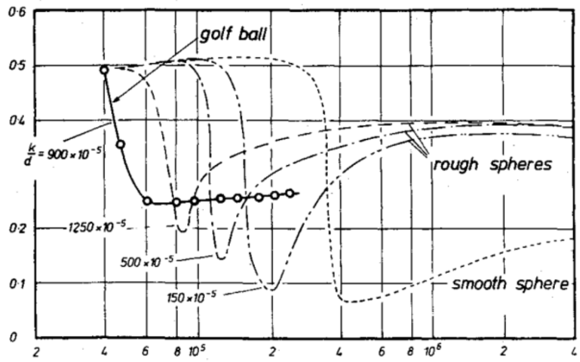

Abbildung 1 Luftwiderstandsbeiwert von Kugeln mit verschiedenen Oberflächen [2]

Methodik:
Zur Analyse der Strömungsformen werden numerische Simulationen mit Hilfe des DLR eigenen Theta-Solvers durchgeführt. Zur Turbulenzmodellierung der URANS-Simulation wird das Wilcox-k-ω-Modell eingesetzt. Die Oberflächenstruktur des Zylindersegments (vgl. Abb. 2) wird so variiert, dass übereinstimmend mit der Literatur eine größtmögliche Variation an Strömungsformen zu erwarten ist. Die Reynoldszahl der Zylinderumströmung beträgt konstant Re=134000. Das Verhältnis von Anström- zur Umfangsgeschwindigkeit liegt konstant bei 1,5. Um eine Zylinderrotation simulieren zu können, wird die sogenannte Chimera-Technik verwendet, bei der der Simulationsraum aus zwei sich überschneidenden Netzen besteht.

Ergebnis:
Eine Validierung der numerischen Methode erfolgt anhand des nicht rotierenden Zylinders mit Dimples und experimenteller Daten aus der Literatur. Der Widerstandsbeiwert weicht um 11%, die Strouhal-Zahl um 2% ab. Diese Abweichungen werden auf Unzulänglichkeiten des k-ω-Modells im Bereich der Strömungsablösung hinter dem Zylinder zurückgeführt. Für die hier im Fokus liegende Strömung innerhalb der Dimples kann eine sehr gute Übereinstimmung der Strömungsformen mit Daten aus der Literatur [3,4] gezeigt werden.

Zur Variation der Oberflächenstruktur wird das Verhältnis von Dimple-Durchmesser zu dessen Tiefe verändert. Für den rotierenden Zylinder mit Dimples können fünf Strömungsformen innerhalb der Vertiefungen voneinander abgegrenzt werden. Für seichte Vertiefungen kann eine konvergent-divergente Strömung beobachtet werden. Mit steigender Tiefe löst die Strömung an der Vorderkante des Dimples ab und formt eine konvergent-divergente Strömung mit Rezirkulationsgebiet aus. In Abhängigkeit der Lage des Dimples zur Anströmrichtung kann zusätzlich hinter einem Dimple ein lokales Rezirkulationsgebiet beobachtet werden. Darüber hinaus stellt sich in bestimmten Fällen eine vorwiegend chaotische Strömungsform innerhalb der Vertiefungen ein. Für den Einsatz von Dimples als Wirbelgeneratoren kann die in den Abbildung 2 und 3 dargestellte Strömungsform von besonderem Interesse sein. Für vergleichsweise tiefe Dimples können in Bereichen mit positivem Druckgradienten gegenläufig rotierende Wirbelpaare beobachtet werden. Aus Abbildung 2 wird bei Betrachtung des Reibungsbeiwertes Cf deutlich, dass diese Wirbelpaare auch außerhalb des Dimples die Strömung beeinflussen. Eine detaillierte Beschreibung der Strömungsformen und deren Einfluss auf die Zylinderumströmung wird in dieser Arbeit vorgenommen.

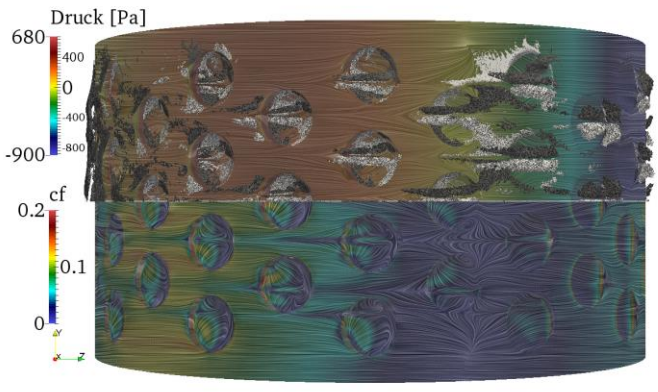

Abbildung 2 Vorderansicht, Anströmung in Blickrichtung

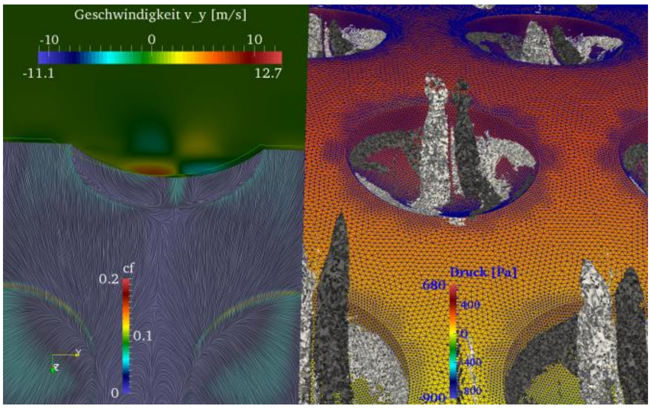

Abbildung 3 Detailansicht aus Abb. 1 der Wirbelstruktur innerhalb eines Dimples

Literatur:

[1]: Seifert, J.: A review of the Magnus effect in aeronautics. In: Progress in Aerospace Sciences 55 (2012) S.17-45
[2]: Achenbach,E.:The Effect of Surface Roughness and Tunnel Blockage on the Flow Past Spheres. In: Journal of Fluid Mechanics 65, Pt 1, (1974) S. 113-125
[3]: Kovalenko G.,Terekhov A.: Flow regimes in a single dimple on the channel surface. In: Journal of Applied Mechanics and Technical Physics 51 (2010) S. 839-848
[4]: Vincent R.,Maple R.: CFD Investigation of Laminar Flow Over a Dimpled Surface Indentation In: AIAA Fluid Dynamics Conference and Exhibit 36 (2006) S. 1-22

Mitteilung

Projektgruppe / Fachkreis:Laminarhaltung und Transition

A simple method to pre-design an outlet flap for a passive HLFC system

Geza Schrauf
Airbus, Airbus Alle 1, 28199 Bremen
geza.schrauf@airbus.com

To achieve laminar flow for larger aircraft, we need to apply hybrid laminar flow control (HLFC). The current state of the art is to stabilize the boundary layer with the help of suction through a micro-perforated titanium surface. The necessary suction power to drive the HLFC system can be obtained by a fan or a compressor. If this is the case, we have an active suction system. We can, however, generate the suction power with the help of an outlet flap. Because such a system does not require a compressor, we call it a passive HLFC system.

In the presentation we will describe a simple method to pre-design such an outlet flap and present comparisons with TAU-calsulations.

References:

Krause, U., Kreuzer, P., Stuke, H.: Air Outlet Design for a Passively Driven Hybrid Laminar Flow Control System.” ECCOMAS 2016.

Rogallo, F. M.: “Internal Flow Systems for Aircraft.” NACA Report N0. 713, 1941.

Rogallo, F. M., Gauvin, W. E.: “Wind-Tunnel Investigation of Air Inlet and Air Outlet Openings for Aircraft.” NACA Special Report No. 95, 1938.

Mitteilung

Projektgruppe / Fachkreis: Flow Control

Control of flow separation in the wake of an axisymmetric space-launcher model

Anne-Marie Schreyer, Gonca Taskin
Institut für Strömungsmechanik, TU Braunschweig,
Hermann-Blenk-Straße 37, 38108 Braunschweig
a.schreyer@tu-braunschweig.de

The afterbody geometry of a classical space launcher is characterized by a step decrease in diameter at the junction between main body and rocket engine. The boundary layer on the main body separates at this step, a large recirculation region forms, and a turbulent shear layer develops (see Figure 1, left). This separation-dominated flow field is highly unsteady and induces strong wall-pressure oscillations that can excite structural vibrations [2,3,6,7]. At stages along the flight trajectory at higher altitude, the displacement effect of the afterexpanding propulsive jet causes an enlargement of the recirculation region and a pressure increase at the main-body base [6,7]. The flow might not reattach on the afterbody, and hot gases from the jet can be convected upstream in the separation zone and harm the structure.
Means to stabilize and reduce the reattachment length to reduce dynamic loads on the launcher are therefore of great interest. Particularly passive vortex generators have drawn a lot of attention [4], both due to promising results on two-dimensional backward-facing step geometries [1,5], and their simplicity and robustness [4].
In the current study, we investigate the influence of a convoluted trailing edge (lobes) on the wake of a generic space-launcher model in supersonic flow (see Figure 2), and analyze the technique's potential to control the separation length and dynamics.
Kähler et al. [1,5] investigated different lobe geometries on a 2D backward-facing step in transonic flow. The lobes introduce counter-rotating streamwise vortices that increase turbulent mixing and create a highly three-dimensional flow field with a spanwise component [1]. Behind lobe peaks, the separation is locally rather strong, but the overall separation length is significantly reduced, and the dynamic motion of the reattachment location is stabilized [1,5]. The induced vortices should be of similar size as coherent structures in the wake [1], and larger lobes have a stronger effect.
Our research goals are to a) contribute to a better understanding of the flow field to enable efficient control, b) study the effect of lobes on the wake topology of an axisymmetric model (Similar as for 2D backward-facing step?), c) characterize the dynamic behavior of the surface pressure signal, since this represents a footprint of coherent structures in the wake [3], and d) analyze the interaction with the afterexpanding jet plume (Will the flow reattach under the influence of control?).
Experimental investigations are performed in the Hypersonic Ludwieg Tube Brauschweig in supersonic configuration, at a free-stream Mach number of $M_\infty = 2.9$ and a Reynolds number based on the model diameter of $Re_D = 1.3 \cdot 10^6$. The model consists of a nose cone and two cylindrical bodies representing the main body and nozzle, respectively (see Figure 1). The implemented TIC-nozzle allows to simulate propulsive jets, a cold air jet in the present case, with an exit Mach number of 2.5. The model is installed in the wind tunnel with a sword-shaped strut support.
In previous studies, we investigated the baseline case (with smooth trailing edge), as well as the effect of the jet plume on the wake [6] in detail. For the baseline case, the mean velocity field from PIV and the power spectral density of the base-pressure

fluctuations are shown in Figure 1. For the current study, we implemented square lobes with a height of 0.2h and a deflection angle of 18° at the main-body base (see Figure 2). Kulite XCQ-093 pressure sensors with a range of 0.35 bar absolute are flush-mounted into the base at a radial position of r/D = 0.42 and at different angles (θ = 180°, 190°, and 240°) to capture 3D effects. Further Kulite LE-062 sensors are installed on the nozzle fairing at x/D = 0.77 (reattachment location in baseline case) and x/D = 0.31, the presumed reattachment location for the controlled case [1,5]. The dynamic behavior and spectral content of the wake is analyzed based on these unsteady wall-pressure signals. In addition, we carry out schlieren flow visualizations to study the effect of the lobes on the mean flow topology, in particular the reattachment length. The wake with and without jet plume is investigated downstream of the lobe peak and valley positions (see Figure 2). The experiments are currently ongoing, and will be concluded and analyzed well before the symposium.

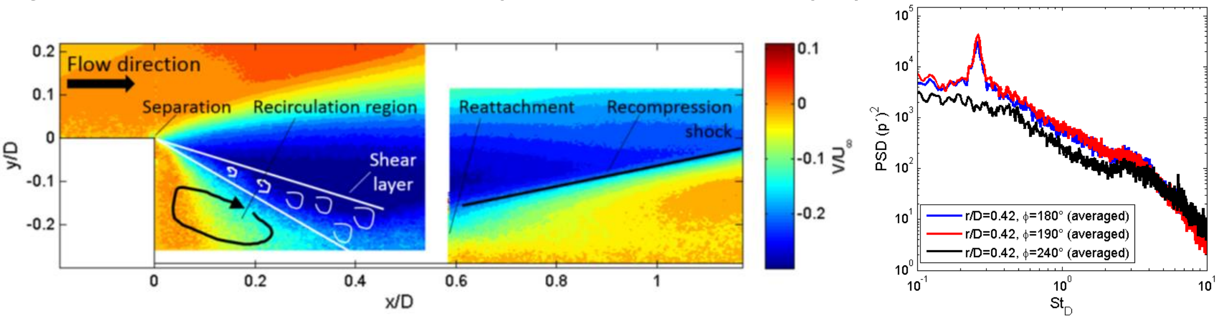

Figure 1 Wake of a launcher model with afterbody (uncontrolled baseline case). Left: Schematic of the mean-flow topology, superimposed on a contour plot of the mean radial velocity component V from PIV (normalized with free-stream velocity U_∞). Right: Base-pressure spectra. Data from [6].

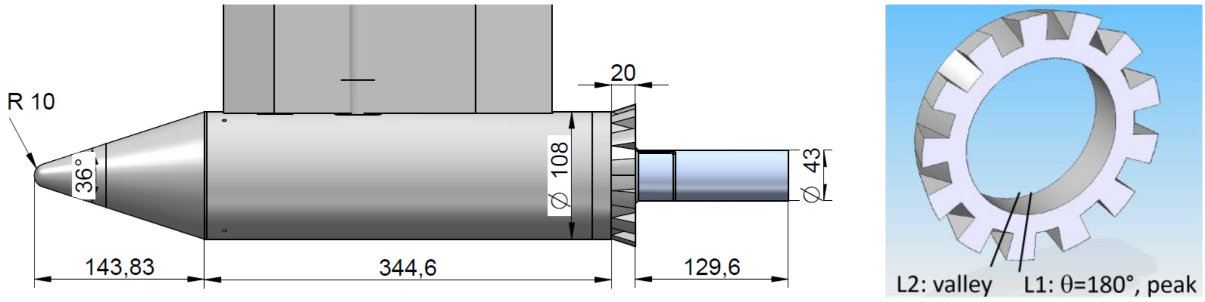

Figure 2 Left: Sketch of the axisymmetric space-launcher model with convoluted trailing edge and strut support (dimensions in mm). Right: Rotatable lobe ring with measurement locations L1 and L2.

Literature

[1] Bolgar, I., Scharnowski, S., Kähler, C. J., Control of the Reattachment Length of a Transonic 2D Backward-Facing Step Flow, Int. conf. on jets, wakes and separated flows, Stockholm, Sweden, 2015.

[2] Bourdon, C. J., Dutton, J. C., Planar visualizations of large-scale turbulent structures in axisymmetric supersonic separated flows. Physics of Fluids 11 (1), pp. 201–213, 1999.

[3] Deprès, D., Reijasse, P., Dussauge, J.-P., Analysis of Unsteadiness in Afterbody Transonic Flows, AIAA Journal, Vol. 42, No. 12, 2004, pp. 2541-2550.

[4] Pearcey, H. H., Part IV: Shock-induced separation and its prevention by design and boundary layer control. In: G. V. Lachmann (Hg.): Boundary Layer and Flow Control: Its Principles and Application. Volume 2. Oxford: Pergamon (2), pp. 1166–1344, 1961.

[5] Scharnowski, S., Bolgar, I., Kähler, C. J., Control of the recirculation region of a transonic backward-facing step flow using circular lobes, 9th International Symposium on Turbulence and Shear Flow Phenomena (TSFP 9), Melbourne, Australia, 2015.

[6] Schreyer, A.-M., Stephan, S., Radespiel, R., Flow structure and unsteadiness in the supersonic wake of a generic space launcher, 54th AIAA Aerospace Sciences Meeting, 2016.

[7] Statnikov, V., Sayadi, T., Meinke, M., Schmid, P., Schroeder, W., Analysis of pressure perturbation sources on a generic space launcher after-body in supersonic flow using zonal RANS/LES and dynamic mode decomposition, Physics of Fluids, Vol. 27, No. 1, 2015.

Mitteilung

Projektgruppe / Fachkreis: Flow Control

Shape optimization of active and passive drag-reducing devices on a D-shaped bluff body

Richard Semaan
Institute für Strömungsmechanik, TU Braunschweig, Hermann-Blenk-Str. 37
38108 Braunschweig, r.semaan@tu-bs.de

The flow around bluff bodies is common in nature as well as in many engineering applications such as road vehicles and bridges. It is mainly characterized by a large vortex shedding and a low pressure region in the wake, which is the main source of the elevated drag. The wake dynamics can also cause serious structural vibrations and acoustic noise. These issues can be minimized or even mitigated with the use of passive or active flow control (AFC) devices.

Various passive means for bluff body drag minimization have been investigated in numerous experiments. For example, Bearman [1] described the benefits of a splitter plate on the wake. Significant drag reduction on a blunt body was achieved by modifying vortex shedding using wavy trailing edges or vortex disruptors (e.g. [2], [3]). However, away from their design operating conditions passive devices are known to have a lot of adverse effects. For this reason, active flow control (AFC) systems became the more popular alternatives. Examples include tangential blowing [4], Coanda blowing [5] and rotating cylinders [6].

The current study aims to numerically optimize passive and active flow control devices for an existing D-shaped model. The two types of devices are: Coanda actuation, and randomly-shaped flap. As illustrated in Figure 1, the optimization sequence was performed using several coupled softwares, which ranged from the genetic algorithm software DAKOTA, to the mesh generator Pointwise, to the CFD solver OpenFoam. The sequence is initialized by DAKOTA, which generates a set of variables characterizing the geometry as well as the actuation intensity. The flap geometry is defined through a cubic polynomial, whereas the Coanda forcing is characterized by the blowing intensity (C_μ) and the radius of the Coanda surface (r_C). These variables are then processed by Matlab to generate the corresponding shape, which is then transferred to Pointwise for meshing. The mesh is subsequently used by OpenFoam for the RANS numerical simulations. After each simulation, the cost functional is calculated and then passed to DAKOTA which evaluates it and generates a new set of variables, and the cycle continues. For the passive device, the cost functional is the drag coefficient, whereas for the active device it is the power ratio.

The optimization leads to a 40% drag reduction for the optimal flap (Figure 3), and a total power savings of ~ 70% for the optimal Coanda actuator (Figure 4). This reduction is mainly achieved through changes in the base flow and a suppression in the vortex shedding. The addition of either an active or a passive device creates two additional smaller recirculation regions near the base that shift the larger recirculation region away from the body and thereby increase the base pressure. The results were validated against more refined URANS simulations for selected cases. Further experimental validation in the wind tunnel are currently ongoing, and their results will be presented in the final paper.

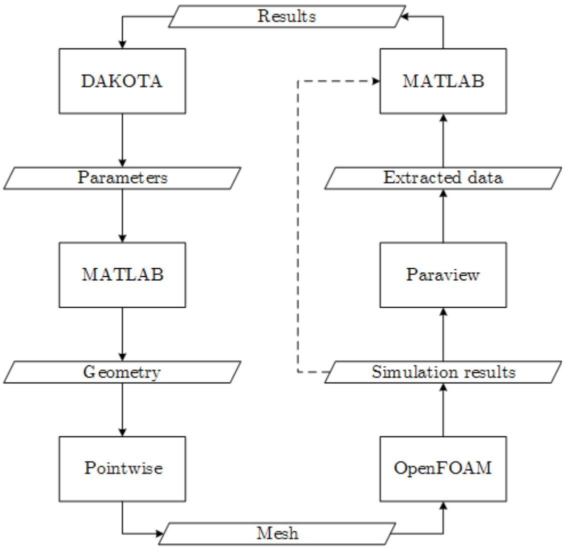

Figure 1: Schematic illustration of the optimization sequence

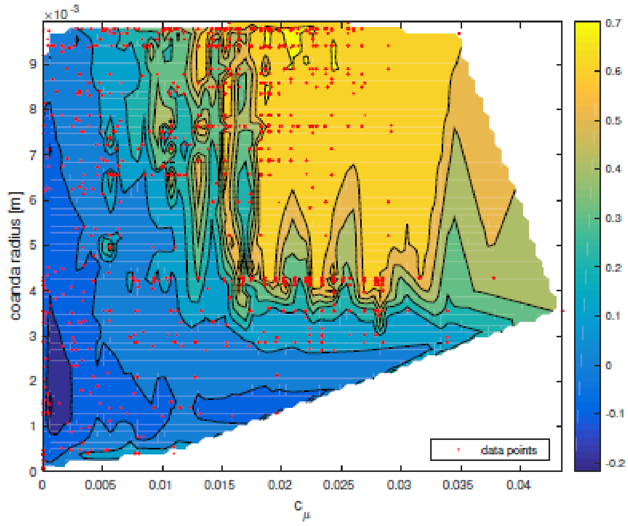

Figure 2: Contour plot of the power ratio over the $r_C - C_\mu$ range. The red points denote individuals

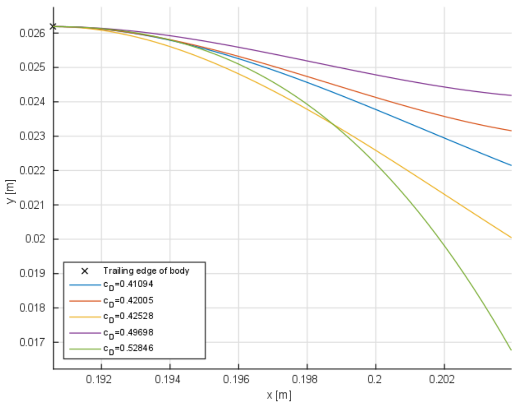

Figure 3: Best five shapes of the trailing edge flaps

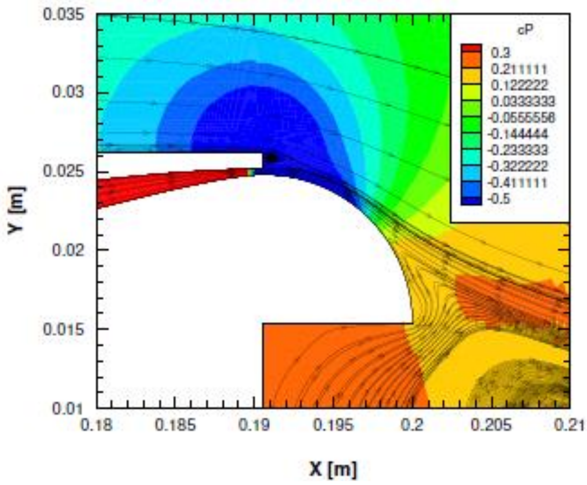

Figure 4: Pressure coefficient distribution around the Coanda jet of the optimized geometry

[1] P. W. Bearman, "Investigation of the flow behind a two-dimensional model with a blunt trailing edge and fitted with splitter plates," *Journal of Fluid Mechanics,* vol. 21.02, pp. 241-255, 1965.

[2] N. Tombazis and P. W. Bearman., "A study of three-dimensional aspects of vortex shedding from a bluff body with a mild geometric disturbance," *Journal of Fluid Mechanics,* vol. 330, pp. 85-112, 1997.

[3] H. Park, D. Lee, W.-P. Jeon, , S. Hahn , . J. Kim, J. Kim, J. Choi and H. Choi, "Drag reduction in flow over a two-dimensional bluff body with a blunt trailing edge using a new passive device," *Journal of Fluid Mechanics,* vol. 563, pp. 389-414, 2006.

[4] M. Pastoor, L. Henning, B. R. Noack and R. King , "Feedback shear layer control for bluff body drag reduction," *Journal of fluid mechanics,* vol. 608, pp. 161-196, 2008.

[5] J. B. Freund and M. G. Mungal, "Drag and wake modification of axisymmetric bluff bodies using Coanda blowing," *Journal of Aircraft,* vol. 31.3, pp. 572-578, 1994.

[6] J. Beaudoin, O. Cadot, J. L. Aider and J.-E. Wesfreid, "Drag reduction of a bluff body using adaptive control methods," *Physics of Fluids,* vol. 18 (8), pp. 85-107, 2006.

Mitteilung

Projektgruppe / Fachkreis: FG Aerodynamik, Institut für Luft- und Raumfahrt, Technische Universität Berlin

Aktive Strömungskontrolle eines komplexen Strömungsfeldes an einer hochbelasteten Verdichterkaskade unter instationären Randbedingungen mit Hilfe von fluidischen Aktuatoren in den Seitenwänden und der Statorbeschaufelung

Marcel Staats, Wolfgang Nitsche
FG Aerodynamik, TU Berlin, Marchstraße 12, marcel.staats@ilr.tu-berlin.de

Eine signifikante Wirkungsgradsteigerung des Kreisprozesses einer Gasturbine ist mittels isochorer Verbrennung zu erwarten [1], [2]. Die angestrebte Wirkungsgradsteigerung liegt bei 10% verglichen mit dem herkömmlich in Turbomaschinen eingesetzten Joule-Prozess, mit isobarer Verbrennung. Das neuartige Verbrennungskonzept ist stark instationär und Rückkopplungen mit den benachbarten Turbokomponenten sind zu erwarten. Eine Möglichkeit die isochore Verbrennung zu integrieren ist es eine Ringrohrbrennkammer zu verbauen, wodurch die Verbrennung sequenziell durchgeführt werden kann und sich eine periodische Androsselung des Verdichteraustritts ergibt. Diese wiederkehrende Instationarität kann die Stabilität des Statorgitters beeinträchtigen. Ein stabiler Verdichterbetrieb ist für eine Turbomaschine allerdings eine essenzielle Forderung. Mittels aktiver Strömungskontrolle kann der stabile Arbeitsbereich des Verdichter Stators vergrößert werden.

In diesem Beitrag werden Experimente an einer 2D Niedergeschwindigkeitsverdichterkaskade vorgestellt. Abbildung 1 zeigt den experimentellen Aufbau der verwendeten Messstrecke. Im Nachlauf des Statorgitters befindet sich ein Drosselapparat, welcher die instationären Randbedingungen einer isochoren Verbrennung simuliert. Zur Beschreibung des Strömungsfeldes sind sowohl Druckmessungen auf der Statorschaufel als auch 2D/3C-PIV-Messungen in der Statorpassage, bei einer Reynoldszahl von Re=600000 und einer Strouhalzahl der Androsselung von Sr = 0,03, durchgeführt worden. Der Versuchsstand ist mit 7 hoch belasteten Verdichterstatorprofilen ausgestattet, welche im Auslegungspunkt einen Umlenkwinkel von $\Delta\beta$=60° besitzen. Abbildung 2 zeigt die sich in Folge des periodisch angedrosselten Nachlaufs ändernde Anströminzidenz eines Statorprofils, welche aus PIV Messungen errechnet wurde. Durch die signifikante Änderung des Einströmwinkels von $\Delta\beta_1$ = +-3,5° wird das Gitter periodisch überlastet, wodurch periodische Strömungsablösung die Folge ist [3].

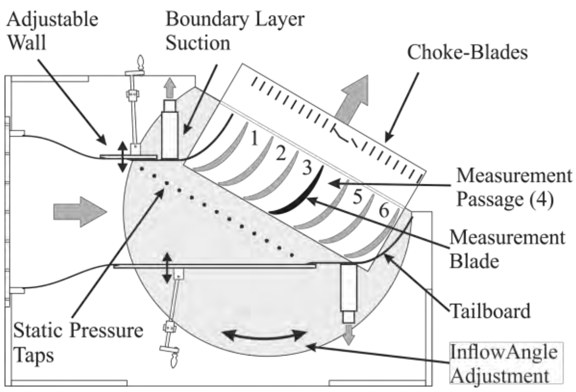

Abbildung 1: Experimenteller Aufbau

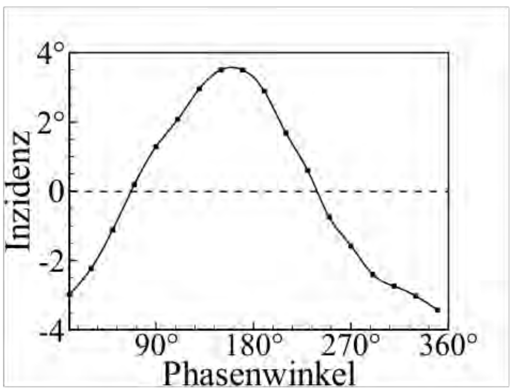

Abbildung 2: Periodische Inzidenzänderung

Mittels PIV und Druckmessungen konnten geeignete Positionen zur Anwendung von aktiver Strömungskontrolle an der Seitenwand und der Schaufel selbst identifiziert werden. Drei verschiedene Aktuationssetups wurden hinsichtlich des Einflusses von eingebrachtem Impuls und der Ausblasfrequenz auf den Druckrückgewinn einer Passage untersucht. Die unternommenen Experimente zeigten eine deutliche Reduktion der periodischen Strömungsablöseerscheinungen.

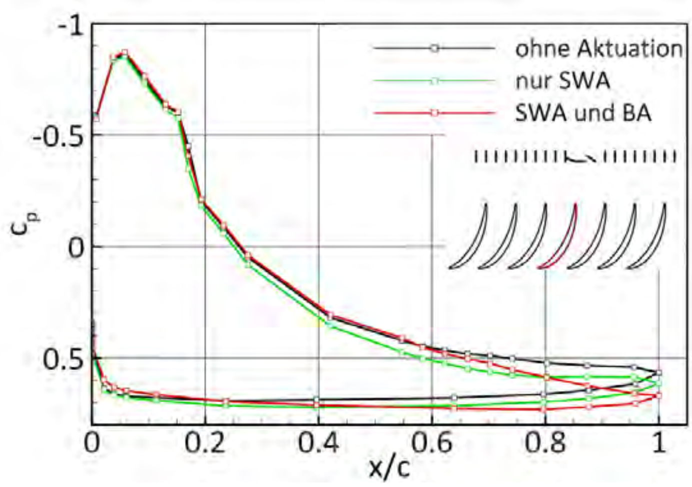

Abbildung 3: Einfluss der Aktuation auf die Druckverteilung der Messschaufel

In den Experimenten wurde pulsierendes Ausblasen eingesetzt. Dabei wurden fluidische Aktuatoren entwickelt welche in die Seitenwand und die Statorschaufel integriert worden sind. In Abbildung 3 sind vergleichend drei Profile der Druckverteilung auf der Statorschaufel im Mittelschnitt gezeigt. Zum gezeigten Phasenpunkt der Androsselung ist die Messpassage maximal verblockt. Die schwarze Kurve zeigt die Druckverteilung im Referenzfall, d.h. ohne Aktuation. Strömungsablösung tritt ab circa x/c = 0,7 Schaufelsaugseitig auf. Durch das anschalten der Seitenwandaktuation (grüne Kurve) werden die im Verdichtergitter auftretenden Sekundärströmungen (Eckenablösung) beeinflusst. Diese Beeinflussung mittels der Seitenwandaktuatorik entblockt die Verdichterpassage und bewirkt einen höheren Druckrückgewinn, welcher sich im erhöhten Hinterkantendruck wiederspiegelt. Wird zur Seitenwandaktuation nun die Schaufelaktuation auf der Saugseite mit verwendet (rote Kurve), ist deutlich ein Druckanstieg bis zur Hinterkante des Statorprofils zu verzeichnen. Die verwendeten Impulsbeiwerte betrugen, für die eingeschalteten Aktuatoren, im dargestellten Fall jeweils $c_{\mu,SWA} = s_{\mu,BA}$=1,6%.

Die Schaufeldruckmessungen wurden genutzt, um geeignete Aktuationsparameter zu finden. Das Strömungsfeld in der Passage wurde phasengemittelt mittels 2D/3C – PIV Messungen in mehreren Schnitten räumlich aufgelöst. Die Messungen lassen detaillierte Schlüsse über die Wirkungsweise des Aktuationskonzepts auf die periodisch instationäre Passagenströmung zu.

Literatur:

[1] F. Schmidt and S. Staudacher, *Generalized Thermodynamic Assessment of Concepts for Increasing the Efficiency of Civil Aircraft Propulsion Systems,* Proceedings of ASME Turbo Expo 2015: Turbine Technichal Conference and Exposition GT2015, 2015

[2] G. Lenoble and S. Ogaji, *Performance analysis and optimization of a gas turbine cycle integrated with an internal combustion wave rotor,* Proceedings of the Institution of Mechanical Engineers, Part A: Journal of Power and Energy, SAGE Publications, 2010, 224, 889-900

[3] M. Staats and W. Nitsche, *Active Control of the Corner Separation on a Highly Loaded Compressor Cascade with Periodic Non-Steady Boundary Conditions by means of Fluidic Actuators,* Proceedings of the ASME Turbo Expo 2015, June 15-18, Montreal, Canada, ASME paper GT2015-42161, 2015

Mitteilung

Projektgruppe / Fachkreis: Projekt MaKoS – Manipulation und Kontrolle turbulenter Strömungen

Drag reduction by Manipulation of Turbulent Flow via Rotating Discs

Christina Voß†, Markus Rütten†, Andreas Schröder†, Reinhard Geisler†

†German Aerospace Center, Institute of Aerodynamics and Flow Technology
Bunsenstrasse 10, 37073 Göttingen, Germany
christina.voss@dlr.de , markus.ruetten@dlr.de , andreas.schroeder@dlr.de, reinhard.geisler@dlr.de

Keywords: hairpin vortices, coherent structures, active flow control

For several decades now, the existence of coherent structures within the turbulent boundary layer has been known. However, it is still unexplained how these structures occur, develop and how they interact with each other in the turbulent boundary layer, it is even not clear how these structures have to be defined mathematically [5]. It is known that they play an important role in the generation of turbulence. Therefore, the manipulation and control of these very large structures is one of the main subjects in turbulence research due to the fact that coherent structures have a major influence on the total drag of conventional aircrafts. Over the last years, the assumption was confirmed that the instability of low- and high-speed streaks alternating within the near-wall region of the boundary layer causes the formation of quasi-streamwise vortices, so called “hairpin vortices”. Their interaction with the viscous sublayer of the boundary layer induces new streaks again [2]. *Large Scale Motions* (LSMs) are formed by individual hairpin vortices with the same velocity and flow direction [5]. Different “hairpin packets” [1] in turn vary in speed and growth rate depending on their structural age and wall distance. An overlap of several packets, the so-called *Very Large Scale Motions* (VLSMs), can be observed [5]. After reaching a critical size, these VLSMs collapse initiating the generation of new hairpin vortices which in the long run merge again to new packets. During this development cycle, also called “autogeneration”, a large amount of turbulent shear stress is produced leading to a second energetic peak which can be detected in the nearwall turbulence production [3].
Focal point of the present work is a new boundary layer actuation concept which is able to disrupt the autogeneration mechanism leading to a reduction of turbulent friction drag. Flush-mounted discs of the same diameter, located next to one another, rotate with the same tip velocity and generate a thin disc boundary layer above each disc and quasi-streamwise vortices between neighboring discs [4] (the installed actuator is shown in fig.1). The disc

Figure 1 : Installed "Rotating Discs concept"

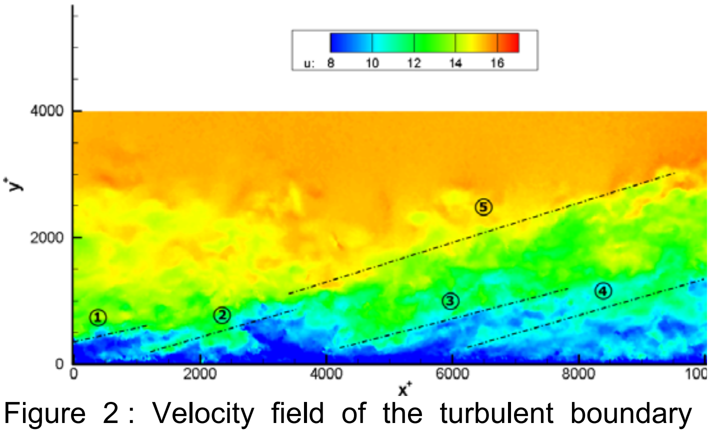

Figure 2 : Velocity field of the turbulent boundary layer at $Re_{\Theta}\approx 10000$ with cascade-shaped hairpin layers

boundary layer causes a phase displacement of near-wall structures whereas the quasi-streamwise vortices retard the flow between the discs with respect to the mean flow [6]. Both processes lead to a weakening of the viscous wall cycle and therefore to minimize the friction drag. For the purpose of understanding the complexity of coherent structures (LSMs and VLSMs) which is necessary to manipulate and control them in order to achieve drag reduction, a basic research experiment on a flat plate was performed in the *Seitenwindkanal Göttingen* (SWG). In the first step, a free, un-actuated turbulent flow was investigated by three single Stereo-PIV-systems. As shown in figure 2, cascade-shaped vortices-packets with different velocities and sizes can be detected within the turbulent boundary layer. Also the overlap of several packets to VLSMs can be identified.Within the framework of the experiment, the development cycle of these coherent structures, especially the drag production and the burst process, is examined in order to specifically use actuator concepts manipulating the stress-producing cycle and minimizing the total drag. After considering the un-actuated flow, the "Rotating Discs" were tested and examined by the use of three Stereo-PIV-systems with regard to its impact on the coherent structures. As can be seen in figure 3, a clear minimization of the spatial coherent structures' extension can be observed by operating the "Rotating Discs" with a tip velocity of $W^+ = 10$.

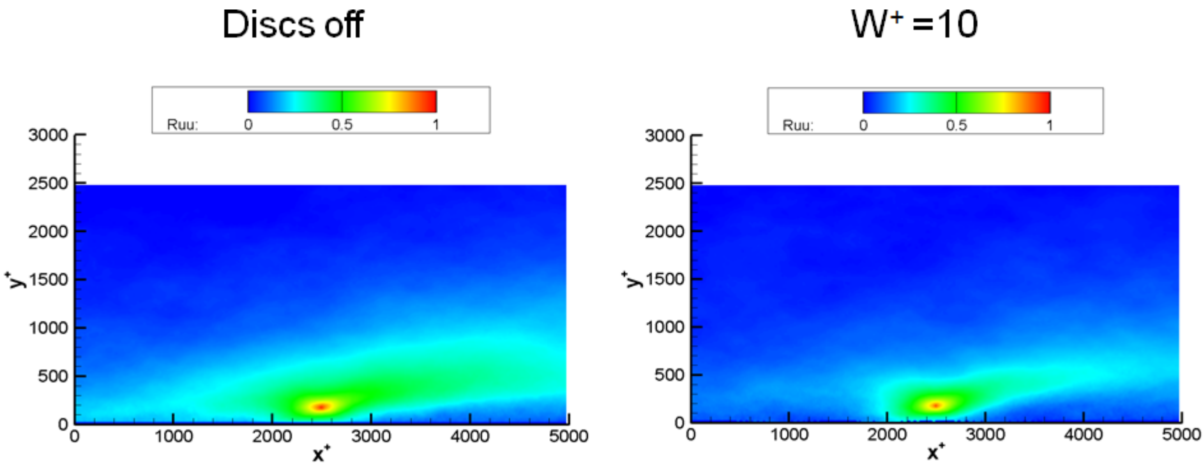

Figure 3 : Two point-correöation of u compponent done at *y/δ* = 0.05

The paper will give a detailed overview of the results obtained by the wind tunnel experiment. The physical understanding of coherent structures within the turbulent boundary layer and their interaction with the viscous sublayer and buffer layer will be considered in detail. In addition to that, the "Rotating Discs actuator concept" and its physical mechanisms within the flow are presented and evaluated with regard to their efficiency to influence the stress-producing cycle and minimizing the viscous drag and therefore the total drag of the model.

References

[1] R. J. Adrian: Hairpin vortex organization in wall turbulence. Physics of Fluids 19, 041301, April 2007

[2] G. Eitel-Amor, O. Flores and P. Schlatter: Hairpin vortices in turbulent boundary layers. Journal of Physics: Conference Series 506 012008, 2014

[3] N. Hutchins, I. Marusic: Large-scale influences in near-wall turbulence. Published an Philosophical Transactions of Royal Society, January 2007

[4] P. Ricco, S. Hahn: Turbulent drag reduction through rotating discs, Journal of Fluid Mech., 722, 2013

[5] A. S. Sharma, B. J. McKeon: On coherent structure in wall turbulence. Accepted for publication in the Journal of Fluid Mechanics, May 2013

[6] D. J. Wise, P. Ricco: Turbulent drag reduction through oscillating discs. Journal of Fluid Mech., vol 746, April 2014

Mitteilung

Projektgruppe/Fachkreis: Flow Control, Laminarhaltung und Transition

Studie zur Grenzschichtabsaugung an einer Fügestelle zur Laminarhaltung der Strömung

J. Zahn, U. Rist
Institut für Aerodynamik und Gasdynamik der Universität Stuttgart
70550 Stuttgart, zahn@iag.uni-stuttgart.de

Bei aktuellen Flugzeugentwicklungen ist niedriger Kraftstoffverbrauch eine wichtige Zielgröße. Aufgrund von reduzierten Luftreibungsverlusten bietet die Laminarhaltung der Strömung auf den Tragflügeloberflächen ein großes Einsparungspotential. Allerdings können kleine Oberflächenunebenheiten wie Rauigkeiten, Stufen und Spalte zu einem deutlich verfrühten laminar-turbulenten Strömungsumschlag führen. Deshalb werden Methoden gesucht, die den negativen Einfluss reduzieren oder gar eliminieren können. Absaugung von Luft durch die Oberfläche stellt eine Möglichkeit dafür dar. Die aktuelle Arbeit befasst sich mit einer vorspringenden Stufe, die an der Fügestelle zwischen zwei Bauteilen auftreten kann, z.B. an der Trennstelle zwischen Flügelvorderkante und Hauptflügel. Hier wird zur Absaugung gezielt der Fügespalt genutzt.

Mittels zweidimensionaler direkter numerischer Simulation wird zuerst die Grundströmung ermittelt, die sich über der Spalt-Stufen-Kombination (Fügestelle) ausbildet. Abgesehen von einer Stufe und einem davor liegendem Spalt ist die Oberfläche dabei glatt und ungekrümmt. Der Umgebungsdruck $p_\infty = 1\,\text{bar}$, die Umgebungstemperatur $T_\infty = 288\,\text{K}$ und Mach-Zahl $Ma_\infty = 0{,}6$ werden in der Arbeit konstant gehalten. Daraus resultiert eine Geschwindigkeit von $204\,\text{m/s}$ im Freistromgebiet oberhalb der Grenzschicht. Die Position der Fügestelle ist, gemessen von der Vorderkante der ebenen Platte, bei der Reynoldszahl $Re_x = 2{,}9 \cdot 10^6$. Stufenhöhen bis zu $h = 0{,}44\,\text{mm}$ werden untersucht. Dies entspricht der zweifachen Verdrängungsdicke der Grenzschicht an der Stufenposition für den Fall der ebenen Platte ohne Fügestelle. Die Reynoldszahl, gebildet mit der Stufenhöhe, beträgt $Re_h = 6000$. Eine scharfkantige, vorspringende Stufe dieser Höhe verursacht laminar-turbulenten Strömungsumschlag direkt an der Stufe, vergleiche Abbildung 1. Um den Einfluss dieser Stufe auf den laminar-turbulenten Strömungsumschlag zu eliminieren, muss die Stufenkante abgerundet werden und durch den Spalt Luft abgesaugt werden, siehe Abbildung 2. Bei dieser besonders kritischen Stufenhöhe und der Spaltbreite von 0,33 mm beträgt die notwendige, mittlere Absaugegeschwindigkeit 20% der Freistromgeschwindigkeit.

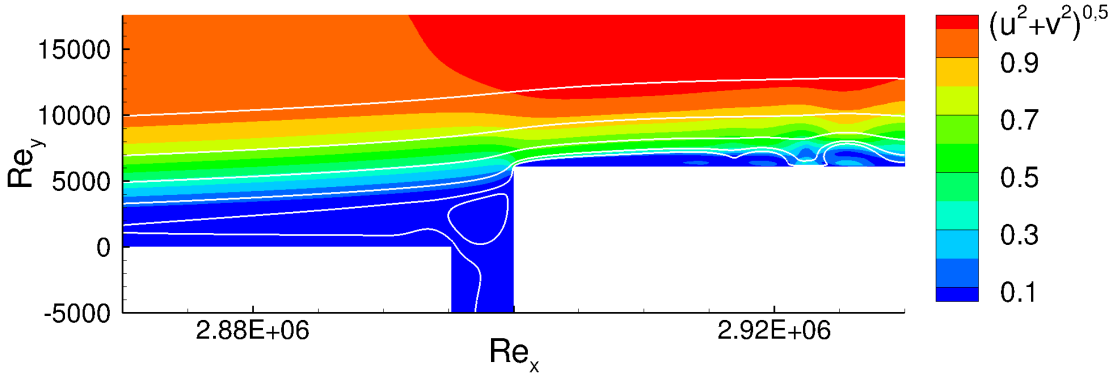

Abbildung 1: Geschwindigkeit und Stromlinien im Bereich einer Fügestelle ohne Absaugung

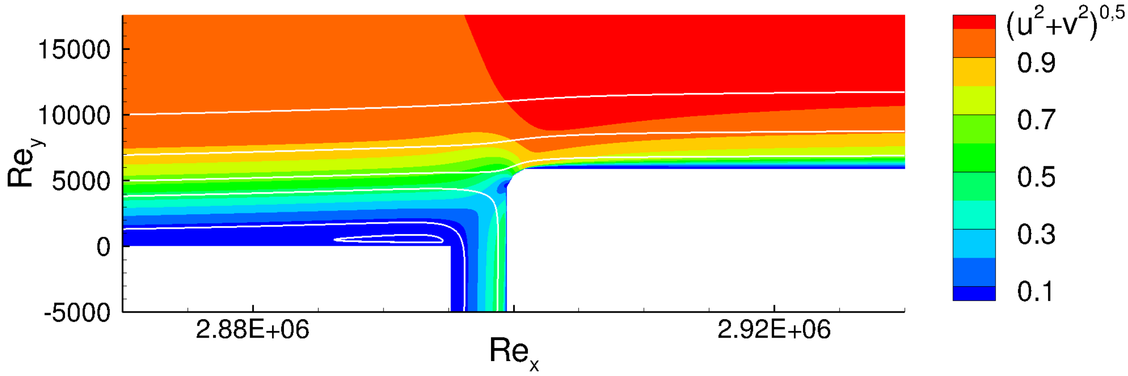

Abbildung 2: Geschwindigkeit und Stromlinien im Bereich einer Fügestelle mit Absaugung durch den Fügespalt

Die Bewertung von Stufen bezüglich des laminar-turbulenten Strömungsumschlags mit und ohne Absaugung wurde bereits auf dem STAB Workshop 2015 vorgestellt, siehe Zahn und Rist [1]. Dazu wurde die e^N Methode verwendet, siehe van Ingen [2]. Basierend auf diesen Ergebnissen wird die Umsetzung des Konzepts in praktischen Anwendungen untersucht. Der Entwurf einer Flügelvorderkante für Laminarflügel von Hühne, Ückert und Steffen [3] sieht eine Fügestelle zwischen der Vorderkante und dem Hauptflügel vor. Diese wird als vorspringende Stufe ausgeführt, weil dadurch eine viel kritischere rückspringende Stufe (z.B. aufgrund von Fertigungstoleranzen) vermieden wird. Im bisherigen Entwurf wird die Trennstelle mit Füllmaterial ausgefüllt. Dadurch kann allerdings ein negativer Einfluss auf die laminare Strömung entstehen. Deshalb wird in der vorliegenden Arbeit untersucht, wie Absaugung hier integriert werden kann. Bei Absaugung an Flügelvorderkanten ist der nötige Unterdruck, der durch die Saugpumpe erzeugt werden muss, für Effizienz von großer Bedeutung. Die Möglichkeit der Integration des vorliegenden Konzepts in bereits entwickelte Absaugesysteme, siehe z.B. Havar et al. [4], wird unter diesem Gesichtspunkt bewertet.

Eine Methode zur passiven Absaugung auf einer ungekrümmten Oberfläche wurde ebenfalls auf dem STAB Workshop 2015 vorgestellt, siehe [1]. Dabei wird der Überdruck durch Aufstauung vor der Stufe ausgenutzt, um über einen Bypass Strömung abzusaugen. Der Auslass des Bypass befindet sich weit stromab der Stelle wo laminar-turbulenter Umschlag ohne Fügestelle erwartet wird. Dadurch wird der laminar-turbulente Umschlag im Vergleich zur glatten Oberfläche deutlich verzögert. Eine Weiterentwicklung dieser Methode sowie die Bewertung des Einsparungspotentials ist ebenfalls Gegenstand dieser Arbeit.

Literatur

[1] J. Zahn, U. Rist, Grenzschichtabsaugung an einer Fügestelle zur Laminarhaltung der Strömung. *Jahresbericht 2015 zum 16. STAB-Workshop 12.-13. November 2015 Göttingen*, 2015.

[2] J. L. van Ingen, A suggested semi-empirical method for the calculation of the boundary layer transition region. *Technische Hogeschool Delft*, Rapport VTH-74, 1956.

[3] C. Hühne, C. Ückert, O. Steffen, Multifunktionale Flügelvorderkante in Multimaterialbauweise. *Lightweight Design*, Ausgabe 1/2016, 2016.

[4] T. Havar, M. Geistbeck, M. Meyer, O. Rohr, T. Meer, Verbindungsanordnung zur aerodynamisch glatten Verbindung zweier Profilelemente, Verfahren zu deren Fertigung und Vorrichtung zur Durchführung des Verfahrens. *Internationales Patent*, WO 2013/000447 A1, 2013.

Mitteilung

Projektgruppe / Fachkreis: Hochagile Konfigurationen

Flugkörperentwicklung unter Nutzung
des „Virtuellen Windkanals“

Dr. Roland Höld; Christian Surrauer, Dr. Mark Förster
MBDA-Deutschland, Hagenauer Forst 27, 86529 Schrobenhausen,
roland.hoeld@mbda-systems.de

Überblick

Bei der Entwicklung neuer Flugkörper sowie der Leistungssteigerung existierender Flugkörper gewinnen numerische Methoden zunehmend an Bedeutung. Dabei liefern numerische Methoden, wie sie beim Konzept des „Virtuellen Windkanals“ eingesetzt werden, einerseits Möglichkeiten zur Reduzierung von Kosten und Entwicklungszeiten, andererseits ergeben sich durch deren Einsatz aber auch neue Chancen im Bereich der Optimierung von Flugkörpern.

Die klassische Entwicklung kompletter aerodynamischer Datensätze, oder erforderlicher Korrekturen, basierend auf experimentell ermittelten Daten im Windkanal ist seit langem „State oft the Art“. Im Gegensatz dazu stellt der Einsatz des „Virtuellen Windkanals“ Herausforderungen dar, die insbesondere im Hiblick auf Verlässlichkeit der erzeugten Daten noch kritisch zu bewerten sind. Dies trifft insbesondere dann zu, wenn Teilbereiche oder auch der gesamte aerodynamische Datensatz ausschließlich auf dem Konzept des „Virtuellen Windkanals“ basieren.

In der vorliegenden Arbeit werden Arbeiten zur numerischen Erzeugung aerodynamischer Daten im „Virtuellen Windkanal“ bei der Flugkörperentwicklung vorgestellt. Als numerische Methode wurde dabei im Wesentlichen der CFD (Computational Fluid Mechanics) Code Tau des DLR eingesetzt. Es wird insbesondere auf die Erzeugung eines kompletten aerodynamischen Datensatzes unter Verzicht auf experimentelle Windkanalversuche eingegangen und Vor- und Nachteile, sowie neuartige Fragestellungen, die sich bei diesem Ansatz ergeben, eingegangen.

Inhalt

Die Entwicklung der numerischen Methoden im Bereich CFD in Kombination mit den verfügbaren Rechenleistungen im Bereich HPC (High Performance Computing) erlaubt es heute, dass bei der Erstellung aerodynamischer Datensätze und bei der Optimierung von Flugkörpern heute ganz oder teilweise auf experimentelle Windkanalversuche verzichtet werden kann. Es ergeben sich hieraus neue Chancen aber auch neue Herausforderungen.

Die Arbeit geht an ausgesuchten Beispielen darauf ein, welche neuen Möglichkeiten der Virtuelle Windkanal bietet und welche Herausforderungen sich bei dessen Einsatz ergeben. Der industrielle Einsatz des Virtuellen Windkanals reicht derzeit von der Bewertung des aerodynamischen Einflusses durch Konturänderungen bis hin zu einer kompletten Flugkörperentwicklung, die ganz auf experimentelle Windkanaldaten verzichtet. Letzteres stellt hohe Anforderungen und Zuverlässiglkeit and die CFD Simulationen. Hieraus leiten sich auch hohe Anforderungen an Flugversuche ab, die erforderlich sind, um die erstellten Datensätze zu verifizieren.

Hauptaugenmerk liegt bei der Arbeit auf der Eintwicklung aerodynamischer Datensätze für ein Flugkörperpdrojekt unter Verzicht auf experimentelle Windkanalversuche. In einer ersten Phase wurde dabei ein Demonstrator entwickelt und dessen Leistungsfähigkeit in Flugversuchen nachgewiesen. In einem zweiten Entwicklungsschritt wird der Flugkörper für eine Einsaztreife weiterentwickelt. Die hierfür erforderliche Aerodynamik ist aus verschiedenen Gründen komplexer als die des Demonstrators und stellt erhöhte Ansprüche an den Datensatz und die CFD Simulationen. In der Arbeit werden die jeweiligen Anforderungen und Herausforderungen dargestellt und bewertet, sowie Vor- und Nachteile des Konzeptes „Virtueller Windkanal“ genannt. Neue Chanchen und Möglichkeiten aber auch aktuelle Grenzen, die der Einsatz des Virtuellen Windkanals derzeit aufweist, werden aufgezeigt.

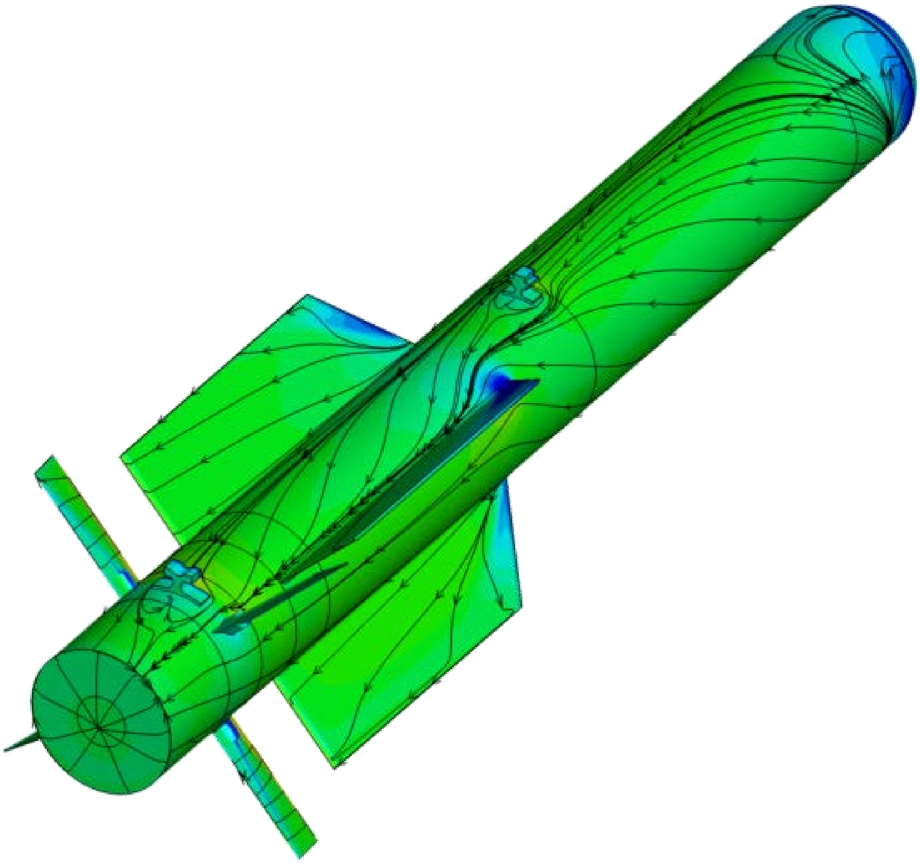

Mitteilung

Projektgruppe / Fachkreis:
Hochagile Konfigurationen / Experimentelle Aerodynamik

Untersuchung zu Gesamtdruckverlusten in der Verdichtereintrittsebene eines integrierten Einlaufs mit eingetragenem Wirbel

Stefan Koch, Markus Rütten, Martin Rein
Institut für Aerodynamik und Strömungstechnik
Abteilung Hochgeschwindigkeitskonfigurationen
Bunsenstr. 10, 37073 Göttingen
Stefan.Koch@dlr.de, Markus.Ruetten@dlr.de, Martin.Rein@dlr.de

Aufgrund der einsatzbedingten Anforderungen für Unmanned Combat Air Vehicles (UCAV) ist die Verwendung eines integrierten Triebwerkseinlaufes mit geringer Einbauhöhe typisch. Die S-Schlag-Geometrie eines solchen Einlaufes ist strömungsmechanisch problematisch, da sie zur Ablösung neigt. Zusammen mit der in den Einlauf eingetragenen Wandgrenzschicht ergibt sich eine ungleichmäßige Gesamtdruckverteilung in der Verdichtereintrittsebene des Triebwerks. Dies führt zu einer Leistungsverminderung und im schlimmsten Fall zum Aussetzen des Triebwerks. In der Vergangenheit wurden bereits verschiedene numerische und experimentelle Untersuchungen von den Autoren zum o.a. Themenkomplex durchgeführt. Hierbei ging es um die Optimierung der Einlaufgeometrie, den Grenzschichteintrag in den Einlauf und damit im Zusammenhang stehende Parameter wie Machzahl, Reynoldszahl und Massenstrom unter besonderer Berücksichtigung der Gesamtdruckverluste in der Verdichtereintrittsebene des Triebwerks, [1]-[4].

In der hier beschriebenen Arbeit wird der Einfluss einer zusätzlichen Störung untersucht, die unter kritischen Flugzuständen am UCAV auftreten kann und die Zuströmung zum Triebwerk u.U. massiv beeinflusst. Es wird der Eintrag eines Wirbels simuliert, wie er sich bei hohen Anstellwinkeln an der Vorderkante einer für UCAVs typischen Deltaflügelkonfiguration bildet. Die Auswirkungen des Eintrags auf die Gesamtdruckverteilung in der Verdichtereintrittsebene wurde sowohl experimentell als auch numerisch für eine Reihe von Testfällen untersucht, bei denen sowohl der Massenfluss durch den Einlauf als auch die Machzahl vor dem Einlauf unabhängig voneinander variiert wurden.

Die Messungen wurden am Kryo-Rohrwindkanal (KRG) der Deutsch-Niederländischen Windkanäle (DNW) an einer ebenen Platte mit integriertem Einlauf durchgeführt, Abb. 1. Anhand numerischer Voruntersuchungen wurden Wirbelgeneratoren in Form von Dreiecksblechen ausgelegt, die einen Wirbel erzeugen, der in seiner Größe einem abgehenden Vorderkantenwirbel eines UCAV entspricht, Abb. 2. Insgesamt wurden drei Wirbelgeneratoren mit verschiedener Höhe und damit unterschiedlicher Zirkulation verwendet.

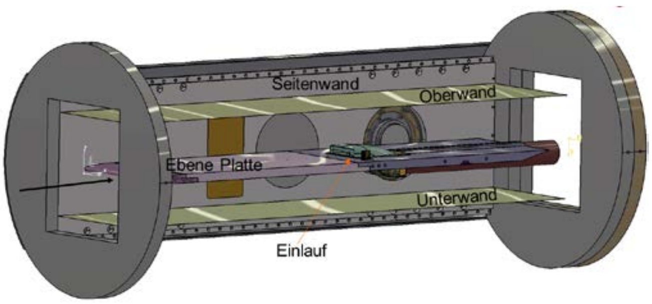

Abb. 1: Messstrecke des KRG mit eingebauter, ebener Platte mit integriertem Einlauf

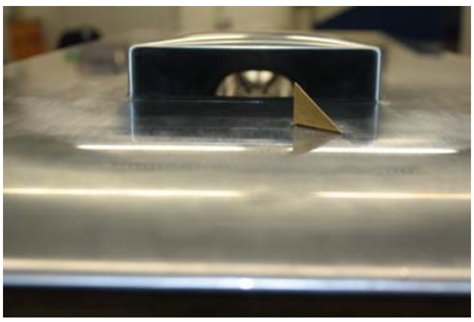

Abb. 2: Wirbelgenerator stromauf vom integrierten Einlauf

Mittels eines drehbaren Sondenrechens mit geringer Verdrängungswirkung konnten Gesamtdruckverluste in der Verdichtereintrittsebene bestimmt und so der sog. DC60-Wert ermittelt werden. Ein kleiner DC60-Wert beschreibt dabei eine gleichmäßige Gesamtdruckverteilung in der Verdichtereintrittsebene und ist ein wichtiger Parameter bei der Auslegung von Triebwerken.

Wird lediglich die Wandgrenzschicht in den Einlauf eingetragen, zeigt sich ein massiveres Gesamtdruckverlustgebiet hauptsächlich im unteren Teil der Verdichtereintrittsebene bedingt durch die dortige Ablöseneigung der S-Schlag-Einlaufgeometrie und aufgrund der Gesamtdruckverluste aus der Wandgrenzschicht, Abb. 3a). Bei Eintritt eines Wirbels in den Einlauf zeigt sich durch die Drehbewegung des Wirbels ein von der Wand hinweg bewegtes Gesamtdruckverlustgebiet. Außerdem kommt es im Einlauf zu einer Seitwärtsbewegung des Wirbels, die mit zunehmender Zirkulation so groß ist, dass der Wirbel die senkrechte Symmetrieebene sogar kreuzt, Abb. 3b). Analysen zeigen außerdem, dass bei zunehmender Zirkulation des eingetragenen Wirbels die Gesamtdruckverluste zwar zunehmen, der DC60-Wert jedoch abnimmt. Die wandnahen Druckverluste im oberen Teil der Verdichtereintrittsebene sind Druckverluste durch Ablösung, die durch die dortige Wandkrümmung und den damit verbundenen Druckgradienten verbunden sind. Die numerischen Ergebnisse aus TAU bestätigen die experimentellen Ergebnisse aus dem KRG, Abb. 3c).

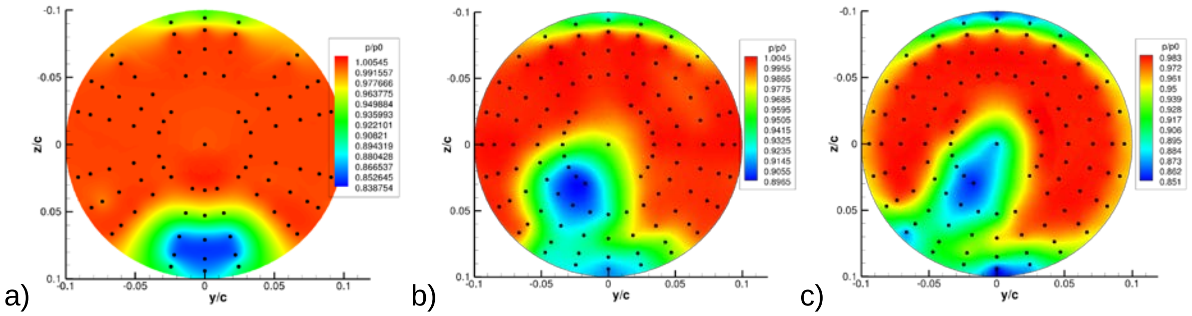

Abb. 3: Gesamtdruckverlustverteilung in der Verdichtereintrittsebene, $Ma_\infty = 0.60$, $Re_1 = 30 \cdot 10^6\ m^{-1}$; a) ohne Wirbeleintrag (KRG); b) mit Wirbeleintrag (KRG); c) mit Wirbeleintrag (TAU)

Der Einfluss des Wirbeleintrags auf die Druckverteilung in der Verdichtereintrittsebene wurde analysiert, ebenso wie der Einfluss unterschiedlicher Wirbelstärken. Die experimentellen und numerischen Ergebnisse wurden gegenübergestellt. Darüber hinaus wurde der Einfluss des Massenflusses bei konstanter Machzahl untersucht, sowie der Einfluss der Machzahl bei konstantem Massenfluss analysiert, wobei in einem Fall mittels der adaptiven Wände der Windkanalmessstrecke zusätzlich ein Stoß vor dem Einlauf erzeugt wurde, wie er bei sehr hohen Fluggeschwindigkeiten auftreten kann.

Literatur

[1] Rütten, M., Kuckenburg, S., Koch, S., Rein, M.: Investigation of the Flow within Partially Submerged Scoop Type Air Intakes; 31st AIAA Applied Aerodynamics Conference, 2013 (doi: 10.2514/6.2013-2912)

[2] Rein, M., Koch, S., and Rütten, M.: “Experimental Investigations on the Influence of Ingesting Boundary Layers into a Diverterless S-Duct Intake,” AIAA Paper 2014-0373, 2014 (doi: 10.2514/6.2014-0373)

[3] Rein, M., Koch, S.: Experimental Study of Boundary-Layer Ingestion into a Diverterless S-Duct Intake,” Journal of Aircraft, Technical Note, Vol. 53, No. 11, 2015

[4] Koch, S., Rütten, M., Rein, M.: Experimentelle und Numerische Untersuchungen zu Integrierten Einläufen für Agile und Hoch Gepfeilte Flugzeugkonfigurationen. DGLR Paper-0173, Deutscher Luft- und Raumfahrtkongress, Rostock, 2015

Mitteilung

Projektgruppe/Fachkreis: Hochagile Konfigurationen

Numerische Untersuchung zum Einsatz von Querschubstrahlen in Flugkörperdüsen zur Schubvektorsteuerung

Christian Schnepf und Erich Schülein
DLR Göttingen, Institut für Aerodynamik und Strömungstechnik
Bunsenstraße 10, 37073 Göttingen
Christian.Schnepf@dlr.de

Die Schubvektorsteuerung stellt eine wirksame Methode zur Erhöhung der Manövrierbarkeit eines Flugkörpers dar. Neben etablierten mechanischen Konzepten (Strahlruder/ schwenkbare Düsen [1]) existieren auch alternative Konzepte. Eine Möglichkeit der fluidischen Schubvektorsteuerung in Überschalltriebwerken stellt ein sekundärer Seitenstrahl dar (QD), der nahezu normal zum Hauptstrahl der Triebwerksdüse ausgeblasen wird (Abb. 1a). Der ausgeblasene Seitenstrahl, im folgenden Querschubstrahl genannt, induziert lokal einen sich stromauf des Querschubstrahls befindlichen Bugstoß. Der Bugstoß und dessen Wechselwirkung mit der Hauptstrahlgrenzschicht induziert eine asymmetrische Druckverteilung an der Triebwerksdüsenwand, die im günstigsten Fall die Steuerkräfte erhöht (Impuls des Querschubstrahls + asymmetrische Druckverteilung). Am Düsenaustritt äußert sich dies in Form einer Hauptstrahlumlenkung. Diese Art der fluidischen Steuerung wird in der aktuellen Arbeit an einer kompletten Flugkörperkonfiguration untersucht. Abweichend zu den meisten anderen Arbeiten zu diesem Thema befindet sich die Querschubstrahldüse relativ nahe am Schubdüsenaustritt (Abb. 1a). Des Weiteren ist die Querschubdüse so orientiert, dass der QD-Schubvektor nicht auf die gegenüberliegende Wand der Triebwerksdüse trifft. Hierdurch kann der Impuls des Querschubstrahls auch bei ausgebranntem Triebwerk noch zur Steuerung des Flugkörpers genutzt werden. Der Hauptteil der aktuellen Arbeit stellt die Untersuchung des Einflusses der axialer Querschubdüsenposition (Abb. 1a) und der Geometrie der QD-Düse (Abb. 1b) auf die entstehenden Steuerkräfte dar. Um die Leistung der fluidischen Schubvektorsteuerung einordnen zu können, findet des Weiteren ein Vergleich mit dem herkömmlichen Querschubsteuerungskonzept statt, bei dem die Querschubdüse an der Außenhaut des Flugörpers platziert ist. Für dieses Konzept wurden zwei Positionen am Flugkörper ausgewählt. Eine befindet sich am Heck (QH), die andere am Übergang der Nase in den zylindrischen Flugkörperteil (QS).

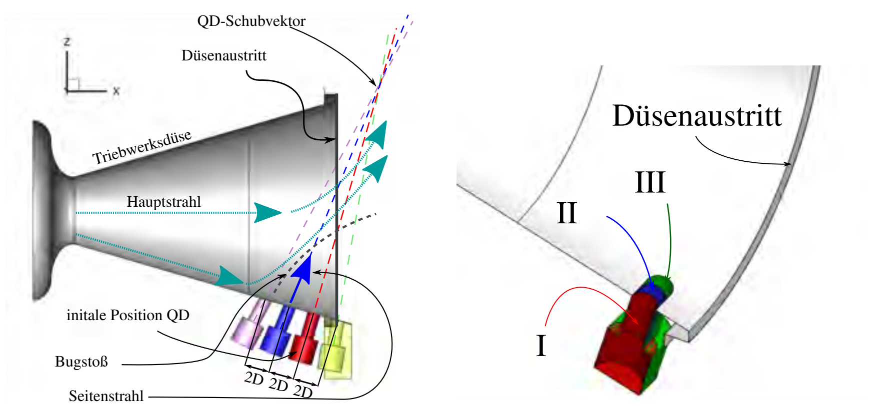

(a) Axiale Variation (b) Variation der Düsenform

Abbildung 1: Skizze der Variation der Querschubdüse.

Die vorliegende numerische Arbeit wurde mit Hilfe des DLR-TAU-Codes [2] durchgeführt. Mit dem TAU-Code werden die stationären RANS-Gleichungen in Verbindung mit dem Menter-SST-Turbulenzmodell gelöst. Vereinfachend werden Realgaseffekte in der Simulation im Bezug auf die heiße Düsenströmung vernachlässigt. Die Machzahl am Düsenaustritt beträgt Ma = 4. Die Querschubsteuerung wird an einem generischen Überschallflugkörper, der sich mit Ma = 4 bewegt, untersucht. Die Simulationen wurden hauptsächlich für eine Flughöhe von 10 km durchgeführt. Punktuell fanden auch Simulationen bei einer Flughöhe von 30 km statt, um den Einfluss des Staudrucks auf die Wirksamkeit der Steuerkonzepte bzw. Düsenpositionen zu untersuchen. Es ist bekannt, dass der Staudruck einen wesentlichen Einfluss auf die Wirksamkeit besitzt.

In Abb. 2 sind Ergebnisse für die I-Düsengeometrie in Form des Gesamtflugkörperkraftbeiwerts C_F für die z-Achsenrichtung aufgetragen. Der Wert C_F-Impuls gibt den Kraftbeiwert an, der sich aufgrund des reinen Impulses der Querschubdüse ergibt. Wie sich zeigt, führt die axiale Variation der Position des Querschubstrahls in der Triebwerksdüse zu keiner wesentlichen Veränderung in der Leistung. Ein betragsmäßiges Maximum für den Kraftbeiwert C_F ergibt sich für die Düse, die zwei Querschubdüsendurchmesser stromauf der Ausgangsdüsenposition (Initial) zu finden ist (Abb. 1a). Interessanter als der Vergleich der Düsenpositionen in der Triebwerksdüse ist der Vergleich der Effektivität der Querschubdüsen für verschiedene Positionen am Gesamtflugkörper. Hier ergibt sich für die Düse am Nasen-Zylinderübergang (QS) der geringste Kraftbeiwert. Dieser liegt sogar unter dem Wert für C_F-Impuls. Verantwortlich hierfür sind Effekte der Querschubstrahl-Grenzschichtwechselwirkung, die sich marginal bis zum Heck auf die Oberflächendruckverteilung des Flugkörpers auswirken. Aufgrund der Länge des Flugkörpers entsteht integral ein negativer Effekt auf die Kräftebilanz. Für die beiden Querschubdüsen im Bereich des Flugkörperhecks (QD/ QH) ergeben sich ähnliche Kraftbeiwerte.

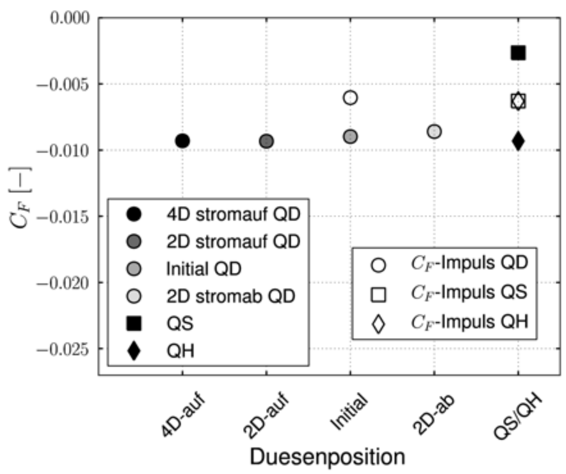

Abbildung 2: Gesamtkraftbeiwert in z-Richtung für Ma = 4 bei einer Flughöhe von 10 km für die I-Düsengeometrie

In der endgültigen Fassung des Artikels werden folgende Punkte zusäzlich bzw. tiefer behandelt:

- Detailliertere Analyse der Strömungsfelder
- Detailliertere Analyse der Beiwerte auch auf Basis des Verstärkungsfaktors [1] und des Massenstroms der Querschubstrahlen
- Detailliertere Analyse des Vergleichs der Düsenlagen, Positionen und Flughöhe

Literatur

[1] K. A. Deere, *Summary of fluidic thrust vectoring research conducted at NASA langley research center*, The 21st AIAA Applied Aerodynamics Conference, AIAA-2003-3800, 2003

[2] D. Schwammborn, T. Gerhold, R. Heinrich,*The DLR TAU-Code: Recent Application in Resarch and Industry*, Invited Lecture in Proceeding on CD of the European Conference on Computational Fluid Dynamics ECCOMAS CDF, 2006

Mitteilung

Projektgruppe/ Fachkreis: Drehflügleraerodynamik

Towards density reconstruction of helicopter blade tip vortices from high-speed background-oriented schlieren data

J. N. Braukmann*, A. Bauknecht, C. C. Wolf, M. Raffel

German Aerospace Center, Aerodynamics and Flow Technology, Bunsenstraße 10, 37073 Göttingen
* johannes.braukmann@dlr.de, Tel. 0551/709-2443

A helicopter main rotor produces blade tip vortices during flight. In certain maneuvers and flight conditions these vortices interact with the following rotor blades. This effect is called blade-vortex interaction (BVI). BVI is one of the main reasons for noise and vibration emissions on helicopters. Therefore, understanding the generation and decay of the vortex is of high interest.

Particle image velocimetry (PIV) and the background-oriented schlieren (BOS) method are commonly used to characterize the flow field of vortices. In contrast to measuring the velocities with PIV, BOS visualizes and also quantifies density gradients in the flow field as deflections of a stochastic background pattern. The vortex rotation and consequent centrifugal forces lead to a lower static pressure and a lower density in the vortex core. The objective of this work is to reconstruct the density distribution of young blade tip vortices from 2D density gradient data measured with a high speed, laser speckle-illuminated BOS setup.

The data for the density reconstruction was aquired within the DLR STAR (Smart-Twisting Active Rotor) project, which was carried out to investigate the functionality and effect of actively twisted blades on the rotor wake. The STAR rotor was a 41% Mach-scaled, 4-bladed BO105 rotor with a diameter of $4\,m$. The blades had a linear pre-twist of $-10°/R$ and a rectangular planform. The described density reconstruction was done for a non-actuated test case in hover conditions at a rotational frequency of $17.35\,Hz$ with blade loadings of $C_T/\sigma = 0.025$ to 0.064. Using a setup with two high speed cameras as depicted in Fig. 1, 15 images with an azimuthal increment of $\Delta\Psi_V = 2.8°$ were taken after each blade passing. This results in an azimuthal range of $\Psi_V = 2°$ to $41°$.

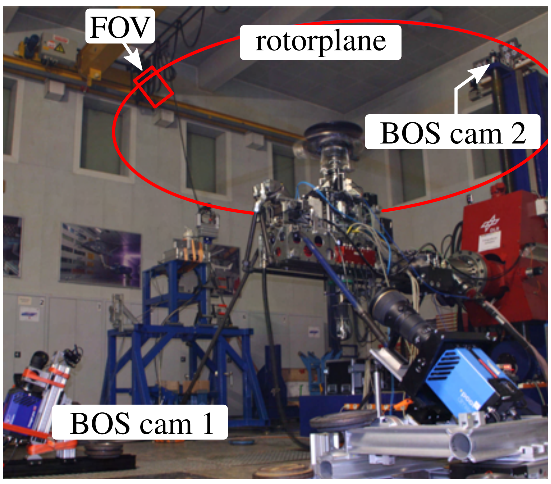

Figure 1: DLR STAR stereo BOS setup after Bauknecht [1]

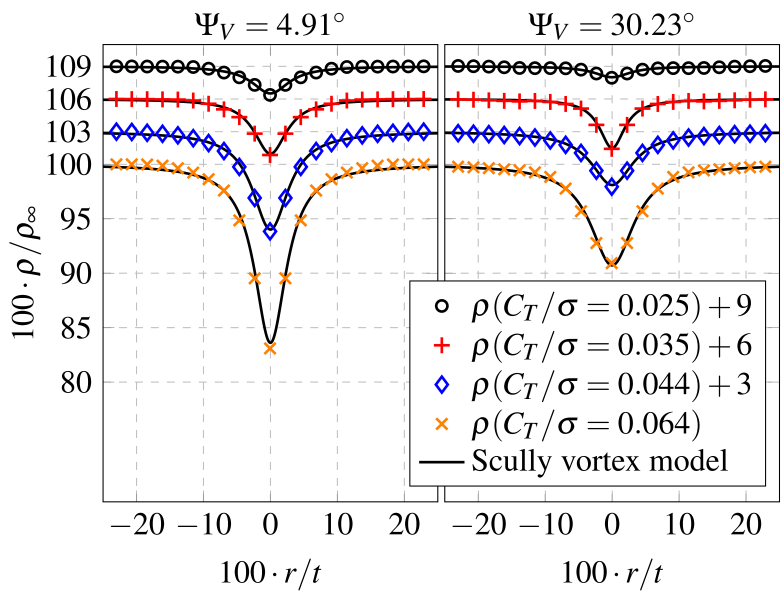

Figure 2: Density distribution at two different vortex ages for a variation of the blade loading

The apparent background shift measured with BOS is nearly proportional to the density gradient along the line of sight. A pseudo-density distribution can therefore be obtained by a spatial integration of the image shift. This distribution then represents a projection of the 3D density object onto a 2D plane. To reconstruct the 3D density distribution, multiple views from different angles are necessary. Using the assumption that a blade vortex is almost rotationally symmetric along its axis, all projections perpendicular to this axis are equal. Therefore, a single projection allows for the 3D reconstruction of a rotationally symmetric object as done in this paper. Due to the complex optical measurement setup a reference measurement with a hot air stream was carried out to calibrate the density magnitude. As a result, density distributions as shown in Fig. 2 were obtained. Figure 2 shows cross-sectional distributions of the reduced density at two vortex ages for different blade loadings. The curves are plotted with a vertical offset of 3 % ρ_∞ for better readability. The density outside the vortex equals the ambient density, and reaches a minimum in the vortex center. For young vortices ($\Psi_V = 4.91°$) and a blade loading of $C_T/\sigma = 0.064$ (marked by ×), this minimal value is about 17 % lower than ρ_∞. For vortices corresponding to $C_T/\sigma = 0.025$ (marked by ∘) at the same age, the minimum is only 3 % lower than ρ_∞. The density deficit recovers with rising vortex age. In addition to the measured data, fits of the Scully [3] vortex model are depicted as black lines in Fig. 2. The model shows a good agreement with the obtained data.

To quantify the vortex size, the vortex core radius $r_{core,BOS}$ was defined as the half-width at the half-height of the density deficit. The development of the core radius reconstructed from the BOS measurement and the radii obtained with PIV by Bauknecht [1], both for $C_T/\sigma = 0.044$, are compared in Fig. 3. An initial decrease in vortex core radius is visible in both datasets. At a vortex age of about $\Psi_V = 15°$, the tendency changes to slightly rising core radii as indicated by the black line. This behavior suggests a vortex roll-up within the first 15° of vortex age, as already described by Bauknecht [1] and Ramasamy et al. [2].

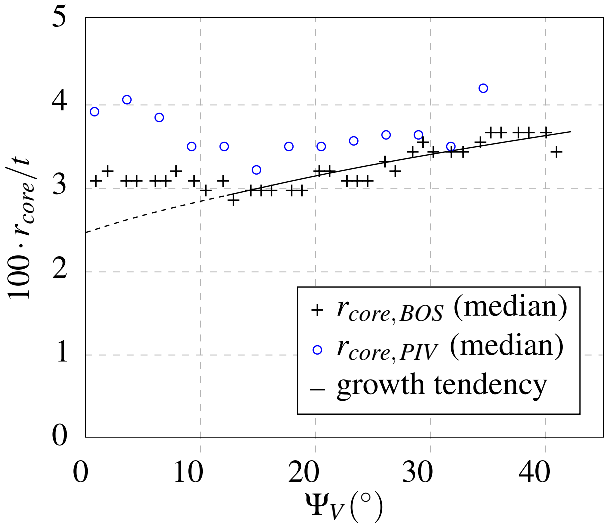

Figure 3: Development of the vortex core radius measured by PIV and BOS after Bauknecht [1]

A further description of the applied methods and an intensive discussion of the results will be given in the full paper.

References

[1] Bauknecht A (2016), *Characterization of blade-tip vortices on large-scale rotors*, Leibniz Universität Hannover.

[2] Ramasamy M, Johnson B, Huismann T, Leishman JG (2009), *Digital Particle Image Velocimetry Measurements of Tip Vortex Characteristics Using an Improved Aperiodicity Correction*, Journal of the American Helicopter Society, vol. 54, pp. 1-13.

[3] Scully M & Sullivan JP (1972), *Helicopter rotor wake geometry and airloads and development of laser Doppler velocimeter for use in helicopter rotor wakes*, TR 179, MIT Aerophysics Laboratory.

Mitteilung

Projektgruppe/Fachkreis: Drehflügleraerodynamik, Versuchstechnik

Unsteady boundary layer transition detection by automated analysis of hot film data

A. Goerttler*, A.D. Gardner†, K. Richter‡

The state of the flow over the rotor blades plays an important role in reducing the power consumption of a helicopter. Currently wind tunnel data is necessary to get results on unsteady transitional characteristics. The state of the art technique for unsteady transition detection is hot film anemometry. This paper will present an algorithm which automatically analyzes the voltage of each sensor to obtain the unsteady boundary layer characteristics.

Data was obtained from 61 hot film sensors operated in constant temperature mode on a DSA-9A airfoil. The airfoil was mounted horizontally in the test section of the Transonic Wind Tunnel Göttingen (DNW-TWG). The 2D model was driven by two hydraulic motors to execute a sinusoidal pitching motion. Every dynamic test case was sampled for 80 periods at a rate of $f = 135$kHz. Automated algorithms replace time-consuming manual analysis and produce results approximately two orders of magnitude faster. Furthermore automated algorithms can analyze every period on their own resulting in a quantification of the scatter between the periods.

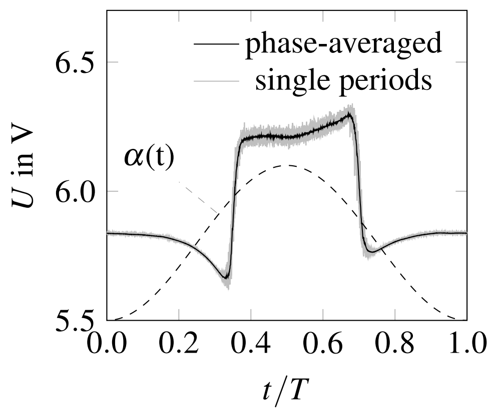

(a) voltage

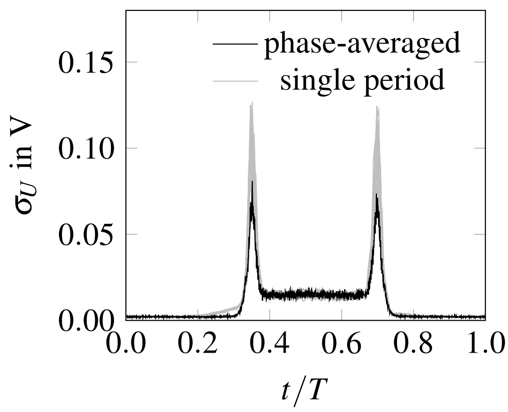

(b) standard deviation

Figure 1: Voltage signal of all periods (a) and their root mean square (b) for the sensor at $x/c = 0.20$ on the upper side for $\alpha = 0^\circ \pm 7^\circ$, $f = 6.6$Hz, $M = 0.3$ and $Re_c = 1.8 \times 10^6$

Fig. 1 shows the voltage (a) and the standard deviation signals (b) of the sensor at $x/c = 0.20$ on the upper side for a sinusoidal pitching case with $\alpha = 0^\circ \pm 7^\circ$, $f = 6.6$Hz, $M = 0.3$ and $Re_c = 1.8 \times 10^6$. Transition can be seen with hot film data results since laminar and turbulent flow develop different heat transfer coefficients, with turbulent flow ($0.35 < t/T < 0.7$) requiring higher power than laminar flow to maintain the constant temperature of the sensor. The skewness is used to evaluate the unsteady boundary layer. The skewness is the third central moment and describes the symmetry of a given distribution. The skewness, taken in a sliding window, is shown in Fig. 2(a). Two similar peaks occur in the graph. These peaks turn out to be a reliable indicator for the transition process. The prominent

*Corresponding Author. German Aerospace Center (DLR), Aerodynamics and Flow Technology (AS), Bunsenstraße 10, 37073 Göttingen, Germany, *Andreas.Goerttler@dlr.de*, Tel. 0551/709-2277
†DLR Institute of Aerodynamics and Flow Technology
‡DLR Institute of Aerodynamics and Flow Technology

zero crossing marks the 50 % intermittency point with equal laminar and turbulent parts. Fig. 2(b) represents the mean of all detected points in the phase-averaged voltage signal. Since the algorithm examines every period, the standard deviation is also computed (not shown). Fig. 3 compares manual and automated results, which both agree well. The standard deviation is for all sensors less than one percent of one period.

Alternative algorithms will be thoroughly explained and their results compared.

References

[1] Richter K., Koch S., Goerttler A., Lütke B., Wolf C.C., Benkel A. (2015) Unsteady Boundary Layer Transition on the DSA-9A Rotor Blade Airfoil, 41st European Rotorcraft Forum, Munich, Germany, 1-4 Sept. 2015.

[2] Goerttler A. (2015) Analyse der instationären Grenzschichttransition am schwingenden DSA-9A Rotorblattprofil, Masterarbeit, Universität Stuttgart

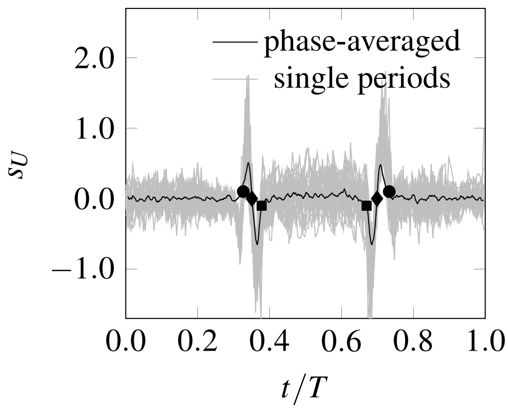

(a) skewness

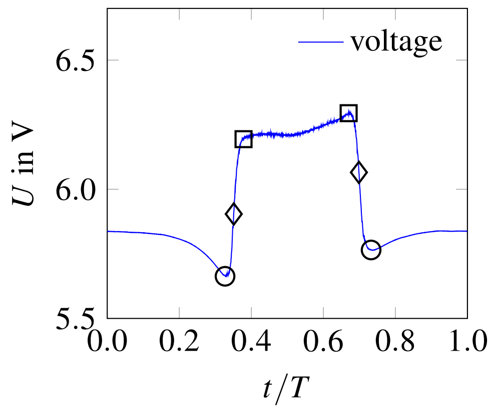

(b) voltage

Figure 2: Positions of the detected transition points in the skewness signal (a) and in the phase-averaged voltage signal (b) for the sensor at $x/c = 0.2$ on the upper side for $\alpha = 0° \pm 7°$, $f = 6.6$Hz, $M = 0.3$ and $Re_c = 1.8 \times 10^6$, detection based on single periods skewness, ◯= onset/end of laminar flow, ◇= 50% intermittency, □= onset/end of turbulent flow

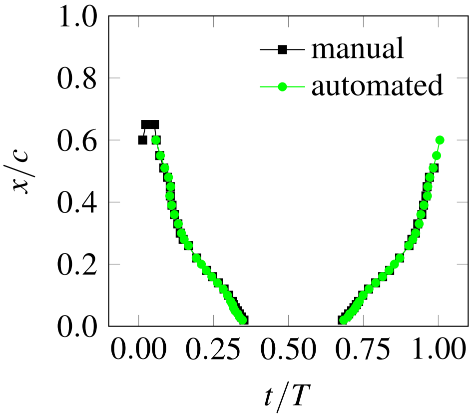

Figure 3: Onset of transition on the upper side for $\alpha = 5° \pm 7°$, $f = 6.6$Hz, $M = 0.3$ and $Re_c = 1.8 \times 10^6$

Mitteilung

Projektgruppe / Fachkreis: Drehflügleraerodynamik

Numerical and Experimental Investigations of Twin-Engine-Light Utility Helicopter Wake Flow

M. Stuhlpfarrer, A. Kümmel, C. Breitsamter
Lehrstuhl für Aerodynamik und Strömungsmechanik, Technische Universität München
85748 Garching bei München
marco.stuhlpfarrer@aer.mw.tum.de

The knowledge of the wake flow of helicopters as well as the related unsteady effects is important concerning comfort and safety. Especially, the interaction of the wake flow with the downstream located components of the helicopter requires accurate information already in the design process. Nevertheless, the precise prediction of the wake flow is a difficult goal by applying computational fluid dynamics. For a precise simulation of the wake flow, the origin of a flow structure as well as the convection has to be captured appropriately. There are high requirements on the modeling of the physical effects, due to the variety of different flow regimes, i.e. laminar or turbulent and attached or separated flow. Furthermore, low numerical dissipation is needed to reproduce the convection accurately [1].
In order to find a suited modelling approach, numerical and experimental investigations are conducted. Latter shall be used to provide a reliable database for validation. The experiments are carried out using a 1:5 scale model of the twin-engine-light utility helicopter configuration. This includes the cabin and skid landing gear as well as a five-bladed rotor head. The blades are truncated at the first aerodynamic effective radial position. Furthermore, a fully functional swashplate is included, which allows cyclic and collective pitch motion. Additionally, the model includes an aerodynamic optimized tail shape with contoured strakes [2], [3]. These shall avoid the up-rolling vortex-pair and reduce the size of the region of separated flow. Figure 1 left shows the helicopter configuration mounted in the wind tunnel A. Figure 1 right shows the setup for the numerical simulation. Therefore, some simplifications at the rotor head were done.


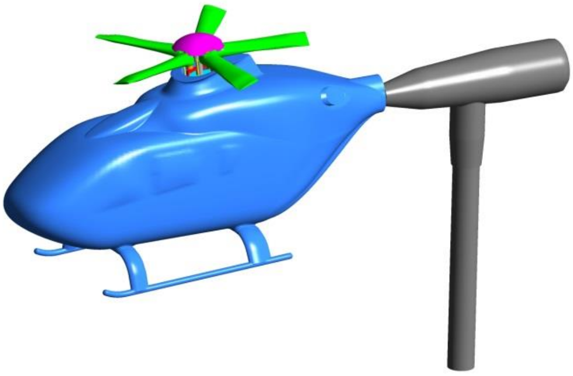

Figure 1: Helicopter configuration mounted in the wind tunnel A (left). Geometry used for the numerical simulation (right).

The experimental investigations are conducted in the wind tunnel A of the chair of aerodynamics and fluid mechanics of the Technische Universität München. Therefore, force measurements with a six-component underfloor balance are carried out, which are mainly used for validating the integral coefficients. For a more detailed investigation of the wake flow field stereo Particle Image Velocimetry (PIV) in different crossflow-section is applied.

The numerical grids are generated with ANSYS ICEM CFD. For this purpose, a block-structured hexahedron mesh is applied. The dimensionless wall distance is set to $y^+ = 1$. The grid is divided into three parts which are connected by sliding mesh interfaces. The static domain contains the helicopter configuration. Furthermore, a rotating disk is embedded to model the motion of the rotor. Therein, an additional domain is designed which realizes the cyclic movement of each rotor blade. The numerical simulations are performed with the commercial software ANSYS Fluent. Therefore, the Reynolds-averaged Navier-Stokes equations are solved. Due to the low Mach number $Ma < 0.3$ the flow is considered to be incompressible. Turbulence is modelled by the scale-adaptive simulation model [4]. In order to obtain low numerical dissipation, for the spatial discretization the „Bounded Central-Difference-Scheme“ is applied and for the temporal discretization the „Bounded Second Order Implicit“ scheme [5] is used. Furthermore, the Courant-Friedrichs-Lewy number of $\mathrm{CFL} < 1$ is set in the wake flow.
Figure 2 left shows the normalized time-averaged axial velocity distribution in a crossflow plane downstream of the fuselage obtained by PIV. Figure 2 right presents the same quantity for the result of the numerical simulation. Both provide a velocity deficit between the strakes as well as in the wake of the skid landing gear. Furthermore, a good accordance between the numerical and experimental solution is shown.

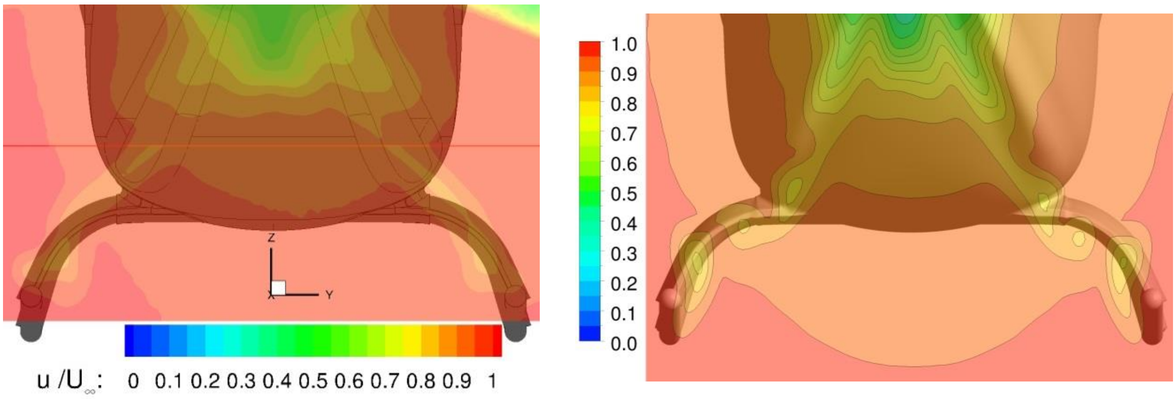

Figure 2: Normalized time-averaged axial velocity distribution in a crossflow plane downstream the fuselage obtained by PIV (left) and provided by the numerical simulation (right).

.

Literaturverzeichnis

[1] P. W. Li Xu, „High Order Accurate Low Dissipation Method for Unsteady Compressible Viscous Flow Computation on Helicopter Rotor in Forward Flight,“ *Journal of Computational Physics,* Bd. 258, pp. 470-488, 2014.

[2] Q. e. a. Zhang, „Advanced CFD-based Optimization Methods Applied to the Industrial Design Process of Airframe Components at Airbus Helicopters,“ *American Helicopter Society 70th Annual Forum,* 2014.

[3] M. Bebesel, A. D'Alascio, S. Schneider, S. Guenther, F. Vogel, C. Wehle und D. Schimke, „Bluecopter Demonstrator - An Approach of Eco-Efficient Helicopter Design,“ in *41st European Rotorcraft Forum*, München, 2015.

[4] F. Menter und Y. Egorov, „The Scale-Adaptive Simultion Method for Unsteady Turbulent Flow Predictions. Part 1: Theory and Model Description,“ *Journal Flow Turbulence and Combustion,* Bd. 85, pp. 113-138, 2010.

[5] ANSYS, Inc., "ANSYS help system," 2014.

Mitteilung

Projektgruppe / Fachkreis: Drehflügleraerodynamik, Windenergie, Numerische Simulation

Wind energy turbine wake vortex influence on helicopter rotor trim

Berend G. van der Wall
German Aerospace Center, Lilienthalplatz 7, 38108 Braunschweig, Germany,
berend.vanderwall@dlr.de

Paul H. Lehmann
German Aerospace Center, Lilienthalplatz 7, 38108 Braunschweig, Germany,
paul.lehmann@dlr.de

Introduction: The wake of wind energy (WE) rotors is modeled as a tip vortex helix with a vortex strength estimated from its rotor thrust. An analytical helicopter rotor model is used to estimate the WE wake vortex impact on rotor trim. Also, a comprehensive helicopter simulation program is used to expose a helicopter to the WE vortex and identify trim perturbations. Figure 1 sketches the WE wake vortex spiral geometry and the aerodynamic problem for a helicopter rotor exposed to the WE vortex swirl velocity field.

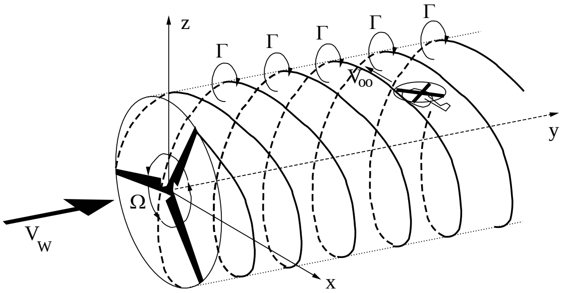

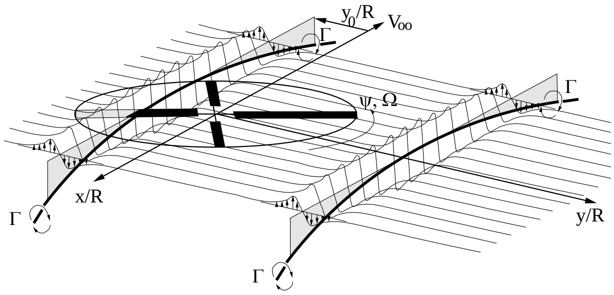

(a) WE turbine wake with a helicopter (b) Helicopter rotor in WE turbine wake

Fig. 1: Sketch of the WE turbine wake – rotor interaction problem

The analytical isolated rotor model: Based on the sketch of Fig. 1 (b) the velocities acting at a rotor blade element tangential (in the rotational plane, normal to the radial axis) and normal to the rotational plane can be established. It is assumed that the helicopter's flight path is parallel to the WE turbine's tip vortex axis and the rotor is horizontal. As indicated in the sketch the vortex center lies in the plane of the rotor disk and therefore only vertical vortex-induced velocities are acting on the blade elements. The vortex axis is assumed to be parallel to the rotor longitudinal x-axis and the vortex-induced velocities are a function of the lateral coordinate y only. By means of blade element theory this allows the analytical computation of rotor collective and cyclic controls to reject the WE vortex induced velocity perturbations. A rotor of the size of a Bo105 is assumed for the calculations.

The helicopter model: For flight mechanics purposes the Institute of Flight Systems at DLR uses the non-linear “Helicopter Overall Simulation Tool” HOST for desktop simulation. HOST was developed by Airbus Helicopters and is now used and further developed in cooperation of them with ONERA and DLR. It is a modular tool that has the ability to simulate any type of helicopter and calculate trim, time domain response and linearization. For the results obtained here HOST was used in a special configuration with the “Big Size Aircraft Vortex Wake Model”. This model includes a pair of wing tip vortices whose parameters are user-specified. The vortex induced velocities are calculated at all specified helicopter aerodynamic bodies and provided to HOST's flight mechanics simulation. In this study, only the main rotor is selected. A helicopter trim without the vortex is performed first, followed by trim including the vortex. The perturbations in rotor trim controls and those of the helicopter pitch attitude and roll angle relative to the undisturbed trim can be compared with results of the analytical isolated rotor model. The helicopter used in simulation is a Bo105 of 2.2 ton gross weight.

Results: The perturbations in rotor trim controls of the analytical isolated rotor model are found to be linear proportional to the peak swirl velocity, made non-dimensional by the rotor blade tip speed and called the peak induced velocity inflow ratio λ_{W0}. The analytical rotor blade begins at 25% radius and blade tip losses are approximated by means of an effective radius of 97% of the physical radius. The computed rotor control perturbations in collective $\Delta\Theta_0$ and longitudinal cyclic $\Delta\Theta_S$ are given in Fig. 2 as a function of the WE vortex core radius r_c, related to the rotor radius R. The largest impact of the WE vortex on collective control is present when it is located at the outer border of the rotor disk because in that case the entire disk is immersed in either downwash or upwash of the WE vortex, depending on its position right or left of the rotor. This also causes large induced velocity gradients across the disk, thus the cyclic control is also large in magnitude to counteract the disturbance. The cyclic control also is large when the WE vortex is located in the middle of the rotor. In this case, one side is subjected to downwash, the other side to upwash.

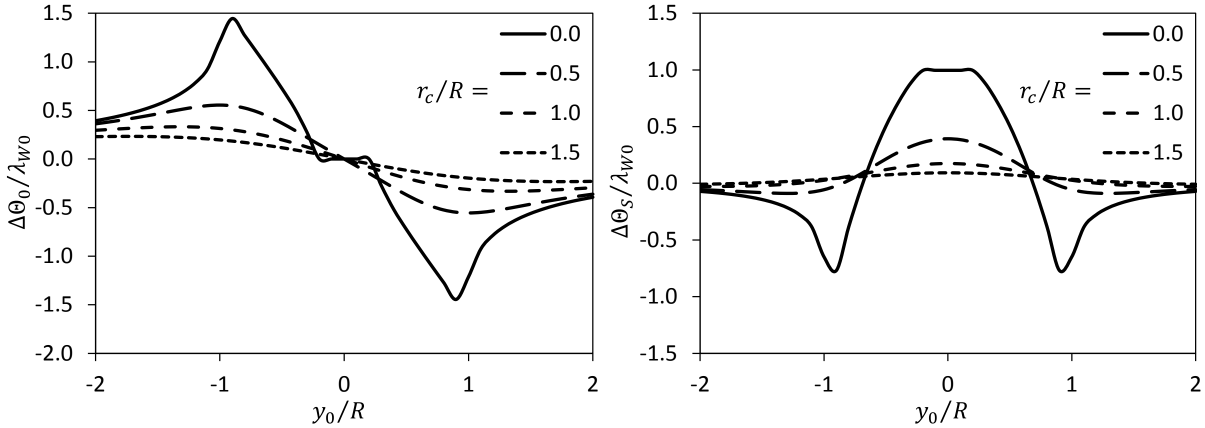

(a) Collective control (b) Longitudinal cyclic

Fig. 2: Isolated rotor trim perturbations due to a WE vortex

The complete helicopter trim involves the WE vortex induced velocities within the main rotor aerodynamics, but not on other components of the helicopter. However, any disturbances of rotor blade aerodynamics cause a modified main rotor power and the tail rotor thrust is used to compensate it, which also causes a roll moment about the helicopter center of gravity. As a consequence, this modifies the helicopter overall trim, including the pitch attitude and roll angle, and requiring additional main rotor control inputs to maintain the trimmed steady flight. Thus, the entire helicopter trim will require larger controls for WE vortex disturbance rejection than the isolated rotor model. The results of Fig. 3 for two WE turbines of 3 and 7 MW power in different distances of $y = 100\ m$ and $500\ m$ downstream of the WE turbines confirm this.

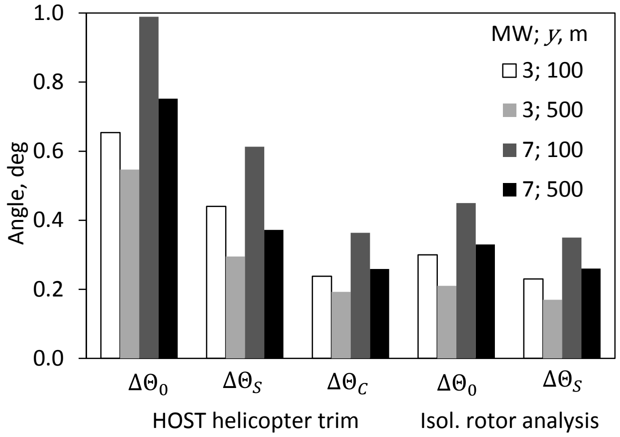

Fig. 3: Comparison of HOST complete helicopter trim perturbations with isolated rotor analysis

Conclusions:

(1) The largest controls required for disturbance rejection occur closest to the WE turbine, where the strongest induced velocities are present.

(2) The controls required are smaller than the available control margin that can be estimated around 8°, but it depends on the flight speed of the helicopter.

(3) The complete helicopter requires more controls than the isolated analytical rotor model, because other components like the tail rotor affect the overall trim.

Mitteilung

Projektgruppe/ Fachkreis: Aeroelastik und Strukturdynamik

Experimentelle Untersuchung von Flattermechanismen in Abhängigkeit des Pfeilungswinkels bei subsonischer Anströmung und kleinen Reynoldszahlen

Marc Braune, Stefan Wiggen
Deutsches Zentrum für Luft- und Raumfahrt (DLR), Institut für Aeroelastik, Bunsenstraße 10, 37073 Göttingen,
Marc.Braune@dlr.de, Stefan.Wiggen@dlr.de

Motivation: Zahlreiche Untersuchungen zum Flatterverhalten und zur aeroelastischen Stabilität von gepfeilten Flügeln sind bekannt [1,2,3]. Diese weisen stabilisierende Effekte einer positiven Pfeilung bzgl. der Flattergrenze, entsprechend einer Verschiebung der Flattergeschwindigkeit hin zu höheren Anströmungsgeschwindigkeiten nach.

Bei bisherigen experimentellen Untersuchungen lag jedoch stets eine Kopplung bei der Variation von strukturmechanischen und aerodynamischen Parametern vor. Eine Veränderung des Pfeilungswinkels führte somit zu einer Veränderung weiterer Systemparameter. Eine klare Trennung zur Identifikation der rein aerodynamischen Auswirkungen der Flügelpfeilung auf die Flattersystematik und eine quantitative Beschreibung der Effekte steht bislang noch aus.

Zielsetzung: Im Rahmen der vorliegenden Arbeit erfolgt eine systematische experimentelle Untersuchung von Flattermechanismen bei Variation der Flügelpfeilung unter einer signifikanten Reduktion auf die wesentlichen aerodynamischen Systemparameter. Hierbei steht insbesondere eine genaue Betrachtung des Pfeilungseinflusses unter Berücksichtigung der Lage der elastischen Achse bzgl. des Flatterverhaltens im Fokus.

Experimenteller Aufbau: Der experimentelle Aufbau besteht aus einem Flatterversuchsstand für einen Niedergeschwindigkeitswindkanal ($Re_{max} \approx 4 \cdot 10^5$) am Institut für Aeroelastik.

Das Versuchssetup umfasst einen Flatteraufbau mit einem elastisch gelagerten Tragflügelsegment mit den Freiheitsgraden Schlag und Drehung. Die Modellaufnahme ermöglicht eine Variation der Position der elastischen Achse. Weiterhin lässt das Setup eine vollständige Drehung des gesamten Flatteraufbaus im Freistrahl des Windkanals zu. Hierrüber wird eine kontinuierliche Verstellung des Pfeilungswinkels (bis maximal 45°) gewährleistet. Zugleich werden die elastomechanischen Systemparameter konstant gehalten.

Lasertriangulatoren und Beschleunigungssensoren zeichnen die Modellbewegung in beiden Freiheitsgraden auf und ermöglichen eine Verfolgung der Amplituden, Phasen und Frequenzen der Schwingungsmoden. Eine elektrodynamische Erregung wird zur aktiven Anfachung oder Dämpfung der Modellbewegung eingesetzt.

Methodik: Für einen Pfeilungswinkelbereich von 0° bis 45° und einer Variation der Lage der elastischen Achse wird bei einer systematischen Erhöhung der Anströmungsgeschwindigkeit eine aktive Modellanregung (unterhalb der Flattergeschwindigkeit) vorgenommen. Oberhalb der Flattergeschwindigkeit wird das selbsterregte Aufklingen der Modellbewegung aufgezeichnet.

Aus dem Ab- bzw. Aufklingen der Bewegungsmoden werden die Frequenzen, Dämpfungen und Phasenbeziehungen ermittelt.

Flattergrenzen werden aus einer Interpolation der Dämpfung in Abhängigkeit der Anströmungsgeschwindigkeit bestimmt. Der Nulldurchgang entspricht dem Flatterpunkt.

Exemplarische Ergebnisse:

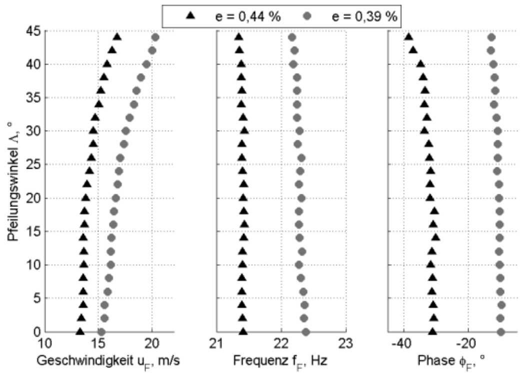

Abbildung 1: Anströmungsgeschwindigkeiten u_F, Frequenzen f_F und Phasenbeziehungen ϕ_F zwischen der Schlag- und der Drehbewegung im Flatterpunkt in Abhängigkeit zum Pfeilungswinkel Λ für zwei Positionen der elastischen Achse e.

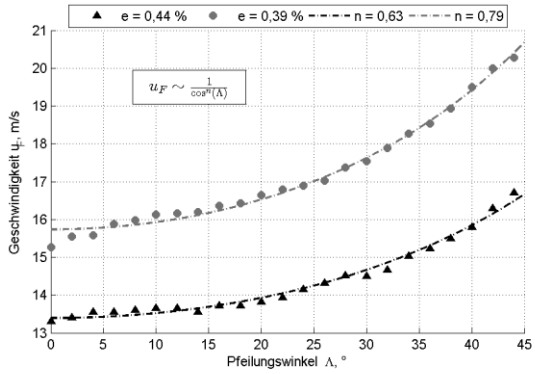

Abbildung 2: Flattergeschwindigkeiten u_F in Abhängigkeit des Pfeilungswinkels Λ sowie Approximation der Messergebnisse mit einer Kosinusfunktion für zwei Positionen der elastischen Achse e.

Exemplarisch sind in Abb. 1 die Verläufe der Strömungs- bzw. Flattergeschwindigkeiten sowie die zugehörigen dominierenden Frequenzen und Phasenbeziehungen zwischen der Hub- und der Drehbewegung in Äbhängigkeit des Pfeilungswinkels dargestellt. Die Messungen wurden für zwei verschiedene Positionen der elastischen Achse, bezogen auf die Flügeltiefe, durchgeführt. Abb. 2 zeigt die Verläufe der Flattergeschwindigkeit über dem Pfeilungswinkel. In Anlehnung an ein Kosinusgesetz, wie es auch bei [1] verwendet wird, wurden die Messergebnisse mit einer $1/\cos^n(\Lambda)$ – Funktion approximiert.

Neben einem erwarteten Anstieg der Flattergeschwindigkeit mit zunehmender Pfeilung zeigen sich quantitative Unterschiede in den Verläufen für die zwei Achsenlagen. Dies zeigt insbesondere die Abweichung des Exponenten (n = 0,63 für e = 0,44 % und n = 0,79 für e = 0,39 %) der Kosinusapproximation untereinander.

Eine Änderung der Flatterfrequenz ist in beiden Fällen nicht zu beobachten, was für einen von der Pfeilung weitestgehend unabhängigen Flattermechanismus spricht. Hier führt insbesondere eine von der Achsenlage abhängige Strukturmechanik zu einer Veränderung der Frequenz.

Ähnliches zeigt sich auch in den Verläufen der Phasenbeziehungen, wobei der starke Abfall der Phase bei hohen Pfeilungswinkeln für e = 0,44 % auf weitere komplexere Zusammenhänge hindeutet.

Die starken Anstiege der Flattergeschwindigkeit, die größer ausfallen als bisherige Experimente [1,2,3] dies vermuten ließen sowie die quantitativen Unterschiede bei einer unterschiedlichen Lage der elastischen Achse geben den Anlass für weitere Messungen. Vorgestellt werden nunmehr systematische Untersuchungen für eine Vielzahl von Pfeilungswinkeln und Lagen der elastischen Achse, wobei die Systematik und Quantifizierung des Pfeilungseinflusses diskutiert wird.

[1] BARMBY, J. G. ; CUNNINGHAM, H. J. ; GARRICK, I. E. : Study of effects of sweep on the flutter of cantilever wings. NACA TN 2121, 1950

[2] BABISTER, A. W. : Flutter and Divergence of Swept-back and Swept-forward Wings. R. & M. 2761, 1950

[3] MOLYNEUX, W. G. : The Flutter of Swept and Unswept Wings with Fixed-Root Conditions. R.& M. 2796, 1950

Fachkreis: Numerische Simulation

Numerical Investigation of an Elasto-Flexible Membrane Airfoil and Validation

Julie Piquee*, Mehran Saeedi#, Christian Breitsamter* , Roland Wüchner#, Kai-Uwe Bletzinger#

* **Institute of Aerodynamics and Fluid Mechanics**,
Technische Universität München,
85748 Garching, Germany
e-mail: julie.piquee@aer.mw.tum.de, web page: https://www.aer.mw.tum.de
\# **Chair of Structural Analysis**
Technische Universität München,
e-mail: mehran.saeedi@tum.de, web page: http://www.st.bgu.tum.de

Throughout the last decades, the wind energy technology has received great of interest due to the environmental concern. One prevailing trend in wind energy technology has been for example to increase the size of the rotor. The respective wind velocities are generally higher, which could offer better conditions for the turbines and larger machines can capture more energy throughout its lifetime. However, larger turbines mean heavier blades, higher structural loads and more fatigue, which results in considerable design issues. One possibility to overcome the structural-design concern could be the use of form variable systems within the blade of the turbine. Active and passive flow control devices showed indeed good promises in load reduction on a wind turbine blade. Basualdo **[1]**, for example, numerically investigated an airfoil, whose geometry could be altered using a rear-mounted flap. The study was conducted using a potential theory method to a variable-geometry airfoil by analyzing the fluctuations of the airfoil displacements. It was found that the use of such a device could lead to load alleviation as it reduces the airfoil displacement fluctuations, which affects directly the fatigue phenomenon. The Princeton windmill research group **[2]** and Béguin **[3]** similarly investigated respectively a Sailwing and an elasto-flexible membrane wing. Both models were based on a structure mainly composed of a rigid leading- and trailing-edge, and an adaptive flexible material wrapped around the structure. It was found out that such an adaptive concept could provide better aerodynamic performance compared with its rigid counterpart. The membrane's flexibility of Béguin permits indeed the airfoil to adapt itself to the surrounding flow field by naturally redistributing the pressure difference on the upper-side and the lower-side of the membrane. This capacity of adaptivity results furthermore in a delay of the stall to higher angles of attack and can produce an increase of the camber and a reduction in the thickness, which could provide more favorable lift-to-drag characteristics.

An elasto-flexible membrane wing concept is investigated via numerical analysis in conjunction with an experimental study at the Technical University of Munich (TUM). The purpose of this present work is to give an overview of the development of a Fluid-Structure-Interaction (FSI) platform using the U-RANS fluid solver TAU from the DLR and the FEM based structural solver CARAT++ from the Chair of Structural Analysis at TUM. The present work is divided in two main parts:

- a first preliminary investigation about a cavity (FSI) bench mark,
- a second 2D FSI analysis of an elasto-flexible membrane airfoil.

The purpose of the first investigation is to identify the possible complications and issues regarding the development of the FSI platform and to verify the coupling between TAU and CARAT++.

The second part focuses on the numerical coupled investigations of a 2D airfoil and a comparison with wind tunnel results to be able to conclude about the accuracy of the numerical FSI results. The studied airfoil consists of an elasto-flexible membrane wrapped around a rigid double-elliptical leading-edge and a rigid trailing-edge, Fig. 1. The membrane is an anisotropic material, whose mechanical properties are different in the weft and the warp directions. The respective E-moduli for the weft and the warp directions are 2.18MPa and 1.01MPa respectively. In the structural model, the upper and lower surface of the airfoil are modeled using membrane elements which are fixed at the trailing-edge. As it was mentioned above, the leading-edge is made with a double-elliptical spar in order to avoid too-high gradient of pressure on the upper-side of the airfoil. Concerning the fluid setup, a hybrid mesh is generated for the fluid using ICEM-CFD. A block method is realized around the airfoil and an unstructured mesh is then used to fill the entire domain. As the interface between structured and unstructured mesh could influence the results, three different meshes differing with in their specific resolution, are tested to realize a mesh independency study.

The FSI investigations on the 2D airfoil are then compared to experimental tests realized in the wind tunnel B of the Institute of Aerodynamics and Fluid Mechanics of the TUM. Force measurements are performed to obtain the aerodynamic forces acting on the airfoil. The photogrammetry technic is used to measure the deformation of the membrane and a hot wire anemometry system is exploited to acquire the flow velocities around the model. Both numerical and experimental analysis are performed for Reynolds numbers (Re) equal to $0.23.10^6$ and $0.56.10^6$ and for different angles of attack (AOA = 6°, 15° and 22°).

Results of the analysis agreed with a typical behaviour of a flexible membrane wing. Compared to its rigid counterpart, the flexible membrane wing presents higher lift values and better aerodynamic efficiency as the camber of the geometry increases with the angle of attack. Furthermore, as the slope of the membrane adapts itself to the flow environment, the flow separation is postponed to higher angles of attack and is smoother. In Fig. 1, some results of the photogrammetry and the hot-wire anemometry tests are represented for an AOA = 15° and U_∞ = 35m/s.

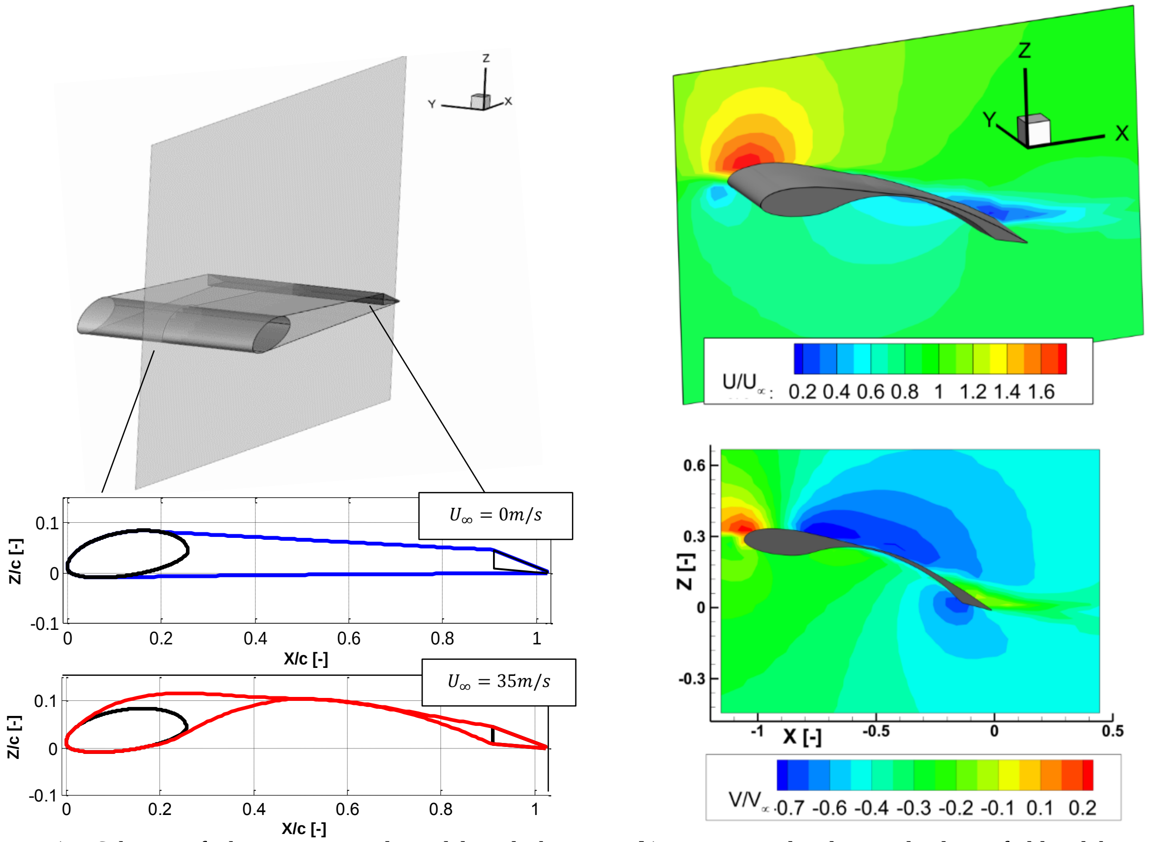

a) Scheme of the experimental model and the associated investigated geometry and results of the photogrammetry test for $U_\infty = 35$ m/s and AOA = 15°

b) Mean axial and vertical velocity field and the respective deformed geometry for $U_\infty = 35$ m/s and AOA = 15°

Fig. 1 -

Acknowledgements

The support of these investigations by the German Research Association (Deutsche Forschungsgemeinschaft) is gratefully acknowledged.

[1] Basulado, S., “Load alleviation on wind turbine blades using variable airfoil geometry”, *Wind Engineering,* Volume 29, No. 2, 2005, pp. 169-182.

[2] Maughmer, M. D., “Optimization and Charateristics of a Sailwing Windmill Rotor”, Princeton Univ. TR, 1976.

[3] Béguin, B., Breitsamter, C., and Adams, N., “Aerodynamic Investigations of a Morphing Membrane Wing”, *AIAA Journal*, Volume 50, No. 11, November 2012, pp. 2588 – 2599.

Mitteilung

Projektgruppe / Fachkreis: Aeroelastik und Strukturdynamik

Coupling of Recurrent and Static Neural Network Approaches for Improved Multi-Step Ahead Time Series Prediction

Dipl.-Ing. Maximilian Winter, Prof. Dr.-Ing. Christian Breitsamter
Lehrstuhl für Aerodynamik und Strömungsmechanik (Technische Universität München)
Boltzmannstr. 15, 85748 Garching bei München
maximilian.winter@aer.mw.tum.de

The industrial design and analysis process of next generation aircraft is characterized by involved multidisciplinary computations and numerically costly optimizations in order to achieve the efficiency goals such as the reduction of emissions and fuel consumption. In this regard, the aspect ratio of the wings tends to be increased, whereas it is envisioned to concurrently decrease the structural weight. Considering those highly-flexible structures, the accurate prediction of aeroelastic phenomena that arise through the interaction of structural, inertial, and flow-induced forces will become of paramount importance in the future. Hence, efficient and precise methods are required to compute motion and gust induced aerodynamic forces as well as the overall aeroelastic response. With respect to the accuracy of the results, the aim of the research efforts is to use modern CFD methods for the unsteady aerodynamic computations. However, due to the vast number of parameters, i.e., various freestream conditions, geometry parameters, flap deflection angles, and fuel levels, the numerical effort of comprehensive multi-physics calculations is still not manageable using the available computer technology.
A possible remedy is to construct and utilize so-called reduced-order models (ROM). For this purpose, CFD-based training data samples describing the input/output relationship of the underlying system are exploited in terms of a linear or a nonlinear system identification. In the context of aeroelastic computations, the system input is regarded with the structural degrees of freedom, whereas the outputs are the motion-induced (generalized) aerodynamic forces. Following this methodology, the time-domain unsteady aerodynamic forces can be predicted with high accuracy, whereas the simulations are performed within seconds once the ROM has been generated.
The ROM methods originating from linear identification principles are proven to provide accurate and reliable results for small structural perturbations, i.e., for a dynamically linear dependence between the flow quantities and the excitation. However, the nonlinear identification that allows for capturing larger amplitude motions or varying freestream conditions are still challenging. Many nonlinear models that are based for example on neural networks or Kriging interpolation exhibit a high precision with respect to the so-called one-step prediction problem. However, often an unstable behavior for multi-step ahead predictions is encountered for these approaches due to the feedback of the model outputs. The methodology for unsteady aerodynamic modeling proposed by Winter and Breitsamter [1] uses a nonlinear identification technique which is not prone to simulation instabilities. Nonetheless, the model is not very accurate if the system is governed by strong dynamic nonlinearities. Therefore, the idea followed here is to favorably combine a model which is suited for highly nonlinear static predictions with the local linear neuro-fuzzy models employed in [1].
The new ROM method depicted in Fig. 1 involves two sequential training steps. Firstly, the recurrent neuro-fuzzy model is trained by the local linear model tree algorithm (LOLIMOT, [2]). In this regard, the model input vector consists of the time-delayed system inputs and the time-delayed model outputs, whereas the neural network parameters are optimized by minimizing the one-step prediction error with respect to the CFD response. After the neuro-fuzzy model is obtained, the multi-step ahead prediction can be evaluated for the given training data. Secondly, a multi-layer perceptron neural network (MLP, [2]), which is a high performance multi-dimensional function approximator, is trained using nonlinear Levenberg-Marquardt optimization. For this step, the input vector comprises the time-delayed system inputs and the time-delayed outputs of the previously generated neuro-fuzzy model. Analo-

gously to the first training procedure, the model parameters are iteratively updated to reproduce the system outputs. The advantage of this coupled approach is that the second model is not operated in a recurrent manner, since no outputs of the MLP neural network are fed back to the respective input vector. Hence, the second model can be considered to perform a nonlinear correction of the neuro-fuzzy model outputs.

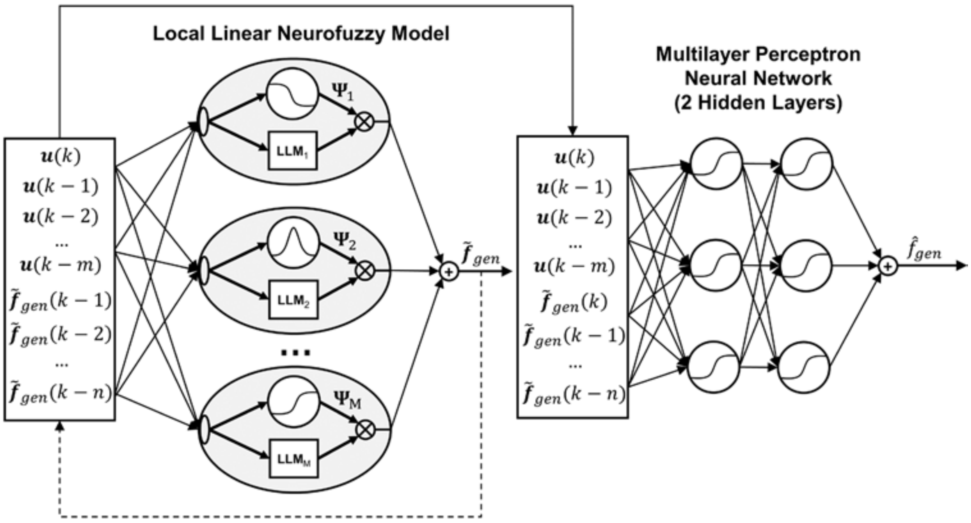

Figure 1: Schematic of the new reduced-order model for highly-accurate unsteady aerodynamic simulations.

In order to evaluate the performance and efficiency of the proposed method, the NLR 7301 supercritical airfoil undergoing a pitch and plunge motion is investigated at transonic flow conditions. For this purpose, a forced-motion CFD computation was carried out to yield the aerodynamic response induced by amplitude-modulated pseudo-random binary deflections. Subsequently, the proposed ROM framework is conditioned according to the described procedure and the model is tested exemplarily by means of amplitude and frequency varying sinusoidal excitations. The result of these considerations is visualized by means of the pitching moment coefficient for both the neuro-fuzzy model without the nonlinear correction (Fig. 2) and the coupled static and recurrent neural network method (Fig. 3), while a comparison with the reference CFD solution is presented for performance classification. It is shown that the new method leads to a notable improvement of the simulation quality, especially, if stronger nonlinear characteristics are encountered. Future work will focus on the coupling of aerodynamic ROMs with structural models in order to perform highly-efficient aeroelastic simulations capable of predicting limit-cycle oscillations.

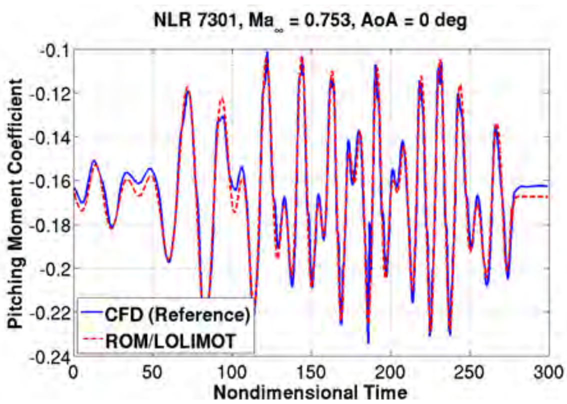

Figure 2: Simulation of the pitching moment coefficient using the neuro-fuzzy model employed in [1].

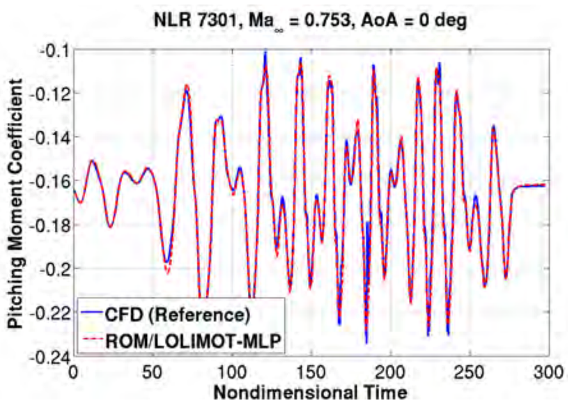

Figure 3: Response of the pitching moment coefficient predicted by the proposed ROM methodology.

References

[1] M. Winter and C. Breitsamter, „Efficient Modeling of Generalized Aerodynamic Forces Across Mach Regimes Using Neuro-Fuzzy Approaches," New Results in Numerical and Experimental Fluid Mechanics X, Notes on Numerical Fluid Mechanics and Multidisciplinary Design, Vol. 132, pp. 467-477, 2016.

[2] O. Nelles, Nonlinear System Identification, Berlin Heidelberg: Springer, 2001.

Mitteilung

Projektgruppe/Fachkreis: Numerische Simulation

Direkte Numerische Simulation von konvektiver Kanalströmung mit Phasenübergang

P. Bahavar, C. Wagner

DLR Göttingen, Institut für Aerodynamik und Strömungstechnik
Bunsenstr. 10, 37073 Göttingen
philipp.bahavar@dlr.de

Die Kondensation von Wasser ist ein generell auftretendes Phänomen in Belüftungssystemen ungeachtet des Einsatzgebiets. Dabei kann das Auftreten von Kondensation an unerwünschten Stellen im System ein erhebliches Problem darstellen, wie beispielsweise das Eindringen von Kondensat aus der Kabinenabluft in das Isolationsmaterial zwischen Kabine und Flugzeugaußenhülle, was langfristig zu einem erhöhten Gewicht und reduzierter Isolationswirkung führt[1].
Die herkömmliche Herangehensweise für die Betrachtung von Kondensation an Oberflächen beruht auf der Nusselt'schen Wasserhauttheorie, die einen Zusammenhang zwischen der Kondensatfilmdicke und dem Wärmeübergang herstellt[2]. Ausgehend von dieser zunächst nur für die eingeschränkte Problemstellung von ruhendem Dampf und laminar abfließendem Kondensat geltenden Formulierung existieren Anpassungen der Theorie, die die Anwendung für Kondensation in der Gegenwart von Inertgasen, bei strömender Dampfphase und mit turbulenter Filmoberfläche erlauben.
Die Durchführung einer Direkten Numerischen Simulation (DNS) von turbulenter Strömung mit Phasenübergang erlaubt die Untersuchung der Wechselwirkung zwischen Oberflächenkondensation und Strömungsstrukturen auf allen relevanten Längenskalen und damit ein besseres Verständnis der Effekte, die die Anpassung der grundlegenden Nusselt'schen Wasserhauttheorie an komplexere Problemstellungen nötig machen. Mit den auf diese Weise gewonnenen Daten wird eine bessere Modellierung von Kondensationsphänomenen über eine breitere Spanne von Strömungssituationen möglich.
Kern der Untersuchung ist die numerische Lösung der zeitlich und räumlich diskretisierten Navier-Stokes-Gleichungen im Rahmen einer DNS mithilfe der Programmbibliothek OpenFOAM. Die Lösung der Impulsgleichung erfolgt mittels eines expliziten Leapfrog-Verfahrens zweiter Ordnung, die räumlichen Ableitungen werden in vierter Ordnung approximiert. Zusätzlich zum Geschwindigkeitsfeld erfordert der Temperaturgradient zwischen der adiabaten oberen und isothermen unteren Kanalwand die Behandlung von sowohl diffusivem als auch konvektivem Transport der Temperatur T mittels $\partial T/\partial t = \kappa\nabla^2 T - \mathbf{u}\cdot\nabla T$ mit der Temperaturleitfähigkeit κ. Durch den Temperaturgradienten induzierte Dichteunterschiede im strömenden Fluid und die damit verbundenen Auftriebskräfte in wandnormale Richtung werden mithilfe der Boussinesq-Approximation erfasst. Darüber hinaus wird auch der diffusive und konvektive Transport der Luftfeuchtigkeit über den Stoffmengenanteil c_{vap} von Wasser in der Luft analog zum Vorgehen bei der Temperatur abgebildet, $\partial c_{\mathrm{vap}}/\partial t = D\nabla^2 c_{\mathrm{vap}} - \mathbf{u}\cdot\nabla c_{\mathrm{vap}}$, dabei ist D die Diffusionskonstante.

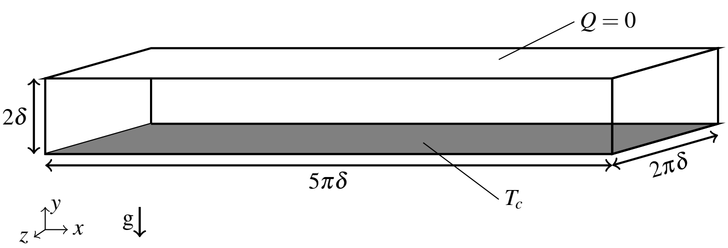

Figure 1: Simulierter Kanal mit festen Wänden in y-Richtung und periodischen Randbedingungen in x- und z-Richtung.

Als Systemgeometrie dient ein Kanal mit periodischen Randbedingungen in Strömungs- und Spannweitenrichtung sowie Wänden mit Haftrandbedingungen in der verbleibenden Richtung, wie in Fig. 1 gezeigt. Die mittlere Strömungsgeschwindigkeit u in x-Richtung ist vorgegeben, sodass sich der Druckabfall in Strömungsrichtung und die Schubspannungsgeschwindigkeit u_τ einstellen.

Die genaue Kenntnis aller thermodynamische Variablen sowie von c_{vap} im kompletten System und zu jedem Zeitpunkt ermöglicht es, lokale Unterschreitungen der Taupunkttemperatur exakt zu erfassen und in den so identifizierten Regionen innerhalb des Kanals Kondensation einsetzen zu lassen. Hierzu wird die Formulierung der Kondensationsrate von Schrage aufbauend auf der Hertz-Knudsen-Gleichung verwendet [3], bei der der Massentransport über die Phasengrenze proportional zur Differenz zwischen dem herrschenden Partialdruck p_{vap} und dem temperaturabhängigen Sättigungsdruck des in der Luft gelösten Dampfes $p_{\text{sat}}(T)$ ist[4]:

$$\dot{m} = \frac{2\sigma_c}{2-\sigma_c}\sqrt{\frac{M}{2\pi RT}}\left(p_{\text{vap}} - p_{\text{sat}}\right).$$

Hierbei ist M die molare Masse von Wasser, R die Gaskonstante und σ_c der Kondensationskoeffizient. Mithilfe des somit bekannten Massenübergangs kann dann der zusätzliche Wärmeeintrag ins System durch Freiwerden der Verdampfungsenthalpie ΔH bestimmt werden. Nach der Kondensation wird das Wasser nicht weiter simuliert, sodass der Einfluss von flüssigem Wasser an der Kanalwand vernachlässigt wird.

Für die vorliegende Untersuchung wurden die Stoffeigenschaften des strömenden Fluids entsprechend derer von Luft gewählt, das heißt eine kinematische Viskosität von $\nu = 1.35 \cdot 10^{-5}\,\text{m}^2/\text{s}$, eine Temperaturleitfähigkeit von $\kappa = 1.898 \cdot 10^{-5}\,\text{m}^2/\text{s}$, eine spezifische Wärmekapazität von $c_p = 1.005\,\text{kJ/kg\,K}$, sowie ein thermischer Ausdehnungskoeffizient von $\alpha = 3.674 \cdot 10^{-3}\,\text{K}^{-1}$. Die Diffusionskonstante von Wasserdampf in Luft beträgt $D = 2.82 \cdot 10^{-5}\,\text{m}^2/\text{s}$, die Verdampfungsenthalpie $\Delta H = 2280\,\text{kJ/kg}$. Die charakteristische Länge des Systems ist die halbe Kanalhöhe $\delta = 0.04\,\text{m}$, damit beträgt die Reynoldszahl $\text{Re} = u\delta/\nu = 2280$, wodurch sich $\text{Re}_\tau = u_\tau\delta/\nu = 150$ ergibt. Die Temperatur der unteren Kanalwand ist $T_c = 278.15\,\text{K}$. Das simulierte Volumen wurde für die DNS in 394 x 180 x 316 Zellen zerlegt, die in x- und z-Richtung mit $\Delta x^+ = u_\tau \Delta x/\nu = 6$ beziehungsweise $\Delta z^+ = 3$ äquidistant verteilt sind und in y-Richtung mit zunehmender Nähe zur Wand feiner aufgelöst sind, mit $\Delta y^+ = 0.2$ direkt an der Wand und $\Delta y^+ = 3$ in der Kanalmitte.

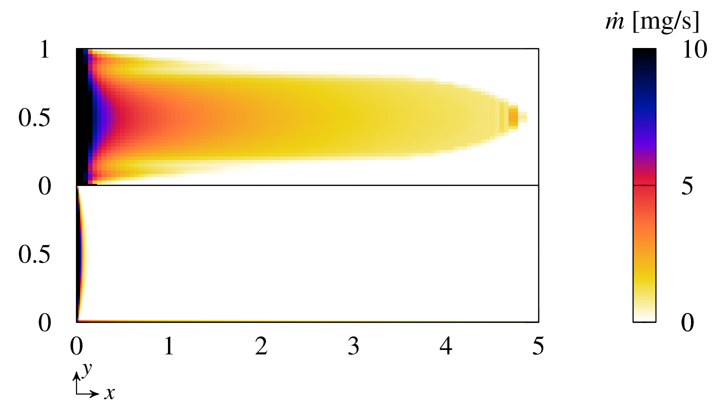

Figure 2: Massentransferrate am Phasenübergang. Oben: Situation während des Einströmens der gesättigten feuchten Luft. Unten: Stationärer Zustand.

Fig. 2 zeigt vorläufige Ergebnisse einer Validierungssimulation für die Massentransferrate am Phasenübergang in einem zweidimensionalen Kanal, in den mit Wasserdampf gesättigte Luft mit laminarem Geschwindigkeitsprofil einströmt. Zu Beginn kondensiert Wasserdampf über die gesamte Kanalhöhe und die gesamte Länge des Kanals hinweg, wohingegen nach Aufheizen des Systems durch das Freiwerden der Verdampfungsenthalpie die Kondensation im stationären Zustand nur am Einlass und in unmittelbarer Nähe zur gekühlten Wand stattfindet. Auf dem Symposium werden stattdessen Ergebnisse für den dreidimensionalen, turbulenten Fall wie oben beschrieben präsentiert werden.

Literatur:

[1] M. Gründer, “Kondenswasser an Bord,” *Flug Revue*, vol. 10, 2003.

[2] W. Nusselt, “Die Oberflächenkondensation des Wasserdampfes,” *Zeitschrift des Vereins Dtsch. Ingeniuere*, vol. 60, pp. 569 – 575, 1916.

[3] R. W. Schrage, *A theoretical study of interphase mass transfer.* PhD thesis, Columbia University, 1953.

[4] R. Marek and J. Straub, “Analysis of the evaporation coefficient and the condensation coefficient of water,” *International Journal of Heat and Mass Transfer*, vol. 44, no. 1, pp. 39 – 53, 2001.

Mitteilung

Projektgruppe / Fachkreis: Numerische Simulation

Modellierung beweglicher Steuerflächen mit dem DLR TAU-Code

Ralf Heinrich, Laia Alcaraz Capsada
DLR Institut für Aerodynamik und Strömungstechnik
Lilienthalplatz 7, 38108 Braunschweig
ralf.heinrich@dlr.de

Ausgangssituation: Für eine Reihe von Anwendungen ist die Modellierung von beweglichen Steuerflächen eine unbedingte Voraussetzung. Genannt seien hier die Trimmung eines Flugzeuges, die Vorhersage von aerodynamischen Lasten infolge von Steuerflächenbewegungen, die Wirksamkeit von Steuerflächen sowie die Simulation eines manövrierenden Flugzeuges. Für letztgenanntes Szenario müssen alle Primärsteuerflächen modelliert werden. Dazu gehören Querruder, Seitenruder, Höhenruder, horizontaler Stabilisator und Spoiler. Insbesondere die Modellierung beweglicher Spoiler stellt für hochgenaue CFD Verfahren eine besondere Schwierigkeit dar.

Ziel: Um mit dem TAU-Code [1] alle Primärsteuerflächen modellieren zu können, sollen entsprechende Strategien entwickelt und umgesetzt werden. Die Techniken sollen an einer Reihe von Beispielen bis hin zur multidisziplinären Simulation eines manövrierenden Flugzeuges demonstriert werden.

Lösungsweg: Im Rahmen dieser Arbeit werden unterschiedliche Strategien vorgestellt, zum einen für Steuerflächen wie Querruder, Höhenruder und Seitenruder, zum anderen für Spoiler. Für die erstgenannten hat sich gezeigt, dass sich die Bewegung der Steuerflächen sehr gut mittels Netzdeformation realisieren lässt. Bild 1 zeigt ein Beispiel für ein generisches Verkehrsflugzeug, bei dem diese Steuerflächen alle mittels Netzdeformation bewegt werden. In diesem konkreten Beispiel werden die spannweitigen Spalte nicht aufgelöst. Die Verschiebungen werden in der Nähe der Außenkanten der Steuerflächen vom ausgeschlagenen Zustand auf den Wert Null übergeblendet. Dies ist für kleinere Ausschläge unproblematisch. Allerdings wächst der Fehler mit dem Ausschlag der Steuerfläche. Daher ist eine weiter Strategie entwickelt worden, die diese Spalten berücksichtigen kann. In ein reguläres Flügelgitter ohne Steuerflächen werden für die Steuerflächen zusätzliche Gitterblöcke über die Chimera-Technik eingebracht, in denen der Spalt modelliert wird. Es werden jeweils ein Gitter für die Steuerfläche selber, sowie zwei weitere Gitterblöcke rechts und links von der Steuerfläche generiert. Die Bewegung der Steuerfläche geschieht mittels Netzdeformation, jedoch ohne „Blending". Für diese Gitterblöcke werden strukturierte Gitterblöcke verwendet, da sich hier die Punkteverteilung insbesondere im Spalt besser steuern lässt. Bild 2 verdeutlicht die verwendet Strategie. Weiterhin wird auch ein Ergebnis einer Simulation für eine ausgeschlagene Steuerfläche gezeigt. Sehr schön zu sehen sind insbesondere die an den Außenkanten der Steuerfläche entstehenden Wirbel.

Für die Modellierung von Spoilern wird ebenfalls, wie für z.B. Querruder, die Chimera-Technik angewendet. In das Gitter für einen Flügel mit Aussparung an der Position des Spoilers wird ein zusätzlicher Gitterblock eingebracht. Die Bewegung des Spoilers wird hier allerdings über Rotation des Gitterblockes eingebracht. Eine wesentliche Voraussetzung dafür ist ein leistungsfähiger Algorithmus zum Lochschneiden [2]. Bild 3 zeigt eine erste Spoiler-Anwendung im 3D, bei der in einen NACA-Flügel insgesamt 3 Spoiler eingebracht worden sind, was üblicherweise auch als „Spoiler-Piano" bezeichnet wird.

Weiteres Vorgehen:
Im Beitrag werden die unterschiedlichen Strategien vorgestellt. Anhand von Beispielen werden die jeweiligen Vor- und Nachteilen verdeutlicht. Weiterhin soll die Strategie mit Blending mit der Strategie mit Auflösung der spannweitigen Spalten verglichen und bewertet werden. Als Anwendung ist unter anderem der Manöverflug eines Flugzeuges geplant (Aerodynamik gekoppelt zur Flugmechanik).

Literatur:
[1] Schwamborn, T. Gerhold, R. Heinrich: The DLR TAU-Code: Recent Applications in Research and Industry. In proceedings of "European Conference on Computational Fluid Dynamics" ECCOMAS CDF 2006, Delft The Netherland, 2006

[2] Spiering, Frank: „Entwicklung eines Verfahrens zum vollautomatischen Lochschneiden in TAU", 19. DGLR-Fachsymposium der STAB, 04.-05. Nov. 2014, München, 2014

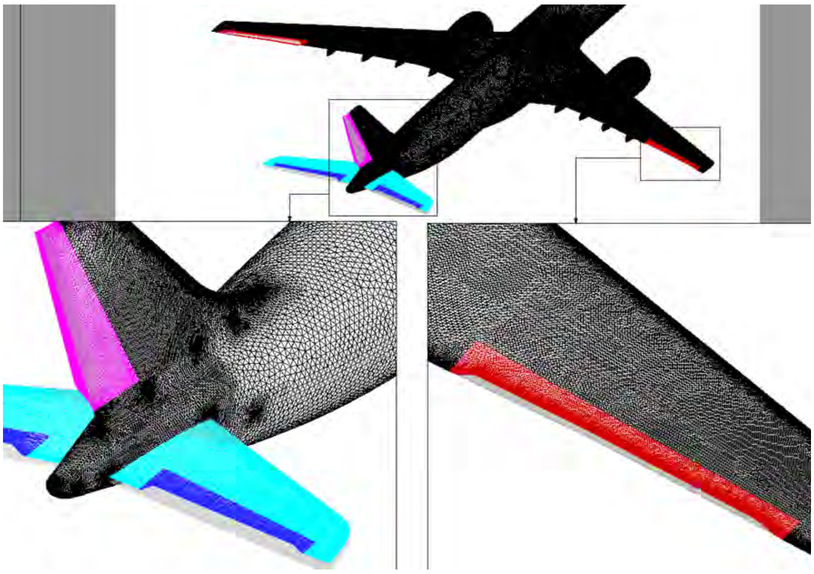

Bild 1: Generische Flugzeugkonfiguration mit Steuerflächen, bewegt mittels Netzdeformation mit Blending

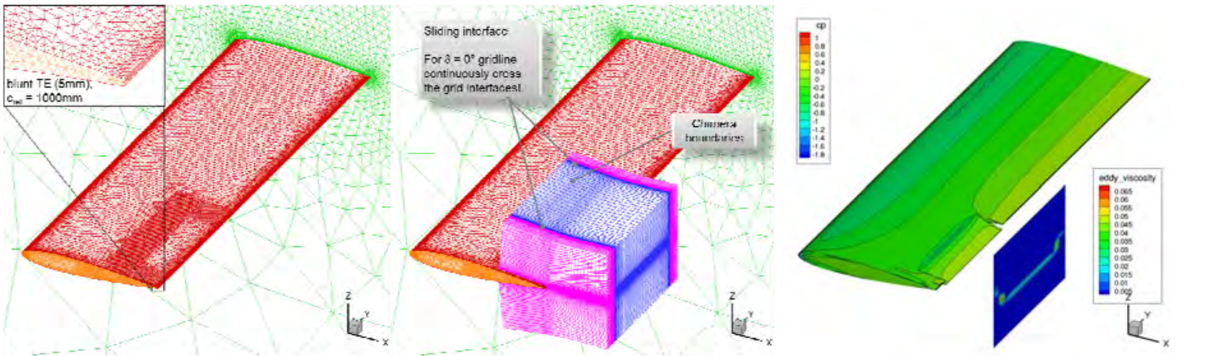

Bild 2: Links: NACAFlügel-Gitter; Mitte: Flügelgitter mit zusätlichen Blöcken für die Steuerfläche; Rechts: Simulationsergebnis mit ausgeschlagener Steuerfläche

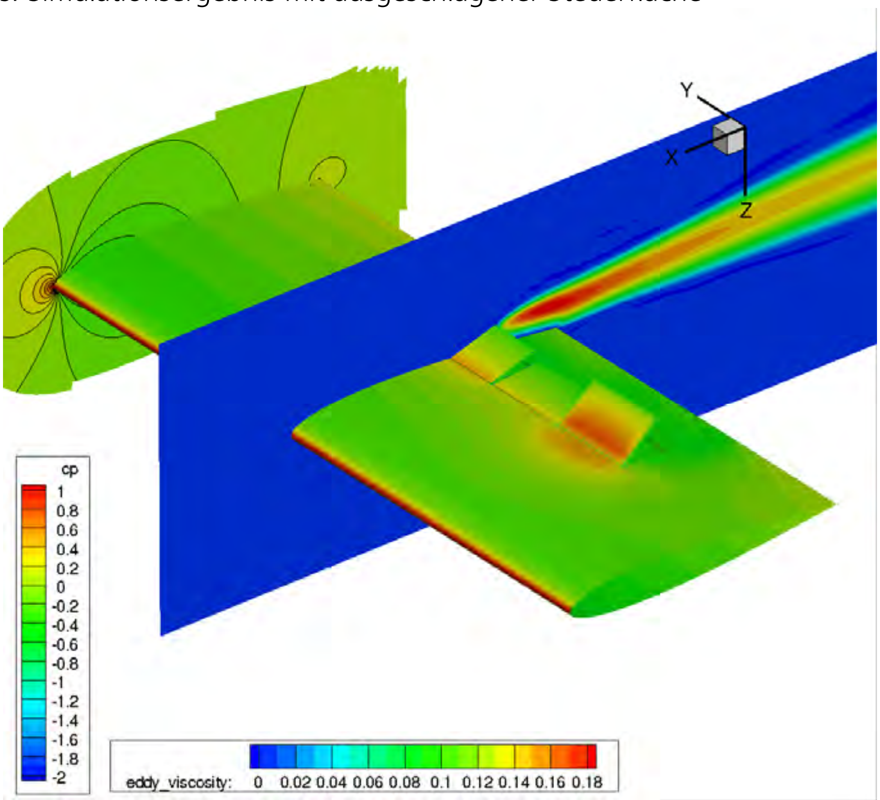

Bild 3: Simulation eines „Spoilerpianos“

Mitteilung

Projektgruppe/Fachkreis: Numerische Aerodynamik

Comparison of optimizer-based and flow solver-based trimming in the context of high-fidelity aerodynamic optimization

Časlav Ilić†, Mohammad Abu-Zurayk, Stefan Keye, Andrei Merle

German Aerospace Center (DLR)
Institute of Aerodynamics and Flow Technology, Lilienthalplatz 7, 38108 Braunschweig
†Corresponding author, caslav.ilic@dlr.de

When performing an aerodynamic optimization of an aircraft configuration in steady flight, it is usual to require some force balance conditions to hold. For typical transport aircraft in cruise flight, these conditions are (neglecting small angles) that the aircraft weight must be balanced by lift, and the pitching moment around the center of gravity by the tail force. When these forces are balanced, it is said that the aircraft is in a *trimmed* state.

There are two ways to achieve trimmed state during the optimization: either the required force balances are posed as constraints for the optimizer to satisfy by the end of optimization [2], or they can be satisfied at each design evaluation by an internal iteration within the flow solver [1]. In the optimizer-based approach, the trim control parameters – angle of attack α and tail deflection angle δ – are included as design parameters in the optimization, together with the actual shape design parameters. With the goal to minimize drag, this approach can be formulated as

$$\begin{aligned} \min_{\tilde{p}} \quad & C_D(u(\tilde{p})), \\ \text{subject to} \quad & C_L(u(\tilde{p})) = C_L^*,\ C_M(u(\tilde{p})) = 0, \\ \text{with flow solver satisfying} \quad & R(u(\tilde{p})) = 0, \end{aligned}$$

where $\tilde{p} = (p, \alpha, \delta)$ is the composite vector of shape design parameters p and trim control parameters, C_D is the drag coefficient, C_L the lift coefficient, C_M the pitching moment coefficient, R the residual of flow equations and u the flow state variables. In the flow solver-based approach, α and δ are treated as flow state parameters, i.e. the force balance equations are solved for during the simulation together with the flow residual equations. This approach is formulated as

$$\begin{aligned} \min_{p} \quad & C_D(\tilde{u}(p)), \\ \text{with flow solver satisfying} \quad & R(\tilde{u}(p)) = 0,\ C_L(\tilde{u}(p)) = C_L^*,\ C_M(\tilde{u}(p)) = 0, \end{aligned}$$

where $\tilde{u} = (u, \alpha, \delta)$ is the composite vector of actual flow state variables and trim control parameters.

The flow solver-based approach may be attractive if it is desired to have a feasible design at each evaluation, or if the chosen optimization algorithm is not able to treat constraints directly [1]. But if maintaining feasibility in each evaluation is not required and a constrained gradient-based optimization algorithm is used, which of the two approaches leads to smaller optimization run time? Intuitively, the optimizer-based approach should be more favorable, since it will not waste time making feasible the initial, far-from-optimal designs, and simulation time may be smaller because of less equations to satisfy.

However, figure 1 shows a case where the opposite is true. An RAE 2822 airfoil is optimized using both approaches, and with only the lift balance equation. The flow is modelled with RANS equations, gradients are computed by the adjoint approach, design parameters are 15 Bezier polynomials, and the optimization algorithm is SNOPT [3]. It can be seen that with the flow solver-based approach only 15 evaluations are needed to reach the optimum, while it

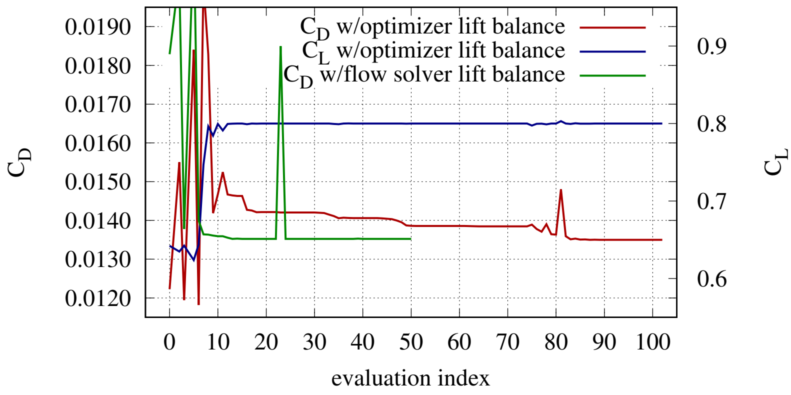

Figure 1: Drag optimization of RAE 2822 airfoil with optimizer-based and flow solver-based control of lift coefficient, at Mach number $M = 0.73$ and target lift coefficient $C_L^* = 0.80$.

takes 85 evaluations with the optimizer-based approach. Even with the run time of single design evaluation in flow solver-based approach being about 30 percent higher than in the optimizer-based approach, this case shows a clear benefit when using the flow solver-based approach.

In the final paper, the two approaches will be compared on a more relevant test case, based on the Common Research Model (CRM) [4] wing-fuselage-tail-nacelle configuration as shown on figure 2. Both lift and pitching moment balance equations will be included, as well as single- and multi-point optimization problems. Design parameters will be free-form deformation (FFD) control points on the wing. The paths by which the optima are reached, as well as any differences in the optima, will be examined, and conclusions on best practice drawn.

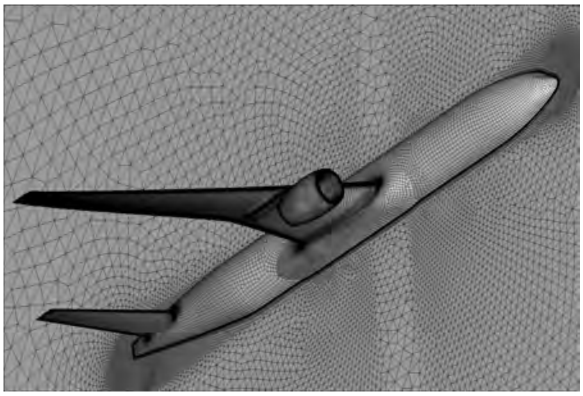

Figure 2: CRM wing-fuselage-tail-nacelle configuration to be used for trimming investigation.

References

[1] J. Brezillon, O. Brodersen, R. P. Dwight, A. Ronzheimer, and J. Wild. Development and application of a flexible and efficient environment for aerodynamic shape optimisation. In *ONERA-DLR Aerospace Symposium (ODAS)*, 2006.

[2] S. Chen, Z. Lyu, G. K. W. Kenway, and J. R. R. A. Martins. Aerodynamic shape optimization of the Common Research Model wing-body-tail configuration. *Journal of Aircraft*, 2015.

[3] P. E. Gill, W. Murray, and M. A. Saunders. SNOPT: An SQP algorithm for large-scale constrained optimization. *SIAM Journal on Optimization*, 12:979–1006, 1997.

[4] J. C. Vassberg, M. A. DeHaan, S. M. Rivers, and R. A. Wahls. Development of a Common Research Model for applied CFD validation studies. In *26th AIAA Applied Aerodynamics Conference*, number AIAA-2008-6919, 2008.

Mitteilung

Projektgruppe / Fachkreis: Numerische Simulation

A new high-order discontinuous Galerkin solver for DNS and LES of turbulent incompressible flow

Martin Kronbichler, Benjamin Krank, Niklas Fehn, Wolfgang A. Wall
Institute for Computational Mechanics, Technische Universität München, Boltzmannstr. 15, 85748 Garching, {kronbichler,krank,fehn,wall}@lnm.mw.tum.de

Incompressible flows in the turbulent regime are of fundamental significance for engineering and biomedical applications. Accurate and reliable numerical simulation of such flows demands for extremely high spatial and temporal resolution despite the steady improvement in modeling of unresolved scales. The INDEXA code (INcompressible Discontinuous Galerkin towards the EXA scale) uses discontinuous Galerkin (DG) for spatial discretization due to their high-order capability, stability in convection-dominated flows, efficiency in massively parallel computations, and geometrical flexibility with respect to complex geometries and curved boundaries. The convective term is written in conservative form and discretized using a Lax–Friedrichs flux formulation. For discretizing the second derivatives in the viscous term and in the pressure Poisson equation, the symmetric interior penalty method is applied.

For efficient time integration, we choose a velocity correction method (dual splitting scheme) that advances the convective term, the pressure term, and the viscous term of the Navier–Stokes equations in separate substeps. The splitting method is based on the third-order accurate backward differentiation formula (BDF3). While the viscous term is treated implicitly for stability reasons, we use an explicit formulation of the convective term that implies a CFL restriction of the time step size. Recent publications have shown that projection methods such as the dual splitting scheme become unstable in the limit of small time steps if they are not stabilized appropriately. This lower limitation of the time step size essentially depends on the grid size h and the viscosity ν. While this time step restriction is less of a concern for well-resolved simulations, it is in conflict with the CFL condition in the marginally-resolved, high Reynolds number regime. The source of instabilities are divergence errors related to a finite spatial resolution that occur as source terms on the right-hand side of the pressure Poisson equation, scaled by the inverse of the time step size. We propose a stabilization technique for this instability by using a consistent divergence penalty term when projecting the intermediate velocity onto the space of divergence-free vectors. This stabilization both enhances the robustness of the method in the sense that the method is stable for arbitrarily small time steps and, more importantly, is crucial when applying the method to flow problems in the under-resolved, high Reynolds number regime.

The temporal splitting leads to easier-to-solve equations such as a pressure Poisson equation and a Helmholtz equation in the viscous step for which optimal solver strategies are available. We use Krylov subspace methods such as the conjugate gradient method and the generalized minimum residual method which represent state-of-the-art iterative methods showing optimal algorithmic performance when combined with appropriate preconditioners. The Helmholtz equation is effectively preconditioned by the inverse mass matrix especially for high Reynolds numbers. From a computational point of view the most demanding part is the solution of the pressure Poisson equation. To obtain mesh-independent convergence rates of the Poisson solver a geometric multigrid method with polynomial Chebyshev smoothing is applied. The solver uses fast matrix-free operator evaluation using recent developments in the deal.II finite element library [3,1]. These developments have recently been rewarded support through the DFG-SPPEXA project ExaDG (PIs: Guido Kanschat, Katharina Kormann, Martin Kronbichler, Wolfgang A. Wall). All substeps in the solver, including the smoother in the geometric multigrid method, evaluate residuals in terms of cell and face integrals. These integrals are computed with a sum-factorization approach that combines low operator complexity with high computational intensity [3]. For example, the code reaches 50-65% of arithmetic peak on Phase 1 of SuperMUC (Sandy Bridge), providing close-to-ideal strong and weak scaling up to all 147,456 cores. Moreover, the code is written in a modular and generic way that allows porting to upcoming computer architecture such as next-generation Intel Xeon Phi (Knights Landing). Our realization brings together a state-of-the-art algorithm with an excellent implementation, ensuring that we reach as low absolute run times as possible for a given solution quality.

The resulting computational approach is highly efficient for direct numerical simulations (DNS) as the cost per time step is approximately independent of the polynomial order. In the talk we present DNS computations of turbulent channel flow up to $Re_\tau = 590$ and up to 131×10^6 DoFs, which is visualized via the Q-criterion in figure 1. We also show that this scheme yields excellent results for implicit large-eddy simulation of the same benchmark cases.

With regard to LES of wall-bounded turbulent flows, the computational cost of resolving the relevant near-wall scales depends on the friction Reynolds number approximately as Re_τ^2 with supplementary restrictions on the time step size if explicit time integration schemes are used. In order to circumvent this dependence, we currently include a novel wall model based on function enrichment in this code, which has recently been proposed in the framework of the continuous Galerkin method and shows excellent performance especially in separated flows with high adverse pressure gradients where many standard wall modeling approaches fail [2]. The basic idea is that classical wall functions such as Spalding's law-of-the-wall are not used to prescribe boundary data, but they are built into the function space, in addition to the standard polynomial part. The computational method is consequently capable of resolving the mean boundary layer, similar to detached-eddy simulation, even if the first off-wall node is located at up to $y_1^+ = 500$.

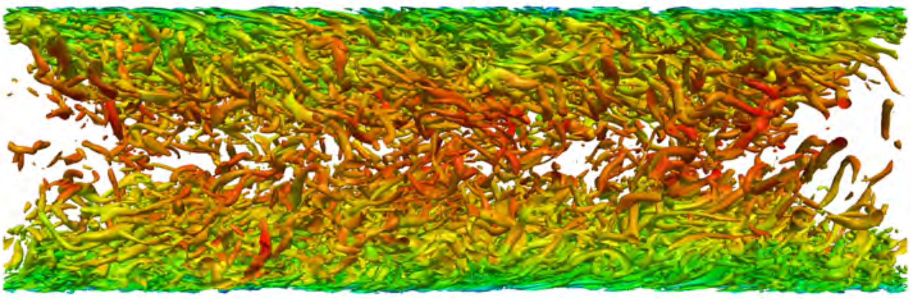

Figure 1: Q-criterion of DNS of turbulent channel flow at $Re_\tau = 590$.

[1] W. Bangerth, D. Davidov, T. Heister, L. Heltai, G. Kanschat, M. Kronbichler, M. Maier, B. Turcksin, D. Wells: The deal.II library, version 8.4. *J. Numer. Math* 24(2), pp. 1–8 (2016), doi:10.1515/jnma-2016-1045, url: http://www.dealii.org

[2] B. Krank, W.A. Wall: A new approach to wall modeling in LES of incompressible flow via function enrichment. *J. Comput. Phys.* 316, pp. 94–116 (2016).

[3] M. Kronbichler, K. Kormann: A generic interface for parallel cell-based finite element operator application. *Comput. Fluids* 63, pp. 135–147 (2012).

Mitteilung

Projektgruppe / Fachkreis: Numerische Simulation

Bayesian calibration of VRANS model parameters for turbulent flow simulations over porous materials

Pradeep Kumar, Konstantin Kutscher, Noemi Friedmann, Rolf Radespiel
TU Braunschweig
Hermann-Blenk Str. 37, 38108 Braunschweig, Germany

Current concepts for airframe noise reduction call for replacing wing trailing edges with materials that effectively reduce local noise sources. This can be performed by employing segments of porous materials. The approach makes it necessary to simulate the aerodynamic effects of porous material inserts at high Reynolds numbers.

A volume and Reynolds averaged Navier-Stokes solver was therefore developed[1,2] for turbulent flow simulations over and inside porous media. This model is based on the Reynolds stress turbulence model JHh-v2[3] and has been extended by volume averaging of the Navier-Stokes equations. This VRANS model was implemented into the DLR-TAU flow solver. In order to accurately resolve the transition across non-porous - porous interface, a number of special conditions are implemented into the turbulence equations leading to a total of six new model parameters governing the flow at the interface with the fluid and inside the porous media. These parameters are:

β : coefficient that defines the jump of velocity-gradients across the nonporous-porous interface.

β_T : coefficient that defines the jump of gradients of Reynolds-stresses over the interface.

C_{wd} : wall distance offset parameter to control the wall-induced damping of wall-normal stresses.

C_{dp} : accounts for additional diffusion of Reynolds normal stresses inside the porous medium.

C_t : parameter for modelling velocity fluctuations triple correlations inside porous medium.

$C_{\varepsilon,h}$: parameter for modelling triple correlations of fluctuating velocity components and velocity-gradients in the dissipation equation.

These modelling parameters were first calibrated in Ref.[1-2], by assessing model sensitivities in an expert-centred manual process and by comparing to DNS-simulations of channel flow from Breugem[4] as reference. This calibration was done for generic porous material that consisted of geometrically aligned cubes. Since several of the model parameter are material-dependant a more general calibration procedure is sought. Hence Polynomial Chaos Expansions (gPCE) based calibration of the model parameters has been recently demonstrated [5,6]. The data for the Bayesian calibrations is assimilated based on the Markov Chain Monte Carlo (MCMC) methods. The data is scanned over a uniform Halton sequence of the modeling parameters based on the prior knowledge of their numerical range. However, a large number of such parametric combinations were non-converging solutions of the VRANS model and the so-called Kernel trick is used to separate these non-physical samples.

As stated above a generic porous medium composed of cubes is considered in the DNS simulations that serve as a calibration reference. A similar porous channel setup has been then designed to obtain the modelling parameters for porous aluminium PA 80-110 material. This material is designed to attenuate broadband trailing edge noise of airfoils and wings. Experimental tests for this porous material at the trailing edge of a DLR-F16 airfoil were performed in the low speed wind tunnel MUB[7] and in the acoustics wind tunnel AWB-DLR. To numerically simulate the flow through the porous medium at the wind tunnel conditions, it is important to achieve similarity with the flow conditions at the trailing edge of the DLR-F16 airfoil at wind tunnel conditions. The Reynolds number in the channel is therefore derived from similarity of the momentum-thickness Reynolds number of the boundary layer

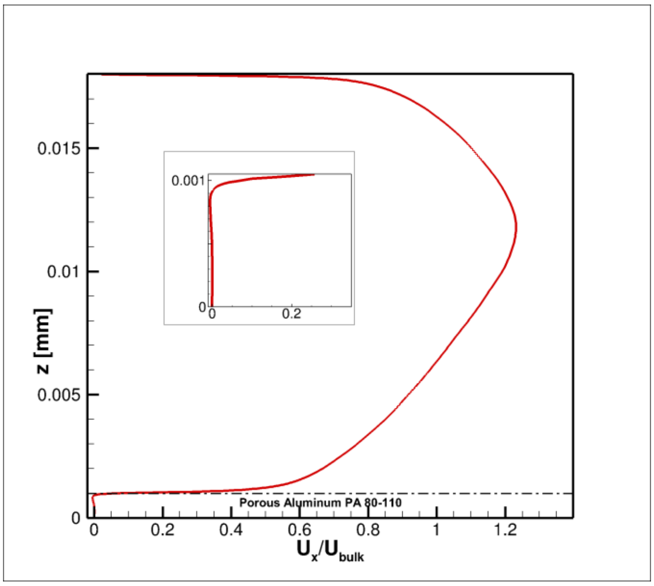

Figure 1. Mean velocity distribution from pore resolving LES simulations along the height of the channel where lower 1mm of the channel is porous material PA 80-110. The picture insert displays a zoom of the porous surface region where negative mean velocities result from secondary vertical flow in within the first pores below the surface.

at the trailing edge of a DLR-F16 airfoil at wind tunnel conditions. Based on the geometry scan data of a PA 80-110 sample, geometry resolving LES simulations are performed for a representative channel flow with the porous wall at the bottom as shown in Figure 1. The various flow and turbulence data e.g. Reynolds stresses as shown in Figure 2, from these LES simulations are used as a reference for a Bayesian calibration of the modelling parameters for the PA 80-110 material. The LES results in mean flow, Reynolds stresses and triple correlations to be used as reference data in the Bayesian update. The full paper will present the sensitivities of the VRANS modelling parameters for porous aluminium material along with the confidence data of the Bayesian update. Validation data will then be provided by comparisons with wind tunnel data of DLR F16 airfoil[7].

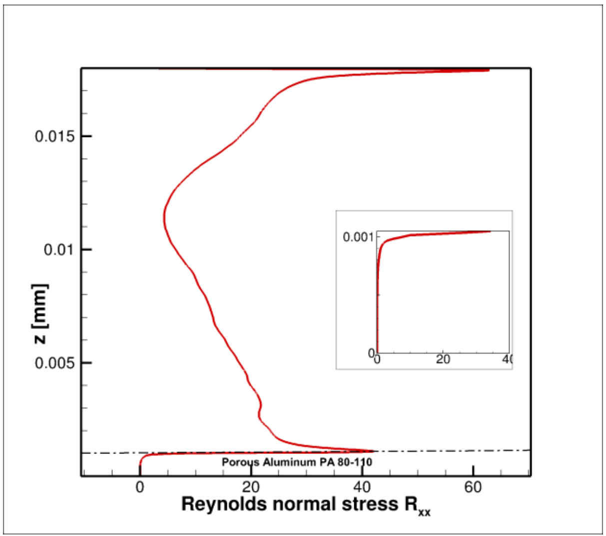

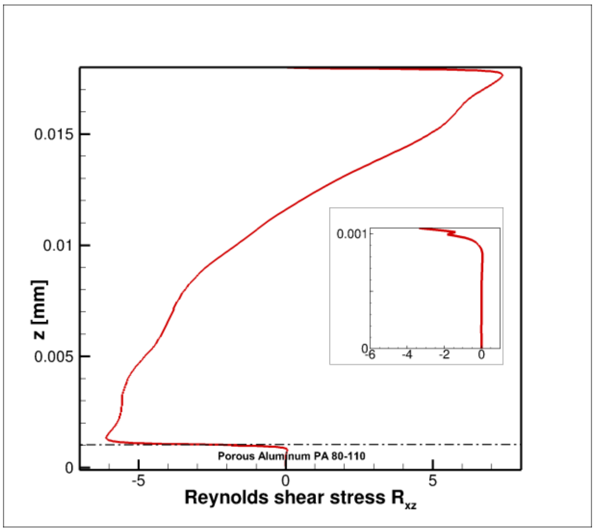

Figure 2 (a) normal and (b) shear Reynolds stresses along the height of the channel from LES simulations.

References:

1. Michael Mößner. Volume-averaged RANS-simulations of turbulent flow over porous media. PhD Thesis, April 2016.
2. Michael Mößner and Rolf Radespiel. Modelling of turbulent flow over porous media using a volume averaging approach and a Reynolds stress model. Computers & Fluids, Vol. 108, pp 25-42, 2015.
3. René-Daniel Cécora, Rolf Radespiel, Bernhard Eisfeld, and Axel Probst. "Differential Reynolds-Stress Modeling for Aeronautics", AIAA Journal, Vol. 53, No. 3 (2015), pp. 739-755.
4. Noemi Friedman, Pradeep Kumar, Elmar Zander, Joachim Rang, Hermann G. Matthies. *Bayesian update of the coefficents of a model of turbulent flow through porous media* March 7-11, 2016, Braunschweig, Germany
5. Noemi Friedman, Elmar Zander, Pradeep Kumar, Hermann G. Matthies. *Probabilistic model identification for the simulation of turbulent flow over porous media,* SIAM Conference on Uncertainty Quantification (UQ16). April 5 - 8, 2016, Lausanne, Switzerland.
6. W.-P. Breugem, The influence of wall permeability on laminar and turbulent flows. PhD thesis, TU Delft, 2015.
7. Michael Mössner and Rolf Radespiel: Flow Simulations over Porous Media – Comparisons with Experiments. Eighth International Conference on Computational Fluid Dynamics, ICCFD8-2014-0272, 2014.

Mitteilung

Projektgruppe / Fachkreis: Numerische Aerodynamik

Scale-Resolving Simulations on Unstructured Meshes with a Low-Dissipation Low-Dispersion Scheme

Axel Probst
DLR, Institut für Aerodynamik und Strömungstechnik
Bunsenstraße 10, 37073 Göttingen, axel.probst@dlr.de

Introduction

Scale-resolving simulations such as hybrid RANS/LES methods (HRLM) are considered as promising approaches for improved numerical predictions of aeronautical flows near the boarder of the flight envelope. Due to the requirement to locally resolve turbulent fluctuations, these methods rely on an accurate spatial discretization, both in terms of the grid resolution and the numerical scheme for the flow equations. For this reason, most scale-resolving flow solvers apply structured grid metrics, which provide regular mesh cells and allow for rather easy implementation of higher-order schemes. However, with the increasing demand for simulations of complex geometries, e.g., high-lift wings with brackets and installed engines, the generation of purely structured grids becomes infeasible and is often abandoned in favour of unstructured methods, such as the widely-used DLR-TAU code.
To qualify the TAU code for accurate scale-resolving simulations, a low-dissipation low-dispersion (LD2) scheme suitable for unstructured solvers has recently been developed [1]. While the LD2-scheme has already been shown to improve HRLM predictions on structured grids [2], the present work comprises first systematic studies on the applicability and accuracy of the LD2-scheme on industry-relevant unstructured or hybrid grids.

Conducted Work and Results

For a systematic assessment of the LD2-scheme on unstructured grids, different flow cases with increasing complexity are computed and validated against experimental or numerical reference data. To estimate the relative accuracy of the new scheme, a standard central scheme (denoted as Reference scheme) is used for comparison.
The investigation starts with the plane periodic channel flow at $Re_\tau \approx 395$ ($Re_\delta = 6875$), which is computed with wall-resolved LES (WR-LES, using the WALE model) on fine grids, as well as wall-modelled LES (using Improved Delayed Detached-Eddy Simulation, IDDES) on coarser grids. The analysis considers different unstructured/hybrid grid topologies which combine hexahedral (structured), prismatic (semi-structured), or tetrahedral (unstructured) cells, see for illustration a mixed hexahedral / tetrahedral grid in Fig. 1 (left). They are designed to approximately retain the original resolution of the hexahedral grids used in [2].
Generally, the channel-flow results confirm the improved accuracy of the LD2-scheme over the Reference scheme on unstructured grids, as exemplarily shown in Fig. 1 (center) for wall-modelled LES on the grid of Fig. 1 (left). However, with such a grid topology large cell-volume jumps at the hexa/tetra interface can hardly be avoided, which results in the disturbed log-law region in the mean velocity profile in Fig. 1 (center). Compared to that, the use of wall-normal prism stacks, as often found in near-wall regions of industrial hybrid grids, allows for accurate WR-LES predictions of the velocity profile (see Fig. 1, right) and the resolved Reynolds stresses (not shown here for brevity). To extend the assessment to more relevant flow conditions, the full paper will also include wall-modelled LES results at higher Reynolds numbers, up to $Re_\tau \approx 4200$.
The next test case under consideration is the flow over periodic hills at $Re_h = 10600$ (where h is the hill height). It features a local separation behind the hill which is usually overestimated by conventional RANS turbulence models. The flow is computed with WR-LES and the LD2-scheme on a prismatic unstructured grid which is approximately derived from the structured grid used in [3]. The results are compared with reference LES results from [3], as well as

TAU results obtained with the Reference scheme. Moreover, grid sensitivities are studied by using coarsened versions of the grids, as well.

Finally, as a complex aeronautical demonstration case, the Delta wing with a sharp leading edge from the VFE-2 project [4] is computed at Re = 1 million and α = 23° using SST-based Delayed DES. The unstructured grid was provided by an industrial partner in the EU-project ATAAC and consists of tetras and near-wall prism layers. To avoid numerical instabilities in coarsely-resolved inviscid flow regions, the LD2-scheme is applied in its hybrid form (HLD2) [2], which blends the LD2-scheme with the more dissipative Reference scheme via a local sensor function, σ. According to Fig. 2 (left), which shows an iso-surface of the Q-criterion coloured by the sensor value, the LD2-scheme is active (1-σ ≈ 1) in most parts of the resolved vortical flow region.

The predictive accuracy is assessed by comparing statistical values of the surface pressure in different spanwise cuts with experimental reference data. The exemplary cut at $x/c_r = 0.6$ in Fig. 2 (center and right) shows convincing agreement of the HLD2 simulations with the measurements of both the mean pressure and the root-mean-square values of the pressure fluctuations, whereas the Reference scheme clearly underpredicts the RMS(c_p)-peak due to the primary vortex. This is primarily attributed to the low-dispersion properties of the LD2-scheme. The further analysis in the full paper will also consider statistical data (mean velocity and turbulent kinetic energy) in field-cut planes along the Delta wing.

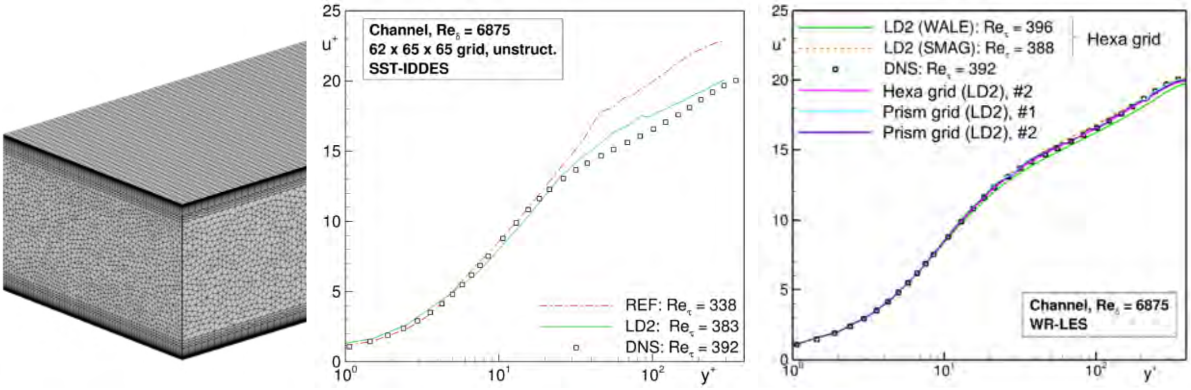

Fig. 1: Periodic channel flow. *Left:* Hybrid hexa/tetra grid. *Center:* Velocity profiles from wall-modelled LES on the hybrid grid. *Right:* Velocity profiles from wall-resolved LES on a prismatic grid.

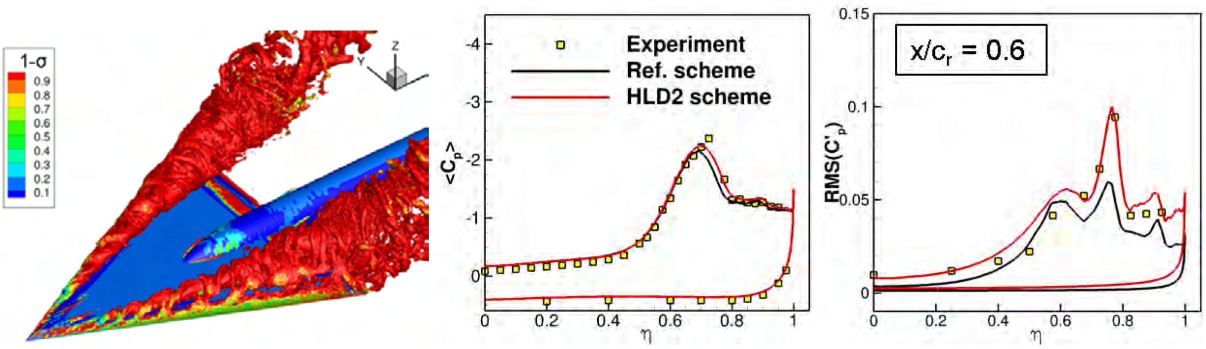

Fig. 2: Delta wing at α = 23° computed on a hybrid grid. *Left:* Iso-surface of Q-criterion coloured by the numerical sensor function of the Hybrid LD2-scheme. *Center:* Mean surface pressure at $x/c_r = 0.6$. *Right:* Root-mean-square of the pressure fluctuations at $x/c_r = 0.6$.

[1] Löwe, J., Probst, A., Knopp, T., & Kessler, R. (2015). A Low-Dissipation Low-Dispersion Second-Order Scheme for Unstructured Finite-Volume Flow Solvers. AIAA 2015-0815.

[2] Probst, A., Löwe, J., Reuß, S., Knopp, T., & Kessler, R. (2015). Scale-Resolving Simulations with a Low-Dissipation Low-Dispersion Second-Order Scheme for Unstructured Finite-Volume Flow Solvers. AIAA 2015-0816.

[3] Fröhlich, J., Mellen, C. P., Rodi, W., Temmerman, L., & Leschziner, M. A. (2005). Highly resolved large-eddy simulation of separated flow in a channel with streamwise periodic constrictions. Journal of Fluid Mechanics, 526, 19–66.

[4] Hummel, D. (2008). Review of the Second International Vortex Flow Experiment (VFE-2). AIAA 2008-377.

Mitteilung

Projektgruppe / Fachkreis: Numerische Simulation

Netzdeformation mit Elastizitätsanalogie in multidisziplinärer FlowSimulator-Umgebung

Arne Rempke
DLR Institut für Aerodynamik und Strömungstechnik
Lilienthalplatz 7, 38108 Braunschweig
arne.rempke@dlr.de

Eine Vielzahl numerischer Anwendungen im Rahmen der Flugzeugauslegung auf Basis hochgenauer Verfahren macht die Berücksichtigung der Geometrieveränderung des Flugzeuges erforderlich. Dazu gehören beispielsweise die Fluid-Struktur-Wechselwirkung, die Manöversimulation, welche die Berücksichtigung beweglicher Steuerflächen erfordert, sowie die Formoptimierung.

Um eine Strömungssimulation für die veränderten Geometrien durchzuführen, ist eine Anpassung des Berechnungsgitters nötig. Dabei werden die Modifikationen an der Oberfläche des Flugzeugs ins Innere des Fluids transportiert. Für diese Volumennetzdeformation sind verschiedenen Verfahren denkbar. Hier wird ein Verfahren verwendet, das das Volumennetz – analog eines physikalischen Körpers – elastisch verformt. Für kleine Deformationen reicht es hierbei aus, eine Linearisierung der physikalischen Modellierung zu lösen. Um den Besonderheiten eines Netzes für reibungsbehaftete Strömungen mit anisotropen Zellen gerecht zu werden, werden dabei kleine Zellen künstlich versteift [1]. Dies bewirkt, dass insbesondere die Randschicht bei der Deformation gut erhalten bleibt. Auch virtuelle Materialparameter wie die Poissonzahl haben wesentlichen Einfluss auf die Netzqualität und die Robustheit der Methode [2]. Zusätzlich zu den linearen wurden auch die nichtlinearen Elastizitätsgleichungen betrachtet, die insbesondere bei großen Deformationen zu qualitativ hochwertigeren Netzen führen.

Um das deformierte Netz für weitere Strömungsrechnungen verwenden zu können, müssen gewisse geometrische Eigenschaften erhalten bleiben. Ein fundamentales Kriterium ist etwa, dass die Volumina aller Zellen positiv sind. Ist dieses Kriterium nicht erfüllt, kann das Netz nicht mehr für Anschlussrechnungen verwendet werden. Selbst wenn nur wenige Zellen negatives Volumen aufweisen, wird daher häufig eine komplett neue Netzdeformation mit anderen Parametern oder einem anderen Verfahren durchgeführt. Um diesen Aufwand zu reduzieren, wurde das hier vorgestellte Netzdeformationsverfahren für lokale Netzreparaturen eingesetzt. Die Problemgröße und Laufzeit können dadurch erheblich reduziert werden.

Neben der Kopplung mit Strukturmechanik oder der Manöversimulation, bei denen sich die Flugzeuggeometrie aufgrund von mechanischen Belastungen oder der Bewegung von Steuerflächen verändert, ist auch die Formoptimierung von Bedeutung. Um eine hochwertige gradientenbasierte Optimierung durchführen zu können, werden die Einflüsse der Netztransformation auf die Zielfunktion mithilfe sogenannter adjungierter Probleme bestimmt.

Die Implementierung der Netzdeformation auf der Plattform *Flow Simulator* ermöglicht die Durchführung oben angesprochener multidisziplinären Anwendungen sowie die Durchführung gradientenbasierter Optimierungen. Aufgrund der Problemgrößen war dabei eine vollständig parallele Vorgehensweise unter Zuhilfenahme von iterativen linearen Lösern und Mehrgitterverfahren von Bedeutung. Die Skalierbarkeit und parallele Effizienz der implementierten Algorithmen wurde anhand von Beispielen untersucht. Die Qualität der Deformation wurde anhand von Zellqualitäten bewertet [3].

Im Rahmen des Beitrages wird die implementierte Methode vorgestellt, sowie eine Reihe von Anwendung zur Demonstration der Leistungsfähigkeit und Effizienz der Methode präsentiert.

Literatur:

[1] Stein, K., Tezduyar, T.E. and Benney, R.: „Mesh moving techniques for fluid-structure interactions with large displacements“, Journal of Applied Mechanics, Vol. 70(1), pp. 58-63, 2003.

[2] Dwight, R.P.: „Robust Mesh Deformation using the Linear Elasticity Equations”, Computational Fluid Dynamics 2006, Deconinck H, Dick E (eds). Springer: Berlin, Heidelberg, 2006.

[3] Knupp, P.M.: „Algebraic mesh quality metrics“, SIAM journal on scientific computing, Vol. 23(1), pp. 193-218, 2001.

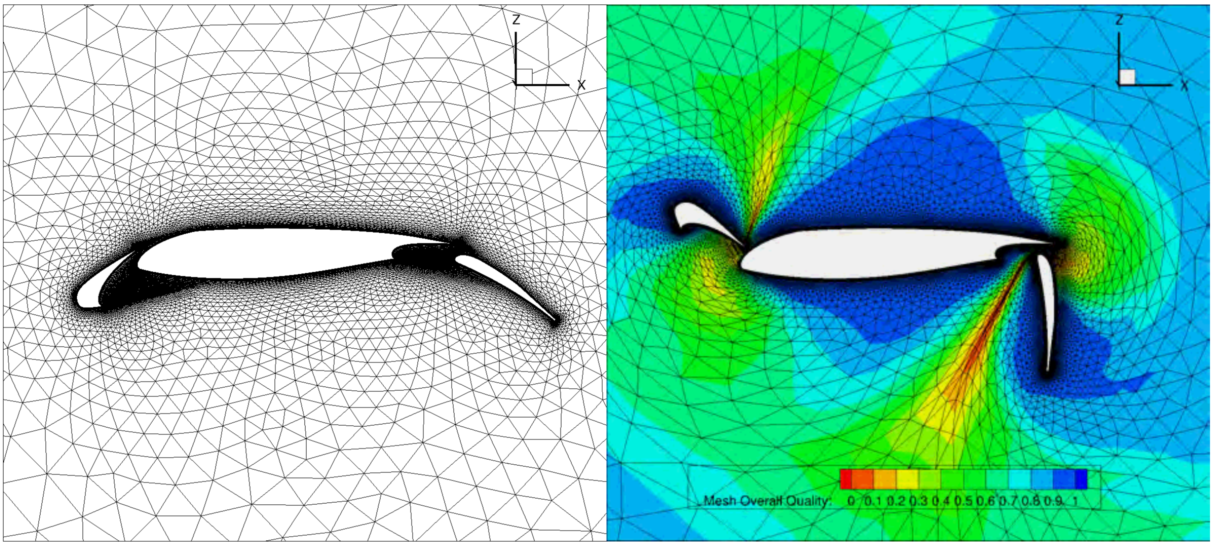

Bild 1 Ausgangsnetz (links) und Deformation (rechts) einer Hochauftriebskonfiguration. Trotz einer Rotation von 70° wurden mithilfe der linearen Elastizitätsgleichungen keine Zellen negativen Volumens erzeugt. Die Farben rechts stellen die Qualitätsänderungen der Zellen dar.

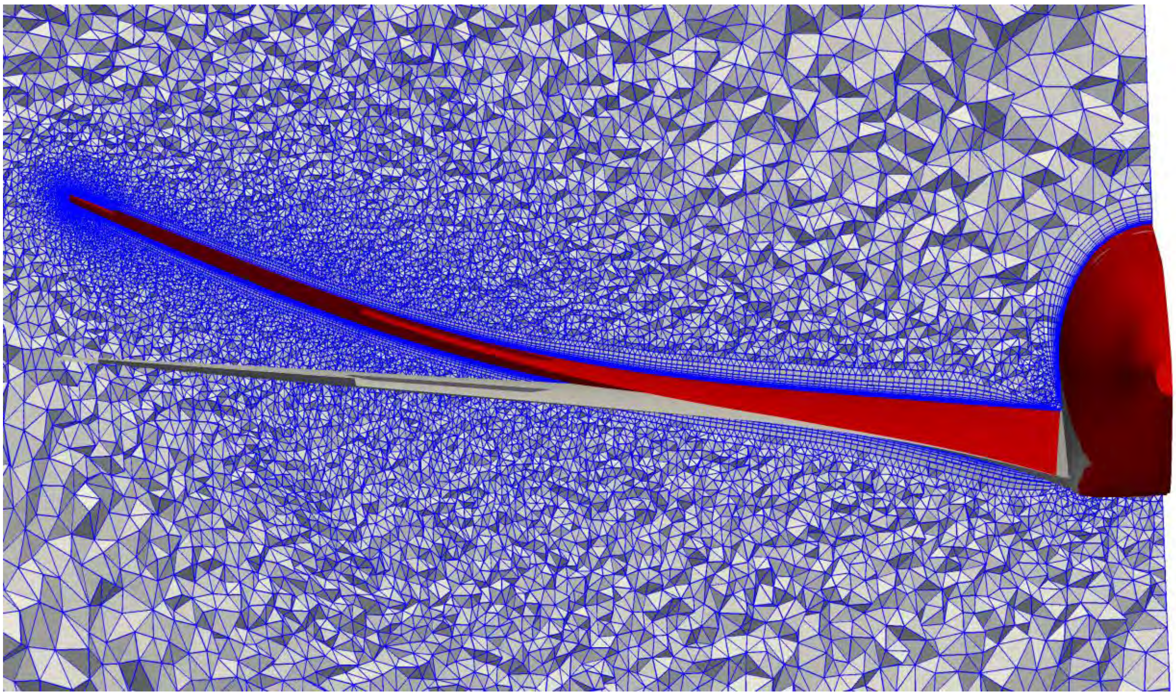

Bild 2 Modifizierte Flügelgeometrie (rot) gegenüber Ausgangflügelgeometrie (grau). Das Volumennetz (blau) wurde mithilfe der linearen Elastizitätstheorie deformiert.

Mitteilung

Projektgruppe / Fachkreis: Mathematische Grundlagen/Numerische Simulation

Building Blocks for an Efficient Solution of the RANS Equations

Cord-Christian Rossow
DLR Institut für Aerodynamik und Strömungstechnik
38108 Braunschweig, cord.rossow@dlr.de

Problem Statement:
Despite substantial progress over the last decades, robust and fast integration of the Reynolds Averaged Navier-Stokes (RANS) equations remains the key challenge in numerical flow simulation. In this contribution, two major problem areas will be addressed.
The first area is the treatment of discrete stiffness due to high aspect ratio cells in an unstructured code. On meshes with high aspect ratio cells the performance of unstructured codes still falls behind the efficiency of structured codes, since structured codes rigorously exploit the directional information inherent in the mesh topology [1]. Despite several attempts, up to now unstructured codes have not been able to adequately cope with such situations, not even for 2D problems. However, for applications in aeronautics with geometries like high aspect ratio wings and blades of rotors and propellers, meshes with large aspect ratio cells are required for reducing the number of cells to increase overall efficiency. Thus, it is highly desirable to establish aspect ratio information in cells of unstructured meshes in a similar way as in structured meshes, however on a purely local basis without the need for information of the general grid topology.
The second area concerns the integration of the equation(s) for the turbulence model. There are two main strategies followed to integrate both the main flow equations and the turbulence equations(s): integrating the equations in a coupled or in a weakly coupled manner, and it is still not clear which strategy is the most efficient one. When fast solution algorithms such as implicit Runge-Kutta (IRK) schemes are combined with multigrid, the different properties of the equations become evident by deteriorated convergence. This situation is aggravated by the fact that it is not yet clear how far multigrid as an acceleration technique is at all suited for equations with such large source terms as occuring in the turbulence equation(s) [2]. Therefore, a common strategy is to treat the turbulence equation(s) differently than the main equations, as accomplishd in [3]. Despite the fact that efficient convergence could be established, solving the main equations and the turblence equation(s) with completely decoupled and different solution strategies increases the code structure to an a much higher level of complexity. Thus, an infrastructure with a high degree of commonality between integration of the main equations and the turbulence equation(s) is highly desirable.

Objective:
The first objective is to replace in a structured code all algorithmic elements which are based on information of the structured grid topology by local formulations suited also for application in an unstructured environment. This mainly concerns the classical aspect ratio scaling [1] based on the spectral radii related to topological grid line directions. Also, all directional grid line solves have to be replaced by topologically independent algorithms.
The second objective is to establish an alternative to the weakly coupled solution strategy of Ref. [3] which at least uses the same multigrid infrastructure for the turbulence equation as for the main equations.

Strategy:
To provide similar information about the cell aspect ratio locally, (i.e., without resorting to global grid topological information), an approach is developed where cell aspect ratio information is established on purely local geometrical considerations. To make additional parts of a structured testbed code independent of grid topological information, algorithmic parts needing such information are reformulated, (e.g., prolongation is established by injection instead

of bi- or trilinear interpolation). Furthermore, all directional solution strategies are replaced either by Jacobi-type methods or red/black Gauss-Seidel is employed. In case that line-solves are strictly required (e.g., to account for stiffness of source terms in the turbulence model), an unstructured line search method which does not refer to topological grid information is established. For the Spalart-Allmaras one-equation turbulence model, an efficient integration strategy for the main flow equations and the turbulence equation is established by using a W-cycle multigrid and a three-stage implicit Runge-Kutta scheme for the main flow equations as general framework. For the turbulence equation, only the first leg of the W-cycle to coarser grid levels is used, and then direct prolongation to the finest grid is performed. Thus for the turbulence equation a typical V-cycle is performed as a subset of the W-cycle of the main flow equations, see the sketch in Figure 1. Instead of using a three-stage implicit Runge-Kutta scheme for the turbulence equation, a point-implicit red/black Gauss-Seidel scheme is used, which is augmented by implicit line solves along lines identified by a line-search algorithm typically applied in unstructured codes. These line-solves are done independently from each other, (i.e., in a Jacobi-type manner), to make the solution algorithm independent of a sweeping direction. In the final algorithm configuration, the implicit system in the Runge-Kutta implicit scheme for the main flow equations is solved by red/black Gauss-Seidel solves, which are intensified by additional sweeps on all points identified by the line-search algorithm used for the line solves of the turbulence equation.

Results:
Results are obtained on the basis of the 3-stage IRK-scheme and 2nd order Roe-upwind dissipation of Ref. [3] for the RAE2822 airfoil using the classical case 9 onflow conditions. A comparison is made between the solution strategy derived in this contribution, which uses no topological grid information any more and solves the main flow equations in a coupled manner, and the implementation of Ref. [3], where a purely structured code is used, and the main flow equations and the turbulence equation are solved in a weakly coupled manner requiring increased complexity. Figure 2 shows, as in Ref. [3], an asymptotic convergence of the turbulence equation similar to that of the main flow equations, demonstrating the viability of the derived strategy.

Future Work:
To show the applicability to a larger range of problems, the method will be applied to airfoil cases with different shock strength and Reynolds number, and to incompressible airfoil flow.

Literature:

[1]*Swanson, R.C., Radespiel, R., Turkel, E.: "On Some Numerical Dissipation Schemes", J. Comp. Phys., 147, 1998.*
[2]*Faßbender, J.: "Improved Robustness of Numerical Simulation of Turbulent Flows around Civil Transport Aircraft at High Reynolds Numbers", Ph.D. Thesis, Technical University of Braunschweig, DLR-FB 2003-09, 2004.*
[3]*Swanson, R.C., Rossow, C.-C.: "An Efficient Solver for the RANS Equations and a One Equation Turbulence Model", Computers & Fluids, 2011.*

Figures:

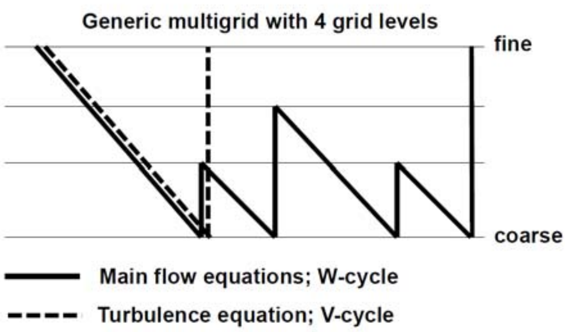

Figure 1: Sketch of multigrid strategy

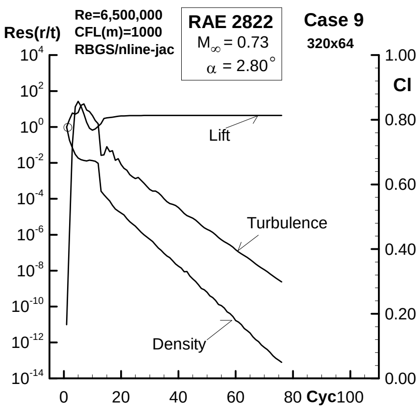

Figure 2: Convergence of coupled scheme

Mitteilung

Projektgruppe/Fachkreis: Numerische Simulation

Subgrid scale modelling of Relaminarization Effects in a differentially heated channel

T. Wetzel, C. Wagner

DLR Göttingen, Institute of Aerodynamics and Flow Technology
Bunsenstr. 10, 37073 Göttingen
tim.wetzel@dlr.de

Introduction It is of great interest in many engineering applications to simulate turbulent mixed convection, i.e. the combination of forced and natural convection, at high Rayleigh and Reynolds numbers. Since simulations of such highly turbulent flows are still not within reach for Direct Numerical Simulations (DNS), reliable turbulence models are needed. Research on Large Eddy Simulations (LES) has yielded a variety of modeling approaches for the approximation of subgrid-scale (SGS) stresses for the momentum equation. Although, only a few of them are applicable to buoyancy driven flows. One turbulence model for the heat flux vector in the filtered Navier-Stokes equations (NSE) has been proposed by Peng & Davidson [1]. This model is formulated in analogy to an eddy-viscosity model for the SGS stresses in the momentum equation. Additionally, in [3] a dynamic scale similarity model was developed to approximate the turbulent heat transport in Rayleigh-Bènard convection. In the present study, both approaches will be applied in LES of mixed convection in a vertical channel in comparison to DNS performed with the same finite-volume method. The objective is to benchmark these different dynamic modeling approaches and to analyse their potentials with respect to the prediction of flow relaminarization in mixed convection.

Computational Details A vertical channel flow with differentially heated walls driven by an upwards pressure gradient at friction Reynolds number based on the channel height and the friction velocity based Reynolds number $Re_\tau = 291$ and a Grashof number of $Gr = 9.6 \cdot 10^5$ are considered. In the LES, the filtered incompressible Navier-Stokes equations (NSE) are solved together with the Boussinesq approximation. A finite volume method based on a fourth-order spatial interpolation technique adapted from Feldmann & Wagner [2] in combination with a second-order Euler-leapfrog scheme for the temporal integration and Chorin's projection method for the velocity – pressure coupling is employed. A grid with equidistantly distributed nodes in the streamwise and spanwise directions is used. The wall-normal grid resolution is non-uniform in order to account for the high velocity and temperature gradients close to the walls. The channel domain extends $L_x = 2.5\pi\delta$ in streamwise direction and $L_y = \pi\delta$ in spanwise direction, with δ being the channel height. The grid resolution for the DNS is sufficiently high with a grid spacing in wall units of $\Delta_x^+ = 4.46$, $\Delta_y^+ = 3.57$ in streamwise and spanwise directions, respectively. The spacing in wall-normal direction is provided by a hyperbolic tangent function leading to $0.26 < \Delta_z^+ < 4.45$. All LES are conducted on a coarser grid with $\Delta_x^+ = 17.86$, $\Delta_y^+ = 14.28$ and $0.99 < \Delta_z^+ < 9.51$.

Results Figure 1 shows the averaged rms velocity profiles obtained with DNS in comparison with the data obtained by means of LES. Figure 2 shows profiles of the temperature rms-values. From the rms-profiles of the velocity fluctuations it can be seen that the turbulence intensities are higher close to the cooled wall. This counter-intuitive behaviour is therefore interpreted as the result of buoyancy induced flow relaminarization close to the heated wall. Figure 3 shows the instantaneous streamwise velocity fluctuations u' at $z^+ = 14.5$ on the left and $z^+ = 276.5$ on the right. The velocity fluctuations are organized in streaky structures and exhibit a more uniform behaviour close to the heated wall (left picture) while they are much more disrupted close to the cooled wall (right picture) which is another indication of the relaminarization effect. Thus, the case considered here is perfectly suited for studying the performance of SGS models in the case of flow relaminarization. The different LES models exhibit different behaviours with the Rotational Rate Smagorinsky model [4] being the best overall candidate out of the eddy-visosity type models so far. Eddy-viscosity SGS models are known to be more dissipative in comparison to structure-based scale similarity models. Thus, it is expected that the LES based on

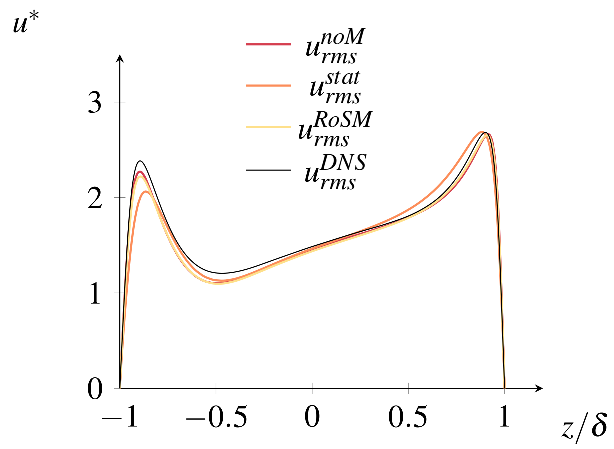

Figure 1: Profiles of streamwise rms velocity fluctuations (noM: no Model, stat: static Smagorinsky model and ROSM: Rotational Rate Smagorinsky Model)

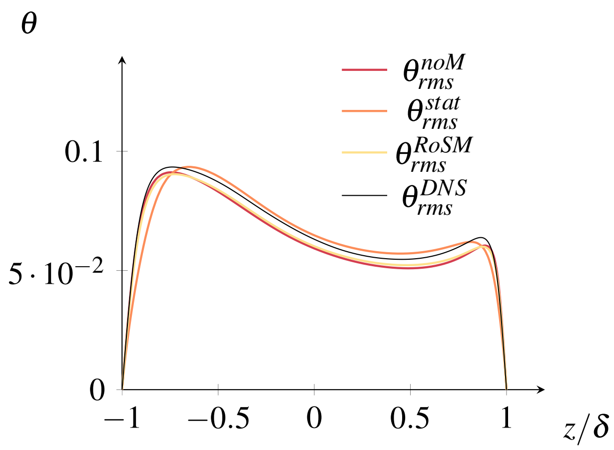

Figure 2: Profiles of temperature rms values

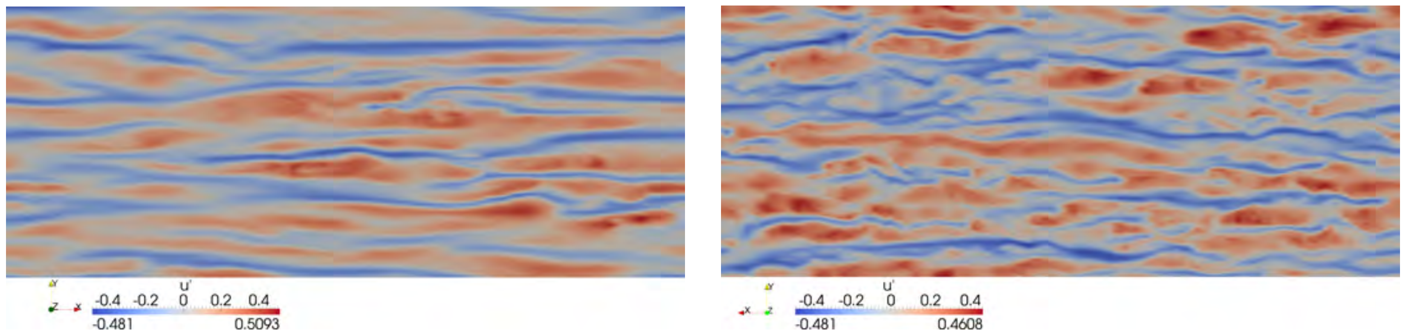

Figure 3: Colour contours of the fluctuating streamwise velocity at $z^+ = 14.5$ (left) and $z^+ = 276.5$ (right) showing streaks, taken from the DNS.

eddy viscosity SGS models will predict a faster decay of the aforementioned streaky structures, while the scale similarity model is expected to be able to represent effects concerning the formation of coherent structures at the walls with better accuracy. This hypothesis is based on a physical reasoning and will be examined in detail and presented at the symposium.

[1] Peng S.H., Davidson L.: On a subgrid-scale model for large eddy simulation of turbulent thermal flow. Int. J. Heat Mass Transfer 45:1393-1405, 2002.

[2] Feldmann D., Wagner C.: Direct numerical simulation of fully developed turbulent and oscillatory pipe flows at Re_tau = 1440. J. Turbulence 13/32:1-28, 2012.

[3] Czarnota T., Wetzel T., Wagner C.: Large eddy simulation of turbulent thermal convection using different subgrid-scale models. New Results in Numerical and Experimental Fluid Mechanics X, ISBN 978-3-319-27278-8, 2014.

[4] Ghorbaniasl, G., Agnihotri, V., Lacor, C.: A self-adjusting flow dependent formulation for the classical Smagorinsky model coefficient. Phys. Fluids 25, 23-26 (2013).

Mitteilung

Projektgruppe / Fachkreis: Experimentelle Simulation und Versuchstechnik

High speed visualization of droplets impacting on dry surfaces
at high Weber numbers

D. Burzynski, S. Bansmer
Technische Universität Braunschweig, Institute of Fluid Mechanics
Hermann-Blenk-Str. 37, 38108 Braunschweig
d.burzynski@tu-bs.de

Introduction

Impact of droplets on solid surfaces has a wide variety of applications. For instance, vehicle soiling and aircraft icing are problems related directly to the splashing phenomena [1,2]. Considering the high impact Velocities and the water droplets Diameter for these cases, it is clear that the associated Weber number, given by $We=\rho u^2 D/\sigma$, where σ is the surface tension and ρ the density of water, is high (We>2,000). There are currently few experimental data available that contributes with information at these high values, due to the complexity of the experiments [1-4]. Investigations conducted by [1] measured the secondary droplets using shadowgraph techniques at We=3,500, 5,000 and 10,000. However, the time evolution of the splashing phenomena is still unexplored. That is why, we report in this publication the results of high speed imaging that visualizes the time development of the droplets at high Weber numbers.

Experimental set-up

A single droplet is released from the droplet generator and falls down by gravity. This droplet impacts on a surface, which is mounted on a motor-driven flywheel using a substrate (see Figure 1). In order to achieve the desired Weber number, we adjusted the angular velocity of the flywheel ω. The free falling droplet is protected from the turbulent gas flow around the flywheel by a shielding tube. This tube and the impacting surface are made of glass. A Shimadzu HPV-2 high speed camera was positioned once perpendicular to the flywheel, and once with 40° respect to the x-z plane.

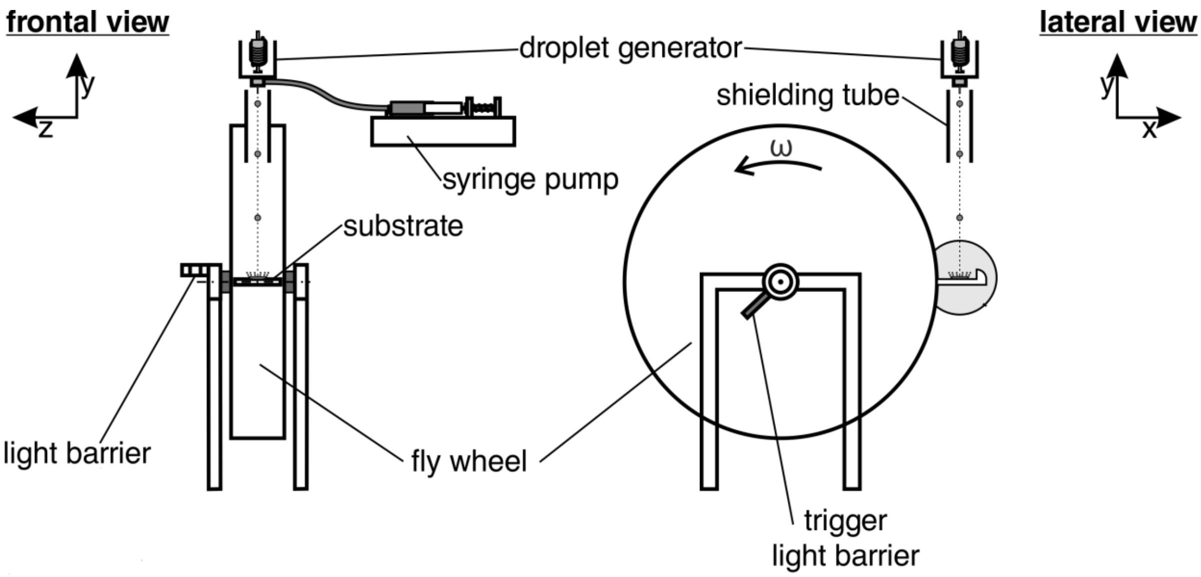

Figure 1: Flywheel experiment

Results

Primarily, we measured the primary water droplet diameter using shadowgraph methods and the standard deviation was 2.8±0.2mm. The Figure 2 and 3 shown different instants and perspectives during the impact of these droplets onto the dry surface at We=10,000. The images were recorded with the high speed camera at 63,000fps for We=5,000 and 10,000 and at 32,000fps for We=3,500. We observed the development of the splashing phenomena and compared the generated secondary droplets. Moreover, we described the time evolution of the corona and the deposited mass. The velocity of them was estimated as well as the maximal spreading diameter for all the three Weber numbers. The data was compared with existing impact models for low Weber numbers.

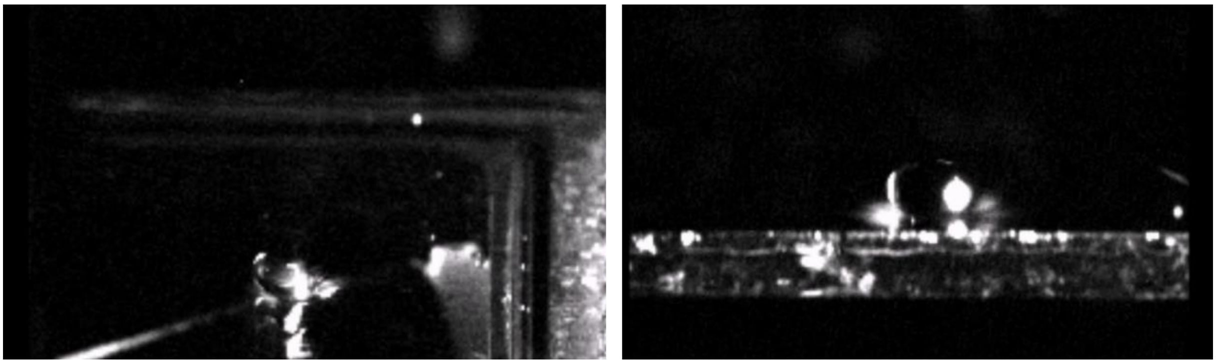

Figure 2 Water droplet impact at We=10,000 and t=1.59e-5s after impact. Perspective view (left) and perpendicular view (right)

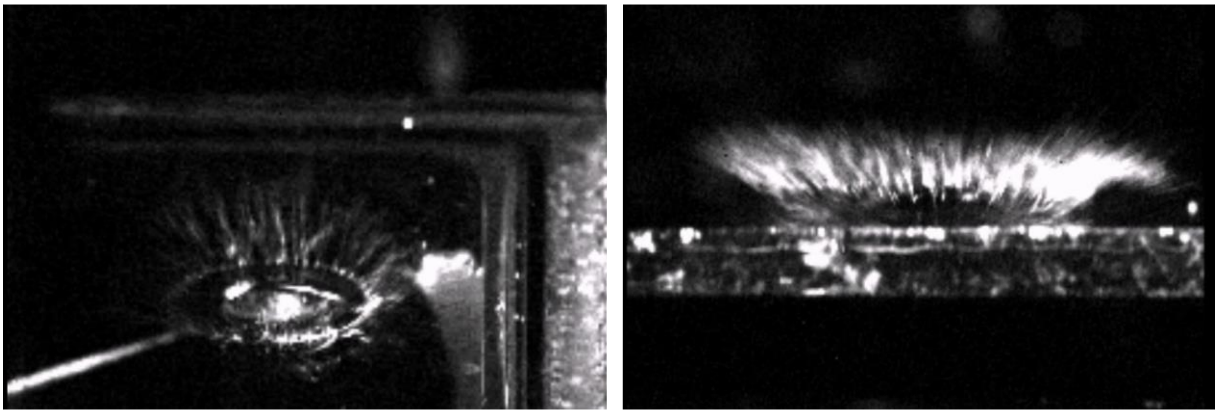

Figure 3 Water droplet impact at We=10,000 and t= 11.13e-5s after impact. Perspective view (left) and perpendicular view (right)

Reference

[1] Faßmann B, Bansmer S, Möller T, Radespiel R, Hartmann M (2013) High velocity impingement of single droplets on a dry smooth surface. Exp Fluids 54 :1516
[2] Josserand C, Thoroddsen S (2016) Drop Impact on a Solid Surface. Annu. Rev. Fluid Mech. 48:365-91
[3] Mehdizadeh N, Chandra S, Mostaghimi J (2004) Formation of fingers around the edges of a drop hitting a metal plate with high velocity. J Fluid Mech, vol 510, pp. 353-373
[4] Rioboo R, Marengo M, Tropea C (2002) Time evolution of liquid drop impact onto solid, dry surfaces. Exp Fluids 33:112-124

Mitteilung

Projektgruppe / Fachkreis: Flow Control / Aerodynamik und Aeroakustik

Challenges in the Quantification of the Momentum Coefficient of Circulation Controlled Wings in Experiments.

Y. El Sayed M., N. Beck, R. Semaan, R. Radespiel
Institut für Strömungsmechanik,
Hermann-Blenk-Str. 37
38108 Braunschweig,
e-mail: y.el-sayed-m@tu-braunschweig.de

An underestimated challenge in experiments with circulation controlled wings is the precise quantification of the blowing intensity. The first experiments with blowing, carried out in the 1930s (Bamber [1]) for boundary layer control, expressed the blowing intensity in terms of a blown air volume coefficient ($C_Q = Q/v_\infty \ S$, where Q is the volume flow rate, v_∞ is the free stream velocity, and S is the projected wing area). The momentum coefficient was first introduced by Poisson-Quinton et al. [2] & [3], as the blowing jet thrust normalised by the product of the free stream dynamic pressure and a reference area ($C_\mu = m_{jet} \ v_{jet}/q_\infty \ S$, where m_{jet} is the jet mass flow rate, v_{jet} is the jet exit velocity, q_∞ is the free stream dynamic pressure, and S is the projected wing area). The momentum coefficient became the ubiquitously used blowing parameter, as it proved most suited in characterising the effect of the blowing jet in suppressing the flow separation.
The main obstacle to the introduction of circulation control in civil aviation is the high bleed air required for blowing. Reductions in the bleed air requirements have been the focus of many studies recently (Pfingsten et al. [4], and Burnazzi et al. [5] & [6]). The development of circulation control wings to reduced bleed air expenditure has demanded more precise measurement of the momentum coefficient, as the current blowing intensity became significantly smaller.
This study investigates the challenges encountered in the quantification of the momentum coefficient of circulation controlled wings with Coanda-flaps in two separate experiments. The first was carried out with a half wing model in the Niedergeschwindigkeits-Windkanal Braunschweig (NWB) in the scope of the Bürgernahes Flugzeug (BNF) project. The second was part of Coordinated Research Centre 880's (CRC-880), and was conducted in the Large Water Tunnel Facility in Braunschweig (Großer Wasserkanal Braunschweig). The figures below show sample results of pressure measurements from the water tunnel experiment.

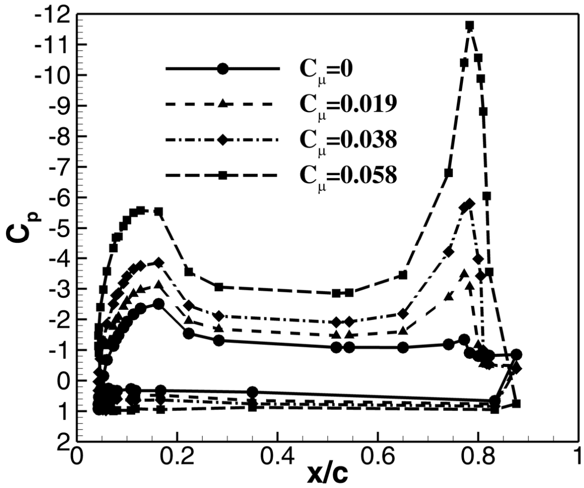

Fig 1 Pressure coefficient distribution at α=0° and Re=2x10^6 with increasing C_μ

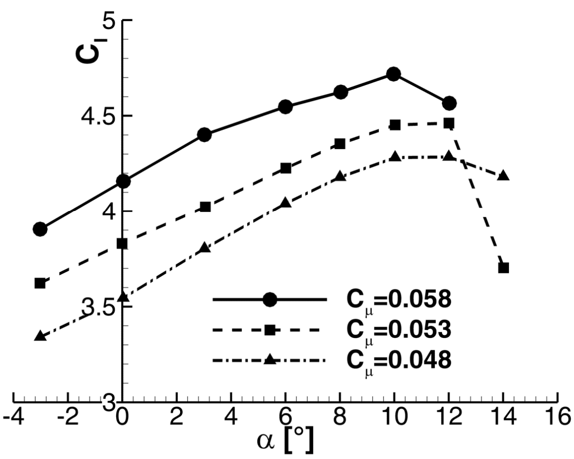

Fig 2 The effect of the C_μ on the amount of lift developed over a range of angles of attack at Re=2x10^6

Four difficulties in accurately determining the momentum coefficient were identified in the two experiments.
1) It is not easy to accurately and dynamically measure the mass flow rate of the Coanda-jet, especially in air, due to thermodynamic effects.
2) The direct measurement of the jet exit velocity is not possible, due to the tiny blowing slot (0.0006c), without extensively obstructing the Coanda-jet. Thus, the jet velocity must be calculated from the pressure difference between the plenum inside the wing and the exit plane correcting for viscous effects and assuming isentropic expansion in air (Jones et al. [7]). If the plenums' pressure is increased beyond the point where the nozzle becomes choked, then additional momentum will be imparted to the flow as the jet expands outside the nozzle.
3) Even with accurate mass flow measurements, the conservation of mass principle cannot be invoked without corrections for changes in blowing slot dimensions under load. Those changes are very small in dimension, and therefore difficult to measure during the experiment, but are still significant in their effect on the momentum coefficient.
4) Guarantying a spanwise evenness of blowing is challenging, as setting a constant slot height along the span is difficult, due to mechanical restrictions and the accuracy of available gap measuring devices. Moreover, the evenness of the jet pressure distribution along the span can be distorted by local disturbances and wall effects, causing an uneven spanwise jet velocity distribution. This unevenness goes quit often unnoticed, since the jet exit pressure is usually measured at only few locations along the span, so not to disturb the Coanda-jet too much.
All those factors have to be considered and compensated for when doing experiments with circulation controlled wings. The present work addresses all these issues and suggests workable solutions and corrections.

References

[1]. Bamber, M.J. "Wind tunnel tests on airfoil boundary layer control using a backward-opening slot". NACA Report 385, 1932.

[2]. Poisson-Quinton, P., Lepage, L.: "Survey of French research on the control of boundary layer and circulation." In: Lachmann, G.V. (ed.) Boundary Layer and Flow Control: Its Principles and Application, vol. 1, pp. 21–73. Pergamon Press, New York (1961)

[3]. Poisson-Quinton, P. "Recherches théoriques et expérimentales sur le contrôle de couche limite." 7th Congress of Applied Mechanics, London, September 1948.

[4]. Pfingsten, K. C., and Radespiel, R.: "Experimental and numerical investigation of a circulation control airfoil", 47th AIAA Aerospace Sciences Meeting, Orlando, AIAA 2009-533.

[5]. Burnazzi, M., Radespiel, R.: Assessment of leading-edge devices for stall delay on an airfoil with active circulation control. CEAS Aeronaut. J. 5 (4), 359–385 (2014).

[6]. Burnazzi, M., R. Radespiel. "Synergies between suction and blowing for active high-lift flaps." *CEAS Aeronautical Journal* 6.2 (2015): 305-318.

[7]. Jones, G.S., J.C. Lin, B.G. Allan, W.E. Milholen, C.L. Rumsey, and R.C. Swanson. "Overview of CFD Validation Experiments for Circulation Control Applications at NASA". Technical Report 20080031119, NASA, NASA Langley Research Center, Hampton, Virginia, 23681, 2008.

Mitteilung

Projektgruppe / Fachkreis: Aerodynamik und Aeroakustik

PIV Measurements of Buffet with Artificial Noise

A. Feldhusen-Hoffmann, M. Klaas, W. Schröder
Institute of Aerodynamics, RWTH Aachen University, 52062 Aachen, Germany
a.feldhusen@aia.rwth-aachen.de

1. Introduction

The shock wave/turbulent boundary-layer interaction with separation in the transonic flow around airfoils may induce large-amplitude, low-frequency, self-sustaining shock wave oscillations without any external forcing. This aerodynamic phenomenon is known as transonic buffet. The initially steady flow around the profile becomes unsteady and induces changes in lift and drag. The interaction between these periodic aerodynamic forces and the wing structure may excite periodic inflection and torsion vibrations of the wing and can lead to dangerous structural failure. Although buffet flows have been investigated intensively in the past, the details of the mechanisms leading to the shock oscillations are not fully understood. Therefore, a deeper understanding of the mechanisms leading to buffet is still of great interest, since it might help to predict the conditions for buffet onset and to find strategies to further postpone the buffet boundary. Lee [3] suggested a feedback loop between up- and downstream propagating disturbances within the flow field downstream of the shockwave which was improved by the formulation of Hartmann et al. [2]. The sound waves generated at the trailing edge are a main feature in this model. They propagate outside the separated recirculation area and impart energy on the shock wave movement. The oscillation period is thereby given by the time it takes a shock induced disturbance to convect downstream towards the trailing edge plus the time it takes the sound waves that originate at the trailing edge to reach the upstream located shock [3]. Figure 1 indicates the main features of the transonic buffet flow over a supercritical airfoil.

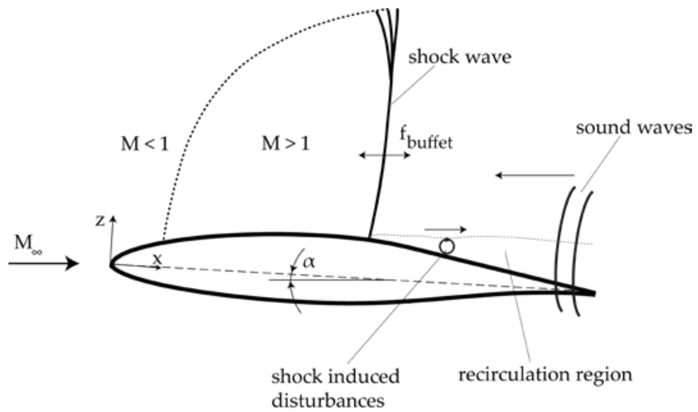

Fig. 1: Schematic of the main features in a transonic buffet flow over a supercritical airfoil.

Experiments conducted by Hartmann et al. [1] of the transonic flow over a supercritical airfoil encountering self-sustained shock wave oscillations gave hints that the sound pressure level of the sound waves originating at the trailing edge and reaching the shock wave varies. As a consequence, the shock is forced to move upstream when the sound pressure level of the sound waves reaching it is high, while the shock moves back to its downstream position when the sound pressure level of the sound waves reaching it is low. It is furthermore expected that the sound waves are of high frequency, i.e., about ten times higher than the shock wave oscillation frequency, but that their sound pressure variation frequency corresponds to the buffet frequency, i.e., shock oscillation frequency. In this study, the buffet flow field over a supercritical airfoil is overlaid with artificially introduced sound waves to study the impact of varying trailing-edge noise on the buffet flow characteristics. Therefore, well defined sound waves are introduced to the flow field downstream of the trailing edge over the airfoil by a loudspeaker.

2. Experimental setup

The experiments are conducted in a transonic wind tunnel equipped with a test section that measures 0.4 m x 0.4 m and which is equipped with flexible upper and lower walls in order to simulate unconfined flow conditions. The DRA 2303 airfoil model has a chord length of 150 mm and is equipped with steady und unsteady pressure transducers. PIV measurements are performed in a measurement region on the suction side of the airfoil. A loudspeaker connected to a horn is installed downstream in the freestream chamber of the wind tunnel and serves as an acoustic sound source (see fig. 2).

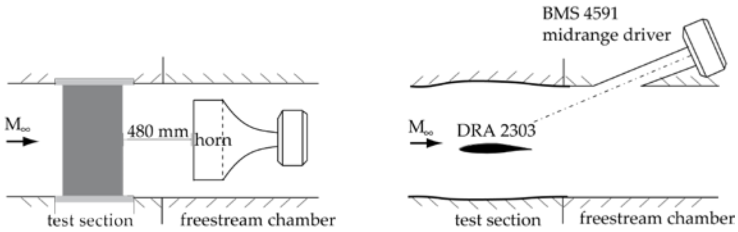

Fig. 2: Top view (left) and side view (right) of the wind tunnel test section with the airfoil model and the artificial sound source.

3. Results

The artificial sound is of high frequency in the range of the natural trailing-edge noise and the sound pressure level varies at low frequency. The results show that the shock oscillation can be influenced by introducing this artificial noise in the trailing-edge region. The signal analysis of an unsteady pressure sensor located in the shock wave region indicates that the sound pressure level variation of the artificially introduced sound waves influence the shock oscillation and force it to "lock" into this excitation frequency (see fig. 3).

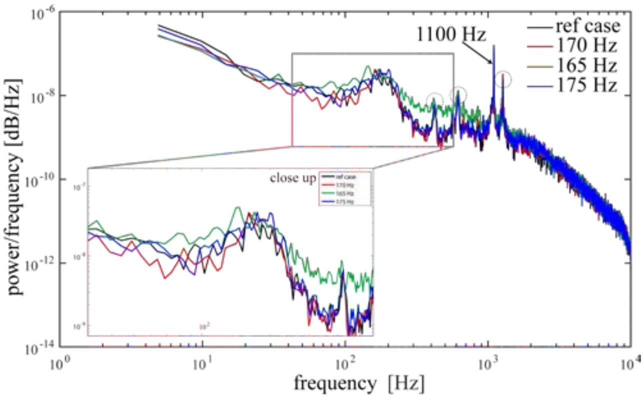

Fig. 3: Frequency spectrum of the signal of a pressure transducer on the airfoil suction side located in the shock wave region for the buffet flow with artificially introduced sound waves, variation of sound pressure level, constant sound frequency of 1100 Hz.

4. References

[1] Hartmann, A., Klaas, M., Schröder, W. (2012). Time-resolved stereo PIV measure ments of shock-boundary layer interaction on a supercritical airfoil. *Experiments in Fluids 10.1007/s00348-011-1074-6.*

[2] Hartmann, A, Feldhusen, A, Schröder, W (2013). On the interaction of shock waves and sound waves in transonic buffet flow. *Phys Fluids. doi: 10.1063/1.4791603*

[3] Lee, B. H. K. Oscillatory shock motion caused by transonic shock boundary layer interaction. *AIAA J*, 28(5):942–944, 1990.

Mitteilung

Projektgruppe / Fachkreis: Experimentelle Aerodynamik

Aerodynamische Flugversuchsanalyse zur Lastenvalidierung

Matthias Held
Airbus Operations Gmbh, Aircraft Aerodynamics, Airbus-Allee 1, 28199 Bremen,
matthias.held@airbus.com

Gemäß der Zulassungsvorschriften für Verkehrsflugzeuge (CS25) müssen die Methoden, die zur Bestimmung der Lasten verwendet wurden, durch Flugversuche validiert werden. Dies wurde in der Vergangenheit vor allem durch direkte Lastmessungen mittels Dehnmessstreifen bewerkstelligt. In jüngerer Zeit wurden diese Messungen vermehrt durch direkte Bestimmung der aerodynamischen Lasten basierend auf der Messung der statischen Drücke unterstützt. Einerseits kann dadurch einer der größten Beiträge zur Gesamtlast direkt bestimmt und somit eine Differenzierung der einzelnen Lastanteile ermöglicht werden, zum anderen eröffnet die genauere Kenntnis der aerodynamischen Lasten die Möglichkeit der Verbesserung der aerodynamischen Modelle, die zur Lastberechnung verwendet werden.

Die Messung der statischen Drücke erfolgte dabei bisher vor allem über kleine Bohrungen in der Oberfläche, die mittels Schläuchen mit zentral installierten Druckmesssensoren verbunden werden. Wo die direkte Einbringung von Bohrungen in die Flugzeugstruktur nicht möglich ist (z.B. im Bereich der Flügeltanks) werden alternativ exakt angepasste Belts angefertigt und aufgeklebt. Diese Art der Instrumentierung ist sehr zeitaufwendig und teuer. Daher werden inzwischen verstärkt elektronische Sensoren (Micro-Electro-Mechanical Systems – kurz: MEMS), die ebenfalls als Belt flexibel auf die Oberfläche aufgeklebt werden, verwendet.

Zur Bestimmung der einzelnen aerodynamischen und flugdynamischen Effekte werden unterschiedliche Flugversuchsmanöver geflogen. Hierzu zählen quasistationäre Manöver wie Stalls und Wind-up-turns, bei denen Anstellwinkeländerungen kontinuierlich oder stufenweise durch Variation von Geschwindigkeit oder Lastfaktor erreicht werden. Aufgrund der Beschränkungen der pneumatischen Messkette eignen sich für die Analyse vor allem diese Manöver. Bei Verwendung von MEMS entfällt diese Beschränkung und auch die Analyse von dynamischen Manövern wird möglich. Hier sind insbesondere Multi-Step-Manöver zu nennen, bei denen durch gegensinnigen Ausschlag von Steuerflächen die Flugzeubewegung angeregt wird [1].

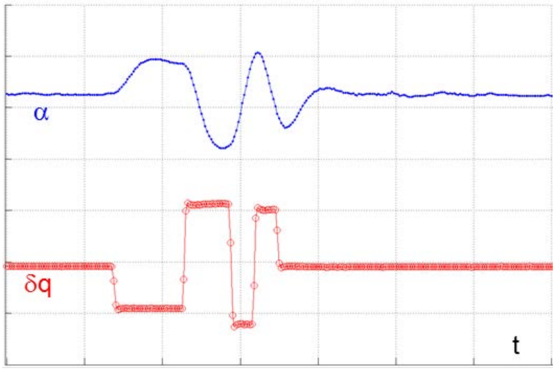

Abbildung 1: Elevator Multistep und Stall Manöver

Aus den gemessenen Drücken werden mittels Integration lokale Schnittlasten und Gesamtlast auf dem Bauteil bestimmt. Aufgrund der beschränkten Anzahl von z.B. spannweitigen Messschnitten ist ein Auffüllen der resultierenden Lastverteilungen erforderlich. Dazu werden vorwiegend vorhergehende Simulationen, die auf Windkanalversuchen oder CFD Rechnungen basieren können, genutzt. Der Prozess der Lastberechnung kann weitgehend automatisiert erfolgen. Voraussetzung ist allerdings eine sorgfältige Analyse und gegebenenfalls Korrektur der gemessenen Druckbeiwerte. Diese umfasst sowohl das Ersetzen fehlerhafter Messungen als auch das Eliminieren unerwünschter Störungen.

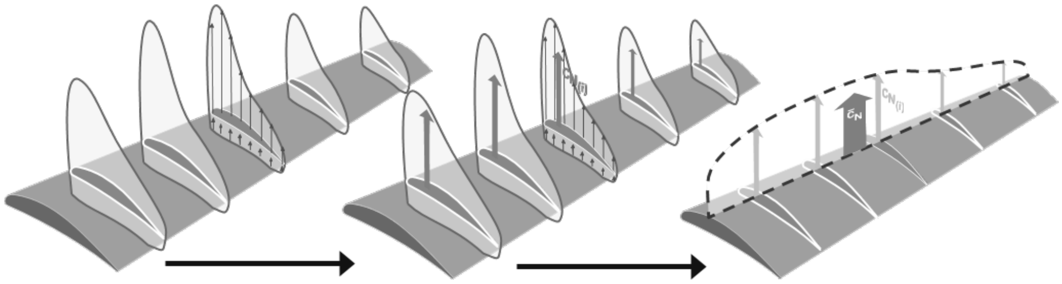

Abbildung 2: Von Druckbeiwert zum Lastbeiwert

Im Rahmen der A350-900XWB Flugversuche wurde dieses Verfahren erfolgreich für die Validierung der Lastenberechnung einiger Bauteile angewendet. Insbesondere die High-Lift Komponenten (Slats und Landeklappen) konnten so ausschließlich basierend auf der aerodynamische Analyse zertifiziert werden. Für weitere Bauteile lieferte die Analyse der statischen Druckmessungen wertvolle komplementäre Erkenntnisse. Diese Ergebnisse konnten als zusätzliche Informationsquelle in der Entwicklung der A350-1000XWB direkt verwendet werden.

Aufgrund der positiven Ergebnisse wird diese Form der Flugversuchsanalyse und -validierung eine noch größere Rolle bei zukünftigen Flugversuchen bei Airbus spielen. Hierzu sind weitere Fortschritte bei der Entwicklung der Messtechnik wie auch der Analysemethoden wichtig. Gleichzeitig kann so die Grundlage für weitere Verbesserungen im Bereich der Vorhersage aerodynamischer Lasten und damit der strukturellen Auslegung zukünftiger Flugzeuge gelegt werden.

Literatur:

[1] Jategaonkar, R. V., Flight Vehicle System Identification: A Time Domain Methodology, Volume 216, AIAA Progress in Astronautics and Aeronautics Series; Published by AIAA Reston, VA, Aug. 2006, ISBN: 1-56347-836-6

Mitteilung

Projektgruppe / Fachkreis: Fluidsysteme

A new Type of Line-Array for Aeroacoustic and Acoustic Source Localization at Drive-by Tests of Trains

Arne Henning*, Andreas Lauterbach*, Maik Bode*, Roland Schuster*, Klaus Ehrenfried*

*German Aerospace Center (DLR e.V.), Institute of Aerodynamics and Flow Technology, Bunsenstr. 10, 37073 Göttingen, Arne.Henning@dlr.de

Introduction

The application of microphone arrays for the allocation of sound sources at objects moving along a known trajectory is of special interest in case of the investigation of noise-sources at trains. Especially in case of high-speed trains it is a challenging task, since the angular velocity of the sound sources is high if the recording takes place at close distances of around 10 m from the track. Different techniques exist for the localization and quantification of sound sources. Examples are elliptical acoustic mirrors and phased microphone arrays. In case of microphone-arrays the focussing process is carried out by means of summing up signals from different sensors with defined phase delay. A short overview of the history of microphone array measurements for train investigations is provided by Michel 2006. In order to detect a flat or even spatial distribution of sound sources with a directional microphone with a concave acoustic mirror, the concave mirror has to be moved with the microphone at its focal point for scanning the volume of interest. This implies a fixed position of the sound sources of interest. When using a microphone-array, the focus point can be varied as desired in the post-processing of the recorded signals, leading to much smaller acquisition times compared to measurements with acoustic mirrors. However, a high spatial resolution requires a large number of microphones distributed on a 2-dimensional mesh.
In the following a new type of microphone-array combining a line array with a two-dimensional elliptical acoustic mirror is described. The combination of both techniques allows a three-dimensional reconstruction of the source distribution. The design was successfully tested on a high speed train track in Germany, which is used by different type of Inter City Express and other passenger trains. It was possible to improve the quality of the results signifficantly and individual wheel sets and aeroacoustic noise caused by roof structures can be identified in the source maps.

Experimental setup

The here presented microphone array combines a line array with a two-dimensional elliptical acoustic mirror. Figure 1 (right) depicts the function principle of the array. An acoustic wave emanating from a sound source located at the first focal line is reflected via the elliptical mirror to the microphones located at the second focal line. Mirror microphones are included in the drawing in order to illustrate the total path length of the acoustic waves. This length has to be taken into account for the phase shift of the time signals when applying the so called delay and sum beamforming algorithm. For the specific geometry of the array used in the study presented here the distance between the two focal lines is 8m. The width of the mirror itself in x-direction is 4m. The array is equipped with a number 31 microphones (type:M51 linearX) positioned along the second focal line of the elliptical mirror with a maximum distance of 2.5m to each other. The individual distances of the microphones to each other follow a non-linear function in order to cover a wide range of frequencies and to avoid aliasing effects occurring in case of equidistant arrangements. The whole setup is mounted on a aluminium frame. Figure 1 (left) shows pictures of the array taken during the drive by tests.

Measurement results

Results from an ICE-3 train with single traction and pantograph at the rear part passing with 55.4 m/s are shown in figure 2 (bottom). Additional results for an ICE-1 train with single traction and rear pantograph are presented in figure 2 (top) for a comparison with results from array measurements with the elliptical mirror unmounted. The figures show the source-maps for the third octave band frequency $f_{1/3}$ = 4 kHz in case of the front part of the train. In order to provide an orientation and identify main components like head, bogie, intercar-gap and pantograph the contour of the train front and rear section is depicted in the background. Additional vertical lines are drawn at the positions of the axles and

junctions of the wagons. Horizontal lines are drawn at the positions of the track, underfloor and roof. The dominant sources are located at the bogie positions. It is known from the literature that in the bogie section of high-speed trains the rolling noise as well as the flow induced noise contributes to the overall emission in this frequency range located at the axle positions. In the front section shown here additional sources are located at three positions at the roof region (x = 22, 28, 46). According to Martens 2006 these sources can be attributed to installations on the roof top of the train including the pantograph in down position (x = 46).
The results show, that the spatial resolution of the resulting source maps can be significantly increased in case of the elliptical mirror array in comparison to a line array without the geometrical reflections and amplification of the acoustic waves emanating at the position of the first focal line of the mirror. The new type of line array is especially improving the results for sources moving along a known trajectory, which is the case for rail vehicles.

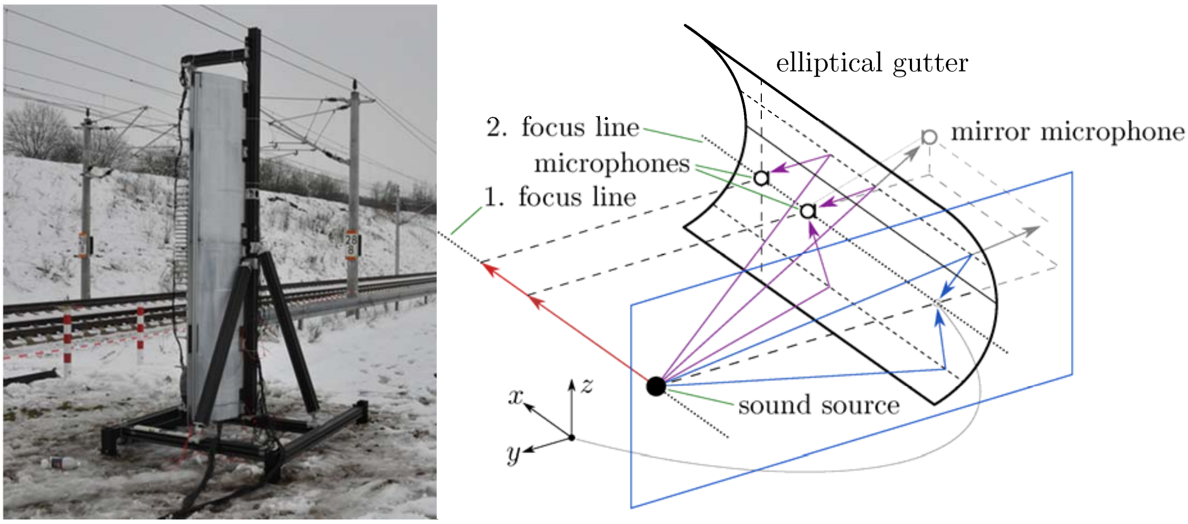

Figure 1: Left: Image of the microphone array during drive-by test. Right: function principle of the array.

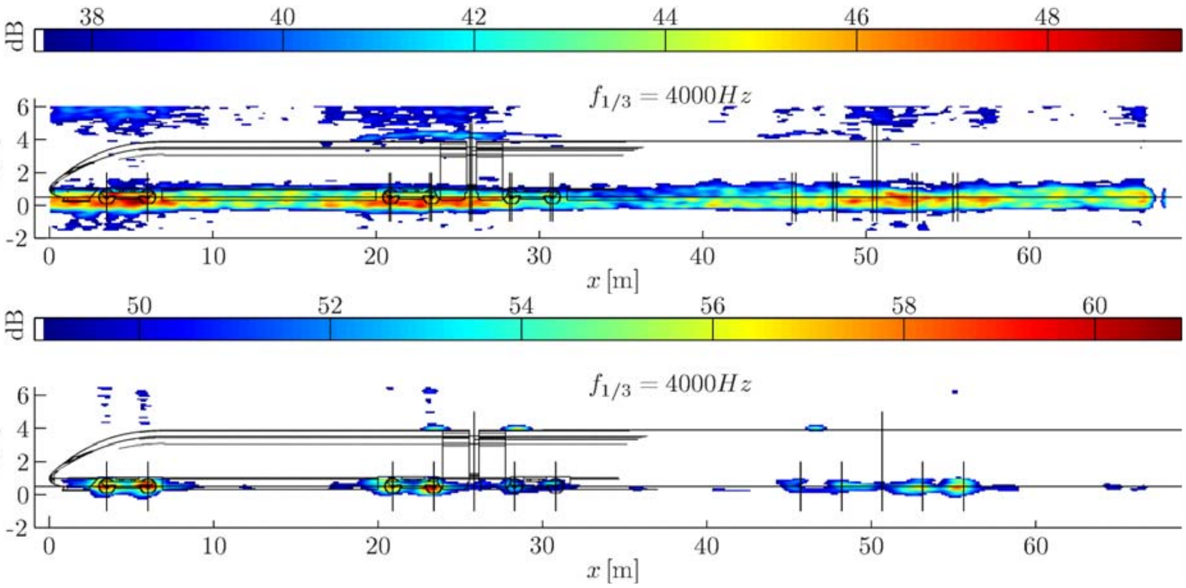

Figure 2: Resulting source-maps for the third octave band frequency f_1/3 = 4 kHz in case of the front part of the train. Top: Without elliptical mirror. Bottom: With elliptical mirror.

Literature

[1] U. Michel, History of acoustic beamforming, in: Proc. Berlin Beamforming Conference (BeBeC), Berlin, volume 1, 2006, p. 1
[2] A. Martens, J. Wedemann, N. Meunier, A. Leclere, High speed train noise - sound source localization at fast passing trains, Sociedad Espanola de Acoustica, S.E.A. 1 (2006)

Mitteilung

Projektgruppe / Fachkreis: Experimentelle Simulation und Versuchstechniken

Optische Wandschubspannungsmessung in dreidimensionalen Strömungen mittels Weißlichtinterferometrie

Jens Lunte, Erich Schülein
DLR, Institut für Aerodynamik und Strömungstechnik (AS),
Abteilung Hochgeschwindigkeitskonfigurationen, Bunsenstr.10, 37073 Göttingen,
jens.lunte@dlr.de, erich.schuelein@dlr.de

Die Wandschubspannung gehört bekanntlich nicht nur zu den wichtigsten, sondern auch zu den am schwierigsten zu erfassenden Oberflächengrößen in der Strömungsmechanik. Obwohl die theoretischen Grundlagen einer berührungslosen Erfassung der Wandschubspannung mittels Ölfilminterferometrie (OFI) in komplexen 3-D Strömungen seit mehreren Jahren bekannt sind [1], bleiben solche Messungen sehr rar. Das Problem liegt vor allem in der aufwendigen Auswertung, die sich nicht ohne weiteres automatisieren lässt. Zur quantitativen Bestimmung der Schubspannung im Rahmen von OFI werden nämlich die Informationen über die Verteilungen der lokalen Ölflussrichtung (Wandströmungsrichtung) und der zeitlichen Änderung der Ölschichtdicke benötigt [2]. Eine möglichst genaue computergestützte (automatische) Bestimmung dieser Daten aus einer erfassten Sequenz von Ölfilminterferenzbildern könnte den Aufwand deutlich verringern und die Messgenauigkeit erhöhen.
Um die Dicke der Ölschicht möglichst genau nach dem Prinzip eines Fizeau-Interferometers bestimmen zu können, wurden bislang überwiegend monochromatische Lichtquellen oder Interferenzfilter (Bandpassfilter) verwendet [1, 2]. Die Nutzung der Weißlichtinterferometrie für diese Zwecke ist nur in [3] an einer 2-D Strömung demonstriert worden. Die Anwendung einer Weißlichtquelle ist wegen der kleinen Kohärenzlänge zwar nur für relativ dünne Ölschichten geeignet (h < 2-3 µm), kann aber in diesem Bereich durch deutlich bessere Genauigkeit punkten. Da bei dieser Methode Farbinformationen anstelle von Intensitätswerten verwendet werden, lässt sich iterativ eine pixelweise Berechnung der kompletten Ölschichtdickenverteilung aus Interferenzbildern durchführen [3].
Die aktuelle Arbeit beschreibt einen Demonstrationsversuch zur Anwendung der Weißlicht-Ölfilminterferometrie auf der Leeseite eines angestellten Deltaflügels (Bild 1). Diese Konfiguration wurde gewählt, weil die komplexe Strömungstopologie am Deltaflügel eine besonders anspruchsvolle Testplattform für vergleichbare Messverfahren darstellt. Die Experimente fanden bei Windgeschwindigkeiten von 50 m/s im Niedergeschwindigkeitswindkanal 1MK des DLR in Göttingen statt. Der Anstellwinkel des Flügels wurde im Bereich von 5° bis 25° in 5°-Schritten variiert.

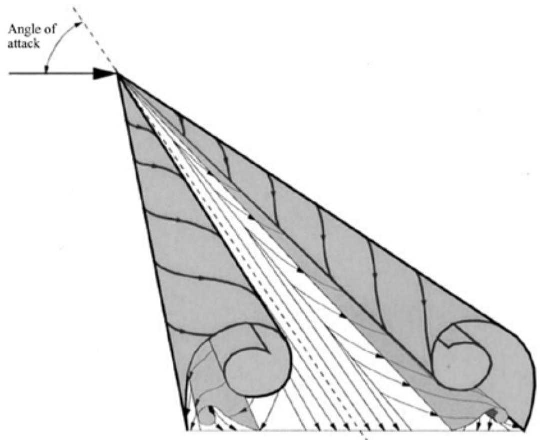

Bild 1: Schematische Darstellung der Strömungstopologie am Deltaflügel [4]

Der optische Teil des Versuchsaufbaus bestand aus einer handelsüblichen 40W-Weißlicht-LED-Flächenleuchte mit Abmessungen 0.6×0.6 m² als diffuse Lichtquelle sowie einer hochauflösenden digitalen Farbkamera SONY NEX-6. Das Spektrum der LED-Leuchte wurde vor Ort mit Hilfe eines AVANTES AvaSpec-USB2 Spektrometers vermessen.
Das Deltaflügel-Testmodell hat eine Pfeilung von 75° mit einer scharfen Vorderkante und einer in Draufsicht abgerundeten Nase (R = 6.9 mm). Die maximale Spannweite des Modells beträgt 150 mm, die Gesamtlänge ist 260 mm, und der Abstand zwischen der virtuellen Nasenspitze und der Hinterkante ist 280 mm. Die Oberfläche des Flügelmodells ist für die Mes-

sungen mit einer schwarzen reflektierenden PVC-Folie (0.1 mm dick) beklebt und kantenbündig zugeschnitten worden. Zum Einsatz kam transparentes Silikonöl ELBESIL B 100 mit einer kinematischen Viskosität von 101.7 mm²/s bei 24°C.
Ein Beispielergebnis der Wandschubspannungsmessung ist in Bild 2 für einen Anstellwinkel von 25° bei 50 m/s dargestellt. Zusätzlich zur ermittelten Verteilung der Wandschubspannung (absolute Werte) sind hier die Wandstromlinien eingezeichnet worden, die aus mehreren Interferenzbildern extrahiert werden konnten. Die lokale Richtung der Wandströmung in Räumen zwischen den eingezeichneten Stromlinien wurde bei der finalen Auswertung interpoliert, so dass eine flächendeckende Auswertung der Interferenzbilder möglich war.
Wie man in Bild 2 gut erkennen kann, kommt es bei erwähnten Testbedingungen zur Bildung des primären Hauptwirbelpaars mit einer gemeinsamen Anlegelinie entlang der Mittelachse des Flügels. Die sekundäre Ablösung der Wandströmung im weiteren Verlauf am Außenrand des Flügels, sowie das erneute Anlegen direkt entlang der Vorderkante entsprechen etwa der Struktur des sekundären Wirbels, die in Bild 1 schematisch dargestellt ist. Aufgrund dieser Strömungstopologie ist es plausibel, dass die ermittelte Wandschubspannung ausgehend von der Mittelinie zunächst unter dem Primärwirbel ansteigt und im weiteren Verlauf zur sekundären Ablöselinie wieder abfällt. Aufgrund der anwachsenden Grenzschicht nimmt das lokale Maximum im Bereich zwischen der primären Anlegelinie und der sekundären Ablöselinie mit der Entfernung zur Flügelnase immer weiter ab.
Weitere Ergebnisse zum Effekt des Anstellwinkels auf die Strömungstopologie und die Wandschubspannungsverteilungen in ausgewählten Querschnitten werden im endgültigen Artikel präsentiert.

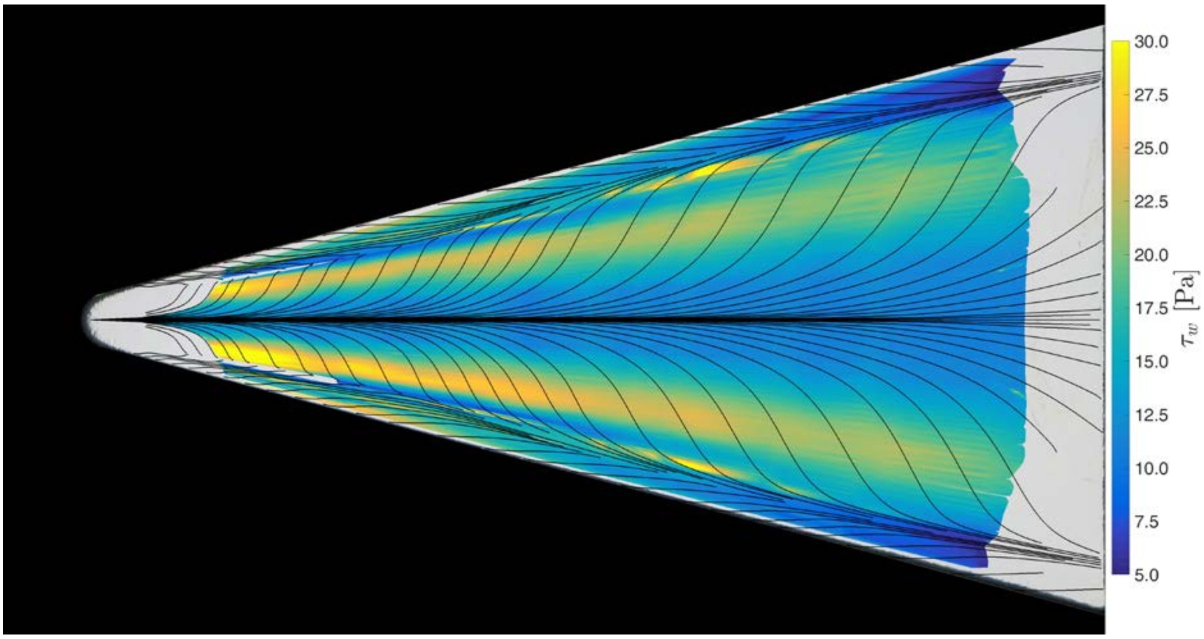

Bild 2: Stromlinien und Wandschubspannungsverteilung auf der Saugseite eines 75°-Deltaflügels bei 50 m/s und 25°

Literatur :

[1] Naughton J., Sheplak M. (2002) Modern developments in shear-stress measurement, *Progress in Aerospace Science*, 2002

[2] Schülein E. (2006) Skin friction and heat flux measurements in shock/boundary layer interaction flows, *AIAA Journal*, 44(8), 2006

[3] Desse J.-M. (2003) Oil-Film Interferometry Skin-Friction Measurement Under White Light, *AIAA Journal*, 41(12), 2003

[4] Riley A., Lowson M. (1998) Development of a three-dimensional free shear layer, *Journal of Fluid Mechanics*, 8 1998

Mitteilung

Projektgruppe / Fachkreis: Experimentelle Simulation und Versuchstechniken

Experimentelle Untersuchung der Deformation des Hochauftriebssystems an der Flügelhinterkante eines subsonischen Transportflugzeugs im Flugversuch

Ralf Meyer, ralf.meyer@dlr.de

Deutsches Zentrum für Luft- und Raumfahrt e.V. (DLR)
Institut für Aerodynamik und Strömungstechnik
Abteilung Experimentelle Verfahren, Bunsenstr. 10, 37073 Göttingen

---

Während des Fluges wird die Leistungsfähigkeit einer Flugzeugtragfläche in Hochauftriebkonfiguration von ihrer aeroelastischen Deformation beeinflusst. Eine genaue Kenntnis der tatsächlichen Flügelform ist von großer Bedeutung, um die ökologische und ökonomische Effizienz im Langsamflug, wie zum Beispiel im Landeendanflug, zu steigern. Der herzustellende Zusammenhang umfasst deshalb den Maximalauftrieb mit zugehörigem Anstellwinkel und die sich einstellende Flügeldeformation.

Mit der optischen Deformationsmesstechnik Image Pattern Correlation Technique (IPCT) lassen sich im Flugversuch dreidimensionale Oberflächeninformationen aufzeichnen, um zum Beispiel das Deformationsverhalten einzelner Segmente oder mehrerer Bereiche zueinander zu analysieren. Dazu werden bei dieser berührungslosen Methode aus Stereobildpaaren des aufgezeichneten Objektes mithilfe von Kreuzkorrelation und Triangulierung flächige Informationen gewonnen [1] [2].

Der hier vorgestellte Beitrag behandelt das Vermessen einer Flugzeugtragfläche in Hochauftriebkonfiguration, welche im Rahmen des LuFo-IV/3-Projektes „High lift INflight Validation“ (HINVA) mit dem DLR Forschungsflugzeug Airbus A320 „ATRA“ durchgeführt wurde [4]. Vier Stereo-Kamerasysteme bestehend aus insgesamt acht monochromen Digitalkameras waren dazu in der Kabine des Versuchsträgers installiert, welche jeweils verschiedene Bereiche einer Tragfläche durch die Kabinenfenster stereoskopisch aufzeichneten [3]. Das Bild 1 zeigt die entsprechende schematische Anordnung.

Aus aerodynamischer Sicht sind insbesondere die globale Flügelverformung (Biegung, Verwindung) sowie die sich tatsächlich im Flug einstellenden geometrischen Parameter des Hochauftriebssystems für das Hochauftriebs- und Überziehverhalten der Tragfläche von Bedeutung. Eine präzise Ermittlung dieser Größen, direkt oder indirekt, ist mir IPCT möglich.

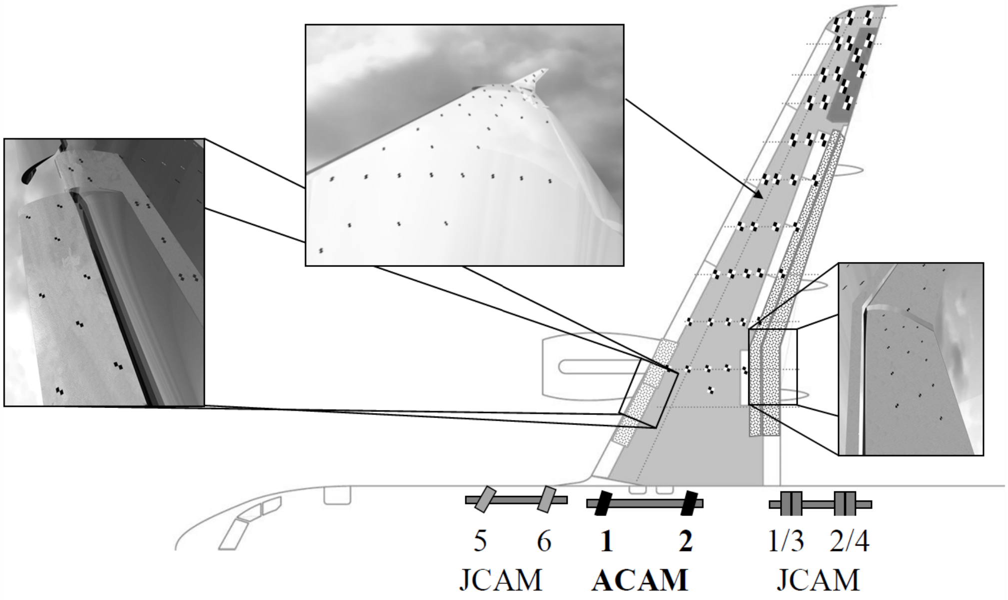

Bild 1: schematische Kameraanordnung zum Vermessen der Tragflächenverformung eines Mittelstreckenflugzeuges mit der Image Pattern Correlation Technique [3].

Der innere Vorflügel und der Bereich der Landeklappen wurden mit IPCT vermessen. Ein markerbasiertes Verfahren erfasste die globale Flügelverformung. Neben stabilisierten Flugzuständen mit Variation unter anderem von Anstellwinkel, Gewicht und Höhe umfasste die IPCT-Versuchsreihe ebenfalls dynamische Flugmanöver mit Anstellwinkelerhöhung bis zum Strömungsabriss.

Nach einleitenden Erläuterungen zu Messprinzip und Versuchsaufbau, beinhaltet dieser Beitrag die Diskussion ausgewählter Messpunkte mit Fehlerbetrachtung. Außerdem erfolgt eine vergleichende Gegenüberstellung mit Ergebnissen aus numerischen Simulationen. Der Beitrag schließt mit einer kurzen Zusammenfassung und einem Ausblick auf zukünftige Arbeiten und Anwendungsgebiete.

Literatur

[1] Boden, F., Kirmse, T., Jentink, H.: Image Pattern Correlation Technique (IPCT), In: AIM² Advanced Flight Testing Workshop - HANDBOOK of ADVANCED IN-FLIGHT MEASUREMENT TECHNIQUES BoD – Books on Demand, Norderstedt, pages 63-85, ISBN 978-3-7322-3740-1 (2013)

[2] Kompenhans, J., Schröder, A., Engler, R., Klinge, F., Stasicki, B.: Development and application of image based measurement techniques for aerodynamic investigations in wind tunnels, DLR Goettingen, conference „High-Speed Flow: Fundamental Problems“, Zhukovsky, Russia (2004)

[3] Meyer, R., Kirmse, T., Boden, F.: Optical In-Flight Wing Deformation Measurements with the Image Pattern Correlation Technique. In: New Results in Numerical and Experimental Fluid Mechanics IX Notes on Numerical Fluid Mechanics and Multidisciplinary Design, 124. Springer Verlag, Cham Heidelberg New York Dordrecht London. Seiten 545-553. ISBN 978-3-319-03157-6. ISSN 1612-2909 (2014)

[4] Rudnik, R., Reckzeh, D., Quest, J.: HINVA – High lift INflight Validation – Project Overview and Status, 50th AIAA Aerospace Science Meeting including the New Horizon Forum and Aerospace Exposition, Nashville, Tennessee, AIAA 2012-0106 (2012)

Mitteilung

Projektgruppe/Fachkreis: **Aerodynamik und Aeroakustik**
Experimentelle Simulation und Versuchstechniken

Full Scale Flow Investigation of a High Lift Vortex System by Means of Particle Image Velocimetry

Christina Politz, Reinhard Geisler, Tobias Kleindienst, Carsten Fuchs

DLR, Institut für Aerodynamik und Strömungstechnik, Abteilung Experimentelle Verfahren,
Bunsenstraße 10, 37073 Göttingen

E-Mail: christina.politz@dlr.de
Tel.: +49 551 709 2462

The understanding and prediction of high lift aerodynamics of a civil aircraft in landing configuration still lacks validated and comprehensively assessed databases involving simultaneous numerical simulations, wind tunnel tests as well as flight tests. The joint research project HINVA (High lift INflight VAlidation) aims on closing this gap for a short to medium range transport aircraft with its specific high lift devices. The research aircraft and hence the common denominator for all three methodologies was the Airbus A320 ATRA (Advanced Technology Research Aircraft) operated by the Research Flight Department Braunschweig. This aircraft was chosen to serve as a flying test bed for two flight test campaigns and as basic configuration for a wind tunnel model as well as baseline geometry for numerical simulations. In the end, all three methodologies fall back on the same realistically shaped and equipped aircraft model in high lift state to provide comparable data.

The herewith presented work comprised an airborne Particle Image Velocimetry (PIV) measurement conducted during the second flight test campaign of the project HINVA. The specific task of the PIV system was the quantification of the outer strake vortex which was initiated by the vortex generator of the nacelle at high angles of attack. To realise such an experimental configuration a high energy laser was placed inside the aircraft cabin. The laser light sheet was propagating through an experimental cabin window and was aligned normal to the longitudinal axis of the aircraft with a significant vertical divergence. Four PIV cameras were placed on both sides of the light sheet in a stereoscopic order to obtain the 3C velocity data inside a predetermined field of view. The flow tracing particles could not be inserted in an artificial manner, hence naturally occurring cloud droplets served as seeding source for this experiment. This however introduced manifold uncertainties regarding the particle dynamics inside the strake vortex and the impact of cloud turbulences on the PIV measurement. These two aspects will be further addressed in the contribution to the symposium.

In the end, two flight tests took place at the beginning of 2015 departing from the Airport Braunschweig-Wolfsburg. PIV data at different Reynolds numbers and angle of attacks was acquired and evaluated. The PIV results indicated a strong vortex system emerging over the wing surface at angles of attack above 10°. A further preparation and utilization of the data can be used to support the experimental outcome of the wind tunnel test conducted at the European Transonic Wind Tunnel (ETW) and numerical simulations with the DLR TAU code.

This contribution summarises this experimental flight test study against the background of its specific boundary conditions, in particular the impact of the free flight characteristics such as turbulences and microphysical properties of clouds. The realised installation inside the aircraft cabin and outside the fuselage will be presented. A brief inside on the qualification and flight test procedure can provide an idea about the complexity of such an installation. Finally a discussion about the 3c-PIV results initiates an analysis about the viability and potential of such a non-intrusive method for full scale applications.

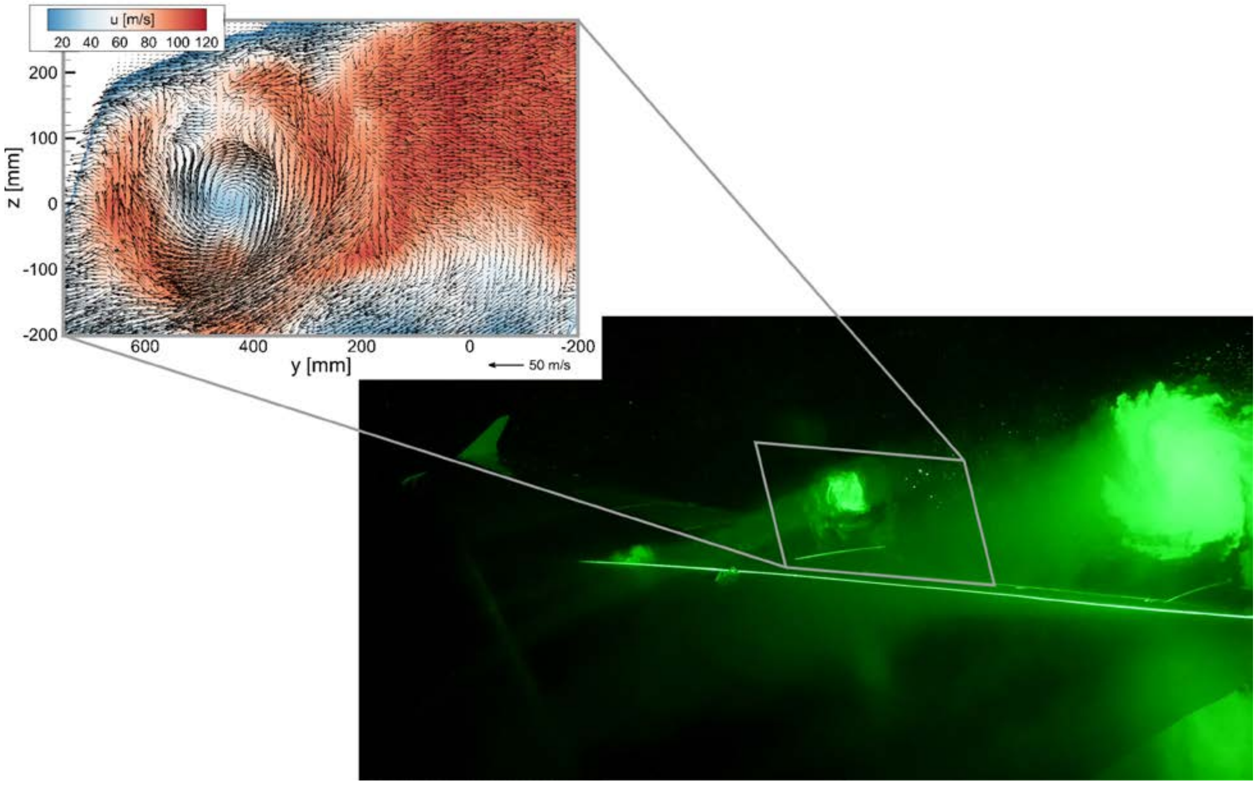

Figure 1: Observed flow field at high angle of attack and the corresponding 3C-PIV result.

References:

[1] Politz C., Lawson N., Konrath R., Agocs J., Schröder A.: Development of Particle Image Velocimetry for In-Flight Flow Measurement. In: Research Topics in Aerospace Advanced In-Flight Measurement Techniques, Springer Verlag, Heidelberg New York Dordrecht London (2013)

[2] Politz C., Roloff C., Philipp F., Ehlers H., Schröder A., Geisler R.: Free flight boundary layer investigations by means of Particle Image Velocimetry, 17th International Symposium on Application of Laser Techniques to Fluid Mechanics, 07.-10. July 2014, Lisbon, Portugal

[3] Rudnik R., Schwetzler D.: High lift INflight VAlidation (HINVA) - Overview about the 2nd Flight Test Campaign, 54nd AIAA Aerospace Sciences Meeting, Aerospace Science and Technology Forum SciTech 2016, San Diego, CA, 04 – 08 January 2016, AIAA 2016-0041 (2016)

Mitteilung

Projektgruppe/Fachkreis: Experimentelle Simulation und Versuchstechniken

Ansprechpartner: Daniel Schanz

Institution: DLR – Institute of Aerodynamics and Flow Technology (AS)
Department of Experimental Methods (AS-EXV)

Adresse: Bunsenstr. 10
37073 Göttingen

Telefon: 0551 709 2883
E-Mail: Daniel.Schanz@dlr.de

Weitere Partner: Andreas Schröder, Sebastian Gesemann, Florian Huhn, Matteo Novara, DLR-AS EXV, Bunsenstr. 10, 37073 Göttingen

Thema: Recent advances in volumetric flow measurements: High-density particle tracking (‘Shake-The-Box’) with Navier-Stokes regularized interpolation (‘FlowFit’)

We present an overview of the activities of our group at DLR over the last three years in the field of volumetric flow measurements. Starting from experimental setups and evaluations using the techniques of tomographic PIV (TOMO-PIV) [1], a novel particle tracking method (‘Shake-The-Box’ [2]) was developed, which utilizes the temporal information residing in successive imaging of a consistent, dynamic particle distribution to enhance the reconstruction of each time step. By effectively separating true particles (which inside a volume cannot disappear in time) from false reconstructions (‘ghost particles’) the technique is able to process particle concentrations at least comparable to TOMO-PIV and more than one order of magnitude above the limits of typical 3D PTV.
The temporal information is captured by predicting the particle positions of all known (tracked) particles in each following time-step. The occurring positioning errors are corrected by successively moving each particle in small steps in space (‘shaking’) until the local residual is minimized. The particle positions of the first four images are reconstructed using Iterative Particle Reconstruction (IPR) [3]. Four-step tracks are extracted as coherent paths with acceleration below a threshold. From there on, the prediction of the particle position simplifies the reconstruction problem by reducing the perceived particle image density on the residual images (see Fig. 1). Within a few time-steps the algorithm converges to a stable number of tracked particles (see Fig. 2, left, top) - close to the real number of particles - allowing for highly accurate particle placement (see Fig. 2, left bottom) and high computational efficiency.
The STB-algorithm was applied to various experimental datasets of time-resolved measurements in water and in air, in volumes ranging from less than a cubic centimeter to

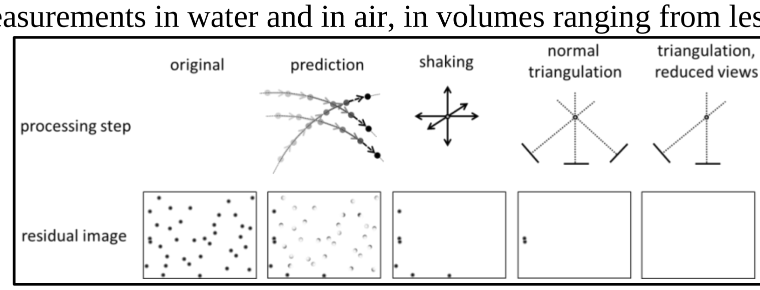

Figure 1: Shake-The-Box scheme for one time-step in the converged phase, illustrating the effects of the different computation steps on the residual image of one single camera (out of multiple).

more than half a cubic meter. Exemplary tracking results are given in Fig. 2 (Middle) and Fig. 2 (Right), showing results from investigations of an impinging turbulent jet (up to 16 m/s) and a thermal plume in air. For the latter, 275.000 instantaneous tracers could be tracked over long sequences of 1000 images.

To quantify flow structures described by the locally highly accurate particle tracks, a spatial interpolation scheme (‘FlowFit’ [4]) was developed. It results in a uniform cubic B-spline representation for velocity and pressure by minimizing a cost function. This cost function connects the measured velocities and accelerations to the B-spline variables where the fitted acceleration is derived from the fitted velocity and pressure according to the Navier-Stokes equation for incompressible and uniform-density flows. The cost function includes physically-motivated regularizations by penalizing divergence of velocity, its temporal derivative and high wavenumber components of velocity. Fig. 2 (Right) shows a FlowFit-result for a single time-step as isosurfaces of Q-criterion for the mentioned thermal plume.

The performance of STB and FlowFit was assessed in comparison to state-of-the-art TOMO-PIV algorithms in the scope of the 4th international PIV Challenge (2014) [5].

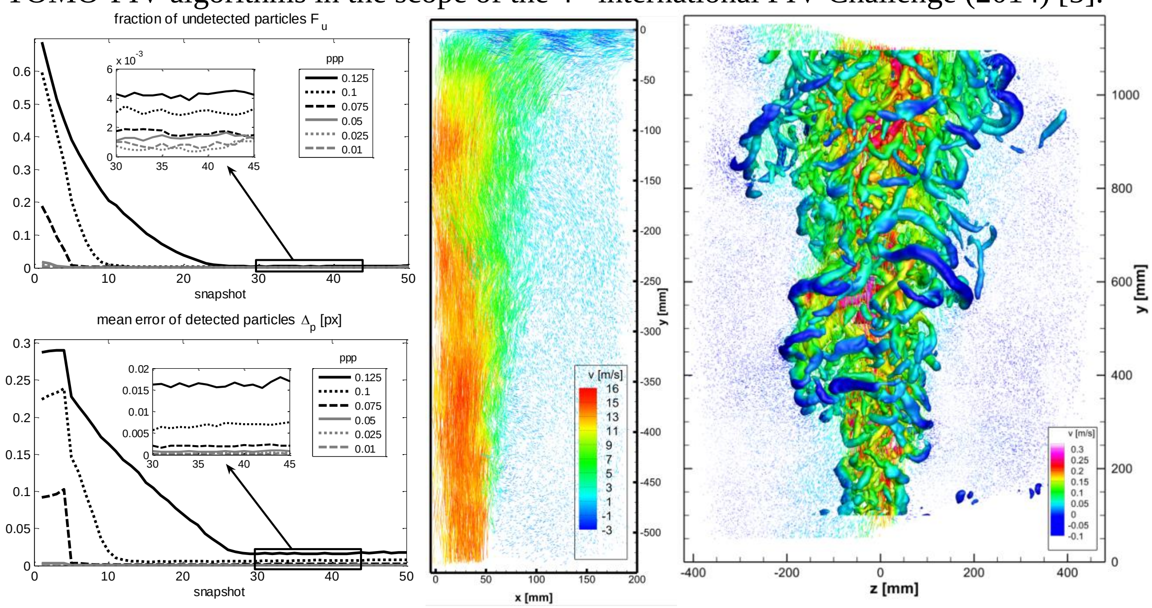

Figure 2: (Left) Development over time-steps of fraction of tracked particles and 3D positional error for different particle image densities (0.01 ppp to 0.125 ppp, synthetic experiement). (Middle) Particle tracks for impinging jet in air at 15 m/s. (Right) Particle tracks as given by STB and isosurfaces of Q-criterion as given by FlowFit for experimental investigation of thermal plume, color-coded by streamwise velocity

Literatur:

[1] Elsinga G E, Scarano F, Wieneke B and van Oudheusden BW (2006) Tomographic Particle Image Velocimetry. Exp Fluids 41:933–947

[2] Schanz D, Gesemann S, Schröder A (2016) Shake-the-box: Lagrangian particle tracking at high particle image densities. Exp Fluids 57: 70

[3] Wieneke B (2013) Iterative reconstruction of volumetric particle distribution. Meas. Sci. Technol. 24:024008

[4] Gesemann S, Huhn F, Schanz D and Schröder A (2016) “From Noisy Particle Tracks to Velocity, Acceleration and Pressure Fields using B-splines and Penalties”, 18th Int Symp on the Application of Laser Techniques to Fluid Mechanics, July 4-7, Lisbon, Portugal

[5] Kähler CJ, Astarita T, Vlachos PP, Sakakibara J, Hain R, Discetti S, La Foy R, Cierpka C (2016), Main results of fourth International PIV Challenge, Exp. Fluids 57:97

Datum: 14.06.2016 **STAB**

Mitteilung

Projektgruppe / Fachkreis: Aerodynamik und Aeroakustik

Towards trailing-Edge noise prediction with Overset LES

P. Bernicke[1], R.A.D. Akkermans[1], R. Ewert[2], and J. Dierke[2]
[1]Institute of Fluid Mechanics, TU Braunschweig, *p.bernicke@tu-bs.de*
[2]Institute of Aerodynamics and Flow Technology, German Aerospace Center (DLR)

Abstract: *In this contribution, an application of a computational aeroacoustic code as a hybrid Zonal LES tool is presented. The here used hybrid approach is based on a novel implementation of the Non-Linear Perturbation Equations extended with fluctuating viscous terms, denoted as "Overset" since a perturbation analysis is performed on top of a background flow. The extension to LES is demonstrated with isotropic decaying turbulence, where the expected temporal decay and scaling of the reference DNS data is recovered with the LES employing a classical Smagorinsky model. Furthermore, investigation of sound sources is illustrated with the application to trailing-edge noise.*

INTRODUCTION

PIANO is a Computational Aeroacoustics (CAA) code from DLR which incorporates many traditional CAA features such as block-structured, high-order, low dispersive and dissipative characteristics [1]. PIANO solves perturbation equations over a time-averaged background flow and therefore represents a hybrid approach. Such hybrid approaches are common in simulating aeroacoustic problems (see, e.g., [2, 3]). The task of computing the sound generation is separated from the sound propagation, where this latter propagation is computed with perturbation equations. Implemented equations include the Linearised Euler Equations (LEE), Acoustic Perturbation Equations (APE), and also nonlinear Euler Equations.
Viscous and nonlinear effects are often negligible in aeroacoustics as they play a minor role when sound propagation over small distances is studied. However, such approaches ignore the direct influence of viscosity on the sound generation and propagation. Furthermore, it is essential to account for viscous effects for Direct Noise Computation (DNC, see [3]) of sound generation and propagation problems. The nonlinear Euler equations have been supplemented by fluctuating viscous terms and therefore represent the full (non-linear) Navier-Stokes equations expressed in perturbation form over a given background flow (see, e.g., [2, 4]). Hence, the CAA-code PIANO can be applied as a Direct Numerical Simulation (DNS) tool to directly simulate laminar or turbulent sound generation or even DNC.
Computational demand is stringent for DNS. Large Eddy Simulation (LES) offers an alternative by resolving only the large energetic scales and model the more universal small scales. Hybrid approaches provide a further alleviation of the computational demand as LES is only performed in regions where it is needed (such as highly unsteady, massive separated flow) and the less computational demanding RANS is performed in the remainder of the domain [5]. As opposed to the so-called embedded approach, the here proposed method is denoted as "Overset" to emphasise that the DNS is performed on top of a background flow.

METHOD

The basis of the present work are the viscous Non-Linear Perturbation Equations, which are derived from the compressible Navier-Stokes equations in nonconservative form. For a detailed derivation the reader is referred to Ref. [2]. The primitive variables are decomposed into a base flow part and a fluctuating part (i.e., p_0 and p', respectively). Terms containing solely background flow contributions are grouped on the right-hand side. Typically, these residuals source terms represent the residual turbulent viscous stress and heat flux whose definition is related to the base flow. In general, the only assumption made is that the background flow is also a solution of the Navier-Stokes equations.

RESULTS

Isotropic decaying turbulence is investigated for the subgrid-scale investigation. The flow is

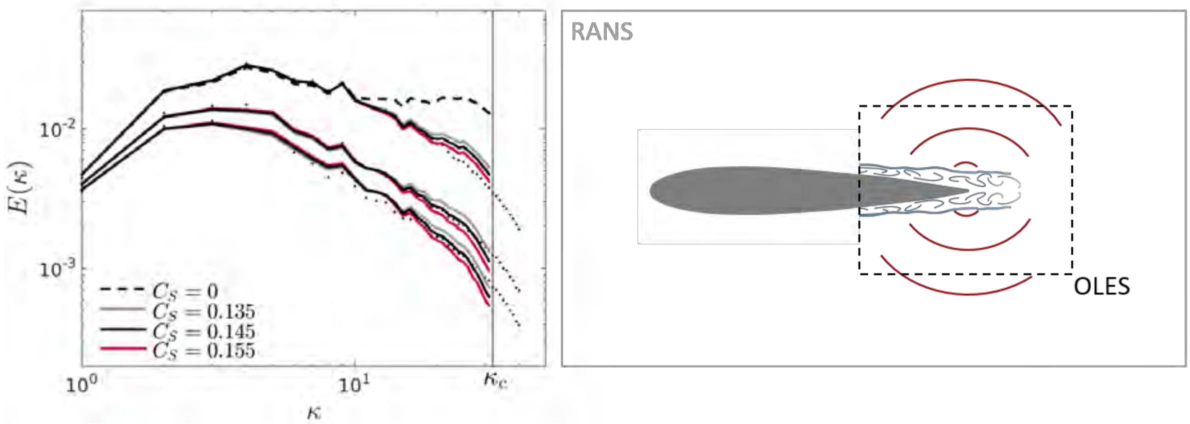

Figure 1: (left) 3D Energy spectrum for various Smagorinsky constants at time t=1/3, 3, and 5. DNS is indicated by points and viscous PIANO with lines. (right) Illustration of an Overset LES computation of trailing-edge noise.

initialised with high-resolved DNS data from Wray [6] after which decay sets in. The simulations were performed at Re_λ=104.5 on a 64^3 grid. By varying the Smagorinsky constant C_S, the scaling and temporal decay can be evaluated as compared to the reference data. This procedure is illustrated in Fig. 1 (left) for only three small variations of the Smagorinsky constant. For the case of no sub-grid scale model (i.e., C_S=0) a significant energy pile-up towards higher wave numbers is observed. By enabling the subgrid-scale functionality, the spectrum can be tuned towards the DNS reference, where C_S=0.145 can provide for the appropriate amount of modelled dissipation. A schematic of an OLES application to trailing-edge noise is presented in Fig. 1 (right). Firstly, the turbulent sound sources are determined with the OLES approach on top of the background flow. In a second step, these sound sources are propagated on a coarser CAA-grid outside the OLES domain.

RESULTS

The Overset LES method was concisely presented. The used numerical code is based on the CAA-code PIANO, here denoted by “viscous PIANO” to emphasise the use of the full Navier-Stokes equations in perturbation form as governing equations. The validation of decaying isotropic turbulence revealed good agreement between the Smagorinsky subgrid-scale model and DNS reference spectra. Further ongoing tests in turbulent channel flow simulations confirmed these promising results. Finally, the application of the OLES is illustrated with trailing-edge noise.

ACKNOWLEDGEMENTS

This work was partly funded by the Collaborative Research Centre SFB880 “Fundamentals of High Lift for Future Civil Aircraft”. Computational resources were provided by the North-German Supercomputing Alliance HLRN.

References

[1] **J.W. Delfs, M. Bauer, R. Ewert, H.A. Grogger, M. Lummer, T. Lauke**: *Numerical Simulations of Aerodynamic Noise with DLRs aeroacoustic code PIANO*, Version 5.2. User Manual, 2008.

[2] **R. Ewert, M. Bauer, M. Lummer**: *A review of state-of-the-art aeroacoustic prediction approaches*, Aircraft Noise, VKI Lecture Series, 2012-02.

[3] **C. Bailly, C. Bogey, O. Marsden**: *Progress in Direct Noise*. International Journal of Aeroacoustics 9:123–143, 2010.

[4] **R.A.D. Akkermans, R. Ewert, M.S.A. Moghadam, J. Dierke, N. Buchmann**: *Overset DNS with Application to Sound Source Prediction*, Proceedings of 5th Symposium on Hybrid RANS/LES Methods, 19-21 March 2014.

[5] **J. Froehlich, D. von Terzi**: *Hybrid LES/RANS Methods for the Simulation of Turbulent Flows*. Progress in Aerospace Sciences 44:349–377, 2008.

[6] **A. Wray**: Unpublished DNS data, ftp://torroja.dmt.upm.es

Mitteilung

Projektgruppe / Fachkreis: Aerodynamik und Aeroakustik

Titel: CFD – CAA slat noise prediction of DLR F15 high lift configuration

Autoren: Dirk Heitmann, Roland Ewert
Institution: DLR Insitut of Aerodynamics and Flow Technology, Technical Acoustics
Adresse: Lilienthalplatz 7, 38108 Braunschweig
e-mail: dirk.heitmann@dlr.de

Introduction
This contribution concerns numerical prediction of slat noise. A hybrid approach based on RANS and CAA with stochastic sources is used. Here, for the first time 3D-computations based on the Eddy-Relaxation source terms are presented. In the final paper this novel approach will be described in detail. Furthermore, the final paper will include comparisons to experimental results obtained in the DNW-LFF test facility in Marknese, Netherlands.

Numerical approach
A hybrid CFD – CAA approach was used for the slat noise prediction of the DLR F15 high-lift configuration. This configuration is depicted in figure 1. A RANS computation using the DLR TAU code was conducted to obtain the mean flow and turbulence data. The mean flow is considered in the following CAA computation using the DLR Piano code. Piano is applied in this work with nonlinear perturbation equations. The sources in this computation are based on the turbulence data obtained from RANS.

The Fast Random Particle Mesh Method (FRPM) was used to insert the sources within the slat region, cp. Fig. 2. The Eddy-Relaxation source model proposed by Ewert et al. [1] was used. Further information about this model will be given in the final paper. This novel source model can be operated in two different modi operandi:

> *Deterministic Mode:* A direct coupling between reference and resolved vorticity is realized, i.e. that vortex dynamics is completely impressed.
>
> *Forced Mode:* The relaxation parameter is defined by a vortex viscosity model according to the actual CAA grid resolution. In this case turbulent scales within the limits of the CAA grid resolution are resolved while smaller structures are modelled by FRPM.

In the forced mode larger structures are directly resolved. The final paper will include a comparison between both modes and highlight the advantages of directly resolving the larger structures.
The CAA-computations were conducted on a structured, curvilinear grid consisting of approximately 18 million points and 109 blocks. The lateral grid extent covers 75% of the slat chord length. This is about 20% of the main chord length. For the lateral sides of the computational domain a periodic boundary condition was chosen. Solid surfaces were treated as adiabatic no-slip walls.

Results
The computations were conducted for the DLR F15 high-lift configuration, depicted in figure 1. In this figure also the c_p-distribution obtained from the RANS is shown.
The sources were inserted within the slat region. The FRPM computational domain is shown in Fig. 2. In this computation the source model was operated in deterministic mode. The con-

tour displays the FRPM forcing and the isolines the realization in Piano. The agreement between contour levels and isolines displays the direct coupling between reference (FRPM) and resolved (Piano) vorticity.
A snapshot of the resulting sound field dis given in figure 3. The contour displays the sound pressure. The sound waves originate from or slightly behind the slat, where the sources are accelerated. Also a microphone is indicated. Figure 4 displays spectra of the sound pressure at this location. The spectra show broad band noise and a single tone at 450 Hz. This tone was also observed in the experiments.

With the chosen computational approach the effects of noise generation in the slat region can be captured properly. The final paper will also include comparisons to experimental data.

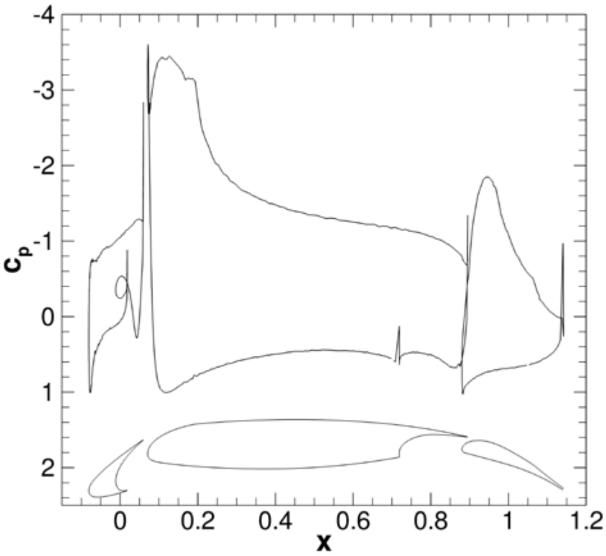

Figure 1: DLR F15 configuration and c_p-distribution

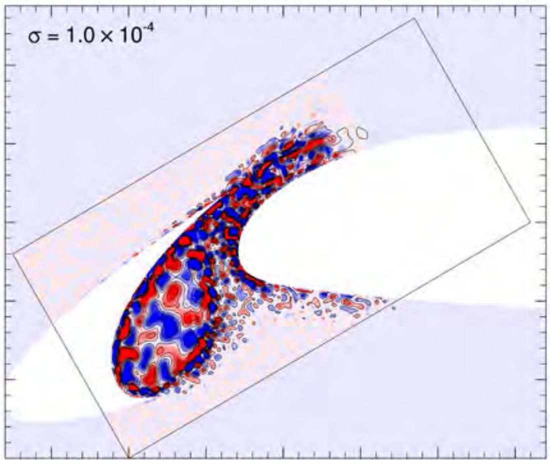

Figure 2: FRPM computational domain within the slat region

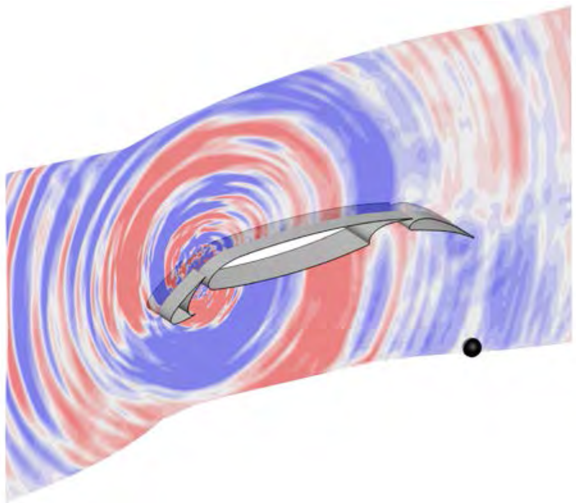

Figure 3: Snapshot of the acoustic pressure emanating from the slat region ; black dot indicates microphone position

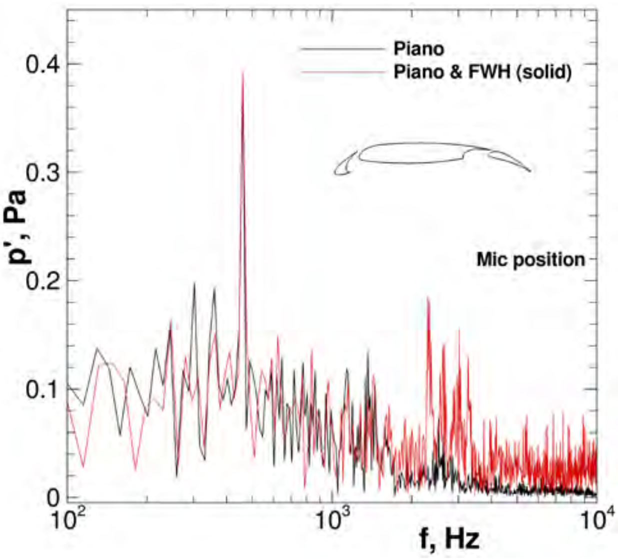

Figure 4: Narrowband spectra of sound pres sure at indicated microphone position

[1] R. Ewert, J. Dierke, A. Neifeld and S.M.A. Moghadam, Linear and Non-Linear Perturbation Equations with Relaxation Source Terms for Forced Eddy Simulation of Aeroacoustic Generation, AIAA Aviation, 20th Aeroacoustics Conference, AIAA 2014-3053.

Mitteilung

Projektgruppe / Fachkreis: Windenergie

Technologien zur Schallreduzierung für Windkraftanlagen

Michaela Herr
Lilienthalplatz 7, D-38108 Braunschweig
michaela.herr@dlr.de
www.dlr.de

Die Perspektiven für den weiteren Ausbau der Windenergie in Deutschland liegen neben der Windenergienutzung auf See bei der optimierten Nutzung der Windenergie an Land, insbesondere dem Repowering. Geräuschminderungstechnologien haben neben der Verringerung der Lärmbelästigung und Erhöhung der Akzeptanz bei Anwohnern auch eine wichtige wirtschaftliche Bedeutung, da in der Genehmigungspraxis Geräuschemissionen als Kriterium für die Festlegung einzuhaltender Abstandsflächen herangezogen werden. Mit Blick auf Repowering-Maßnahmen von Onshore-Parks wird dieses deutlich. Gelänge etwa eine Lärmminderung der einzelnen Windenergieanlage um 1 dB, 2 dB oder 3 dB, wäre theoretisch das Potenzial geschaffen, die Anzahl der Windkraftanlagen (und mithin die Leistung) des Parks um 25 %, 58 % oder 100 % zu erhöhen bei gleichem Gesamtschall des Parks. Weiterhin kann eine Lärmabsenkung notwendig sein, um nach gegenüber der Erstzulassung verschärften Vorschriften eine Betriebsgenehmigung des erneuerten Parks zu erwirken.

Das Vortragsthema ist bewusst auf Rotorblatttechnologie fokussiert mit Blick auf die für Windenergieanlagen zentralen Güteparameter Leistung und Lärm. Nach heutigem Kenntnisstand stellt die Schallentstehung an der Hinterkante im äußeren Bereich der Rotorblätter den wichtigsten Lärmentstehungsmechanismus an modernen Windkraftrotoren dar. Belege hierfür finden sich einerseits in der gemessenen typischen Abstrahlcharakteristik, der Schallquelllokalisation am Rotorblatt mittels Arraytechnologie sowie der messtechnisch nachgewiesenen Effizienz von Maßnahmen der Hinterkantengestaltung auf die Gesamtschallabstrahlung der Anlage. Der Beitrag der äußeren Blattspitze, allgemein eher im höheren Frequenzbereich zu erwarten, spielt bei sauberer akustischer Auslegung heute keine wesentliche Rolle mehr: Gemäß gängiger Praxis wird der äußere Bereich des Rotors zum Zwecke der Lärmminderung entlastet, was allerdings den Ertrag limitiert. Zusätzlich treten am Rotor auch partiell Ablösungen auf, die zu gesteigerter Hinterkantengeräuschemission im niedrigen Frequenzbereich führen. Die Quantifizierung des ebenfalls im tieferen Frequenzbereich auftretenden Vorderkantengeräusches ist gegenwärtig aufgrund seiner Abhängigkeit von der Eingangsturbulenz noch mit großen Unsicherheiten behaftet.
Zielsetzung laufender Forschungsarbeiten am DLR im Rahmen des BMWi-geförderten Projektes BELARWEA – Blattspitzen für effiziente und lärmarme Rotoren von Windenergieanlagen – ist der Entwurf effizienter und gleichzeitig geräuscharmer Windenergierotoren mit abschließender Verifikation an 3D-Blattspitzenmodellen im Niedergeschwindigkeitswindkanal Braunschweig (DNW-NWB). Dies impliziert einerseits den Entwurf aeroakustisch günstiger, leistungsfähiger Rotorblattprofile (äußere 20 % des Rotorblatts) sowie andererseits den Entwurf geeigneter Winglets (äußere 4 % des Rotorblatts). Hierzu werden numerische Simulationsverfahren sowie vorerprobte passive Geräuschminderungstechnologien aus der Luft-

fahrt für die Anwendung am Windkraftrotor weiterentwickelt. Die Projektschwerpunkte liegen auf der gezielten aeroakustischen Methodenerweiterung und -validierung sowie auf der Übertragung passiver Minderungsmaßnahmen für Kantengeräusch.

Neben einer allgemeinen Projektübersicht werden im Vortrag aktuelle Zwischenergebnisse aus numerischen Simulationen im Vergleich zu Windkanalmessungen an 2D-Profilen im Akustischen Windkanal Braunschweig (AWB) des DLR präsentiert, siehe Abbildungen. Das Geräuschminderungspotential von Kantenmodifikationen (gezahnte bzw. anderweitig poröse Hinterkanten) sowie bestehende Einschränkungen in der Umsetzbarkeit werden anhand vorliegender AWB-Messdaten diskutiert.

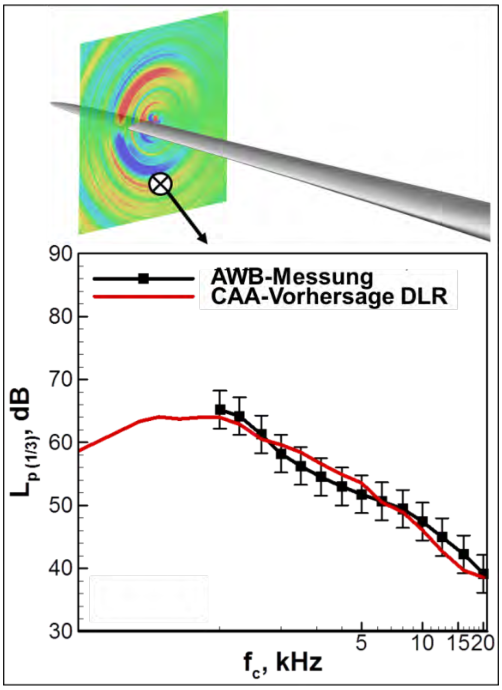

2D-Simulation des Schallfeldes für einen Schnitt durch ein Rotorblatt mittels Computational Aeroacoustics (CAA); unten: Vergleich mit Schalldruckspektrum aus 2D-Profilmessung für eine (im Bild markierte) Mikrofonposition.

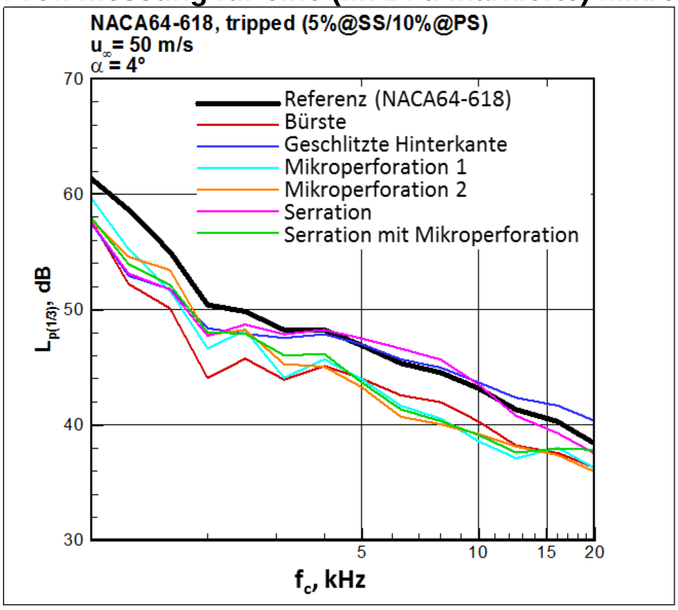

Gemessene Schalldruckspektren für ausgewählte Geräuschminderungsmaßnahmen am NACA64-618-Profil im AWB.

Mitteilung

Projektgruppe / Fachkreis: Aeroakustik

Numerical simulation of the sound generation in cabin air intakes and the sound propagation in an aircraft cabin

Mikhail Konstantinov[1], Claus Wagner[1,2]
[1]German Aerospace Center (DLR), Institute of Aerodynamics and Flow Technology, Bunsenstraße 10, 37073 Göttingen, Germany, mikhail.konstantinov@dlr.de
[2]Ilmenau University of Technology, Institute of Thermodynamics and Fluid Mechanics, Am Helmholtzring 1, 98693 Ilmenau, Germany, claus.wagner@dlr.de

The prediction of the sound pressure level in an complex aircraft cabin is still challenging. There are three major aerodynamic noise sources contribute to the sound level in the cabin. Besides engine and boundary layer noise, there is also the noise generated in the air distribution system of the air conditioning system. In this respect, it is the objective of this study to predict the sound generation realistic cabin air intakes (CAI) and the propagation in segment of aircraft cabin Do728. For this purpose the cabin air flow has been computed with the CFD Code StarCCM+ using Large Eddy Simulation (LES), Delayed Detached Eddy Simulation (DDES) and unsteady Reynolds-averaged Navier-Stokes Simulations (URANS). All these simulations provide the the pressure fluctuations at the cabin walls. Based on the latter, the sound propagation in the cabin is simulated using the Ffowcs Williams-Hawkings model. In the last decade aeroacoustical simulations from heating, ventilation and air conditioning (HVAC) systems of passenger cars has been addressed in many studies, for example in [1].They showed that the main noise sources are located in the air intakes. Thus, in the present study we first focus on the sound generation in aircraft cabin air intakes (CAI). .

Numerical Simulations were carried out applying LES, DDES and URANS. In LES the WALE (Wall-Adapting Local-Eddy Viscosity) Subgrid Scale model has been used. DDES calculations were carried out with DDES-based SST (Menter) $k - \omega$ turbulence model. Finally the URANS simulations were performed with $k - \omega$ (SST) model.. In all simulations the governing equations have been solved with second-order accurate schemes for spatial discretization and second-order time discretization. In addition the Ffowcs Williams-Hawkings [2] model is applied to predict the sound propagation in the cabin.

Calculations have been conducted with two different sets of boundary conditions (bc). In the first set of bc the mass flow is prescribed at all inlets and a flow-split outlet conditions are used at the outlet boundaries (velocity is computed from adjacent cell value with correction using the prescribed split mass flow rate and the pressure values are extrapolated from the adjacent cell using reconstruction gradients). Further, a symmetry plane is enforced at the front and back frame of the segment, and no-slip velocity condition are prescribed at all walls. The second set of bc combines free-stream boundary conditions on all inlets and outlets surfaces..

The presented predictions of the sound generation in cabin air intakes and sound propagation in segment of aircraft cabin are based on the solutions of the unsteady and weakly compressible Navier-Stokes equations. Any of the unsteady simulation provide pressure and density fluctuations. The latter are then used for applying computational aeroacoustic (CAA), which deliver the distribution of acoustical pressure and SPL spectra at characteristic probe points. Additionally, the noise contributions from different wall elements to the total sound are investigated.

The LES and DDES of the flow in the aircraft cabin resulted in similar pressure spectra. However, the computations reveal that the boundary layer structures has a strong impact on sound propagation. Since DDES use RANS in the boundary layer they predict weaker pressure signals, (see Fig.1). It is also observed that the sound level resulting from URANS are substantially lower than those obtained from LES and DDES. Finally, a comparison with sound measurements performed in the Do728 showed that the LES based predictions agreed best. Additionally, the SPL distributions for fixed frequencies in cross-sections of aircraft cabin are calculated with the LES model (Fig. 2). The presented work demonstrates clearly that the sound propagation is closely connected with the flow development in the cabin. The comparison of sound propagation from the CAI in the segment of aircraft cabin and from individual CAI in free space [3] revealed that the cabin walls have to be considered in CAA computations of the sound propagation in aircraft cabins.

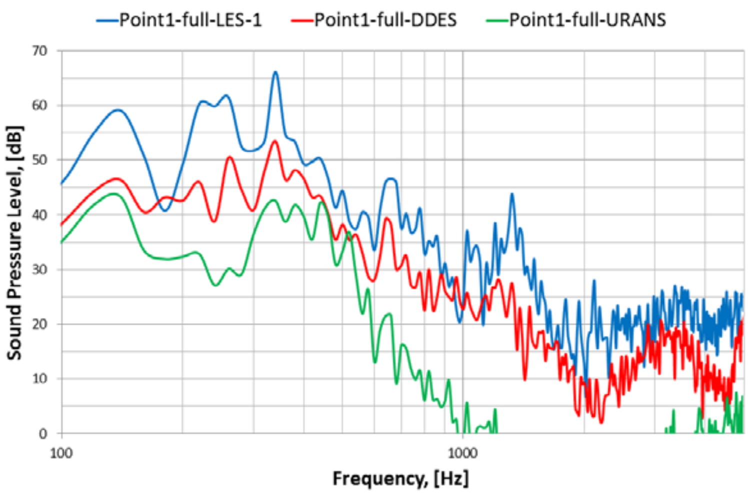

Figure 1: SPL spectra for probe point 1 calculated with different turbulence models.

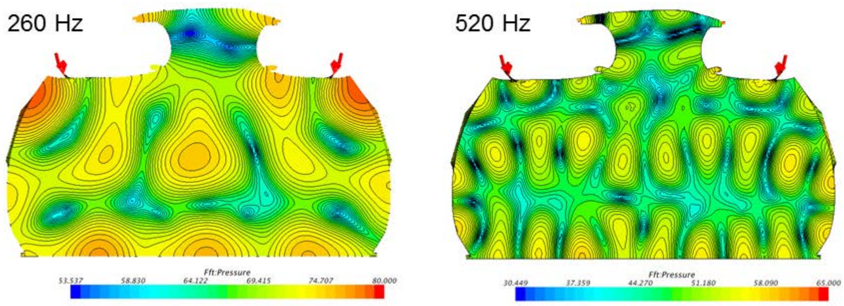

Figure 2: Distribution of acoustical pressure at two characteristic frequencies.

References:

1. S. Caro, J. Manera, R. Toppinga, F. Mendonca, AIIA Paper 09-3352, (2009).
2. J. Ffowcs Williams, D. Hawkings, Phil.Trans. Roy. Soc. (London), **A262**, (1969).
3. M. Konstantinov, C. Wagner, DLRK 2013, DocumentID: 301330, (2013).

Mitteilung

Projektgruppe / Fachkreis: Strömungsakustik/Fluglärm

CAA Prediction of Jet-Wing Interaction Noise Using an Eddy Relaxation Source Model

A.Neifeld[e], C. Appel[d], J.Dierke[c], R. Ewert[b], J.W. Delfs[a]
Institute of Aerodynamics and Flow Technology, Technical Acoustics,
German Aerospace Center (DLR), Lilienthalplatz 7, 38108 Braunschweig, Germany
[e]Andrej.Neifeld@dlr.de, [d]Christina.Appel@dlr.de, [c]Juergen.Dierke@dlr.de,
[b]Roland.Ewert@dlr.de, [a]Jan.Delfs@dlr.de

In this work a hybrid RANS/CAA method as described in Ewert et al. in [1] is applied to study jet-wing interaction noise for a generic problem based on a single stream jet and a NACA 0012 wing section. An Eddy Relaxation (ER) source model proposed in Ewert et al. [2] is applied, which realizes a partly scale resolving simulation of the aeroacoustic sound generation and radiation problem using non-linear disturbance equations (NLDE) in conjunction with an active stochastic forcing method (FRPM) [1]. Herein, the synthetically generated vorticity fluctuations realize turbulent backscattering from unresolved scales [5]. Quantitative correct levels of vorticity fluctuations are derived with FRPM from a precomputed RANS solution. First studies with this approach have been already performed with an isolated single stream jet ($Ma_j = 0.9$) at rest, which delivered encouraging results as reported in Neifeld et al. [3].

The present work is dealing with a generic Jet-NACA0012 configuration as defined in the framework of the European project JERONIMO. The configuration consists of a single stream jet with $Ma_j = 0.6$ and ambient conditions at rest in combination with a rectangular unswept wing with NACA0012 airfoil. The airfoil chord is oriented parallel to the jet axis. The chord length is four nozzle diameters. The wing trailing edge (TE) is located one nozzle diameter vertically above the jet axis ($H/D_j = 1$) and has axial displacement $L/D_j = 4$ from the nozzle exit plane. At the moment, the only available measurement that can be used for comparison is a Jet-Flat Plate interaction experiment conducted by Cavalieri et al. [4]. Nevertheless, equivalent noise radiation from both configurations is expected since the position of the TE with respect to the jet position as well as other flow conditions and geometrical dimensions are identical. Based on this presumption, the flat-plate measurement is subsequently used for the validation of the CAA results.

The comparisons between computed and measurement spectra are illustrated in Fig.1. Two different polar angles are shown, i.e. θ=90° (normal to the jet axis and trailin edge) with a predominant radiation of fine-scale jet noise and at θ=40° with predominant noise radiation from large-scale (coherent) jet structures. A low frequency hump is observable in the spectra for both polar angles, which can be attributed to trailing edge noise. The noise generation mechanism that underlies TE noise can be explained by the scattering of hydrodynamic instabilities of the jet. The good match between measured and computed spectra for different azimuthal and polar angles leads to the conclusion that effects like shielding and relative levels of jet and TE noise are numerically well reproduced and turbulent dynamics from large-scale jet structures are well captured by the simulation.

List of references

[1] R. Ewert, J. Dierke, J. Siebert, A. Neifeld, C. Appel, M. Siefert and O. Kornow, *CAA broadband noise prediction for aeroacoustic design*. 2011, J. Sound Vib. 330, pp. 4139-4160.

[2] R. Ewert, J. Dierke, A. Neifeld, and S.M.A Moghadam, *Linear and Non-Linear Perturbation Equations with Relaxation Source Terms for Forced Eddy Simulation of Aeroacoustic Sound Generation*, AIAA Aviation 2014, 20th AIAA/CEAS Conference, AIAA 2014-3053.

[3] A. Neifeld, D. Boenke, J. Dierke and R. Ewert, *Jet Noise Prediction with Eddy Relaxation Source Model*, AIAA Aviation 2015, 21st Aeroacoustics Conference, AIAA 2015-2370.

[4] A.V.G. Cavalieri, P. Jordan, W.R. Wolf, Y. Gervais, *Scattering of wavepackets by a flat plate in*

the vicinity of a turbulent jet, Journal of Sound and Vibration, Vol. 333, No. 24, December 2014, pp. 6516-6531.

[5] U. Schumann, *Stochastic backscatter of turbulence energy and scalar variance by random subgrid-scale fluxes,* Proc. R. Soc. Lond. A 451 (1995), pp. 293-318.

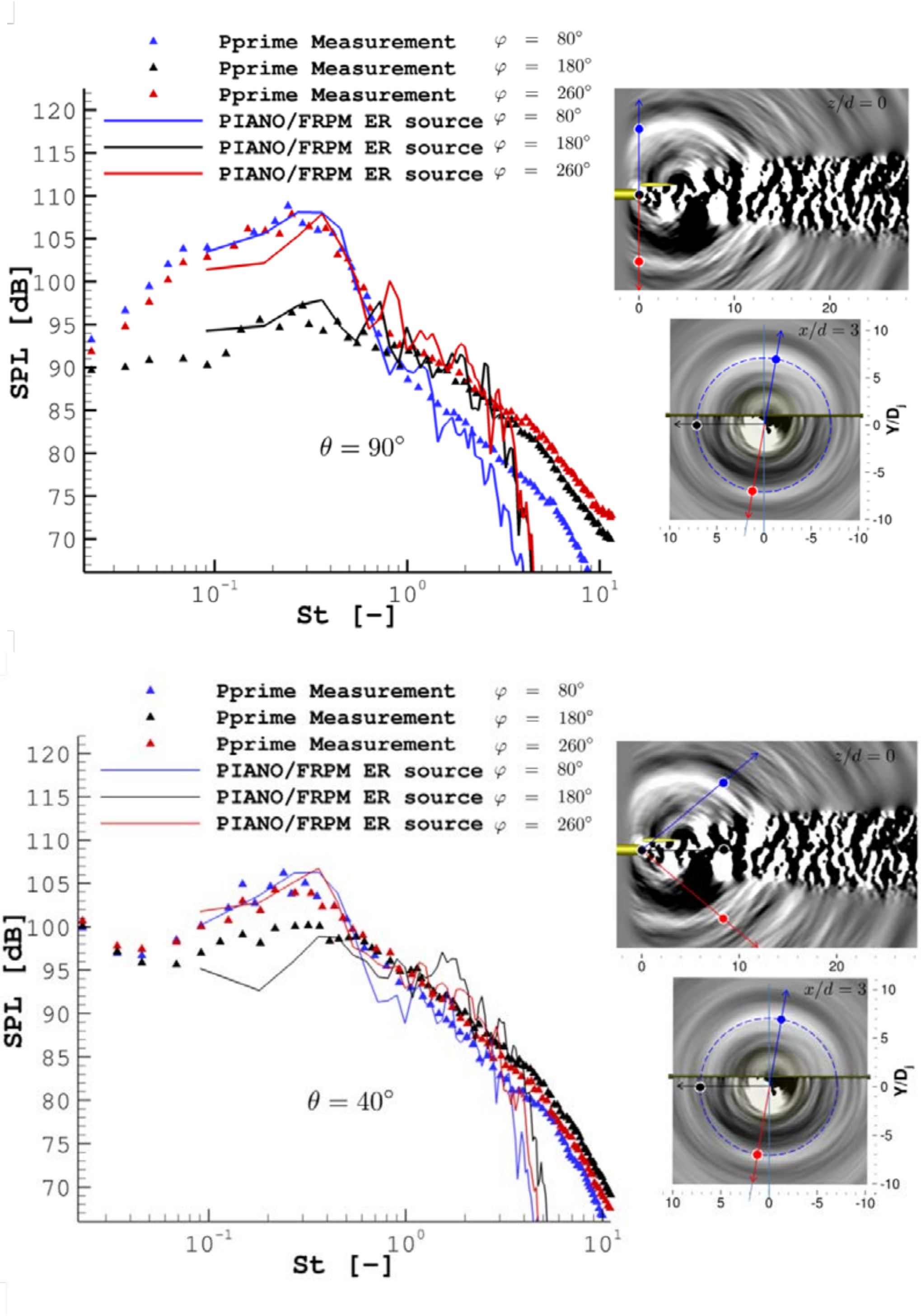

Fig. 1 **Sound pressure level spectra of CAA computation and measurement for a single stream nozzle ($Ma_j = 0.6$, $Ma_\infty = 0.0$) and NACA0012 wing; comparison between three different azimuthal ($\varphi = 80°, 180°, 260°$) and two polar positions ($\theta = 90°, 40°$)**

Mitteilung

Projektgruppe / Fachkreis: Aeroakustik

Prediction of Airfoil Trailing Edge Noise Reduction by Application of Complex Porous Material

Lennart Rossian[1], Benjamin W. Faßmann, Roland Ewert, Jan W. Delfs

Deutsches Zentrum für Luft- und Raumfahrt (DLR), Lilienthalplatz 7, 38108 Braunschweig

With the growing interest in the reduction of air traffic noise over the past years, a significant reduction of the emmited engine noise and jet noise has been achieved. Contrariwise, a similar progress concerning airframe noise still requires continued research. Thereby, a prominent noise source mechanism is the broadband turbulent-boundary-layer trailing-edge noise (TBL-TEN), which is generated by the interaction of turbulent eddies with the pointed trailing edge of an airfoil. In 1974, Hayden and Chanaud showed, that the application of porous material at airfoil trailing edges has a beneficial effect on the emitted noise [1]. Recently, experimental investigations on a high-lift airfoil by Herr et al. demonstrated, that a broadband noise reduction of about 6 dB to 8 dB can be achieved with rigid, porous permeable materials [2]. In the meantime, Faßmann et al. povided a numerical prediciton of the noise reduction by said porous materials. Thereby, a hybrid CFD/CAA (Computaional Fluid Dynamics / Computational Aeroacoustics) approach has been developed, which involves a stochastic source model to generate the TBL-TEN [3]. The present abstract will give an overview of the subsequent work, which involes modeling of complex porous materials. These feature an anisotropic and a non-uniform, gradual distribution of the permeability. Aim of the current work is to come up with a physical understanding of the beneficial effects of a porours trailing edge on an airfoil by conducting simulations with different sets of porous parameters.

As proposed by Faßmann et al., the porous material is modeled by a volume averaged notation of the flow variables [3]. By this, a set of volume averaged Linearized Euler Equations (LEE) is derived. These depend on the parameters of the porous material, which are namely the porosity Φ, the permeability κ and the Forchheimer coefficient c_F. For a solid material, these parameters would be $\Phi = 0$, $\kappa = 0$ and $c_F = 0$, whereas for $\Phi = 1$ and $\kappa \to \infty$ the derived set of volume averaged LEE become the well-known LEE for free flow.

To take into account complex porous materials, the above mentioned parameters κ and c_F are symmetrical 3x3 tensors. Hereby, anisotropic characteristics are modelled, which might be favourable in finding optimized materials that meet both aerodynamic and aeroacoustic constraints. Furthermore, the ability to simulate effects of non-uniform porous materials is pursued to avoid discontinuities in the transition from the solid airfoil to the porous trailing edge. It is asumed that such edge may act as a source region for turbulent-boundary-layer induced noise.

The two-step hybrid CFD/CAA procedure to simulate the generated TBL-TEN is based on the DLR PIANO-CAA-Code [4]. First, a time-averaged turbulent flow needs to be computed by a CFD solver. Then, in the CAA step, time dependent linear propagation equations are solved to obtain the acoustic field. Thereby, the sound sources need to be posed explicitly. In the case of trailing edge noise, a vorticity based forcing sound source is applied to the momentum equation. This source is computed by the Fast Random Particle-Mesh Method (FRPM), a synthetic turbulence method based on the turbulent statistics of the time averaged CFD solution [5].

[1] Corresponding author, Lennart.Rossian@dlr.de

Within the simulation framework, the interface between either two different porous materials or a free flow and a porous material is of special interest. To model the physical link between the two different regimes, Rossian et al. proposed a set of acoustic jump conditions [6], which have later been modified. For now, the primitive variables ρ, v_i, p and their normal derivatives with respect to the interface are taken to be conserved directly. On the numerical side, a new compact boundary scheme has been implemented into PIANO to provide the ability to implement the acoustic jump conditions.

For now, a series of numerical test cases have demonstrated the capability to simulate acoustics inside and around complex, meaning anisotropic and non-uniform, porous materials. Thereby, the means to simulate the possible trailing-edge noise reduction of an airfoil with an arbitrary porous trailing edge are at hand. First results presented in [6] already show a good overall quality of such simulation.

For the final manuscript, further improvements in the FRPM turbulence reconstruction will be applied to enhance the quality of the numerically determined sound spectra. Furthermore, the effects of anisotropic as well as non-uniform pourous materials will be studied. The aim is to develop a deeper physical understanding of the beneficial influence of a permeable airfoil trailing edge.

[1] R. E. Hayden and R. C. Chanaud, ”Foil Structures with Reduced Sound”, 1974.

[2] M. Herr, K.-S. Rossignol, J. W. Delfs, M. M¨oßner and N. Lippitz, ”Specification of Porous Materials for Low-Noise Trailing-Edge Applications”, AIAA Paper 2014-3041, 2014.

[3] B. W. Faßmann, C. Rautmann, R. Ewert and J. W. Delfs, ”Prediction of Porous Trailing Edge Noise Reduction via Acoustic Perturbation Equations and Volume Averaging”, AIAA Paper 2015-2525, 2015.

[4] J. W. Delfs, M. Bauer, R. Ewert, H. A. Grogger, M. Lummer and T. G. W. Lauke, ”Numerical Simulation of Aerodynamic Noise with DLR’s aeroacoustic code PIANO”, 2008.

[5] R. Ewert, J. Dierke, J. Siebert, A. Neifeld, C. Appel, M. Siefert and O. Kornow, ”CAA Broadband noise prediction for aeroacoustic design”, Journal of Sound and Vibration, Vol 330, No. 17, 2011, pp. 4139-4160.

[6] L. Rossian, B. W. Faßmann, R. Ewert and J. W. Delfs, ”Prediction of Porous Trailing Edge Noise Reduction Using Acoustic Jump-Conditions at Porous Interfaces”, AIAA Paper 2016-2920, 2016.

Mitteilung

Projektgruppe/Fachkreis: Aerodynamik und Aeroakustik

Numerical simulation of acoustic radiation of a 3-D jet-wing-flap configuration

Daniel Schütz, daniel.schuetz@uni-siegen.de
Holger Foysi, holger.foysi@uni-siegen.de

Chair of Fluid Mechanics, University of Siegen, Paul-Bonatz-Str. 9-11, 57068 Siegen, Germany

The prediction of flow noise is still not fully understood for a variety of real world applications. An important area of research is the noise emitted during the interaction of flows with structures in aerodynamics. A currently relevant example here is the sound emission from the jet-wing-flap interaction, as considered in this work. As a result of efficiency-optimizing measures the engine diameter are getting bigger, which results in engines being installed closer to the wing. Thus, there is an interaction between the flap and engine jet in the case of an extended flap, which can lead to an increased noise emission. Since this is the case primarily at takeoffs and landings, in the acoustically most relevant flight phase, this situation gained increased attention from aircraft manufacturers.
In this project, the 3-D jet-wing-flap interaction of a real geometry will be investigated numerically, by using large-eddy simulation in the acoustic near field and acoustic analogies in the far field. One objective of this work is to develop a hybrid solution method for the accurate numerical prediction of the interaction between jet and flap. Moreover, the influence of different Mach numbers, Reynolds numbers, flap angles and wing positions on the emitted sound field should be investigated. Furthermore, a deeper insight into the sound-generating mechanisms is sought, with comparisons to experiments and simulations performed by EADS. Since the simulation of the entire configuration is very complicated, fundamental studies were performed first, using simplified test cases originating from the planned configuration, see figure 1 for example. A verification of the far-field solver based on analytical solutions of generic test cases and the flow around a 2-D NACA0012 profile was performed. Moreover, a comparison with the DLR code PIANO [1] is sought.

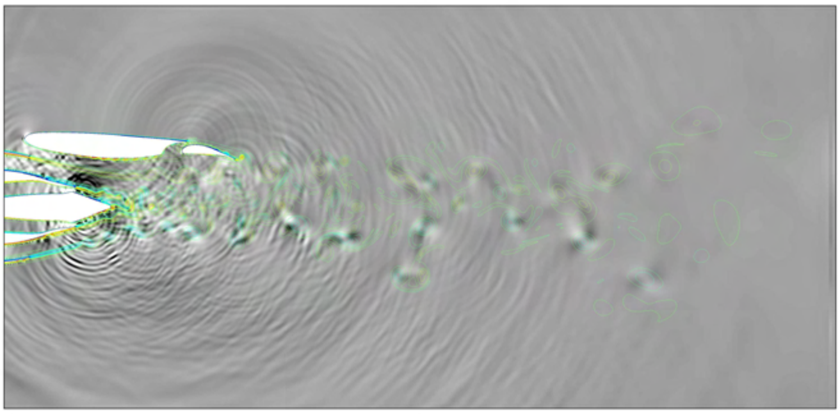

Fig. 1: Preliminary work: 2-D jet-flap-interaction. Dilatation field and contours of vorticity are shown.

As a basis for the LES simulations, the open source package Overture [2] is used. The program offers the possibility of fluid mechanical calculations using finite differences on overlapping grids, see Figure 2. Thus, more complex geometries can be handled efficiently using structured grids. The compressible solver was already modified for acoustic purposes and extended to

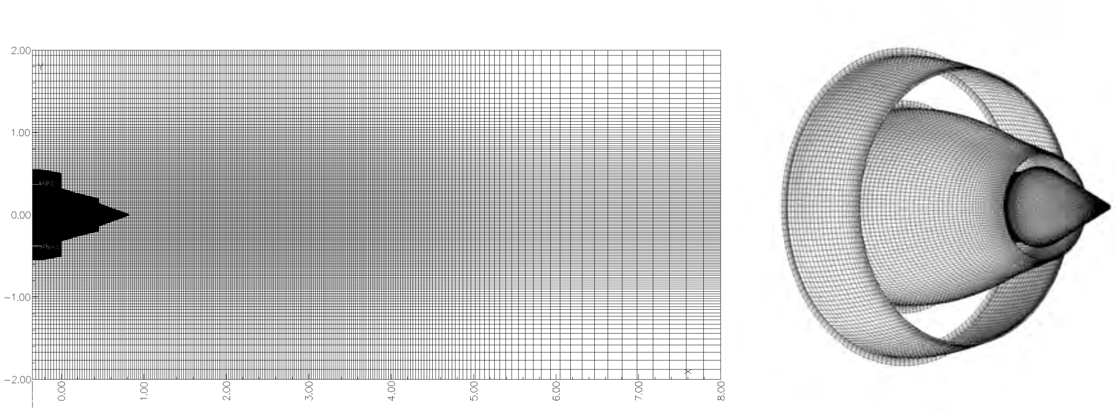

Fig. 2: Preliminary work: 3-D Nozzle. Whole domain (left), 3-D nozzle surface grid (right).

handle wave propagation over far-field boundaries [3]. Radiation and outflow boundary conditions, proposed by Tam and Dong [4], were implemented. Time integration is performed using a 3rd-order Runge-Kutta scheme and 4th-order finite difference schemes for the spartial derivatives. The explicit filter variant [5, 6] of the approximate deconvolution model [7] is used for subgrid modelling, alternatively implicit LES is possible.
During the conference first results of the three-dimensional turbulent flow interacting with the wing are presented and discussed, for different flap angles. The Reynolds and Mach numbers for these cases are fixed at $Re_{D_s} = \rho_s U_s D_s/\mu = 1.32 \times 10^6$ and $M_s = U_s/c_\infty = 0.37$. Furthermore, the sound pressure level for these configurations is plotted and compared.

References

[1] DLR - German Aerospace Center in the Helmholtz-Association (Hrsg.): *Finite Difference Operators and Boundary Conditions for Overture, User Guide, Version 1.0.* Institute of Aerodynamics and Flow Technology, Department of Technical Acoustics, Braunschweig: DLR - German Aerospace Center in the Helmholtz-Association, 2008

[2] Henshaw, W. D.: *OverBlown: A Fluid Flow Solver For Overlapping Grids, Reference Guide, Version 1.0.* Lawrence Livermore National Laboratory, Livermore, California: Centre for Applied Scientific Computating, 2003

[3] Schütz, D.: *Implementierung und Anwendung von asymptotischen Fernfeldrandbedingungen in den kompressiblen Strömungslöser des Open-Source Pakets Overture*, Universität Siegen, Lehrstuhl für Stömungsmechanik, MSc Thesis, 2015

[4] Tam, C. K. W. & Dong, T. Z.: Radiation and outflow boundary conditions for direct computation of acoustic and flow disturbances in a nonuniform mean flow. *J. Comput. Acoust.* **4** (1996), 175–201

[5] Mathew, J., Lechner, R., Foysi, H., Sesterhenn, J. & Friedrich, R.: An explicit filtering method for large eddy simulation of compressible flows. *Phys. Fluids* **15** (2003), 2279–2289

[6] Bogey, C. & Bailly, C.: Large eddy simulations of round free jets using explicit filtering with/without dynamic Smagorinsky model. *Int. J. Heat Fluid Flow* **27** (2006), 603–610

[7] Stolz, S., Adams, N. A. & Kleiser, L.: An approximate deconvolution model for large-eddy simulation with application to incompressible wall-bounded flows. *Phys. Fluids* **13** (2001), 997–1015

Mitteilung

Projektgruppe / Fachkreis: Aerodynamik und Aeroakustik

Numerical Simulation of a Resonant Cavity: Acoustical Response under Grazing Turbulent Flow

L. Stein, J. Reiss and J. Sesterhenn
Institute of Fluid Dynamics and Technical Acoustics, Technical University of Berlin
Müller-Breslau-Str. 12, 10623 Berlin
stein@cfd.tu-berlin.de

Aim

Helmholtz resonators play a key role as silencers in many technical applications. The aim of this work is to study the mechanism that governs the emission and reduction of noise. For the first time we closely monitor the interaction between the acoustic field of a Helmholtz resonator's detailed geometry and a fully turbulent shearing flow by a Direct Numerical Simulation. We compare our results to an experimental study by [Golliard, 2002]. Further quantities beyond the scope of experimental measurements are extracted from our Direct Numerical Simulation: This helps to better understand the damping mechanism of acoustic resonators in general.

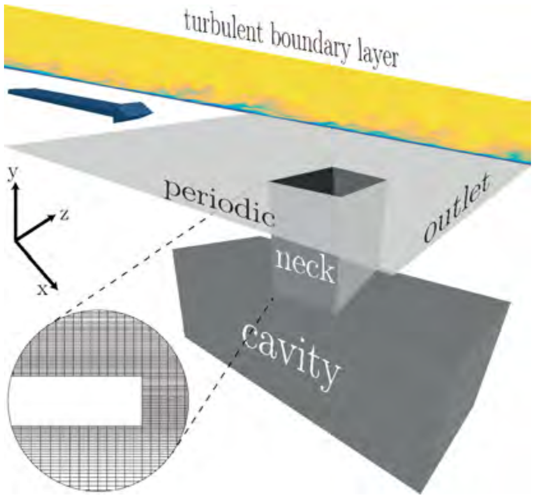

Figure 1: Three dimensional geometry of the investigated Helmholtz resonator with grid refinement. Details are found in the PhD thesis by [Golliard, 2002] (S. cavity C1, δ_{99}=11 mm with 14 mm stream wise opening).

Method

This work uses a skew-symmetric formulation of the compressible Navier-Stokes equations [Reiss, 2014]. The resulting finite-difference scheme is fully conservative and of arbitrary order in space and time as needed for acoustics. The parallelization (MPI) is achieved by a hybrid approach using a multi-block-code with a ghost layer synchronization as well as block internal decomposition. This allows load balancing. Additionally, mesh refinement reduces the cost of the computation. Thereby the resolution of the Direct Numerical Simulation resolves the acoustic Stokes boundary layer as well as the viscous lengthscale δ_v of the viscous sub-boundary layer. A recycling-rescaling strategy is implemented [Pirozzoli und Bernardini, 2011] to stimulate physical inflow turbulence. The case under investigation (S. Fig. 1) has a Mach number of M = 0.1 (38.5 m/s), a Reynolds number of Re_θ = 2900 with respect to the momentum thickness θ, a constant Prandtl number of Pr = 0.7 and standard temperature and pressure (273 K, 100 kPa).

Results

The performed simulation of a Helmholtz resonator under grazing flow (S. Fig. 2) is successfully compared to the experimental result by [Golliard, 2002, Kooijman et al., 2008]. New aspects of the coupling between ordered acoustic phenomena and turbulent flow are revealed. The resonator's eigenfrequencies are identified by a frequency analysis. The turbulence statistics and mean flow features are investigated and contrasted for example with the analytic solution of Van Driest (S. Fig. 2). In particular, we show the differences between the modifications of the characteristic fluid structures (and their respective frequencies) due to the presence of the Helmholtz resonator and the case of the turbulent flat plate flow without any resonating volume.

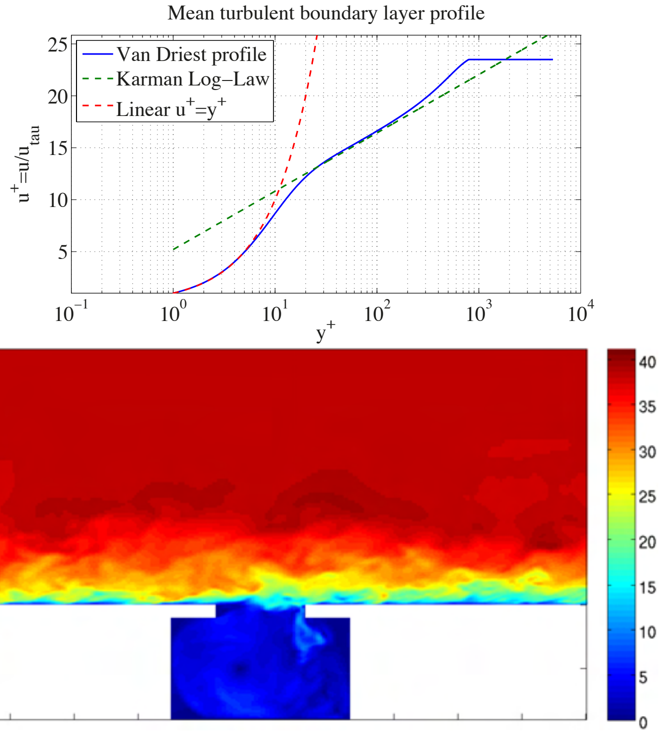

Figure 2: Top: Mean flow profile of the here considered turbulent boundary layer (in terms of wall units). Bottom: Velocity norm m/s in the xy-plane of the turbulent flow over the investigated cavity (u_0 = 38.5 m/s).

Acknowledgement

The provision of computational resources (ACID11700) by the Federal High Performance Computing Center Stuttgart (HLRS) are gratefully acknowledged. This work is possible through the Elsa-Neumann-Stipendium des Landes Berlin (NaFöG).

References

[Golliard, 2002] Golliard, J. (2002). Noise of Helmholtz-resonator like cavities excited by a low Mach-number turbulent flow. *PhD-thesis*, Université de Poitiers.

[Howe, 1981] Howe, M. (1981). The influence of mean shear on unsteady aperture flow, with application to acoustical diffraction and self-sustained-cavity oscillations. *Journal of Fluid Mechanics*, 109:125-146.

[Kooijman et al., 2008] Kooijman, G., Hirschberg, a., and Golliard, J. (2008). Acoustical response of orifices under grazing flow: Effect of boundary layer profile and edge geometry. *Journal of Sound and Vibration*, 315(4-5):849–874.

[Pirozzoli und Bernardini, 2011] Pirozzoli, S. and Bernardini, M. (2011). Turbulence in supersonic boundary layers at moderate Reynolds number. *Journal of Fluid Mechanics*, 688:120–168.

[Reiss, 2014] Reiss, J. and Sesterhenn, J. (2014). A conservative, skew-symmetric finite difference scheme for the compressible Navier–Stokes equations. *Computers & Fluids*, 101: 208–219.

Mitteilung

Projektgruppe / Fachkreis: Fahrzeugaerodynamik

Wall Shear Stress Measurements on a Stadler-KISS

Johannes Haff*, Erich Schülein*, Arne Henning*, Steve Cochard**, Sigfried Loose*

*German Aerospace Center (DLR e.V.), Institute of Aerodynamics and Flow Technology, Bunsenstr. 10, 37073 Göttingen, Johannes.Haff@dlr.de

**Stadler Rail, CH-9423 Altenrhein, Switzerland

Introduction

The prediction of the total energy consumption of new or further developed rail vehicles is a fundamental task in the railway industry. The aerodynamic drag is the dominant part of the driving resistance for most rail vehicles [1]. An educated estimation of the energy consumption therefore requires information of the aerodynamic drag. Current state-of-the-art computational studies fail to meet the high accuracy level required to reliably predict the total energy consumption of a rail vehicle. Wind tunnel experiments do not simulate realistic near wall flow conditions on scale models and cannot predict the friction drag. Besides, no test facility exists to measure the aerodynamic drag of full-scale trains. Nowadays, coasting test is the primarily tool used by the industry to predict the aerodynamic drag of rail vehicles.

One disadvantage of coasting tests is the strong impact of the environmental conditions on the measurement results. Therefore, a large number of test runs - associated with high costs - is necessary to produce reliable experimental results. A key interest from DLR industry partners is the reduction of development costs by increasing the performance of computational studies to predict the aerodynamic drag of a rail vehicle.

The friction drag combined with the pressure drag from the leading nose and the trailing nose account for most of the aerodynamic drag. The friction drag is the result of the developing boundary layer on the train surface and is defined by the wall shear stress.

This article presents an experimental study performed on an electric double-deck train KISS to measure the wall shear stress under real operating conditions. The results are compared to theoretical values and results published in the literature. The measured wall shear stresses will help to improve the predictability of computational studies by modifying the surface roughness of the vehicle surface to achieve the same values as measured in the experiment. The oil film interferometry used to measure the wall shear stress is a non-intrusive method [2].

Experimental setup

To measure the wall shear stress, the oil film interferometry technique [2] was used. To avoid any influence of measuring probes, the experimental setup was installed inside the train. The measurements were performed on one side of a four car double-deck train KISS (Figure 1, left), provided by the Swiss Federal Railway (SBB), at driving velocities of 120 and 160 km/h. The second door of the first car located 19.09 m from the vehicle front (Figure 1, middle) served as measuring position. Based on two driving velocities and two driving directions, measurements at four different length-scale Reynolds numbers were performed. The measurements took place on the SBB railway line between Martigny and Sion in Switzerland. The 30 km long track is flat and straight.

The oil film interferometry method is based on an interference pattern generated by the overlap of light reflection on the oil film and the ground. Before the test, an oil film was applied on an exterior of a window. Depending on the measurement position and the driving speed of the train, silicone oils of two different viscosities (50 and 100 cSt) were used during the investigations. A LED panel type Ecolight-PLs-40n with 40W and a size of 600 × 600 mm from Xtend EcoLight GmbH served as light source to generate the interference pattern (Figure 1, right). The panel has a maximum light flux of 3800 lumen. A thermoelectrically cooled 1.92 megapixel CCD camera from PCO (pco.1600) with a resolution of 1600 × 1200 pixels and a grey-scale resolution of 14 bit was used to record the interference pattern. The camera was equipped with a Zeiss Planar T* 1.4/100 camera lens and a interference filter (589 nm) in front of the camera lens to increase the image contrast. It was controlled using the software tool CamWare installed on a notebook connected via a GigE interface and was installed on a mounting device above the light source (Figure 1, right). The electric energy to power camera and light source was provided by the train infrastructure.

Figure 1. Electric double-deck train KISS (left), measuring position in the first car (middle) and experimental setup consisting of a CCD camera and a LED panel (right).

The challenge by measuring the interference pattern from inside the train is the additional reflection from the double glass windows which reduce the contrast of the interference pattern and therefore decrease the quality of the raw data (low dynamics).

Measurement results

In Figure 2, left, the recorded interference after 190 s measuring time at a driving velocity of 160 km/h and a length-scale Reynolds number of $5.56 \cdot 10^7$ is shown. The visualisation in Figure 2, right, presents the measured skin friction coefficients at two different driving velocities and two different train direction. In total, results at four different length-scale Reynolds numbers are available.

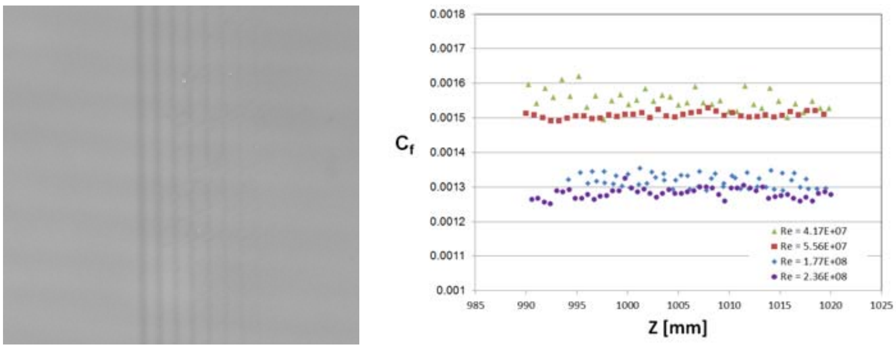

Figure 2. Recorded interference pattern at $Re_x = 5.56 \cdot 10^7$ with flow direction from the left (left) and measured skin friction coefficient at the four investigated Reynolds numbers (right).

The article will compare the experimental results with the theory and results from the literature. Further, a comparison is made with performed computational studies at different surface roughnesses to improve the transferability to the reality.

Literature

[1] Brockie N., Baker C.: *The Aerodynamic Drag of High Speed Trains*, Journal of Wind Engineering and Industrial Aerodynamics, No. 34, pp. 273-290, 1990.

[2] Schülein E.: *Optical Skin Friction Measurement in Short-duration Facilities (Invited)*, AIAA-2004-2115, 2004.

Mitteilung

Projektgruppe / Fachkreis: Fahrzeugaerodynamik

Aerodynamische Untersuchungen zum dynamischen Flügeln an zwei NGT-Zügen

Henning Wilhelmi*, Thomas Thieme*, Arne Henning*, Claus Wagner*

*German Aerospace Center (DLR e.V.), Institute of Aerodynamics and Flow Technology, Bunsenstr. 10, 37073 Göttingen, henning.wilhelmi@dlr.de

Einleitung

Um dem zukünftig zu erwartenden gesteigerten Verkehrsaufkommen im Schienenverkehr auf der vorhandenen Schieneninfrastruktur gerecht zu werden, müssen Lösungen zur Steigerung der Streckenkapazitäten gefunden werden. Eine Möglichkeit dies zu erreichen besteht in der abschnittweisen Kopplung mehrerer Züge zu einem Verbund. Der Vorgang des Koppeln wird als Flügeln bezeichnet. Bisher wird das Flügeln in den meisten Fällen stationär an Bahnhöfen durchgeführt; auf dem deutschen Schienennetz wird dies z.B. abschnittsweise bei ICE-Zügen umgesetzt. Der Nachteil dieser Art des stationären Flügelns besteht in der geringen Flexibilität und der limitierten Anzahl von koppelbaren Zügen aufgrund der eingeschränkten Bahnsteiglänge. Um diese Nachteile zu überwinden, wird im Rahmen des DLR-Projekts „Next Generation Train“ (NGT) die Methode des sogenannten dynamische Flügelns untersucht. Dabei handelt es sich um eine berührungslose Verbindung von mehreren Zügen zu einem Zugvberbund. Im Gegensatz zur mechanischen Kopplung im Stand, wird beim dynamischen Flügeln lediglich eine drahtlosen Datenverbindung zwischen den Zügen zur fernwirkenden Kopplung benötigt. Diese Methode wird daher auch als „virtuelles Flügeln“ bezeichnet.
Die Methode bietet den Vorteil, dass der Rangierstoß am Bahnhof vermieden wird und eine Kopplung geschwindigkeitsunabhängig und nicht zwingend an einem Bahnhof stattfinden kann. Durch flexibles Bilden von Verbünden, auch von unterschiedlichen Zugtypen, fahren die Züge in konstantem Relativanstand hintereinander her. Das dynamische Flügeln bietet damit eine Lösung, um die Streckenauslastung ohne größere Strukturmaßnahmen zu erhöhen und diese je nach Tagesbedarf an die Anforderungen durch vergrößern oder verkleiner der Verbände anzupassen.
Aus aerodynamischer Sicht sind bei dieser Aufgabenstellung verschiedenste Aspekte von Interesse. So kann das dynamische Flügeln, vergleichbar zum sogenannten Platooning im Automobilbereich [1, 2], zu einer Reduzierung des Strömungswiderstandes und somit des Verbrauches führen. Instationäre Effekte durch aerodynamische Wechselwirkungen zwischen den Zügen sind darüber hinaus sowohl komforttechnisch (z.B. Akustik oder Schwanken), als auch regelungstechnisch von Bedeutung.

Versuchsaufbau

Die Versuche zum dynamischen Flügeln werden im Wasserschleppkanal Göttingen (WSG) mit eingesetzten Plexiglasflächen zur Bodensimulation (siehe Abb. 1) durchgeführt. Dies bietet gegenüber einem klassischen Windkanal mit festestehendem Modell den Vorteil, dass mit deutlich geringerem Aufwand d.h. ohne den Einsatz eines laufenden Bandes und Grenzschichtabsaugung die Bodeninteraktion simuliert werden kann. Auch die Aufdickung der Kanalgrenzschicht über die Lauflänge der Zugmodelle kann damit vermieden werden. Der zur Bodensimulation benötigte eingehängte Boden besteht aus je 4m langen linken und rechten Hälften, die in dem Kanal mittels Aluminiumprofilen befestigt werden. Zwischen den Hälften besteht ein kleiner Spalt, um die Modellbefestigung durchführen zu können.
Als Versuchsträger wurden zweitilige NGT-Modelle im Maßstab 1:50 inklusive der Drehgestelle mittels 3D-Druck gefertigt. Die Gesamtlänge beträgt jeweils x_{ref}=820mm. Die Höhe z_{ref} ist 90mm und die Breite y=60mm.
Die Bewegung durch das Wasser erfolgt durch einen Wagen, der auf dem Wasserschleppkanal durch ein Seil mit bis zu 4m/s vorbewegt wird. Unterhalb dieses Schlittens sind für die Kraftmessungen an jedem Zug eine piezo-elektrische 6-Komponenten Kraftwaagen angebracht. Die Verbindung zwischen Zug und Waage erfolgt mit Hilfe von vier, 30mm langen, NACA-0021 Profilen (Schwerter), welche an der Unterseite des Zuges angeschraubt sind. Aufgrund der Form und der Befestigung unter dem Zug soll der aerodynamische Einfluss minimiert werden. Zwischen Waage und Schwerter wiederum befindet sich ein X-95-Profil, welches einen Versatz des Züge auf der x-Achse ermöglicht, um den Abstand variieren zu können.
Um den Einfluss der Schwerter abschätzen zu können., wurden auch Fahrten ohne Zug durchgeführt. Die Messungen werden bei einer Reynoldszahl von Re=360000 (basierend auf der Modellbreite)

durchgeführt. Die Ermittlung der instationären Kräfte erfolgt lediglich über dem Bereich mit eingesetzem Boden, ausgelöst durch Lichtschranken.

Abbildung 1: (l.)Wasserschleppkanal mit Schlitten und Zügen (vom Boden verdeckt) über Bodeneinsatz. (r.) ICE-Zugmodell im Verbund unter dem Boden.

Ergebnisse:

Es wurde der Verbund von zwei NGT Zügen bei 5 verschiedenen Abständen gemessen. Die benötigte Anzahl von 35 Fahrten für stabile Mittelwerte wurde in Voruntersuchungen ermittelt. Die Abstände betrugen 1,2%; 12,2%; 24,4%; 36,6%; 48,8% und 60,1% der Einzelzuglänge.

Abbildung 2 zeigt die Entwicklung des Beiwerte der einzelnen Zugmodelle, wobei bei zwei Abständen die niedrigsten c_w-Werte von 0.57 für den gesamten Verbund ermittelt wurden. Betrachtet man die Einzelfahrzeuge, so ist beim kleinsten Abstand von 1,2% der geringere Widerstand des vorderen Zuges die Ursache für den niedrigen Gesamtwiderstand. Bei 36,6% ist hingegen der Widerstand am zweiten Fahrzeug Auslöser für die Widerstandsreduktion. Ein ähnliches Verhalten zeigt sich bei Zabat et al.[1], welcher zeigt, dass in einem Verbund aus zwei PKW der Widerstand für den vorderen Wagen bei kleineren Abständen stark abnimmt. Auch der zweite Wagen zeigt bei größeren Abständen nochmals einen vergleichbaren Einbruch im Widerstandsbeiwert. Es wird von den Autoren keine Ursache angegeben, aber eine ähnliches Strömungsphänomen scheint plausibel. Derzeit finden PIV-Messungen im Wasserscheppkanal am DLR Göttingen statt. Die Analyse der instationären und gemittelten Geschwindigkeitsfelder soll Aufschluss über die Wechselwirkung der Nachlaufstruktur mit dem Zugkopf des hinterhereilenden Zugteiles und eine physikalische Erklärung für die Widerstandsreduktion geben

Der von Zabat et al.[1] beobachtete geringere c_W-Wert des vorderen Fahrzeuges bei kleinen Abständen kann im Zugverbund nicht bestätigt werden.

Im Vergleich zum vorderen Zugteil zeigt sich während der gekoppelten Fahrt allderings durchweg eine Widerstandsreduktion für den hinteren Zug.

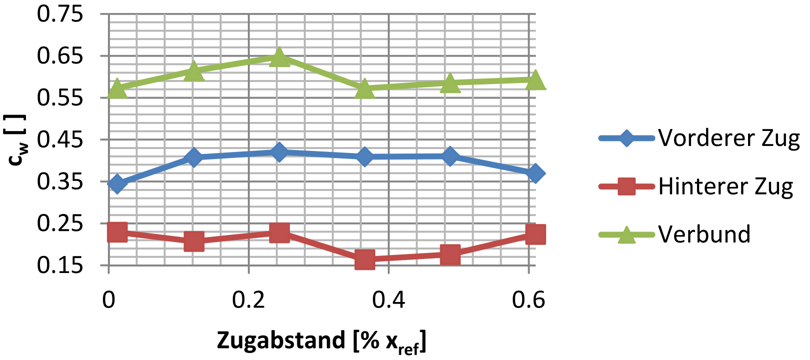

Abbildung 2: Entwicklung des Widerstandsbeiwertes beim dynamischen Flügeln von zwei Zügen bei verschiedenen Abständen

Literature

[1] Zabat, M., Stabile, N., Farascaroli, S., & Browand, F. (1995). *The Aerodynamic Performance Of Platoons: A Final Report*. *California Partners for Advanced Transit and Highways (PATH)*. Los Angeles, CA.

[2] Jootel, P. S. (2013). *SARTRE - Project final report*. Retrieved from www.sartre-project.eu

Mitteilung

Projektgruppe / Fachkreis: Windenergie

Hybrid RANS/LES simulations of the three-dimensional flow at root region of a 10 MW wind turbine rotor

Galih Bangga, Pascal Weihing, Thorsten Lutz and Ewald Krämer
Institut für Aerodynamik und Gasdynamik, Universität Stuttgart,
Pfaffenwaldring 21, 70569 Stuttgart,
bangga@iag.uni-stuttgart.de

Introduction

Three-dimensional (3D) flow occurring in the near hub region of a rotating wind turbine blade is a complex flow phenomenon involving massive flow separation and a strong 3D effect due to rotation. Centrifugal and Coriolis forces were identified to have a strong influence on the flow under such situation, and this leads to an increase of sectional lift coefficient (Cl) compared to two-dimensional (2D) airfoil data [1].

Accurate predictions of this effect is important for the design of more reliable wind turbine blades and RANS simulations have been shown to innacurately predict these phenomena at high operating wind speeds [2]. Unfortunately, even the use of the most modern turbulence models could not essentially improve the situation [3]. Large Eddy Simulations (LES) offer a better prediction for massively separated flow field, but the computational cost is way more expensive than RANS. Detached Eddy Simulations (DES) use the capability of LES in resolving large eddies while the smaller flow structures near the wall are modelled using RANS. By doing so, the 3D flow characteristics are better captured but the computational cost can be kept small. It has been shown by Johansen *et al.* [4] that DES calculations were able to resolve more 3D flow structures near the blade root compared to RANS which allowed a better examination on the 3D effects. Using the same turbine, Li *et al.* [5] confirmed this observation.

On this basis, the present study aims to obtain a better insight into the 3D effects by employing the capability of DES in resolving the eddies. The predicted sectional loads are examined and compared with RANS prediction. At last, the centrifugal and Coriolis forces influence on the velocity profiles within the blade boundary layer is presented.

Test Cases and Computational Setup

The examinations were performed on the AVATAR (Advanced Aerodynamic Tools for Large Rotors) blade [6]. The blade is 102.9 *m* in radius (*R*) and designed to operate at rated wind speed of 10.5 *m/s*. Two different wind speeds (U) were investigated, rated and stalled wind speeds, listed in Table 1. By doing so, two variations of the geometric angle of attack (α_g) were obtained. The rotational speed and pitch angle in the stalled wind speed case (Case 2) was purposely set not according to the original blade design [6] in order to artificially generate massive separation on the blade.

The unsteady simulations were carried out using the multi-block structured CFD code FLOWer [7], employing Improved Delayed DES (IDDES) simulations [8] based on the (URANS) SST k-ω model. The simulations were carried out with fully turbulent boundary layer. The implicit residual smoothing with variable coefficients and third level multigrid were used. The time integration was carried out by an explicit hybrid multistage Runge-Kutta scheme with dual time-stepping scenario. The timestep value was 0.052 s, an equivalent to three degrees blade revolution for every physical time step. The blade mesh was C-H type and grid independency studies have been carried out in [9]. The periodic boundary condition was used, assuming periodicity of the flow from one blade to the other blades, so that only one blade was modeled. The Chimera interpolation method was employed in the overlapping grid area.

Table 1. Simulated cases.

Label	U [m/s]	n [rpm]	Pitch [°]
Case 1 (Rated)	10.5	9.02	0
Case 2 (Post stall)	20	9.02	0

Results

Figure 1 shows CFD predictions of the sectional loads for two different cases. The forces are non-dimensionalized by the local kinematic velocity, $V = (U^2 + (\Omega r)^2)^{0.5}$ with Ω is the rotational speed in

rad/s. It can be seen that IDDES predicts much larger aerodynamic forces than RANS especially for the blade inner region. The largest differences between the two CFD methods are observed at 0.15 < r/R < 0.4 for Case 1. For higher wind speed (larger α_g), this region is shifted further outboard and the affected area is much larger especially for F_t (see the arrow).
These differences are driven by the flow behavior near the blade as illustrated from the kinematic streamwise velocity (u_{kin}) plot in Fig. 2. Separation is delayed and its area is much reduced in IDDES prediction compared to URANS. The velocity profiles in Fig. 2 (right) show that IDDES predict stronger chordwise and radial velocities than RANS in the vicinity of the wall (point *P*). This indicates a stronger Coriolis and centrifugal forces so that separation is delayed considerably. Thinner boundary layer (δ) is also observed for IDDES. Furthermore, the wake downstream the airfoil section at 0.24*R* is better resolved (Fig. 2, left). URANS predicts smeared velocity field at *L* distance downstream of the airfoil which seems unphysical. This behavior, however, is not shown in IDDES prediction.

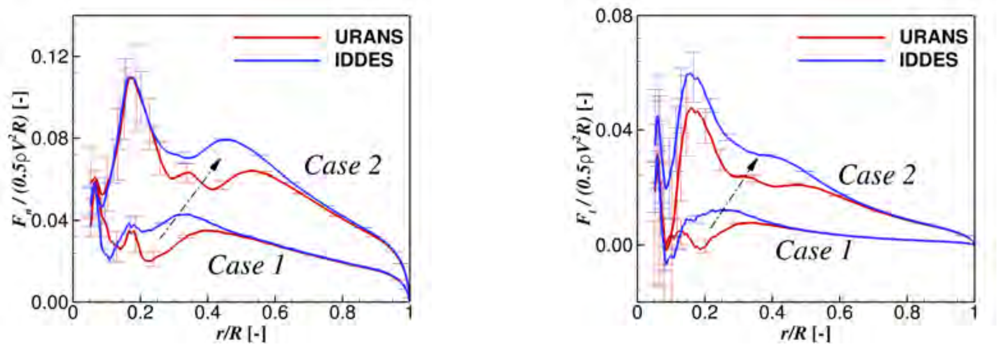

Fig. 1: Time-averaged non-dimensional sectional loads; (left) *Fn* and (right) *Ft*.

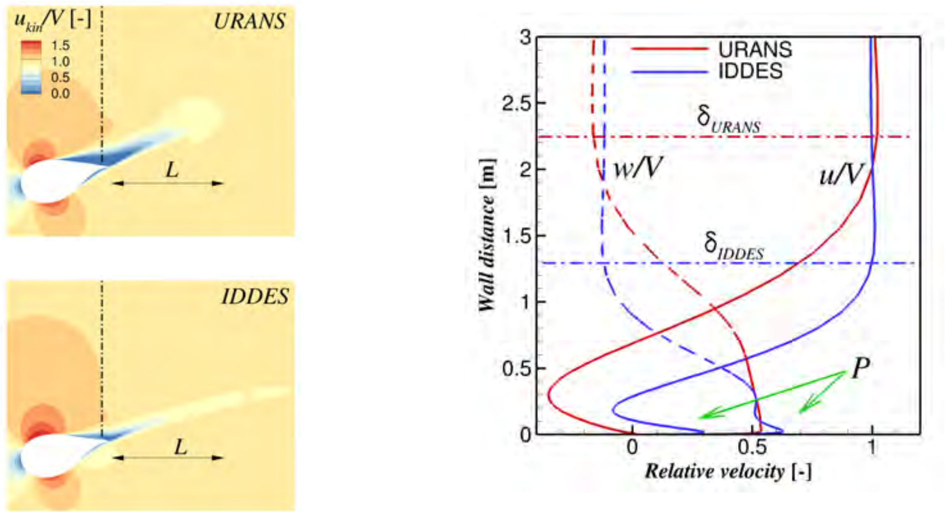

Fig. 2: Velocity field at 0.24*R* (left) and (right) velocity profiles extracted from the black - dashed lines in the left figures for Case 1.

References

[1] Himmelskamp H.: Profile investigations on a rotating airscrew, Ph.D. thesis Universiät Göttingen, 1945.
[2] Pape AL, Lecanu J.: 3D navier–stokes computations of a stall-regulated wind turbine, Wind Energy 7(4), 309–324, 2004.
[3] Breuer M *et al.*: Comparison of DES, RANS and LES for the separated flow around a flat plate at high incidence, Int. J. Numer. Meth. Fluids 41, 357–388, 2003.
[4] Johansen J, Sorensen N, Michelsen J, Schreck S.: Detached-eddy simulation of flow around the NREL phase VI blade, ASME 2002 Wind Energy Symposium, 106–114, 2002.
[5] Li Y *et al.*: Dynamic overset CFD simulations of wind turbine aerodynamics, Renewable Energy 37, 285-298, 2012.
[6] Lekou D et al.: Avatar deliverable d1.2 reference blade design, Tech. rep. ECN Wind Energy, 2015.
[7] Kroll N, Rossow C-C., Becker K, and Thiele F.: The MEGAFLOW project, Aerospace Science and Technology 4, pp. 223-237, 2000.
[8] Gritskevich M *et al.*: Development of DDES and IDDES formulations for the k-ω shear stress transport model, Flow, Turbulence and Combustion 88(3), 431-449, 2012.
[9] Bangga G., Lutz T., and Krämer E.: An examination of rotational effects on large wind turbine blades, EAWE PhD Seminar 11, Stuttgart, Germany, 2015.

Mitteilung

Projektgruppe / Fachkreis: Drehflügleraerodynamik/ Windenergie

Numerische Untersuchungen einer Modellwindenergieanlage

Annette Fischer, Amélie Flamm, Eva Jost, Thorsten Lutz, Ewald Krämer
Institut für Aerodynamik und Gasdynamik (IAG), Universität Stuttgart
Pfaffenwaldring 21, 70569 Stuttgart
fischer@iag.uni-stuttgart.de

Einleitung

Lastschwankungen an Windenergieanlagen (WEA) haben zwei wesentliche negative Einflüsse auf die Wirtschaftlichkeit der Windenergie. Auf der einen Seite sind Windkraftanlagen während ihrer Lebenszeit einer Vielzahl solcher Lastwechsel ausgesetzt. Diese entstehen beispielsweise durch die Turbulenz in der atmosphärische Grenzschicht, den Nachlauf anderer Windkraftanlagen, die Positionierung in komplexem Gelände, Schräganströmung oder den Turmvorstau [1]. Diese Lastfluktuationen rufen Ermüdungslasten hervor, was die Lebensdauer der Anlagen negativ beeinflussen kann. Auf der anderen Seite können Lasten, beispielsweise hervorgerufen durch das Eigengewicht der Blätter, eine weitere Vergrößerung der Rotordurchmesser verhindern. Aus diesen Gründen werden Lastreduktionsprinzipien an Windkraftanlagen immer wichtiger. Im Zuge des DFG PAK780 Projektes werden verschiedene aktive und passive Systeme sowohl experimentell, als auch numerisch untersucht. Neben 2D Untersuchungen werden die Konzepte auch in rotierenden Systemen analysiert. Da die Implementierung der Systeme in eine reale Windkraftanlage zu einem so frühen Entwicklungsstatus schwer umsetzbar ist, wurde an der Technischen Universität Berlin, in Zusammenarbeit mit der SMART BLADE GmbH, die Modellwindkraftanlage BeRT (Berlin Research Turbine) entwickelt [2]. An dieser Modellanlage, die einen Rotorradius von R=1,5m hat, können die Blätter ausgetauscht und somit verschiedene Lastreduktionssysteme getestet werden.

In der vorliegenden Mitteilung wird kurz auf das numerische Setup eingegangen. Die CFD-basierten numerischen Untersuchungen befassen sich vorerst mit einem reinen Rotor, welcher als 120°-Modell mit periodischer Randbedingung realisiert wurde. Darüber hinaus wird auf ein Vergleich der Lasten zwischen einem Setup mit Fernfeldrandbedingung und einem Setup mit einem approximiertem Windkanal der TU Berlin mit Euler-Wänden eingegangen, um so den Einfluss des Windkanals auf den Rotor abzuschätzen. Ein vollständiger Artikel wird zusätzlich eine Gitterkonvergenzstudie nach Celik [3], sowie Untersuchungen mit reibungsbehafteten Windkanalwänden und Anstellwinkelauswertungen enthalten.

Numerisches Setup

In den vergangenen Jahren wurde am IAG eine Prozesskette für die numerische Untersuchung von Windenergieanlagen entwickelt [4], auf deren Grundlage die hier vorgestellten Simulationen durchgeführt werden. Als Strömungslöser wird der CFD-Code FLOWer, welcher vom Deutschen Zentrum für Luft- und Raumfahrttechnik (DLR) entwickelt wurde und am IAG für Windkraft- und Hubschrauberanwendungen weiterentwickelt wird, eingesetzt [5]. FLOWer verwendet ein Finite-Volumen-Verfahren zur Lösung der kompressiblen Navier-Stokes-Gleichungen für blockstrukturierte Netze. Die einzelnen Komponenten der WEA werden separat vernetzt und die Netze mit Hilfe der Chimera-Technik überlappt, wodurch ein körperangepasstes Netz für jede Struktur verwendet werden kann. Die Vernetzung der Rotorblätter erfolgt automatisiert durch ein am IAG entwickeltes Skript [4], wobei darauf geachtet wird, dass für die wandnächste Zelle y^+<1 ist. Die restlichen Netze werden von Hand erstellt. Abbildung 1 zeigt das Drittelmodell der BeRT-Anlage im Hintergrundnetz.

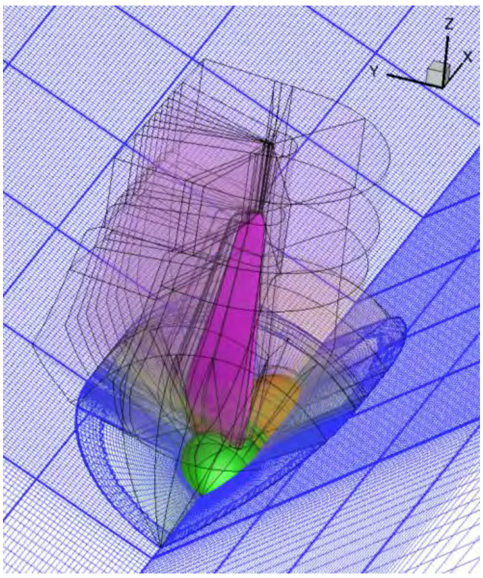

Abbildung 1: Netze des BeRT 1/3-Modells.

Das Hintergrundnetz selbst besteht aus einem Drittel eines Zylinders. Die Rotorebene befindet sich in der Mitte der ca. 64m (≈43R_{BeRT}) langen Domain. Im Bereich der

Anlage haben die Zellen eine konstante Größe von 0,25mx0,25mx0,25m. Das Hintergrundnetz mit Fernfeldrandbedingung hat einen Radius von ca. 17m (≈11R_{BeRT}), wohingegen das Netz mit Eulerwand einen Radius von ca. 2m hat, was der Hälfte des hydraulischen Durchmessers der Messstrecke im Windkanal entspricht. Das Blattnetz enthält ca. 5,5 Mio. Zellen, das gesamte Setup mit Fernfeld ca. 13,1 Mio. Zellen, das mit Eulerwänden ca. 11,4 Mio. Zellen.

Exemplarische Ergebnisse

Die Anlage wurde stationär vorgerechnet und anschließend instationär mit 3° pro Zeitschritt bis zur Konvergenz der Lasten simuliert. Die Anzahl an inneren Iterationen lag zwischen 30 und 100 pro Zeitschritt. Das Strömungsfeld um die Anlage entwickelt sich im Fall mit Fernfeldrandbedingung aufgrund des großen, zur Verfügung stehenden Raumes nur sehr langsam, wodurch eine lange Simulationszeit bis zur vollständigen Expansion des Nachlaufs benötigt wird. Dadurch ändern sich die Induktion und damit der Anstellwinkel an der Anlage über einen langen Zeitraum hinweg, was wiederum Einfluss auf die Umströmung der Blätter hat. Hat sich die Strömung voll ausgebildet, sinkt der Anstellwinkel nicht weiter, die Strömung am Blatt liegt über den gesamten Radius an (Abbildung 2, links) und die Lasten an der Anlage konvergieren. Bei der Simulation mit Windkanal ist die Expansion des Nachlaufs aufgrund des Wandeinflusses sehr klein, sodass eine Konvergenz der Lasten schneller erreicht wird. Im Vergleich zur Simulation mit Fernfeld führt die geringe Expansion zu einem Anstieg der Strömungsgeschwindigkeit in der Rotorebene, sowie um die Anlage herum, wodurch die Spitzenwirbel schneller abtransportiert werden. Durch die höhere Geschwindigkeit sieht die Anlage einen höheren Anstellwinkel, der auf der Saugseite zu Ablösungen führt (Abbildung 2, rechts) und der damit einen großen Einfluss auf die Aerodynamik des Blattes hat. Abbildung 3 zeigt den Verlauf des Schubes (F_x, oben) und der antreibenden Kraft (F_y, unten) über dem Radius, jeweils normiert mit dem Maximum der Fernfeldlösung, über fünf Umdrehungen, sowie gemittelt über fünf Umdrehungen. Aufgrund der erhöhten Geschwindigkeit im Fall mit Windkanal steigen Schub (≈35%) und Leistung (≈65%). Für diesen Fall treten Ablösungen im Bereich der Blattwurzel, sowie zwischen R=0,8m und 1,2m auf, was an F_x gut zu erkennen ist. Somit haben die Wände des Windkanals einen bedeutenden Einfluss auf das Geschwindigkeitsfeld der Anlage und damit auch auf deren Lasten.

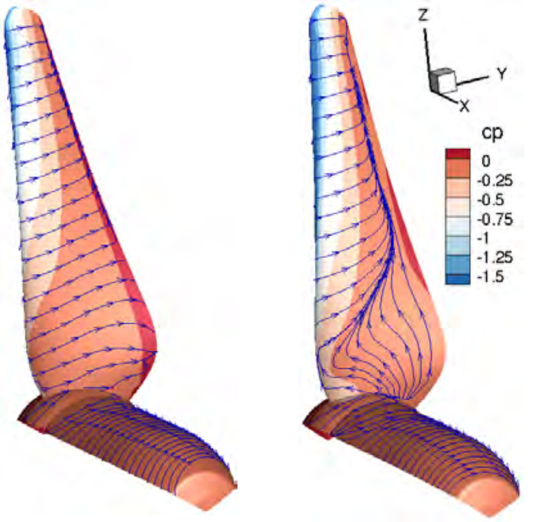

Abbildung 2: Oberflächenlösung der Saugseite mit Stromlinien für den Fall mit Fernfeld (links) und mit Eulerwand (rechts).

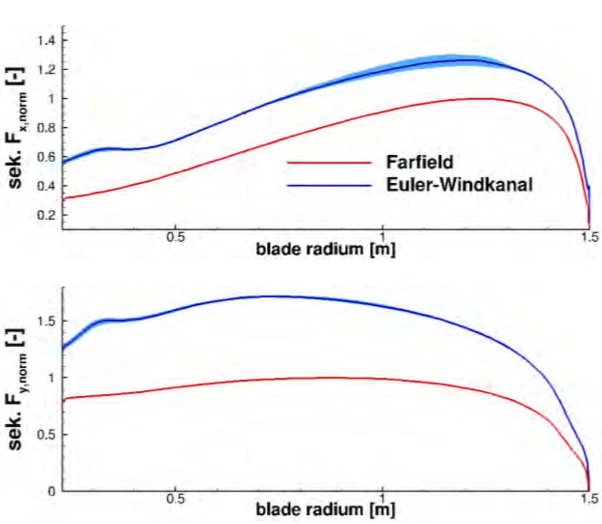

Abbildung 3: Normierte, sektionale Lasten in x-Richtung (Schub, oben) und y-Richtung (antreibende Kraft, unten)

Die Präsentation wird sich näher mit den hier aufgeführten Effekten befassen und dabei auch auf die Entwicklung das Anstellwinkels und der Induktion eingehen. Darüber hinaus wird eine Gitterkonvergenzstudie sowie die Simulation eines Windkanals mit reibungsbehafteten Wänden präsentiert.

Literatur

[1] Schulz C, Fischer A, Weihing P, Lutz T and Krämer E *High Performance Computing in Science and Engineering 15* (Springer)

[2] Pechlivanoglou G, Fischer J, Eisele O, et al. 2015 *DEWEK* (Bremen)

[3] Celik I B, Ghia U, Roache P J, et al. 2008 *Journal of fluids {Engineering-Transactions} of the {ASME}*, 130(7)

[4] K. Meister et al., 2009 EUROMECH 508

[5] Kroll N and Fassbender J 2002 *MEGAFLOW Numerical Flow Simulation for Aircraft Design* (Berlin: Springer)

Mitteilung

Projektgruppe / Fachkreis: Windenergie

An Experimental Setup for Airfoil Characterizations in Customized Turbulent Flow

Hendrik Heißelmann, Joachim Peinke, Michael Hölling
ForWind – Institute of Physics, University of Oldenburg, 26111 Oldenburg, GER
hendrik.heisselmann@uni-oldenburg.de

1. Introduction

Airfoil characterizations are usually performed in highly laminar flows. In order to incorporate unsteady effects, either pitched airfoils in laminar inflow have been used or the inflow has been periodically altered with a fixed airfoil. These cases are mainly representative for helicopter applications. Attempts to include turbulence were made using classical and fractal grids [6][5], but they do not cover the typical operational conditions of wind turbines very well [2]. The consideration of wind energy applications will be addressed in our presentation of an experimental setup for the investigation of airfoil characteristics in different turbulent inflows with customizable features, which was developed at the University of Oldenburg. An active grid is used to manipulate either the flow velocities or inflow angles. The presented study on a DU 00-W-212 airfoil was carried out within in the EU FP7 project «AdVanced Aerodynamic Tools for lArge Rotors» (AVATAR), which is aiming at a comparison and validation of simulation tools based on BEM methods, CFD and wind tunnel experiments.

2. Experimental Setup

An experimental setup for airfoil characterizations in the return-type acoustic wind tunnel at the University of Oldenburg is presented. The wind tunnel is operated in laminar condition with a background turbulence level of 0.3% for the measurement of classical airfoil polars - constituting the baseline case for the comparison presented later on.
An active grid can be inserted between the wind tunnel nozzle and the test section in order to generate reproducible, customized turbulence patterns with different characteristics [7][8]. The turbulent patterns can be tailored using 16 individually controlled shafts with attached flaps. However, only the nine vertical shafts were used for the presented work as all seven horizontal shafts remained in open position (least blockage) to render a quasi two-dimensional turbulence pattern with customized inflow angle variations. A grid transfer function was therefor recorded and used to translate the desired inflow angle variations into flap movements – so-called grid protocols. This method allows not only to impose a statistical distribution of inflow angles but also to mimic atmospheric wind time series (of inflow velocity or angle) in the wind tunnel.
The investigated DU 00-W-212 airfoil is a wind turbine dedicated airfoil, designed by the TU Delft as a blend of two other DU airfoils [9]. It is designed for the use in the tip region of state-of-the art wind turbine blades and is part of the AVATAR reference wind turbine. For the experiments at Re 500,000 and Re 900,000, an aluminum airfoil model with a chord of 0.3m is vertically mounted inside the closed wind tunnel test section with cross-section of 1.0m x 0.8m (w x h) and 2.6m length. The airfoil has an aspect ratio of 2.68 and is fixed to two rotating plates at its ends, which are fitted flush with the test section floor and ceiling. Two 3-component load cells at the top and bottom axis are used for the highly resolved force measurements. The angle of attack is adjusted with a stepper motor and is monitored with an angle encoder at the bottom airfoil mount. Chord-wise pressure distributions are measured via 48 pressure taps connected to a system of three synchronized multi-channel scanners.

3. Results

Two different unsteady turbulent inflows were generated with the active grid in order to compare the impact of different turbulence on the airfoil performance. A sinusisoidal exitation protocol was used to generate periodically varying inflow angles with a frequency of 5Hz. A second turbulent grid protocol features intermittent angle variations. Both inflow cases were characterized in the empty wind tunnel prior to the installation of the airfoil model using highly-resolving x-wire measurements on the wind tunnel center line at the downstream position of the designated airfoil's leading edge. While both grid protocols were designed to produce inflow angle variations within approximately ±6° and yield almost similar turbulence intensities (5% and 3.7%), they deviate in other features significantly. Unstead flow situations are usually characterized by a reduced frequency [1], but the absence of a pronounced frequency in the intermittent inflow makes such a characterization more difficult. To be still able to compare both cases, the power spectral density of the inflow angle variations is considered in dependence of the reduced frequency. The reduced frequency spectrum of the intermittent inflow covers a wider range of reduced frequencies (0<k<0.5) as it is expected for the operation of wind turbine blades in turbulent atmospheric flows [4], while the sinusoidal case exhibits one pronounced reduced frequency at k=0.18. It is therefore more likely to mimic the natural flow conditions with turbulence of this characteristics.

Averaged polars of the measured load cell data were compared for both turbulent cases with the laminar reference case at Re 500,000 and Re 900,000. The results for both Re numbers are almost similar for the laminar case. The lift polars show a clear lift peak with a rather quick drop in the stall region, while the larger Re number leads to a slight reduction in $C_{L,max}$. In contrast, the turbulent inflow causes a significantly larger Re-effect on the polars as shown in Figure 1. In both Re cases, all three lift polars differ in the slope of the linear region and the turbulent cases show a delayed stall with an extended stall region and increased $C_{L,max}$. While the increase is rather small in the low Re number range, it is significant for the larger Re number.

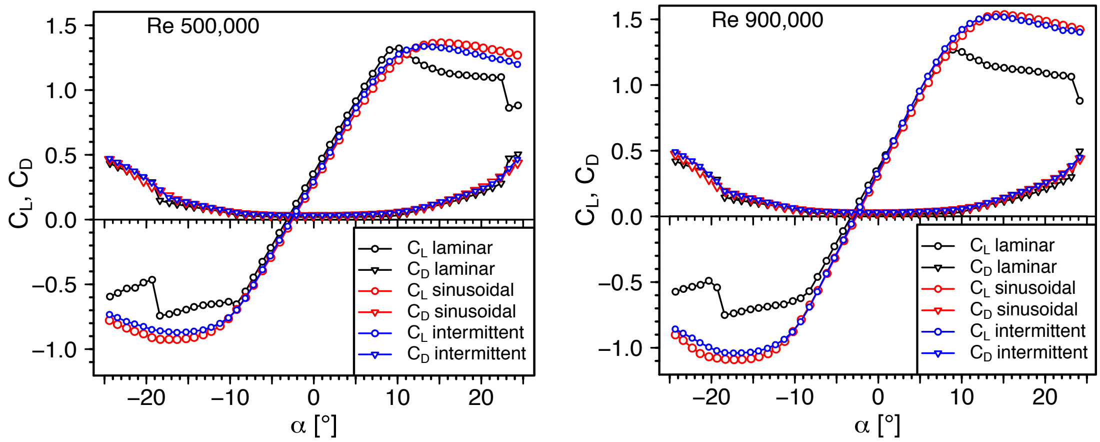

Figure 1: Polars for Re 500,000 (left) and Re 900,000 (right) measured in laminar, sinusoidal and intermittent inflow cases.

Analysis of the fully resolved data sets show similar minimal and maximal lift values for the sinusoidal and intermittent cases, while the standard deviations were significantly lower in the intermittent case. Further examination of the full data will be performed to improve the description of turbulence and grasp its impact on the airfoil performance.

References

[1] Leishman J G 2006 Principles of Helicopter Aerodynamics 2nd ed Cambridge Aerospace Series (Cambridge University Press)

[2] Wolken-Möhlmann G, Knebel P, Barth S and Peinke J 2007 Journal of Physics: Conference Series 75 012026 URL http://stacks.iop.org/1742-6596/75/i=1/a=012026

[3] Wächter M, Heißelmann H, Hölling M, Morales A, Milan P, Mücke T, Peinke J, Reinke N and Rinn P 2012 Journal of Turbulence 13 N26URL http://www.tandfonline.com/doi/abs/10.1080/14685248.2012.696118

[4] Pereira R, Schepers G and Pavel M D 2013 Wind Energy 16 207–219 ISSN 1099-1824 URL http://dx.doi.org/10.1002/we.541

[5] Schneemann J, Knebel P, Milan P and Peinke J 2010 Proceedings of EWEC 2010

[6] Eisele O, Pechlivanoglou G, Nayeri C and Paschereit C 2013 Proceedings of ASME Turbo Expo 2013: Turbine Technical Conference and Exposition

[7] Knebel P, Kittel A and Peinke J 2011 Experiments in Fluids 1–11 ISSN 0723-4864 10.1007/s00348-011-1056-8 URL http://dx.doi.org/10.1007/s00348-011-1056-8

[8] Weitemeyer S, Reinke N, Peinke J and Hölling M 2013 Fluid Dyn. Res. 45 061407 (16pp)

[9] Timmer W and van Rooij R 2003 Journal of Solar Energy Engineering 125

Mitteilung

Projektgruppe / Fachkreis: Drehflügleraerodynamik / Windenergie

RANS Simulation of the New MEXICO Rotor Experiment Including Laminar-Turbulent Transition

C. C. Heister
German Aerospace Center (DLR), Lilienthalplatz 7, 38108
Braunschweig,christoph.heister@dlr.de

Within the framework of International Energy Agency (IEA) Task 29 a key interest is the general improvement and calibration of aerodynamic models for wind turbine applications. During the associated Mexnext-III project, detailed wind tunnel measurements have been undertaken in order to provide a database for the assessment and improvement of current aerodynamic methods. The wind tunnel measurements have been conducted on a model wind turbine in the open test section of the DNW-LLF wind tunnel facitilty, as shown in Figure 1. The rotor of the model wind turbine has a diameter of 4.5m and was operated at a rotor speed of 425.1 rpm at a blade pitch of -2.3°. During the wind tunnel experiment detailed flow data has been collected under axial and yawed flow conditions including blade pressures and loads, near field velocity measurements (PIV) as well as accoustic measurments. The present paper presents RANS simulations using the DLR TAU code for three axial flow testcases of the New MEXICO rotor experiment and gives a comparison of the RANS results to the available wind tunnel measurements. The RANS simulations assume an isolated, rigid rotor geometry as previously used by e.g. Lutz et al. [1] or Bechmann et al. [2]. For the present simulation the wind tunnel test section was neglected since its influence on the rotor flow field has been found to be small (Réthoré et al. [3]). For the RANS simulation an overset grid with a total of 29 million grid points was used, consisting of a cylincrical background grid with farfield boundary conditions and three blade grids. TAU simulations were run for three testcases corresponding to wind tunnel speeds of $v_{tunnel} = 10, 15$ and $24 m/s$ using the Wilcox-kω turbulence model. As shown by Figure 2 the axial flow upstream ($x<0$) and downstream ($x>0$) of the rotor could be simulated in general good agreement to the experiment. Due to the momentum extraction of the rotor, the velocity deficit in the downstream region is clearly visible. Axial velocity fluctuations caused by the tip and root vortex are well resolved, especially for the high wind tunnel speed at $v_{tunnel} = 24 m/s$ with large areas of separated flow at the suction side of the rotor. For this flow case the Menter-SST turbulence model was found to improve the prediction of largley separated blade flow.The computation of the pressure distributions at the rotor blade sections is considered in general good agreement to the experiment, as exemplary shown for $v_{tunnel} = 15 m/$ in Figure 3. The RANS simulation slightly underestimates the pressure measurements on the suction side. In order to study the infuence of the rotor blade boundary layer state on the rotor thrust and torque, laminar-turbulent RANS simulations were conducted as well. Since the rotor blades were equipped with zigzag tape up to 70% of rotor radius during the experiment, the TAU simulations were run with locally tripped and free transition, as exemplary shown in Figure 4. The final paper will analyze axial and radial traverses, pressure distributions and rotor thrust and torque for all three wind tunnel speeds, including laminar-turbulent results.

References :

[1] Lutz, Th.; Meister, K.; Krämer, E. : « Near Wake Studies of the MEXICO Rotor«, EWEA-2011, Brussels, 14-17 March, 2011.
[2] Bechmann, A.; Sørensen, N. N.; Zahle, F.: « CFD simulations of the MEXICO rotor«, Wind Energy, Wiley Online Library, Vol. 14, pp. 677-689, 2011.
[3] Réthoré, P.-E.; Sørensen, N. N. ; Zahle, F. : « MEXICO Wind Tunnel and Wind Turbine modelled in CFD«, 28th AIAA Applied Aerodynamics Conference, Honolulu, Hawaii, 27-30 June, 2011.

Figure 1: New MEXICO rotor experiment in the DNW-LLF – smoke visualization of the blade tip vortices under axial flow conditions (Photo from Boorsma, K.; Schepers, J.G.:, "Description of Experimental Setup", ECN, 2015).

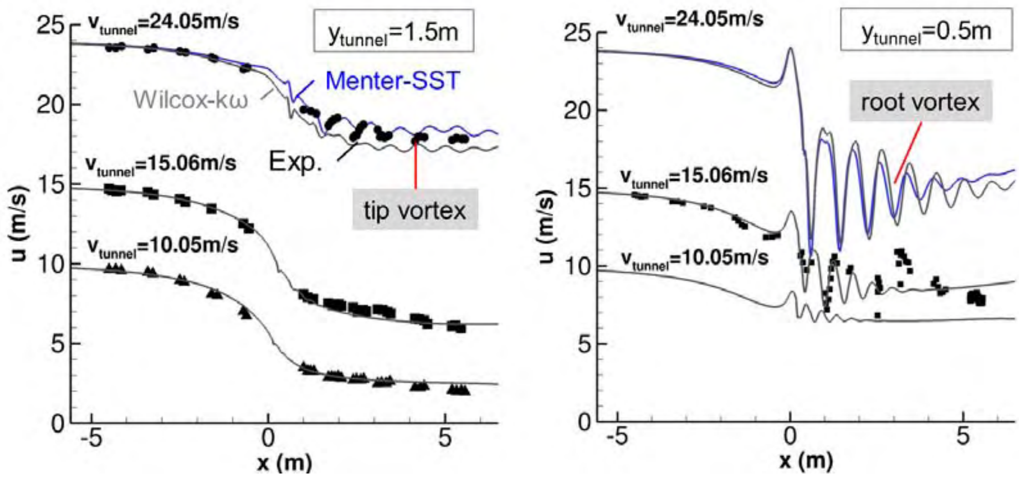

Figure 2: New MEXICO rotor experiment–axial flow u upstream and downstream of the rotor for three different wind tunnel speeds v_{tunnel} comparing PIV measurements and TAU RANS simulation results near the blade tip (y_{tunnel}=1.5m) and near the root (y_{tunnel}=0.5m).

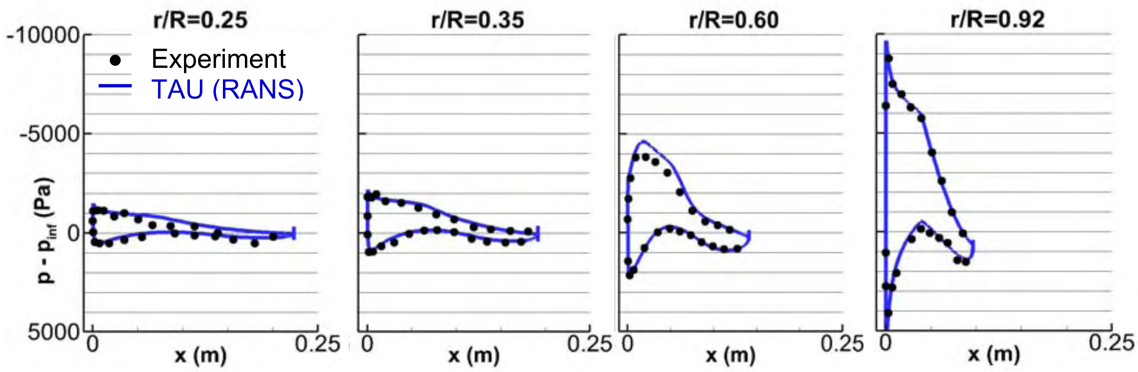

Figure 3: New MEXICO rotor experiment (v_{tunnel}=15,06m/s) – pressure distributions at four rotor blade sections comparing experiment and TAU RANS simulation (isolated rotor, fully turbulent, Wilcox-kω turbulence model).

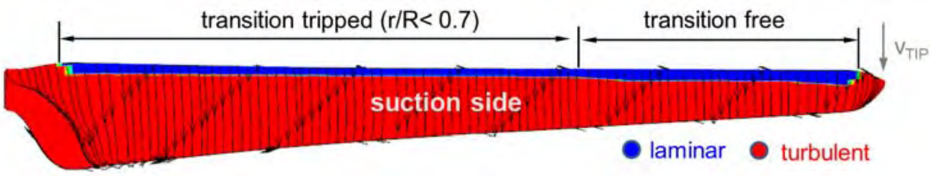

Figure 4: New MEXICO rotor experiment (v_{tunnel}=15,06m/s) – computed skin friction lines and predicted laminar-turbulent flow areas on the suction side of the rotor blade with locally tripped and free transition (TAU RANS simulation, isolated rotor, Wilcox-kω turbulence model, AHD and C1 transition criteria).

Mitteilung

Projektgruppe / Fachkreis: Drehflügleraerodynamik/ Windenergie

CFD study of trailing edge flaps for load control on wind turbines

Eva Jost, Thorsten Lutz, Ewald Krämer
Institute of Aerodynamics and Gas Dynamics, University of Stuttgart
Pfaffenwaldring 21, 70569 Stuttgart
{e.jost, lutz, kraemer}@iag.uni-stuttgart.de

As ultimate and fatigue loads play an important role in today's wind turbine design, load reduction and control is one of the focus points of today's wind energy research. A reduction would lead to reduced rotor weight and costs, to an increase of turbine reliability or allow a further enlargement of the diameter to increase power output. Active trailing edge flaps applied to the outer part of the rotor blade constitute a very promising approach for these matters. As flaps are able to increase or decrease the local lift by adapting the deflection angle, it is possible to partly compensate load variations due to variations of the effective inflow angle. These variations are caused by changes in the incoming wind speed resulting from e.g. tower blockage, atmospheric shear and turbulence or yawed inflow.

The suitablility of trailing edge flaps for wind turbine load control has been shown in various publications, both experimentally (e.g. [1]) and numerically (e.g. [2]). Fatigue load reductions up to approximately 30 % have been found for a trailing edge flap covering up to 25 % of the blade span of a 5 MW turbine [3]. Most numerical studies were conducted on the basis of blade element momentum (BEM) theory. As viscous and unsteady aerodynamics have a great influence, it is however important to also apply higher fidelity models in order to validate the results. Within the European FP7 project AVATAR extensive studies on trailing edge flaps have been performed including models of various fidelity ranging from BEM to CFD [4]. The paper will in detail present an extract of the CFD simulations performed at the IAG with the main focus point on a study on the flap design parameters meaning flap shape (rigid/morphing), flap length, radial positioning of the flap center and radial sizing.

The simulations have been conducted making use of the process chain for the simulation of wind turbines developed at the IAG, University of Stuttgart. The main part constitutes the CFD code FLOWer, which originates from the German Aerospace Center (DLR) [5]. Trailing edge flaps are realised with the use of grid deformation by deforming the flap part of the airfoil or respectively rotor blade while the rest is kept rigid. This approach allows to vary the design parameters easily without the need to generate new meshes for each case.

2D simulations are performed for a representative airfoil located at 75% rotor blade radius. Within this 2D simulations paramters like flap length and shape are varied at realistic inflow conditions. In 3D a pure rotor model is at first analysed in a 120°-model with periodic boundary conditions. Different flap positions and sizes along the blade span are evaluated for a deflection angle of 10° as shown in Figure 1 and Figure 2 for the DTU 10 MW turbine [6].

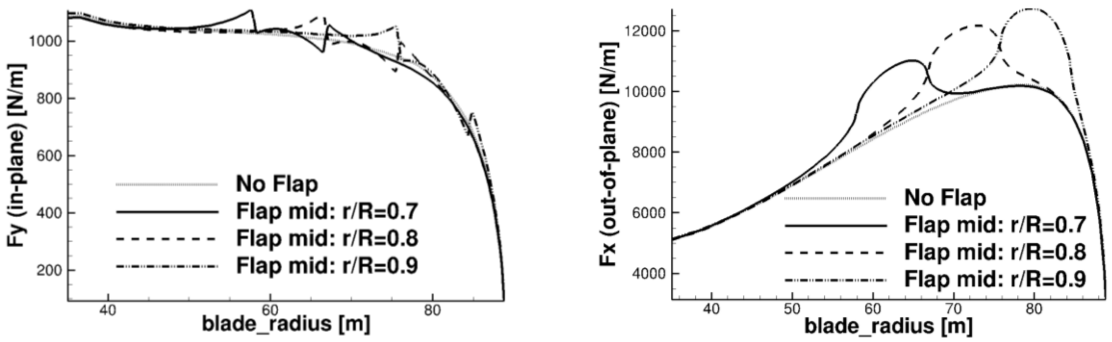

Figure 1: Variation of flap radial position

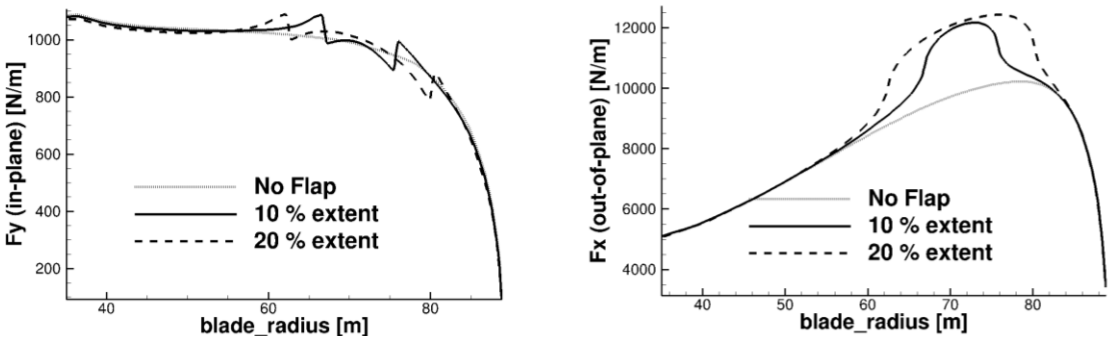

Figure 2: Variation of flap radial size

Most important with regard to load control is the impact of the flap on the out-of-plane forces meaning the blade thrust and resulting moment at blade root. As it is visible in the plots the variation of the position along the blade span shows that the flap is more effective the further outboard it is located. A higher increase of the force is possible leading to an even higher impact at blade root due to the longer lever arm. The variation of the radial size indicates that a larger extension along the blade span is favourable. Apart from the bigger area that is covered, 3D effects are reduced as the thrust increase is higher at mid flap position for the 20% extension. Vortices which appear at the flap edges due to the gradient of bound circulation decrease the flap effectiveness in the flap section as a downwind is induced.
The presentation will include a description of the numerical setup and gradually go through the different steps of the study.

References

[1] D. Castaignet, T. Barlas, T. Buhl, N. Poulsen, J. Wedel-Heinen, N. Olesen, C. Bak and T. Kim, «Full-scale test of trailing edge flaps on a Vestas V27 wind turbine: active load reduction and system identification,» *Wind Energy 17,* pp. 549-564, 2014.

[2] S. Navalkar, J. van Wingerden, E. van Solingen, T. Oomen, E. Pasterkamp and G. van Kuik, «Subspace predictive control to mitigate periodic loads on large scale wind turbines,» *Mechatronics 24,* pp. 916-925, February 2014.

[3] T. K. Barlas, G. J. van der Veen and G. A. M. van Kuik, «Model predictive control for wind turbines withdistributed active flaps: incorporating inflow signalsand actuator constraints,» *Wind Energy,* vol. 15, p. 757–771, 2012.

[4] M. Aparicio, R. Martín, Arturo Muñoz and A. Gonzalez, «Deliverable 3.3: Results of a parametric study of flow devices, guidelines for design,» AVATAR project, 2016.

[5] N. Kroll and J. Fassbender, MEGAFLOW – Numerical Flow Simulation for Aircraft Design, Berlin/Heidelberg/New York: Springer Verlag, 2002.

[6] C. Bak, F. Zahle, R. Bitsche, T. Kim, A. Yde, L. Henriksen, P. Andersen, A. Natarajan and M. Hansen, «Design and performance of a 10 MW turbine,» [Online]. Available: dtu-10mw-rwt.vindenergi.dtu.dk.

Mitteilung

Projektgruppe/Fachkreis: Drehflügleraerodynamik/ Windenergie

Aerodynamisches Verhalten von Windenergieanlagen im komplexen Gelände unter turbulenter atmosphärischer Zuströmung

Christoph Schulz, Thorsten Lutz, Ewald Krämer
Institut für Aerodynamik und Gasdynamik (IAG), Universität Stuttgart
Pfaffenwaldring 21, 70569 Stuttgart
schulz@iag.uni-stuttgart.de

Einleitung

Im Rahmen der süddeutschen Verbundprojekte LidarComplex und KonTest wurden Untersuchungen an einem potenziellen Testfeldstandort für eine Forschungswindenergieanlage in Baden-Württemberg durchgeführt. Eine der zentralen Zielstellungen der Projekte war die Charakterisierung der Strömung im Gelände sowie der Interaktion zwischen atmosphärischer Turbulenz, Gelände und Windenergieanlage. Zunächst wurden auf Basis von verschiedenen Messverfahren die grundlegenden Strömungszustände im Gelände charakterisiert. Hierbei kamen Schalenkreuz- und Ultraschallanemometer an einem Messmasten, Lidar-Messungen (Light Detection And Ranging) sowie Messungen mit einem unbemanntem Luftfahrzeug (UAV) zum Einsatz [Schulz2015]. Auf Basis der so gewonnen Daten wurden mit numerischen Modellen atmosphärische Zuströmfelder generiert und als Eingabegrößen für die Simulation verwendet. Die sich an die Messungen anschließenden Simulationen des Testgeländes konnten eine gute Übereinstimmung mit den Messungen erzielen, weswegen in einem weiteren Schritt eine Windenergieanlage in die Simulation eingegliedert wurde. Anhand dieser Simulationen wurden Untersuchungen zum aerodynamischen Verhalten und dem Nachlauf der Anlage durchgeführt. In dieser Mitteilung soll kurz auf die Simulation der Windenergieanlage im komplexen Gelände unter atmosphärischer Turbulenz und einen analogen Vergleichsfall im ebenen Gelände eingegangen werden. Ein vollständiger Artikel wird ebenfalls detaillierte Informationen zu den Messungen und den Simulationen des Geländes ohne Anlage enthalten. Die zentrale Bedeutung der Untersuchungen liegt in der bisher ungenügenden Vorhersagegenauigkeit des Verhaltens von Windenergieanlagen und deren Nachlauf im komplexen Gelände.

Numerisches Modell

Die numerischen Simulationen von Windenergieanlagen werden am IAG basierend auf einer eigens entwickelten Prozesskette Windenergieanlagensimulation durchgeführt [Meister2009]. Als Strömungslöser wird dabei der CFD-Code FLOWer des Deutschen Zentrums für Luft- und Raumfahrt (DLR) eingesetzt. Durch Verwendung der Gitterüberlappungstechnik (Chimera) wird es ermöglicht die Netze der einzelnen Strukturen der Windenergieanlage unabhängig zu gestalten. Für die Vernetzung der Rotorblätter wird dabei auf ein erprobtes Skript zurückgegriffen [Meister2009]. Zur Erstellung des Hintergrundnetzes im Gelände wurde ein über MPI parallelisiertes Vernetzungsprogramm entwickelt, welches ein kartesisches Hintergrundnetz erstellt und auf Basis von Geländeoberflächen deformiert. Insgesamt wurden für die Simulation der Windenergieanlage im Testgelände ca. 180 Mio. Zellen verwendet. Als Randbedingung am Einströmrand des Hintergrundnetzes wurde ein konstantes exponentielles Geschwindigkeitsprofil vorgegeben. Stromab des Einströmrandes wurden anschließend turbulente Fluktuationen in Form von Körperkräften in einer Ebene senkrecht zur Strömungsrichtung zeitlich aufgelöst in das Feld eingebracht [Troldborg2014]. Dabei berechnet sich der in das Feld eingebrachte Kraftvektor $\vec{f}$ wie folgt:

$$\vec{\mathrm{f}} = \frac{\rho\vec{\mathrm{u}}}{\Delta n}\left(U_n + \frac{1}{2}u_n\right)$$

Dabei sind $\vec{u}$ der zu modellierende Geschwindigkeitsschwankungsvektor und u_n dessen Normalkomponente, Δn die Gitterweite und U_n die mittlere Geschwindigkeit in Normalenrichtung. Die so berechneten Körperkräfte werden durch Manipulation des Residuums, ähnlich des Aktuatorscheiben-ansatzes, in das Feld eingebracht. Die Fluktuationen $\vec{u}$ werden in der Simulationsvorbereitung nach dem Modell von Mann bestimmt [Mann1998].

Alle Simulationen in den oben genannten Projekten wurden als DES97 durchgeführt. Nahe der Windenergieanlage, in deren Zuströmung und Nachlauf wurde ein WENO-Verfahren fünfter Ordnung zur Berechnung der konvektiven Flüsse benutzt [Liu1994]. Die zeitliche Diskretisierung erfolgte mittels dual time stepping Methodik nach Jameson. Für alle Simulationen wurden neun Minuten simuliert, bevor die Daten über eine Minute ausgewertet wurden. Die benötigten Ressourcen belaufen sich dabei auf sieben Tage auf ca. 4600 CPUs auf der Hazel Hen des HLRS.

Exemplarische Ergebnisse

Die Wechselwirkung zwischen atmosphärischer Zuströmung und Gelände führt zu einer starken Geschwindigkeitsüberhöhung an der Anlagenposition. Durch eine geeignete Wahl der Zuströmgeschwindigkeit im Fernfeld wurde die Simulation so kalibriert, dass an der Anlagenposition im Gelände die gleiche Geschwindigkeit herrscht wie im ebenen Vergleichsfall. Bedingt durch den Geländeanstieg werden Strömgungswinkel von unten stärker betont (Abbildung 1).

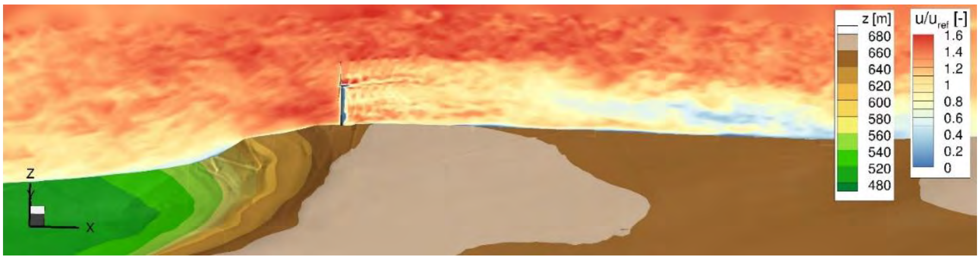

Abbildung 1: Strömungsfeld um die Anlage im Gelände; relative Geschwindigkeit als Kontur

Dies führt zu ähnlichen aerodynamischen Effekten wie eine Schräganströmung der Rotorblätter, lediglich um eine Viertelrotorumdrehung gedreht. Das Rotorblatt bewegt sich auf die Strömung bei seiner Abwärtsbewegung zu und ist bei der Aufwärtsbewegung nachlaufend. Infolge dessen kommt es zu einer Anstellwinkeländerung im Vergleich zur ebenen Zuströmung. Diese bewirkt neben einer Lastveränderung auch eine Ablenkung des Nachlaufes der Anlage, da sich die Induktion über den Umlauf des Rotors stark ändert. Verstärkt wird diese Anstellwinkelinhomogenitiät durch die vom Gelände verursachte Geschwindigkeitsüberhöhung. Das Grenzschichtprofil der Zuströmung wird vor allem im unteren Rotorbereich völliger, wohingegen es im oberen lediglich eine geringe Geschwindigkeitszunahme erfährt. Dies ist in direkter Konsequenz in einer Erhöhung der Lasten im unteren Rotorbereich zu sehen (Abbildung 2). In größerer Höhe über dem Grund ist die Übergeschwindigkeit durch den Hügel also geringer als am Boden, weswegen die mittlere Strömungsgeschwindigkeit hier niedriger ist als im ebenen Vergleichsfall. Ein weiterer auftretender Effekt ist die Reduzierung der Standardabweichung in longitudinaler Richtung auf dem Hügel, welche sich ebenso in einer Abnahme der Fluktuationen der Lasten zeigt (Abbildung 2). Die Ursache ist vergleichbar mit dem Düseneffekt, welcher longitudinale Schwankungen dämpft. Überdies verwischt der Turmschatteneffekt im Gelände sowohl in Standardabweichung der Last als auch in den Spektren des Anstellwinkels. Dies beeinflusst die Nachlaufausbreitung vor allem in Bodennähe neben anderen Effekten. Bedingt durch die atmosphärische Turbulenz kommt es zudem zu einem früheren Aufbrechen des Nachlaufes und zu einer stärkeren Interaktion dessen mit der Umgebungsturbulenz, was in Ansätzen in Abbildung 3 verdeutlicht wird. Die Präsentation wird sich näher mit den Schwankungen des Anstellwinkels, der Lasten und den Einflüssen auf die Nachlaufausbreitung befassen. Zudem werden nähere Details zur Modellierung der turbulenten Zuströmfelder erörtert.

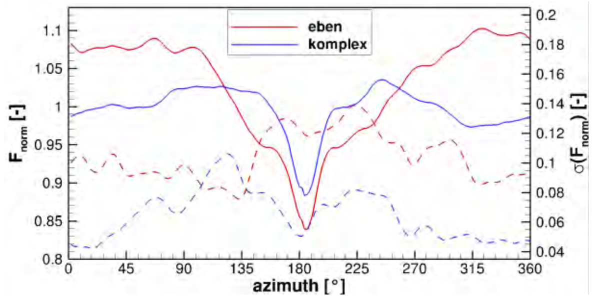

Abbildung 2: Rotorschub (Last in x-Richtung) und Standardabweichung über dem Azimutwinkel.

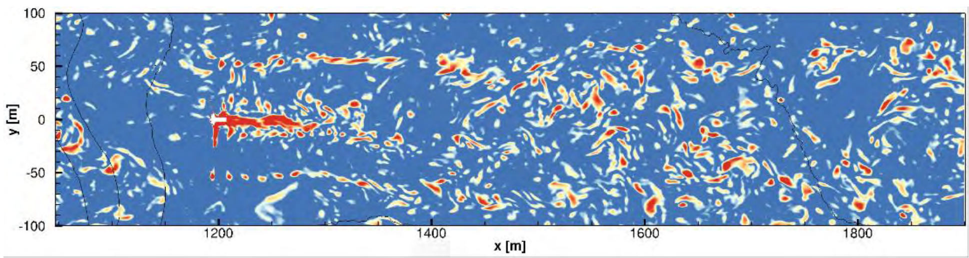

Abbildung 1: Wirbelviskosität auf Nabenhöhe; Draufsicht; Anlage bei x=1200 m

Literatur

[Liu1994] Liu X et al., 1994 Journal of computational physics 115 200–212
[Mann1988] Mann J, 1998 Probabilistic engineering mechanics 13 269–282
[Meister2009] K. Meister et al., 2009 EUROMECH 508
[Schulz2014] Schulz C et al., 2014 Journal of Physics: Conference Series vol. 524
[Schulz2015] Schulz C et al., 2015 11th EAWE PhD Seminar on Wind Energy
[Troldborg2014] Troldborg N et al. 2014 Wind Energy 17 657–669

Mitteilung

Projektgruppe / Fachkreis: Biofluidmechanik

Development of an Enhanced Blood Viscosity Model for Numerical Simulations of Complex Blood Flow Regimes in Membrane Oxygenators

Lars Krenkel[a,b], Franz Süß[a,b], Markus Rütten[c]

[a]Ostbayerische Technische Hochschule (OTH) Regensburg
Lehr- und Forschungsgebiet Biofluidmechanik
Galgenbergstr. 30, 93053 Regensburg
Lars.Krenkel@oth-regensburg.de, Franz.Suess@oth-regensburg.de

[b]Regensburg Center of Biomedical Engineering (RCBE) , OTH und Universität Regensburg
Am Biopark 9, 93053 Regensburg

[c]Deutsches Zentrum für Luft-und Raumfahrt e.V.
Institut für Aerodynamik und Strömungstechnik, Abteilung Hochgeschwindigkeitskonfigurationen
Bunsenstr. 10, 37073 Göttingen
Markus.Ruetten@dlr.de

Ausgangssituation: Blood is a rather complex heterogeneous multi-phase mixture of solid corpuscles suspended in a liquid plasma showing several non-linear and non-Newtonian properties. These are e.g. shear-thinning, viscoelasticity or stress-relaxation. In general, the rheological characteristics of blood are determined by the properties of these blood components and their interaction with each other as well as with the surrounding. Hemodynamic phenomena as e.g. flow separation, secondary flow structures in curved vessels, oscillatory wall shear stress, as well as flow induced blood coagulation are dominated by the complex blood rheology and are believed to play important roles in the development of the numerous problems in long term application of artificial ("extra-corporal") lungs. Therefore, a complete understanding as well as a sufficient modelling of the hemodynamics in complex flow regimes, as e.g. in membrane oxygenators, is of big importance.

Ziel: Within this work, a newly set-up environment for reliable numerical simulation of blood flow regimes in rather complex realistic geometries will be presented by the example of blood flow through an extracorporeal membrane oxygenator (ECMO). An ECMO is a medical treatment which is a cardiopulmonary bypass circuit. The blood is removed from the venous system, oxygenated by an oxygenator and then returned back into the body by a pump. Typical complications associated with ECMO in long term use are decreasing gas exchange efficiency by coagulopathy (induced by biocompatibility issues and flow) and finally (pharmacologically induced) bleeding.
Some research groups already implemented successfully innovative numerical models for coagulation representation in highly resolved simple vessel configurations. Nevertheless, the complexity of a complete oxygenator system prevents the application of higher order simulation techniques for coagulation representation due to its immense computational costs. Another important fact is, that blood viscosity shows many non-linear effects with respect to shear rate, haematocrit as well as with vessel diameter. Especially for diameters below 300 microns. The first two effects are mostly considered in recent numerical blood viscosity models. Whereas the clear width impact on viscosity is mostly neglected although it affects the relative viscosity by a factor of ~3 (lower viscosity in smaller vessels, Fåhraeus-Lindqvist-Effect, *FLE*).

Lösungsweg: Presented will be a numerical approach which allows not only the consideration of blood viscosity changes due to shear rate and haematocrit (Carreau-Yasuda) but also due to clear diameter changes. This enhancement is necessary for realistic oxygenator flow analysis. The membrane fibres are stacked crosswise and by that they build sinuous wave-like channels with varying diameters between 100 and 400 microns.

Blood coagulation on the other hand is represented statistically by means of flags which are transported with flow. They represent either activated or inactivated platelets. On a statistical base they can be activated by shear stress or by interaction with an already activated platelet. If activated platelets approach each other (come close together) this region will be marked as coagulation regime and local viscosity modifications as well as mesh movement will take place. Activated platelets without any interaction, on the other hand, will be inactivated with time.
All model enhancements are adjusted/validated by means of real blood flow experiments and, furthermore, comparison with medical image micro-ct data analysis of real oxygenators. The effect of viscosity change in accordance to the diameter of blood vessels results mainly from tumbling motions of erythrocytes caused by velocity gradients within the flow. Depending on the vessel diameter, this results either in the formation of a so-called plasma skimming layer close to the vessel wall without erythrocytes for intermediated vessel diameter or in a pseudo haematocrit reduction which leads to the formation of a plasma bolus between single erythrocytes for small vessel diameter (see figure 1). Both effects result in a significant change of the local viscosity. Since most investigations on blood viscosity change due to *FLE* have been undertaken in straight or tapered pipes, not much is known on the erythrocyte motion and its effect on viscosity in wavy channels. Therefore, additional experimental investigations on erythrocyte motion at different velocity gradients and haematocrit levels are carried out in wavy micro channels using optical tracking techniques.

Ergebnis: Preliminary results of numerical investigations on blood flow in complex membrane oxygenators using standard non-Newtonian blood viscosity models showed a more or less equally distributed flow shear between the single membrane fibres in the membrane stack. The calculated shear rate for this case exceeded the physiological level capable of triggering (flow induced) blood coagulation. However, comparison of potential blood coagulation regions derived from CFD data compared to medical image data from real clinical oxygenators revealed, that CFD overpredicts the appearance of flow induced coagulation. Therefore, as a first approach, a clear width based enhanced blood viscosity model was implemented into DLR CFD THETA code based on published data of viscosity change due to vessel diameter for straight vessels. Due to the fixed assignment of viscosity change and clear width of the flow, the local viscosity changes directly with change in flow shape, which is a non-realistically behaviour. Therefore, the need arose to take into account the tumbling motion induced phase shift between change of geometrical flow shape and viscosity change. These temporal and spatial effects have to be investigated in wavy micro ducts of different shapes.

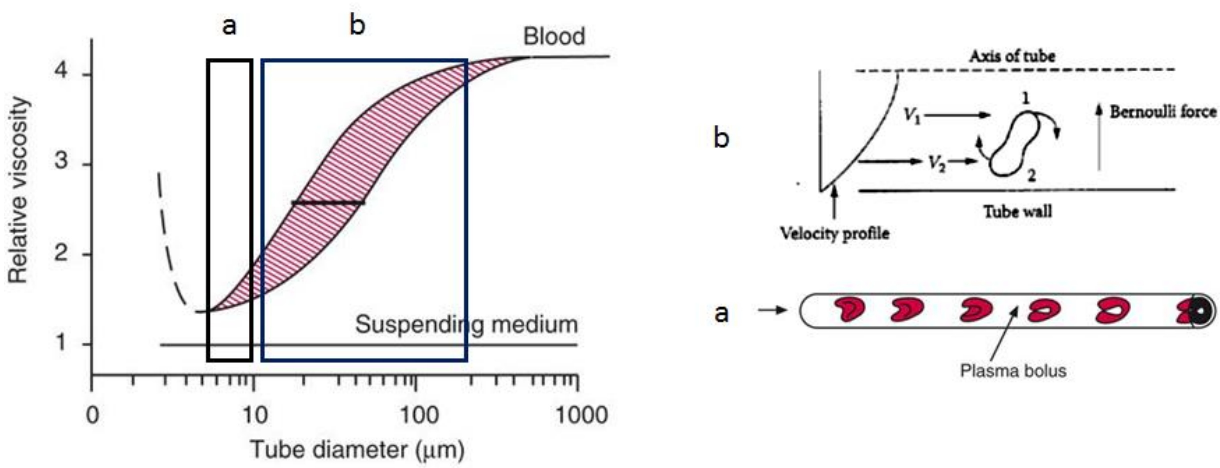

Figure 1: Principle mechanisms of the Fåhraeus-Lindqvist-Effect [Elsevier]

[1] K. Lehle, A.Philipp, T. Müller et al. “Flow Dynamics of Different Adult ECMO Systems: A Clinical Evaluation”, Artif. Organs., Vol. 38, Issue 5, pp. 391-398, (2014).

Namensverzeichnis der Autoren und Koautoren